Coal Classification by HPLC and Three-Dimensional Detection

Michael J. Sepaniak and Edward S. Yeung

Ames Laboratory* and Department of Chemistry
Iowa State University
Ames, Iowa 50011

Coal liquefaction products include a fraction known as the asphaltenes, which are operationally defined as the pentane insoluble, benzene soluble components. The asphaltenes have been postulated as intermediates in the conversion of coal to oil and contain a high concentration of the coal impurities. It is the goal of this work to characterize the asphaltenes derived from various solvent refined coals, so that similarities and differences between various refining processes can be identified. Such information can lead to the optimization of the processing conditions, improved quality control, reduced environmental pollution, and the understanding of the fundamental chemical reactions involved.

A typical coal-derived asphaltene sample contains hundreds of components, mostly in the 200-800 molecular weight range. Considering the complexity of these samples, it is imperative to resolve the components as much as possible, to obtain the maximum amount of information for classification purposes. Recent advances in microbore columns have resulted in extremely high efficiencies in liquid chromatography. Chromatographic runs however can last tens of hours. Also, the reliability, reproducibility, and useful life of these columns for repeated injections of such complex samples have not been adequately tested. We have therefore chosen for these studies standard commercial reversed-phase HPLC columns, which, with the proper eluant gradient, are not much lower in efficiency than those mentioned above. The use of a pre-column switching technique significantly prolonged column life and reduced contamination. The use of multidimensional detectors allows the extraction of a maximum amount of information, and the high sensitivity of the detectors allows small injection quantities and again more reliable separation.

Three optical detectors are used for this work, based on the fact that these are sensitive and that they complement one another in the type of information each provides. The first is a conventional uv absorption detector operating at 254 nm. This has a demonstrated detectability in the nanogram range and is a general and versatile detector. The second is a laser-excited fluorometeric (LF) detector that has a detectability in the picogram range. In addition to the higher signal levels because of the higher photon fluxes in a laser, the monochromaticity in excitation results in correspondingly narrower Rayleigh and Raman lines and permits larger spectral windows for fluorescence observation. In order to obtain information as different from that in the first detector as possible, visible wavelengths are used in excitation and in emission. This favors the detection of the larger molecules, where conjugation shifts the absorption bands to longer wavelengths. The third is a two-photon excited fluorometric

*Operated for the U.S. Department of Energy by Iowa State University under contract No. W-7405-Eng-82. This research was supported by the Director for Energy Research, Office of Basic Energy Science, WPAS-KC-03-02-03.

(TPF) detector. A detectability in the nanogram range has been demonstrated with continuous-wave lasers, but picogram levels can be achieved if high-power pulsed lasers are used. The net excitation is into electronic states comparable in energy with those in uv absorption, but the unique selection rules of the TPF process provide complementary information. Furthermore, the TPF process is enhanced when a real electronic state matches the energy of one of the photons, in our case a visible photon. The selectivity again favors the larger molecules with a higher degree of conjugation.

Pattern recognition studies were performed using the subroutines CORREL, WEIGHT, BACLAS, SICLAS, MULTI, TREE, and KNN from the standard package known as ARTHUR. To limit the number of features in the statistical pattern recognition programs, an intra-sample feature correlation was first performed.

Reproducibility

Even though the injection quantities were kept to 40 µg, contamination still prevented the use of a single column for all the work, and 6 different columns (from the same production batch) were used. In the process of correlating the chromatographic peaks to extract features, we found that the normalized retention times and signal magnitudes among all injections had relative standard deviations of 2.5% and 9.2% respectively. Considering the complexity of these samples, the reproducibility is good.

Detector comparison

Chromatograms from each of the three detectors for a particular run are shown in Figure 1, indicating that information obtained from each is quite independent and the three complement one another. It should be noted that even if peaks occur at the same retention time, they need not correspond to the same component. A distinctive feature in Figure 1 is the positions of the different "center-of-mass", i.e., when about 50% of the weighted response has passed the detector in question. These are in the order uv, TPF and LF. The nature of reversed-phase separation using this gradient generally makes the smaller components elute early and the larger components elute late. Since the LF detector requires electronic conjugation for the necessary spectral red-shift, very little response shows up early in the chromatogram. Even when the individual concentrations of the components decrease towards the end of the chromatogram, as a result of our pre-column switching and as evidenced by the falling response in the uv detector, the LF response remains high. Chromatograms from the TPF detector present an interesting case. Presumably the abundance of two-photon states around 244 nm (twice the photon energy) is not too different from one-photon states at 254 nm (uv detector). The smaller response of TPF early in the chromatogram is an indication of the lower overall sensitivity of the process. The components towards the later part of the chromatograms are rich in electronic states in the 488 nm region, as seen from the LF chromatogram. These same electronic states serve to resonantly enhance the TPF process, thus providing a larger signal. The TPF still falls off a bit earlier than the LF signal, probably because of gradually decreasing concentrations and the lower overall sensitivity of the former process. Our choice of visible wavelengths in excitation and emission is thus justified, since the uv detector is not suitable for these components. Even if a uv fluorometric detector is used, one still favors the smaller, less conjugated components.

Sample comparison

Figure 2 shows chromatograms for the four different samples studied, all from the LF detector. Some consistent, distinctive features can be identified even without statistical analysis. The locations and the relative heights of the two major peaks in each chromatogram are sufficient to distinguish the PAMCO and the Cat. Inc. samples from the two Synthoil samples, and from each other. As expected, the two Synthoil samples are more difficult to distinguish. Minor features around 33 mins. and 37 mins. are useful for visual comparison in that case. At first sight it may seem that features after 50 mins. are distinctive for each sample. However, intra-sample correlation of these features is not good due to the pre-column switching procedure, and these features cannot be used.

A more objective comparison can be made using pattern recognition analysis. This was performed first for each detector with the 38, 38, and 41-dimensional vectors derived from the peaks via feature extraction. The results are presented in Table I. Then, the WEIGHT subroutine was used to determine the 6 or 7 most important features for each detector to the classification process. These were then used by themselves in a second pattern recognition analysis, the results of which are also shown in Table I. Finally, the combination of these 20 most important features and the 7 most important of these were also analyzed. It is significant to note that the combined set of 20 features did even better in every classification scheme than the individual sets of 38, 38, and 41 from the three detectors. In the combined set of 7 features, the success at classification is better than either the 6 TPF features or the 7 LF features, and about equal to the 7 uv features. This is consistent with the fact that in general having more independent types of measurements is better than having more of the same type of measurement for classification purposes. In Table II we list the overall ranking of the set of 20 combined features and the average retention times in the whole data set. The first observation is that the detectors are quite different, as expected. Features that are important in classification for one detector need not be important for another detector. This is seen from the relative locations of the selected features in the three chromatograms, and the lack of correlation among the individual rankings. One can infer that a distribution of molecular sizes and polarities can be important as features in classification, and that whole chromatograms rather than parts of chromatograms are needed. The second observation is that sometimes an important feature in one detector does correspond to an important feature in another detector. An example is the set of features UV2, LF3 and TPF2, which have indistinguishable retention times. Such situations magnify the significance of a given feature. Since the ultimate use of these classification and feature extraction studies is to identify compounds or classes of compounds that are important to the liquefaction processes themselves, these should be the most favorable starting points. Fractions can be collected on a semipreparatory scale in these regions, so that structural studies by infrared, nmr, or mass spectroscopy can be performed. Also, whenever the relative signals of a given feature at all three detectors remain constant in going from one sample to the next, more confidence can be put on the possibility that only a single component is involved. The third observation is that major peaks are not necessary useful features for classification. This points out the dangers of relying on just visual comparisons for classification. The human perception is easily biased towards the larger, seemingly better resolved, peaks.

In these complex samples, peaks may contain several components, so that slight differences in the gradient can dramatically alter the peak height. Also, if only one of the several components is important for classification, one would not be able to use it due to interference from the other components. The fourth observation is that the internal standard peak in the TPF chromatograms was actually identified as the eighth most important feature for classification. This apparent paradox can be resolved by noting that there is a continuous background at that location that is real. The "feature" therefore is simply the magnitude of this background at the retention time of the internal standard, not at all unreasonable to be important for classification. The fifth observation is that the six TPF features rank low in the group of 20 combined features for classification. This is more due to the poorer signal to noise levels and greater dependence on focusing and positioning, rather than an indication of the type of information. A higher response using e.g. pulsed lasers should improve things.

To assess the importance of the unresolved components that make up the broad background, we have extracted features based on the chromatographic valleys. The same pattern recognition calculations were performed using the signal levels in each detector at these "valleys". In general, the valleys are slightly poorer features for classification compared to the peaks. The fact that they perform this well indicates that the unresolved components can also be useful for characterization of the coal liquids. This is not surprising considering the diversity of components that are present, and that a large response in any detector need not be related to the importance of a given component. It is however incorrect to conclude that low-resolution chromatograms can be equally useful for classification purposes, since the success of these "valleys" is due in part to the reproducibility of the locations of the "peaks" that are around them. There are regions where both useful peaks and useful valleys are found, for example between 5 and 10 mins. in retention time. This then points to a particularly interesting region for further studies, possibly at higher chromatographic resolution and by collecting fractions for other analytical methods. The usefulness of the valleys in classification shows that the human bias towards recognizing peaks as features can be deceptive in complex systems.

Table I. Success at classification for each detector.

Detector	# Features	Success(%)			
		SICLAS	BACLAS	KNN	MULTI
TPF	38	90	100	42	100
TPF	6	74	94	52	87
LF	38	87	100	42	100
LF	7	90	94	74	94
UV	41	97	100	61	100
UV	7	90	100	90	100
All	20	100	100	94	100
All	7	97	100	84	100

Table II. Ranking of importance of peaks as features.

Rank	Feature*	Retention Time (min.)
1	LF1	21.1
2	UV1	26.6
3	LF2	8.1
4	LF3	40.5
5	LF4	26.0
6	LF5	6.3
7	UV2	40.3
8	LF6	9.1
9	UV3	21.8
10	TPF1	5.9
11	UV4	7.0
12	TPF2	40.0
13	UV5	19.7
14	UV6	5.3
15	TPF3	43.0
16	TPF4	52.5
17	TPF5	27.2
18	UV7	34.1
19	LF7	33.4
20	TPF6	24.4

*Features are identified in Figure 1. Letters refer to the respective detectors and numbers refer to those on the chromatograms.

FIGURE CAPTIONS

Figure 1. Information from the three detectors for the same injection. Numbers are peaks used as features as explained in the text. (a) uv detector; (b) LF detector; and (c) TPF detector.

Figure 2. Sample comparison using the LF detector. The labels refer to the four solvent-refined coals specified in the text.

FIGURE 1

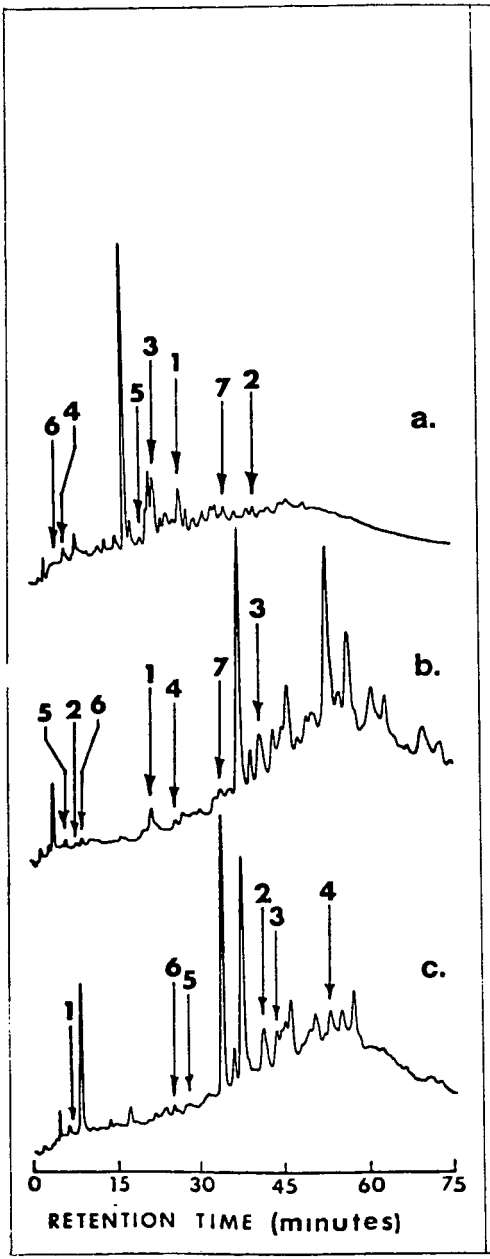

FIGURE 2

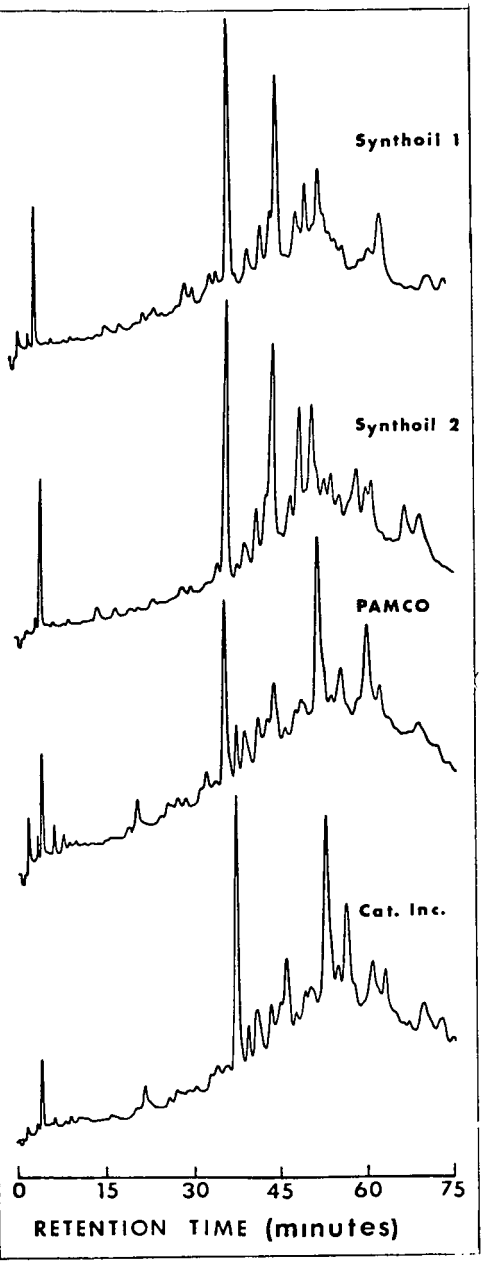

APPLICATIONS OF ON-LINE MULTIDIMENSIONAL CHROMATOGRAPHY TO SOLVENT REFINED COAL

T. M. Chen, J. A. Apffel, H. M. McNair

Department of Chemistry, Virginia Polytechnic Institute and State University, Blacksburg, Virginia 24061

Solvent refined coal (SRC) is predominately aromatic in nature and contains many polyaromatic hydrocarbons (PAHs). Several PAH's are highly carcinogenic and therefore a knowledge of PAH distribution in SRC is important for health reasons as well as the basic information about the composition of SRC.

SRC is a complex mixture and attempts to elucidate structure or compositional details by a single analytical technique have had limited success. We have chosen several on-line multidimensional chromatographic techniques to examine the hexane soluble fraction of SRC. These techniques include LC (silica gel)/ LC (reverse phase); LC/GC; and LC/LC/Fluorescence. The latter technique proved to be the most useful and will be discussed in detail in this paper.

An SRC sample from AMAX feed stock (obtained from Southern Services, Inc., Wilsonville, Ala) was continously extracted with hexane.

A prepacked silica gel column (size A; 24 x 1 cm; S1-60 silica gel) from E. M. Laboratories, Cinn. Ohio was the first column. HPLC grade hexane, 1.8 ml/min was used to elute a 250 microliter solution of approximately 50 mg of sample. Typical results are shown in figure 1. Note in figure 1 that it was necessary to backflush the column after 70 minutes to elute high molecular weight material. The column was also washed with methylene chloride for 30 minutes before another sample was injected. The fractions containing PAHs are numbered 5 to 10.

Silica gel separates PAH's roughly by the number of condensed aromatic rings. Six fractions of potential PAH content wer chosen based on the retention times of a standard sample containing: Napthalene, 1-Methylnaphthalene, 2-Methylnaphthalene, Acenaphthalene, Flurene, Phenanthrene, Anthracene, 2-Methylanthracene, Fluorathene, Pyrene, Benzo(A)Anthracene, Chrysene, Fluoranthene, Perylene, Benzo(A)Pyrene, Benzo(G,H,I)Perylene, Indeno(1,2,3)Pyrene.

In early work the six fractions were collected manually, dried by nitrogen, dissolved in acetonitrile and injected onto an analytical reverse phase column, Vydac RP Column, 25x0.32 cm (Separations Group, Hisperia Ca.). Mobile phase was a mixture of acetonitrile and water (composition and flow rate changed for different fractions). Detection was a UV-254 nm photometer coupled in series with a Spectrofluorometer (Varian Model SF-330, Palo Alto, CA) equipped with a 16 ul HPLC flow cell.

PAH's were identified by 3 chromatographic techniques: (1) rentention time; (2) ratio of fluorescence/UV detector response; (3) fluorescence spectrum of trapped fractions in the SF 330 flow cell.

PAH distribution in the fractions is shown in Table 1. Characterization by simple retention time, and fluorescence/UV response ratios was difficult. Figures 2,3,4 show fraction 7 eluted under identical chromatographic conditions, but recorded at 3 separate fluorescence excitation and emission wavelengths. The selective fluorescence response of the various PAH's was the key to identification. Note that standard samples are shown under the SRC samples in Figures 2, 3 and 4 to aid in identification.

Table 1 PAH Distribution in SRC Fraction

Fraction	PAH
5	napthalene, 2-methylnaphthalene
6	naphthalene
7	phenanthrene, anthracene, 2-methylanthracene and pyrene
8	fluoranthene
9	benzo (a) anthracene, perylene and benz (a) pyrene
10	benzo (a) anthracene, perylene and benz (a) pyrene

INSTRUMENTATION

Figure 5 is a schematic of the multidimensional or LC/LC/Fluorescence system. The LC is a Varian model 5040, a single reciprocating piston pump with 3 solvent inlet valves controlled by a microprocessor. For LC/LC operation two Valco automatic six-port valves are used to trap fractions and divert the proper fraction to the second LC column. One limitation of the on-line LC/LC system is the incompability of solvent for the different LC columns. Small volumes of hexane (10-30 ul) such as used here can be injected onto the reverse phase system.

The LC/GC system used employed a Varian model 8070 LC/GC interface and has been reported by Apffel elsewhere (1). In this application a hydrocarbon group separation was performed by HPLC on a 5 μ silica column using hexane as a mobile phase (See figure 6). The PAH's were sampled at points determined by standards and automatically injected into a capillary GC. The GC separation was temperature programmed and run on either an SE-30 or a SE-52 WCOT capillary. GC detection was by FID (See Figure 7).

CONCLUSIONS

On-line coupled chromatographic techniques allow separations not easily done off-line. The on-line techniques are easily automated (increasing reproducibility) and allow small transfer volumes between systems. The main limitation with LC/LC is the incompatibility of mobile phases when the columns are normal phase and reverse phase. With LC/GC the main problem is quantitation (since only a portion of the peak is injected) and degradation of GC columns with some LC mobile phases. The use of selective detectors in series is a good technique to examine complex fractions like SRC and enhances the separating power.

REFERENCES

(1) A. Apffel, R. Majors, H. McNair, "Quantitative Studies Using an LC/GC System"; paper presented at Pittsburgh Conference March 1980; submitted to J. Chromatography Science.

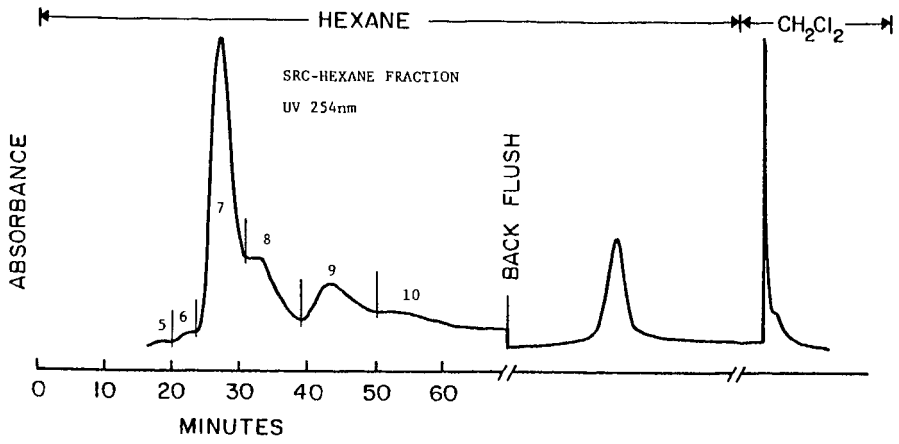

Fig. 1 Fraction of SRC from LC Analysis for Further Work

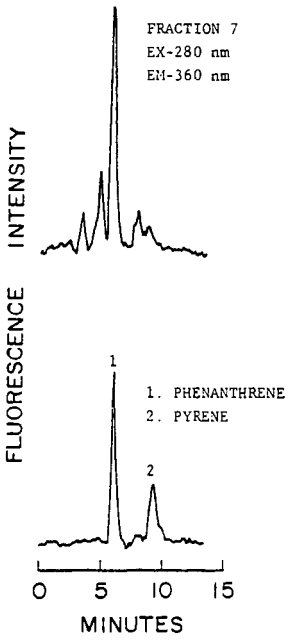

Fig. 2 Fraction 7

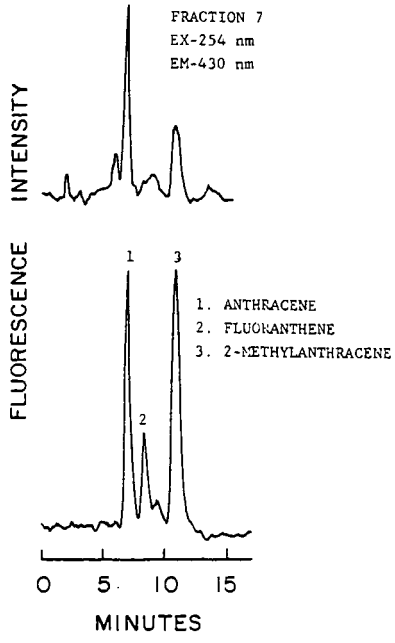

Fig. 3 Fraction 7

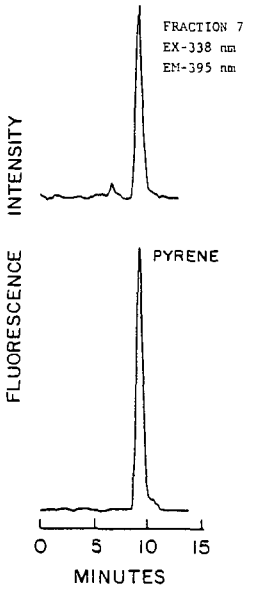

Fig. 4 Fraction 7

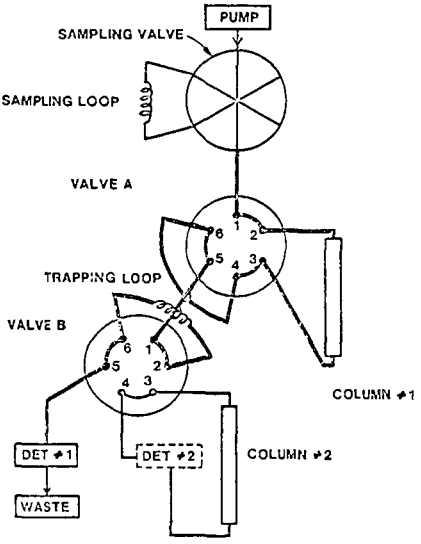

Fig. 5 Column Switching Schematic-LC/LC/Fluorescence

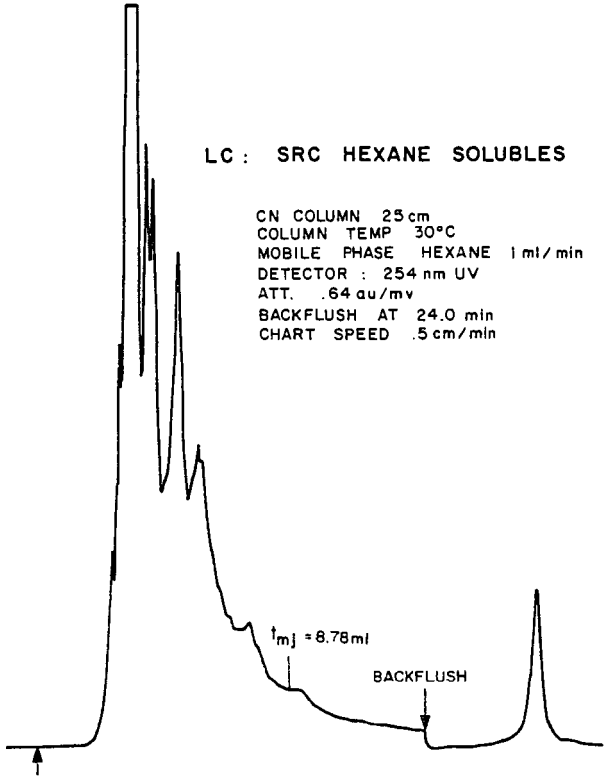

Fig. 6 LC Trace of Hexane Soluble Fraction of SRC

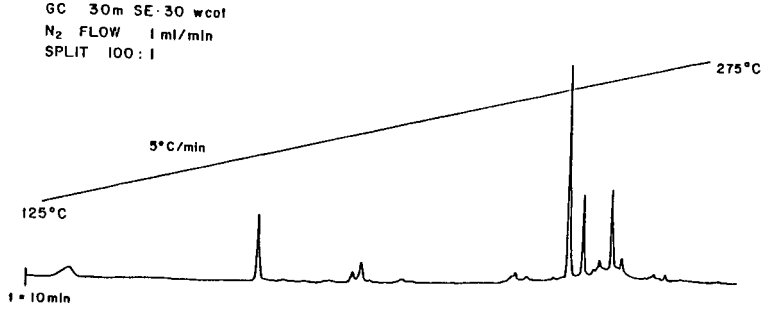

Fig. 7 Analysis of PNA Fraction From LC

Coupled-Column Chromatography Used For The Analysis of Coal-Derived Liquids

E. Katz and K. Ogan
The Perkin-Elmer Corporation
Main Avenue, Norwalk, CT 06856

Our goal is to utilize the newest LC technology to provide significant improvements in areas of analytical interest. The analysis of complex samples is a challenging problem. Conventional analytical methods for complex samples involve several steps, and hence are long and laborious. Modern LC technology offers speed and efficiency, particularly for the sample clean-up and fractionation steps.

We have developed a fractionation method which makes use of two different types of columns: a low-resolution partition column and a size-exclusion column. The low resolution column has the same separation mechanism as the ultimate analytical column. This fractionation stage limits the retention range of compounds to be chromatographed in the analytical step. The selected fraction from this low resolution column is transferred to a size-exclusion column which separates compounds on the basis of their molecular size. This second stage of fractionation greatly reduces the number of compounds within this retention range.

We have utilized the coupled-column chromatography (CCC) system to obtain fast and qualitative characterization of a sample prior to the analytical step.

We have demonstrated the compatibility of the CCC system with analytical methods, specifically, the determination of PAHs and phenols by reversed-phase LC.

Use of the CCC fractionation system with samples such as coal liquids resulted in very reproducible performance of analytical columns, performance which is required for identification and quantitation of individual compounds.

Additional verification of individual PAHs was provided by fluorescence detection at two selective excitation and emission wavelength sets.

In the case where the determination of many compounds in very complex samples is needed, additional resolution is required.

CHARACTERIZATION OF HIGH BOILING FISCHER-TROPSCH LIQUIDS

FRANK P. DI SANZO

MOBIL RESEARCH/DEVELOPMENT CORP., PAULSBORO, NEW JERSEY 08066

INTRODUCTION

Fischer-Tropsch liquids obtained through the indirect liquefaction of coal via synthesis gas ($CO+H_2$) are expected to become an important source of fuel during the next several decades. Their commercial feasibility has already been demonstrated (1).

The hydrocarbon products from the Fischer-Tropsch process range from methane to high molecular weight compounds. In addition, relatively large amounts of oxygenates are produced. The quality of the gasoline product is such that extensive upgrading is required to produce stable, high octane motor fuels. Synthesis gas has been converted to high octane gasoline by a combination of Fischer-Tropsch synthesis followed by product upgrading with a ZSM-5 class catalyst. The application of ZSM-5 class catalyst to the production of high octane gasoline from methanol has already been demonstrated (2-4).

In conjunction with process development for the conversion of synthesis gas to high octane gasoline analytical methods are being developed to characterize in considerable detail the hydrocarbons and oxygenates in Fischer-Tropsch stage one effluent prior to their passage over a reactor with ZSM-5 class catalyst. These techniques will enable the effects of process variables on the composition of stage one products to be measured and subsequent effects of variations in Fischer-Tropsch composition on ZSM-5 catalysis to be defined.

Published Fischer-Tropsch analytical methods (5-11) have dealt mainly with relatively low molecular weight components produced during Fischer-Tropsch catalyst studies with little emphasis on the higher boiling hydrocarbons and oxygenates which may be produced in large scale reactors.

In this paper, gas and preparative liquid chromatographic methods for the characterization of Fischer-Tropsch hydrocarbons and oxygenates boiling above 170°C (C10+) are presented.

EXPERIMENTAL

Materials. Fischer-Tropsch samples obtained under various process conditions were studies in detail. All three samples represented mostly components boiling above 170°C (C10+).

Separation Scheme. The separation scheme (Figure 1) devised to isolate and characterize the various compound classes found in Fischer-Tropsch liquids consisted of preparative low pressure liquid chromatography (LC) and gas chromatography. Total hydrocarbons isolated by silica LC were resolved into paraffins and olefins by argentation liquid chromatography as previously described elsewhere (12).

Silica Low Pressure Liquid Chromatography. The LC system consisted of a Waters 6000 pump (Waters Associates, Milford, Mass.)

and a Rheodyne 70-10 valve containing a 10 ml sampling loop. Solvents were distilled in glass (Burdick & Jackson, Muskegeon, Michigan). A 30cm x 15mm i.d. glass column was packed with 20-44 micron Bio-Sil silica gel (Bio-Rad, Richmond, Calif.) activated in air at 150 C for 12 hours.

2.7 gms of the Sample A Fischer-Tropsch liquid was injected directly onto the liquid chromatographic column. Samples B and C contained an insoluble high molecular weight wax which was removed prior to liquid chromatographic analysis to prevent plugging of the injection valve and column. Soluble hydrocarbons and oxygenates were extracted from this insoluble wax by weighing approximately 3 grams of the Fischer-Tropsch samples into a centrifuge tube, adding 3-5 ml of toluene, shaking until the total sample was dispersed, and then centrifuging for five minutes. The supernatant liquid was removed and filtered over a pre-weighed 4-5.5 micron frit. This procedure was repeated until the extracting toluene was clear (usually 3-4 extractions). Finally, the remaining insoluble wax was transferred quantitatively to the frit which upon drying was reweighed to calculate percent insoluble wax. The toluene solution containing the extracted hydrocarbons and oxygenates was reconcentrated to obtain a 3 ml solution which was injected onto the LC column described above. The injected sample was eluted sequentially with hexane (250 ml), methylene chloride (250 ml), and methanol (150 ml) at flow rates of 5-6 ml/min. The solvents were removed with a three ball Snyder column and modified nitrogen purged pre-weighed beakers. After solvent evaporation the beakers were re-weighed to obtain a weight percent analysis on each LC fraction (Table 1). 99.6% of the total sample injected onto the silica column was recovered. Samples containing residual C5-C9 hydrocarbons may exhibit lower recoveries due to the loss of these hydrocarbons during solvent evaporation.

Argentation Liquid Chromatography. A 30 cm x 9 mm i.d. glass column was packed with 20% silver nitrate impregnated on 32-63 micron Woelm silica gel (12). The silica was prepared by dissolving the silver nitrate in acetonitrile and then adding the silica. The solvent was removed in a dark room by rotary evaporation while purging with nitrogen and heating with an infra-red lamp. The packed glass column was protected from light by completely covering with aluminum foil.

The capacity of the silver nitrate column was approximately 100 mg of total hydrocarbons isolated from the silica column. Three separate injections were made for each sample.

Gas Chromatography. Gas chromatographic analysis on each LC fraction was performed on a SIGMA 2 GC (Perkin Elmer, Norwalk, Ct.) equipped with a flame ionization detector. OV-101 Glass SCOT columns were purchased from SGE (Austin, Texas). Samples were injected in the splitless mode.

A packed 6' x 1/8" SS 1.5% Dexsil 300GC on Supelcoport (Supelco, Bellefonte, Pa.) column was used for the paraffin fraction. Peak integration was performed with a Varian 620 Data System.

RESULTS/DISCUSSION

Major Functional Groups. IR spectra of the three Fischer-Tropsch samples prior to liquid chromatographic analysis are given

in Figure 2. The major absorption bands of interest are the carbonyl (1700-1750 cm^{-1}), olefin (910 cm^{-1}, 955 cm^{-1}) and the $(CH_2)_x$ (1720-730cm^{-1}). The carbonyl bands for all three samples indicate the presence of more than one carbonyl functional group. In Sample A α-olefins (910 cm^{-1}) predominate; however, sample B has approximately equal amounts of α-(910 cm^{-1}) and β-olefins (960cm^{-1}) while in sample C the β-olefins are the major olefins.

The bands at 720-730 cm^{-1} which are characteristic to long chain paraffins are proportional to the high molecular weight wax present. Samples B and C exhibit a strong absorption due to the high content of insoluble wax present in these samples. Sample A which contained no detectable insoluble wax has a low absorption at 720-730 cm^{-1}.

Paraffins. Gas chromatographic fingerprints (Figure 3) of the paraffins isolated by argentation LC indicate that Samples B and C contain normal paraffins up to approximately C45. In contrast, Sample A contains normal paraffins up to approximately C35. In addition, the latter sample contains a distinct second maximum at C21-C22 and a relatively large envelope. Components appearing between the normal-paraffins (Figure 3) are believed to be iso-paraffins (13,14).

Olefins. Gas chromatograms of the three olefinic fractions isolated by argentation LC are shown in Figure 4. The two major olefin types observed in all samples are the linear α-olefin and the β-olefin. In Sample A the linear α-olefins are the major components whereas in Sample B both the linear α- and β-olefins predominate. In Sample C linear β-olefins are the major components. These results are consistent with the IR data presented in Figure 2.

Other minor olefins believed to be methyl-substituted are also present. In all three samples olefins were detected up to C22-C25.

Ketones and Esters. Infra-red analysis of the methylene chloride LC fraction (Figure 5) indicated that the major functional groups were ketones (1705 cm^{-1}) and esters (1735 cm^{-1}). The aldehyde content is very low as evidenced by the lack of significant absorption at 2720-2820 cm^{-1}. No aldehydes were detected by FT H-NMR. In addition to IR analysis these compound classes were confirmed by wet chemical functional group micro-reaction. Gas chromatograms were compared before and after reaction and the shifting and/or decrease in peak areas indicated a positive reaction. Esters were confirmed by reaction with methanolic-sodium hydroxide and ketones by reaction with 2,4-dinitrophenylhydrazine (15). Individual components were identified by co-injection with authentic standards. Figure 6 compares the SCOT column chromatograms of Samples A and C methylene chloride fraction. Sample B produced a gas chromatogram similar to that of Sample C.

Methylketones are the major components in all three samples. This was confirmed by gas chromatography and FT H-NMR and C13-NMR. Sample A contains detectable esters which were confirmed by the methanolic-sodium hydroxide reaction.

Alcohols and Acids. IR analysis of the methanol LC fraction (Figure 5) indicated the presence of alcohol (3420 cm^{-1}) and carbonyl (1705 cm^{-1}) bands. The carbonyl band was attributed to carboxylic acids as confirmed by a separate extraction of the total sample with aqueous $NaHCO_3$ (Figure 5). No methylketone contamination from the methylene chloride fraction was detected by gas chromatography.

The alcohols in this fraction were confirmed by gas chromatography by acetylating with acetic anhydride in the presence of pyridine (16) which resulted in peak shifting and improved peak efficiency (Figure 7). Individual components were identified by co-injection with standard compounds. Sample A alcohols (Figure 7a) consisted mostly of normal alcohols up to C20 whereas Sample B contained both normal and secondary alcohols which paralleled the linear α- and β-olefin concentration (Figure 4C). Sample C contained only trace amounts of alcohols. Initial studies of the methyl derivatives of the extracted acids indicated that normal-carboxylic acids of C5 to C10+ are present in these samples.

Carbon Number Distribution Plots. Distribution plots for two of the three samples were reconstructed for the major components of various functional groups (Figures 8 and 9). Oxygenates, having boiling points higher than their corresponding hydrocarbons of the same carbon number reached a maximum at lower carbon numbers. This maximum may vary depending on the exact boiling point cut of the Fischer-Tropsch sample.

Distribution plots of oxygenates (methylketones, n-carboxylic acids and alcohols) follow closely those of the linear α-olefins and β-olefins. The ratio of linear α-olefins to β-olefins is strongly dependent on process conditions (e.g. temperature). Both the olefins and the oxygenates contain detectable carbon numbers up to approximately C22-C25.

Except for the linear α-olefins and alcohols the other products are probably formed in secondary reactions (14). Of interest is the carbon number distribution plot for the major esters detected in Sample A (Figure 8) which exhibits a maximum at higher carbon number than the other oxygenates. These esters are believed to be mixed esters as a result of secondary reactions occurring in the reactors among the major carboxylic acids and the major alcohols present:

$$\underset{(R_1=n,\ n+1,\ n+2\ \ldots)}{R_1\overset{O}{\overset{\|}{C}}-OH} + R_2-OH \longrightarrow \underset{(R_2=m,\ m+1,\ m+2\ \ldots)}{R_1\overset{O}{\overset{\|}{C}}-OR_2}$$

CONCLUSION

Chromatographic techniques have been developed which will allow a detailed characterization of Fischer-Tropsch high boiling hydrocarbons and oxygenates obtained under various process conditions. These techniques are currently being refined to include newer chromatographic techniques (e.g. fused silica capillary columns-GC, GC/FT-IR) and mass spectrometric characterization of the minor and major components.

ACKNOWLEDGMENTS

The author wishes to thank S. J. Lucki, J. A. Brennan and J. Kuo for kindly providing the Fischer-Tropsch samples, and J. G. Ehlers and M. E. Landis for obtaining the IR and NMR data. Permission granted by Mobil Research/Development Corp. to publish the results of this study is also appreciated.

REFERENCES

1. "South Africa Commits to Oil from Coal Process", C&EN News, Sept. 17, 1979. pp 13-16.
2. P. D. Caesar, J. A. Brennan, W. E. Garwood and J. Ciric, J. of Catalysis, 1979, 56, 274-278.
3. C. D. Chang and A. J. Silvestri, J. of Catalysis, 1977, 47, 249-259.
4. S. L. Meisel, J. P. McCullough, C. H. Lechthaler and P. B. Weisz, Chemtech, 1976, 6, 86.
5. J. J. Blekkingh, Fischer-Tropsch Synth, 1976, 3, 6.
6. Z. H. Shirazi and C. Stoianov, Pak. J. Sci. Ind. Res., 1977, 20, 1-10.
7. A. G. Sharkey, Jr., J. L. Shultz and R. A. Friedel, U-S. Dept. Interior Bur. Mines Bulletin No. 634, 1967.
8. V. Konik, J. Smejkal and Z. Celeryn, Prare Ustavu Vyzkum Poliv, 1964, 7, 233-245.
9. P.W. Darby and C. Kemball, Trans. Faraday Soc., 1959, 55, 833-41.
10. L. B. Itsikson, Khim i Tekhnol Topliv i Mosel, 1965, 10, 62-64.
11. M. H. Studier and R. Hayatsu, Anal. Chem., 1968, 40, 1011-13.
12. F. P. Di Sanzo, P. C. Uden and S. Siggia, Anal. Chem., 1980, 52, 906-909.
13. J. H. Le Roux, J. Appl. Chem. (London), 1969, 19, 230-234.
14. G. Henrici-Olive and S. Olive, J. of Catalysis, 1979, 60, 481-83.
15. R. L. Shriner, R. C. Fuson and D. Y. Curtin, The Systematic Identification of Organic Compounds, 4th edition, John Wiley & Sons, Inc., New York, 1962, p 219.
16. S. Siggia, Quantitative Organic Analysis via Functional Group, 3rd edition, John Wiley & Sons, Inc., New York, 1963, Chapter 1.

TABLE 1

LIQUID CHROMATOGRAPHIC ANALYSIS OF 170°C+ COMPONENTS

	SAMPLE A	SAMPLE B	SAMPLE C
Paraffins	72.7	70.4	78.4
Olefins	16.2	13.2	9.4
Esters + Ketones	10.6	1.5	6.3
Acids + Alcohols	1.1	2.0	0.2
Insoluble Wax	0	12.5	5.7
Loss	0.4	0.4	0.4

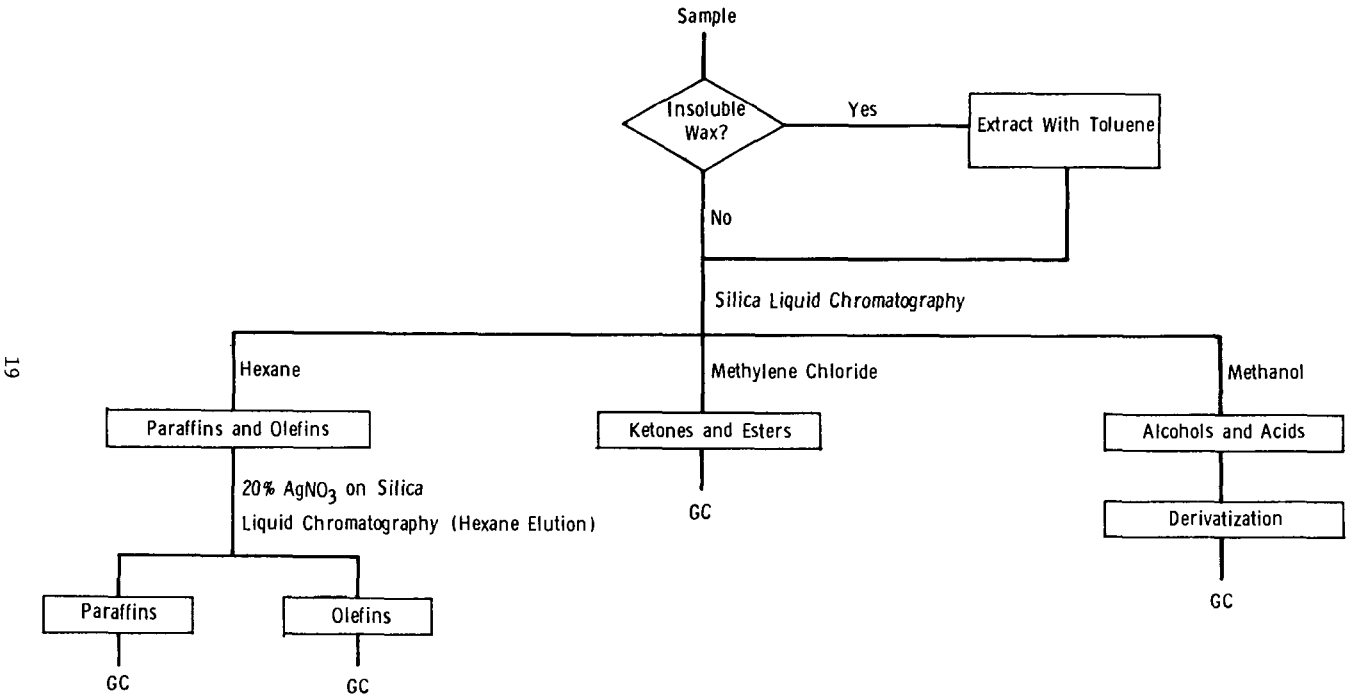

FIGURE 1: SEPARATION SCHEME FOR FISCHER-TROPSCH MATERIALS

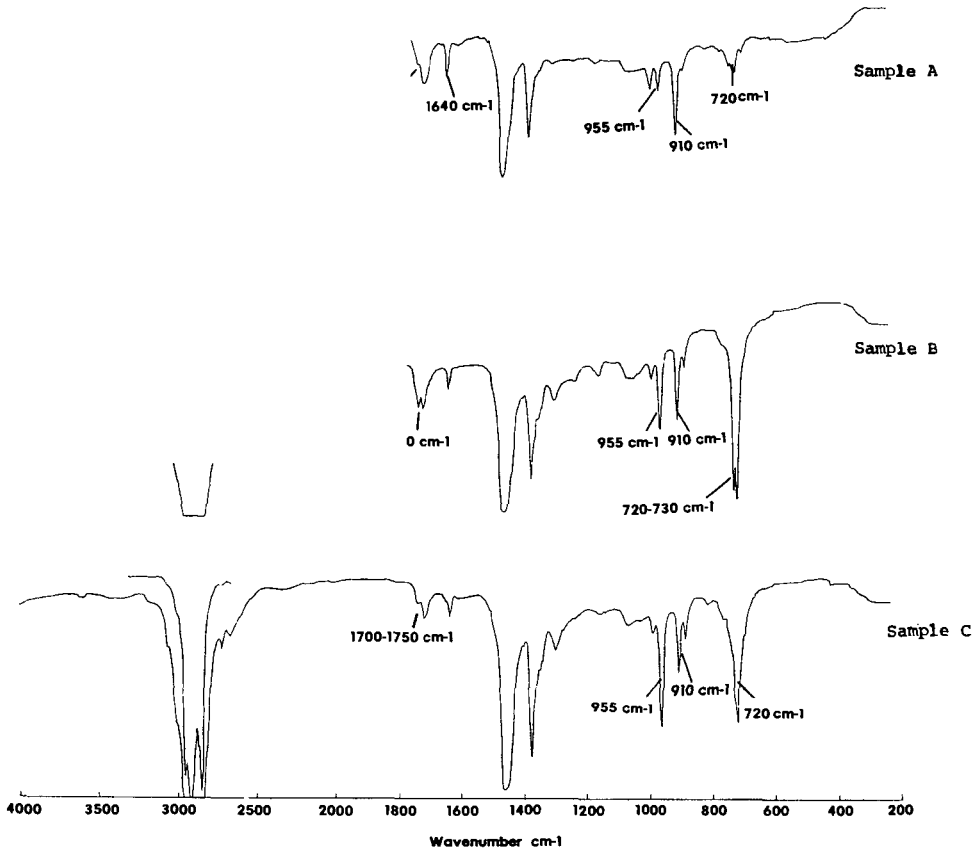

FIGURE 2: IR SPECTRA OF FISCHER-TROPSCH MATERIALS PRIOR TO LC FRACTIONATION

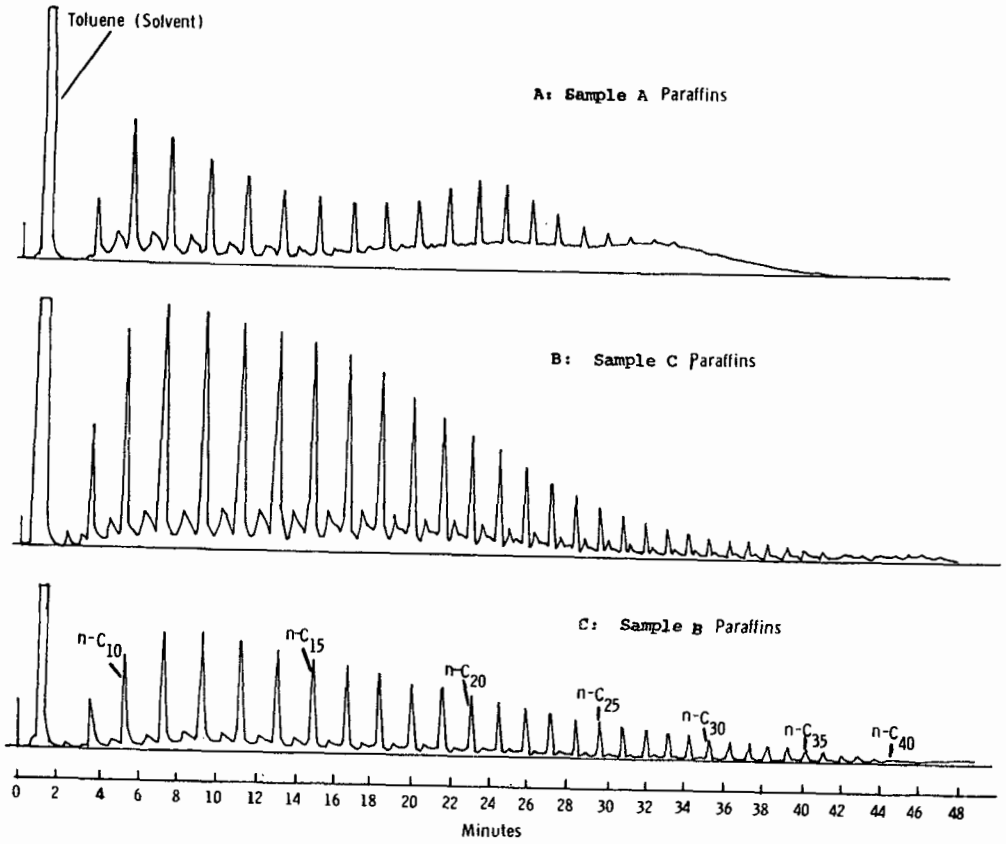

FIGURE 3: PACKED COLUMN GAS CHROMATROGRAMS OF PARAFFINS FROM ARGENTATION LC

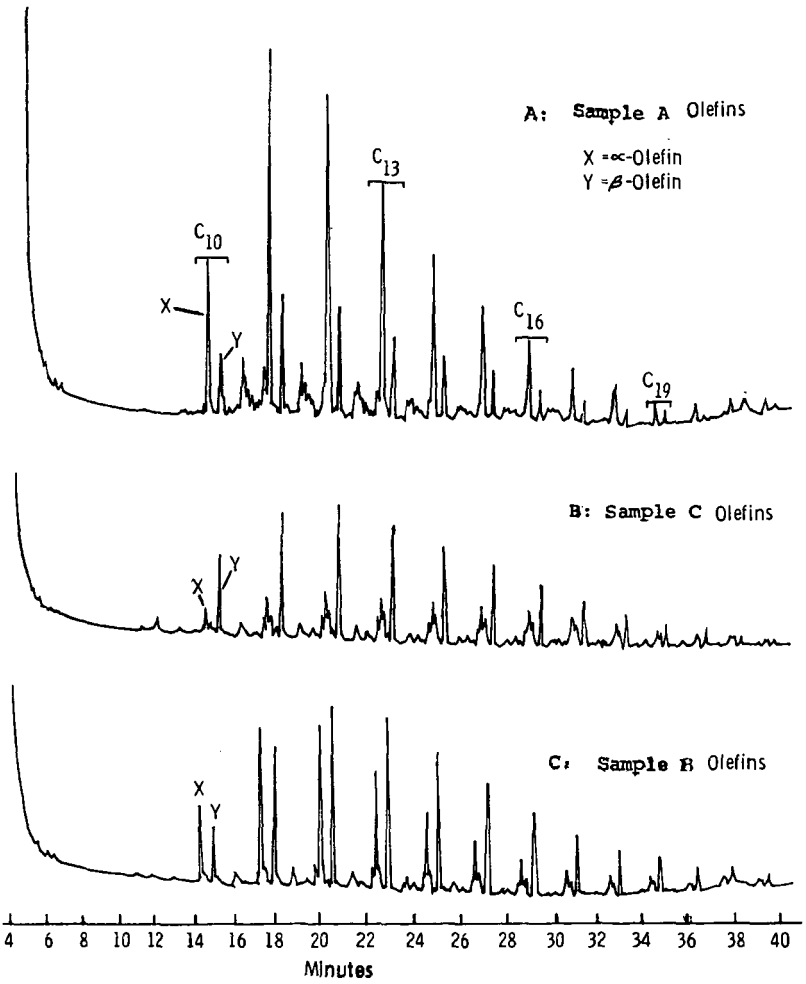

FIGURE 4: OV-101 SCOT COLUMN GAS CHROMATOGRAMS OF OLEFINS FROM ARGENTATION LC

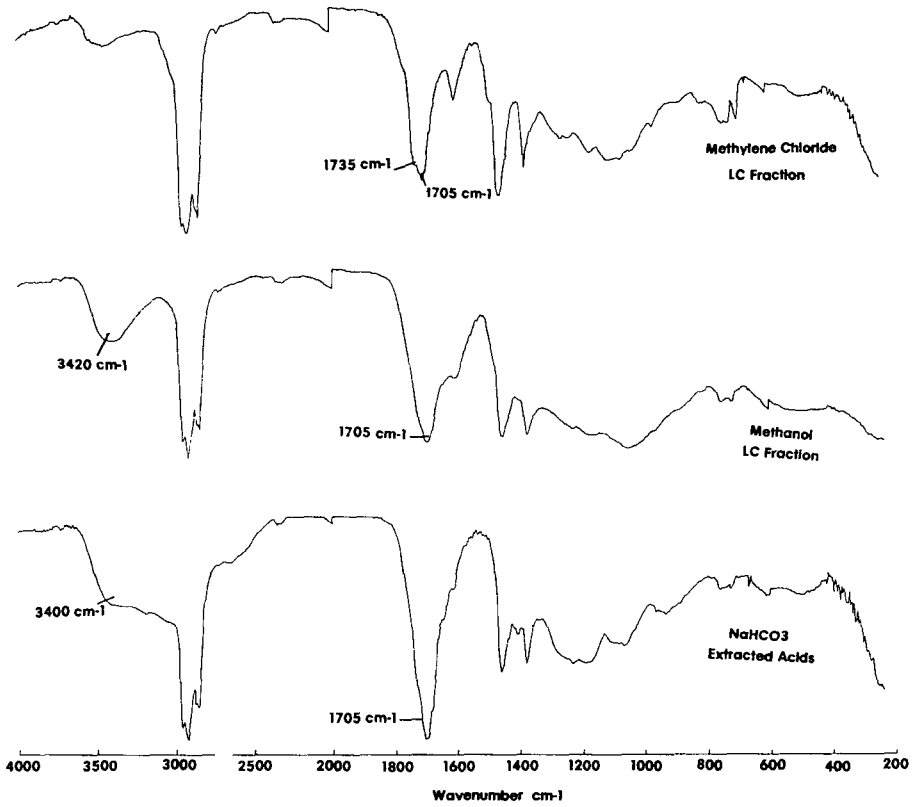

FIGURE 5: SAMPLE A METHYLENE CHLORIDE-METHANOL LC FRACTIONS AND $NaHCO_3$ EXTRACTED ACIDS

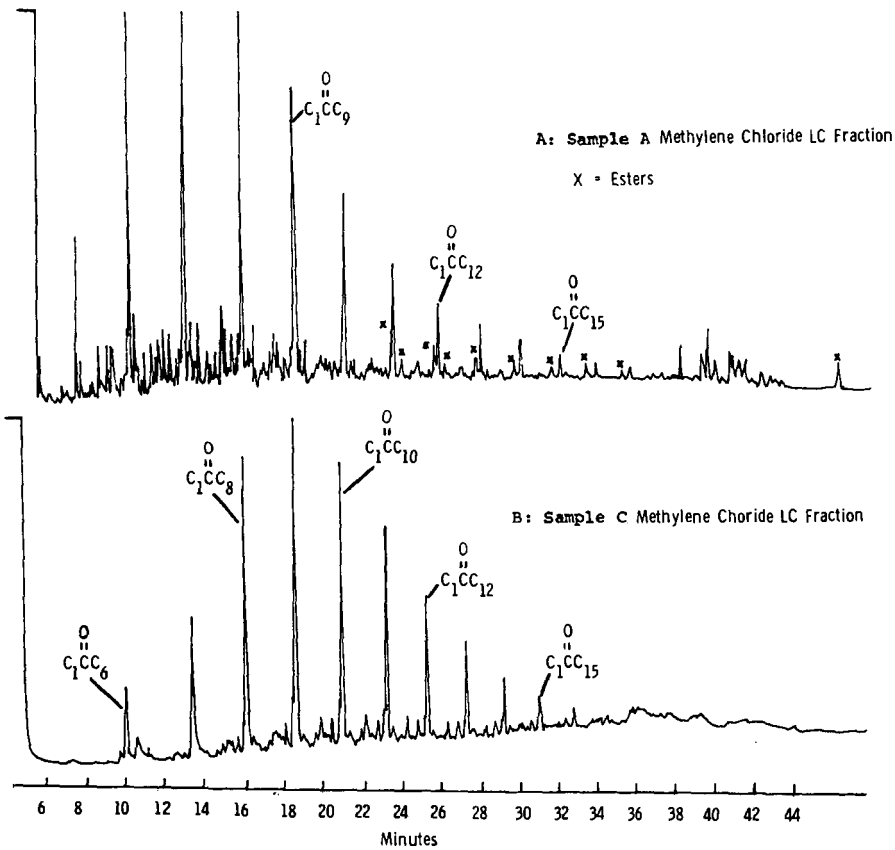

FIGURE 6: OV-101 SCOT COLUMN GAS CHROMATOGRAMS OF SAMPLE A AND SAMPLE C METHYLENE CHLORIDE LC FRACTIONS

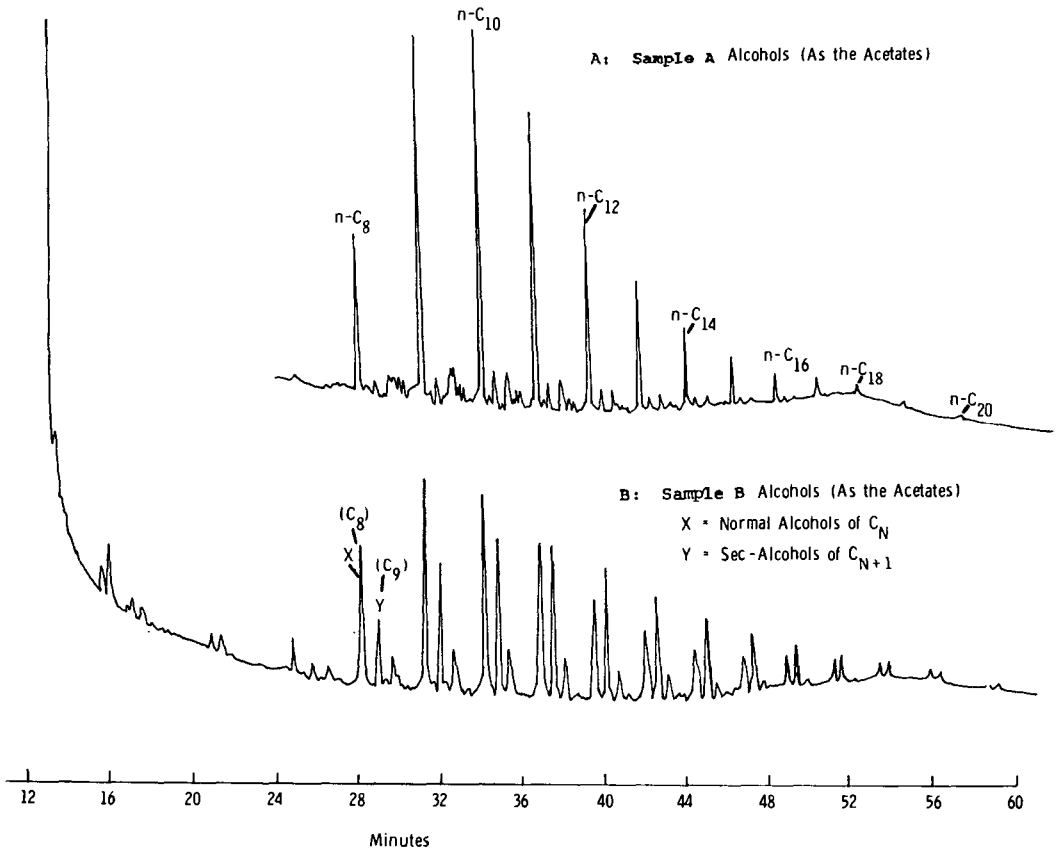

FIGURE 7: OV-101 SCOT COLUMN GAS CHROMATOGRAMS OF ALCOHOLS PRESENT IN THE METHANOL LC FRACTIONS

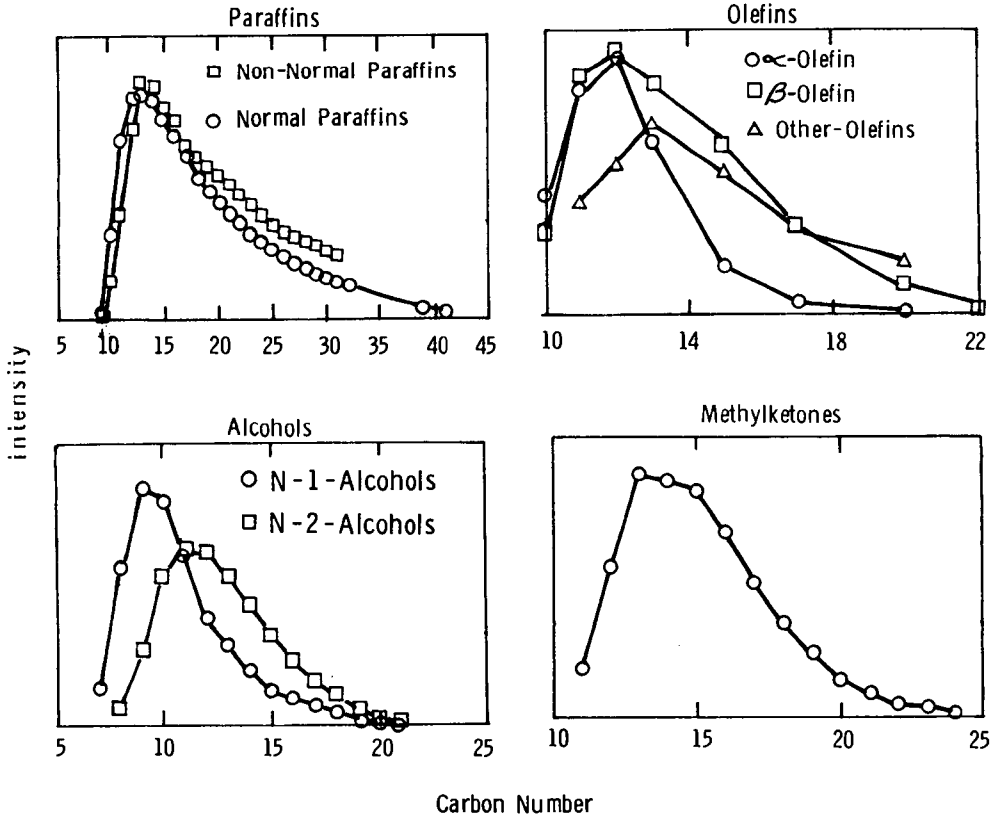

FIGURE 8: CARBON NUMBER DISTRIBUTION PLOTS: SAMPLE B

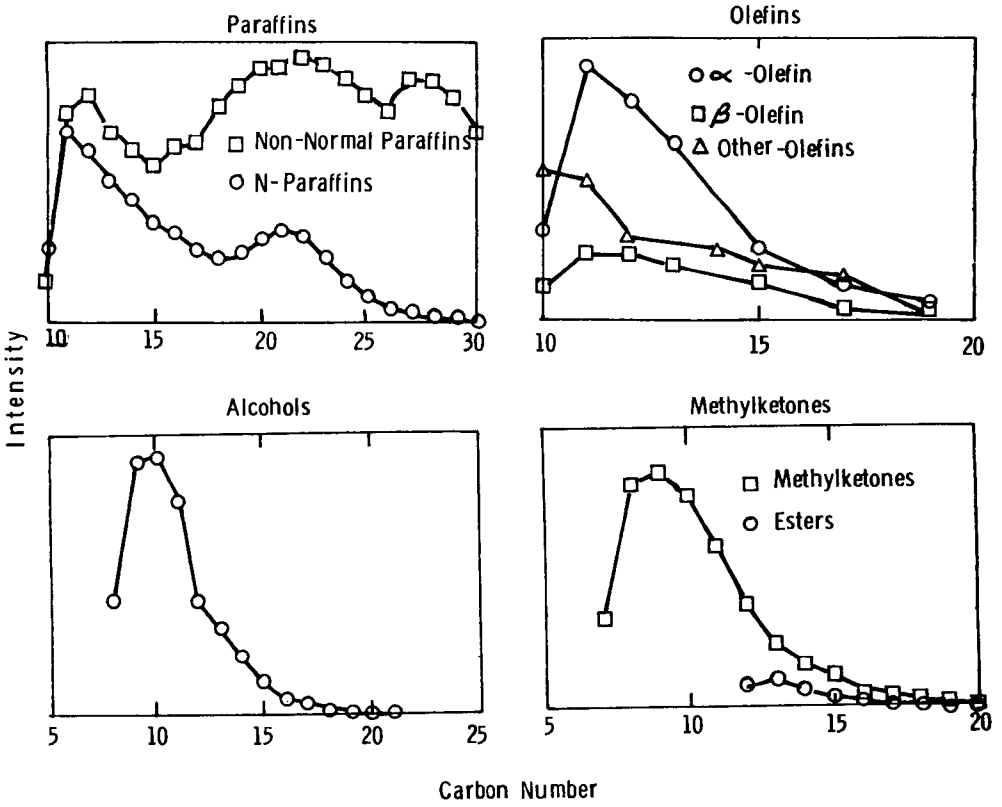

FIGURE 9: CARBON NUMBER DISTRIBUTION PLOTS: SAMPLE A

CALIBRATION CURVE FOR GPC ANALYSIS OF ASPHALTS

B. Brulé

Laboratoire Central des Ponts et Chaussées, Service de Chimie,
58 Boulevard Lefèbvre, 75732 Paris Cedex 15, France

INTRODUCTION

A better understanding of the structure of asphalts is important not only for scientific purposes, but also from the technological and economic viewpoints because this binder is used in very large quantities in road construction. Research workers therefore seek to acquire in-depth knowledge of this binder, making it possible to relate compositional parameters to practical properties. Among the physical and chemical analysis techniques capable of contributing to the characterization of such a medium, gel permeation chromatography (GPC) is a good choice because of its efficiency and its ease of application. Further, the development of finely graded subgrades has added to the preceding advantages that of a response time of the same order of magnitude as that obtained with gas chromatography.

The application of GPC to the characterization of heavy petroleum residues has already been dealt with in a certain number of publications. Among these mention may be made of the work of Altgelt (1,2) on the scatter range of the molecular weights of asphaltenes and maltenes, that of Richman (3) and of Bynum and Traxler (4) on the qualitative characterization of road asphalts. The problems raised by molecular weight calibration were investigated by Albaugh et al. (5) as well as by Dickson et al. (6,7). Snyder (8) studied the problems involved in the application of analytical GPC to asphalt characterization and demonstrated that, unlike polymers, the response of refractometric and ultraviolet detectors was not independent of elution volume. Reerink and Lijzenga (9) have proposed a molecular weight calibration method based upon the comparison of results obtained by ultracentrifugation. Significant experimental work involving fractionation of asphalt by preparative GPC and the characterization of fractions by analytical GPC, viscosimetry, vapor pressure osmometry, infrared and nuclear magnetic resonance spectrometry have been published by Kiet et al. (10).

All of this work has demonstrated that the quantitative interpretation of GPC asphalt chromatograms raises two types of problem. The first, that of correcting the response of the detectors, has been dealt with in earlier publications (11,12). The second, relative to the establishment of a calibration curve in molecular weight, is dealt with in the present paper.

FRACTIONATION OF ASPHALTS BY PREPARATIVE GPC

To plot a calibration curve in GPC the best approach consists in injecting a sufficient number of standards having a chemical structure and make-up identical to those of the product to be characterized. If these standards do not exist, they must be prepared and characterized. We have thus used preparative GPC to isolate a sufficient number of narrow fractions of asphalts of various origins. The classical conditions of a preparative fractionation are given below:

- Apparatus: Waters Chromatoprep 101
- Columns: 2 columns (10^3 and 10^4 Å), diameter 5 cm, length 120 cm
- Solvent: redistilled chloroform
- Flow rate: 20 ml/min
- Injected volume: 100 ml

- Injected solution concentration : 10 %
- Volume of fractions : 125 ml.

The efficiency of the fractionation is evaluated by the injection, in analytical GPC on two micro-Styragel columns of 10^3 and 10^4 Å, of 0.3 mg of the most representative fractions. Figure 1 shows the chromatograms of the fractions 6 to 18.

It is noted that, apart from the heaviest fractions (fractions 6, 7 and 8) for which the behavior is special and which represent less than 1 % of the initial product, the preparative separation is indeed carried out according to the molecular weight. A calculation of the average characteristics carried out on the largest fraction (fraction 16) leads to the following numerical values : Mn (in equivalent polystyrene) = 555, Mw (in equivalent polystyrene) = 690. The polydispersity is thus 1.24, which can be regarded as satisfactory.

CALIBRATION CURVE BY VAPOR PRESSURE AND MEMBRANE OSMOMETRY

The determination of the number average molecular weights - either by vapor pressure osmometry (VPO) or by membrane osmometry - of the asphalt fractions obtained by preparative GPC makes it possible to establish a first experimental relationship between elution volume (in analytical GPC) and molecular weight. Most of the measurements were performed by means of a Mechrolab 301A vapor pressure osmometer. Some determinations were carried out, for the fractions of high molecular weight, with a membrane osmometer of the same make. The measurements were conducted in benzene at 37°C on solutions with concentrations varying between 20 and 5 $g.l^{-1}$. It was thus possible to determine the number molecular weights of preparative GPC fractions of four asphalts, namely two 80/100 samples (ELF Feysin and ELF Grandpuits) and two 40/50 samples (Shell and CFR). The representative points of the molecular weight as a function of distribution coefficient are given in Figure 2. The values of the molecular weights corresponding to the points located in the upper part of the curve (Mn higher than 10,000) were obtained by membrane osmometry. This figure also shows (continuous bold line) the calibration curve in molecular weight plotted for polystyrenes.

It is noted that the experimental points, although obtained from four asphalt samples having different crudes and manufacturing processes, describe a single curve. This calibration curve, specific to asphalts, is not very different from the polystyrene curve for distribution coefficients between 0.5 and 0.7. Beyond these values, the asphalt curve moves either toward the largest elution volumes, for the same molecular weight, or toward the higher molecular weights, for a given elution volume. It can be noted that the lower part of the curve (weights lower than 1000) which corresponds to substances of high aromaticity, moves substantially away from the polystyrene curve, probably owing to the superposition of an adsorption process which increases as the aromaticity of the products increases and as their molecular weight decreases. For molecular weight values higher than 10,000, we shall see in the discussion of the viscosimetric measurements that part of the shifting can be explained by the fact that the molecular weight is determined on non-ideal solutions.

INTRINSIC VISCOSITY OF ASPHALT FRACTIONS

The viscosimetric measurements were carried out in THF at 30°C by means of an FICA automatic dilution viscosimeter. The sample analyzed is a CFR 40/50 asphalt which we fractionated under classical conditions. Figure 3 shows the experimental points corresponding to the variation of the expression (t-to)/to.C as a function of the concentration C of the solution (t being the solution flow time and t_o the solvent flow time).

This figure shows that, unlike what is observed in the case of ideal solutions, the relationships are not linear for the high molecular weight fractions except beyond a concentration of the order of 2 to 3 $g.l^{-1}$. Below this value, the curves bend downward in proportion to the molecular weight. This illustrates the dissociability of the species as a result of dilution and the existence of a critical concentration beyond which the solutions have a "normal" behavior. The intrinsic viscosity values determined by extrapolation, to zero concentration, of the linear part of the curve are thus apparent values which take into account a partially associated state. As the molecular weights measured by vapor pressure osmometry or membrane osmometry were determined on solutions whose concentration was higher than the critical concentration indicated by viscosimetry, we conclude that, here too, what is involved is the apparent molecular weights taking into account the associability of the species.

CONSTRUCTION OF $|\eta|$ M CURVE OF ASPHALTS

The numerical values of intrinsic viscosities and molecular weights make it possible to plot the curve $|\eta|$ M = f (Kd) for 40/50 CFR asphalt fractions. This curve is shown in Figure 4 together with the universal calibration curve (continuous bold line). The dotted line is the calibration curve in $|\eta|$ M proposed by Reerink and Lijzenga (9) for asphaltenes.

The discrepancy between the curve in $|\eta|$ M established for asphalt fractions and the universal calibration curve is qualitatively of the same order as that which was observed in the calibration of molecular weight. It may be considered that the observed deviation in the lower part of the curve is due to the elution lag caused by adsorption of aromatic substances of low molecular weight. For fractions with high molecular weight we have shown that the numerical values of intrinsic viscosity and molecular weight were apparent values higher than the real values because the measurements were not carried out on ideal solutions but on solutions whose concentration was higher than the critical value. The product $|\eta|$ M thus measured is hence greater than that which is obtained in GPC.

CALIBRATION CURVE USING UNIVERSAL CALIBRATION

As the micellar behavior of solutions of asphalt fractions of high molecular weight leads to apparent values during the determination of molecular weight by membrane osmometry, it is difficult to plot a calibration curve in molecular weight of asphalts by traditional means. Under these conditions, we have assumed - as a working hypothesis - that the universal calibration of Benoit et al. (13) is applicable to asphalt fractions. The use of universal calibration in the case of GPC on micro-packings calls for continuous measurement of the viscosity of the eluate. It was Ouano (14) who first substituted for the measurement of a flow time that of the pressure drop at the terminals of a capillary tube. The principle was taken up by Lesec (15) who demonstrated that the measurement of the pressure at the inlet of a capillary tube placed between the outlet of the columns and the inlet of the refractometer could be interpreted in terms of viscosity. We therefore set up the viscosimetric detector described by Lesec and formed a capillary tube of 0.23 mm diameter and 3 m length. A branch at the inlet of this capillary allows pressure measurement. A data acquisition system permits the processing of data from the detectors by computer.

After calibrating the analytical GPC system in terms of hydrodynamic volume by means of polystyrene standards, we fractionated the asphalts (four samples of 180/200, two of 80/100, two of 60/70 and two of 40/50) under usual conditions for preparative GPC. Each fraction was analyzed by analytical GPC with viscosimetric detection in order to determine its intrinsic viscosity under the real conditions of the GPC. Its molecular weight was then determined by reference to the universal calibration curve.

We also used VPO to determine the number average molecular weights for the fractions of small molecular weight which have an ideal behavior in solution. All the measurement points are shown in Figure 5 in which we have reproduced the calibration curve for polystyrenes (bold line) and the calibration curve in molecular weight of asphalts previously established by membrane osmometry (thin line).

It is noted that these measurements make it possible to define a new calibration curve in molecular weight for road asphalts, a calibration curve which is independent of the origin of the crude and of the manufacturing process. This curve is much more realistic than that established by membrane osmometry because it is plotted by measuring the intrinsic viscosity by GPC with viscosimetric detection, but its validity is limited by the hypothesis initially made regarding the applicability of the universal calibration to asphalt fractions. It is also seen that this curve moves further away from the curve for polystyrenes and molecular weight increases, thus verifying the classical hypothesis that the compactness of heavy asphalt fractions increases with molecular weight.

In order to utilize this new calibration curve easily, we compared the calibration curve for asphalts with the calibration curve for polystyrenes. The relationship obtained is shown in Figure 6.

The adjustment of this relationship on a second-degree equation leads to the following expression:

$$\log Y = 3.21 - 1.04\ X + 0.331\ X^2$$

in which Y = asphalt weight and X = polystyrene weight.

Furthermore, we deemed it of interest to compare the values of intrinsic viscosity and of molecular weight obtained by GPC with the results published by Altgelt (16), on the one hand, and Kiet et al. (10) on the other hand. The different relationships $\log |\eta| = f \log (M)$ are given in Figure 7.

Fairly good agreement is found for the low molecular weights, and then significant bending of the viscosity curve obtained by GPC with viscosimetric detection.

CONCLUSION

The work reported in this paper shows that it is possible to approach experimentally the problem of the plotting of a calibration curve in molecular weight for GPC on a micro-packing applied to the characterization of asphalts. It is shown that if one determines, for different asphalts, a specific calibration curve relating the number average molecular weight, measured by membrane osmometry, of narrow fractions to their elution volume, one obtains a single curve independent of the origin of the crude and of the manufacturing process. This curve is very close to the polystyrene curve for values between about 1000 and 3000. It moves away toward the higher elution volumes, for small molecular weights, owing to the increase in the aromaticity of the asphalt constituents as molecular weight decreases. It also moves away, and in the same direction, as the weight increases: in this case, molecular weight measurements lead to apparent values higher than the real values owing to the non-ideal behavior of the solutions. This difficulty may be overcome by accepting the hypothesis of the applicability of universal calibration to asphalt fractions and by using a viscosimetric detector to plot a new calibration curve with reference to the calibration curve in hydrodynamic volume. The interpretation of the results makes it possible to establish a calibration relationship of the form: $\log M \text{ (asphalt)} = 3.21 - 1.04\ X + 0.331\ X^2$, in which X = log M (polystyrene), and to elucidate, for asphalt fractions, the relationship between intrinsic viscosity and molecular weight.

REFERENCES

(1) - K.H. Altgelt, Die Makrom. Chem., 1965, 88, 75.
(2) - K.H. Altgelt, J. Appl. Polym. Sci., 1965, 9, 3389.
(3) - W.B. Richman, Proc. Ass. Asphalt Paving Technol., 1967, 36, 106.
(4) - D. Bynum, R.N. Traxler, Proc. Ass. Asphalt Paving Technol., 1970, 39, 683.
(5) - E.W. Albaugh, P.C. Talarico, B.E. Davis, R.A. Wirkkala, A.C.S. Symposium on GPC, Houston, 1970.
(6) - F.E. Dickson, R.A. Wirkkala, B.E. Davis, A.C.S. Symposium on GPC, Houston, 1970.
(7) - F.E. Dickson, B.E. Davis, R.A. Wirkkala, Anal. Chem., 1969, 41, 10, 1335.
(8) - L.R. Snyder, Anal. Chem., 1969, 41, 10, 1223.
(9) - H. Reerink, J. Lijzenga, Anal. Chem., 1975, 47, 13, 2160.
(10) - H.H. Kiet, L.P. Blanchard, S.L. Malhotra, Sep. Sci., 1977, 12 (6), 627.
(11) - B. Brulé, Rapport de Recherche LPC n° 76, LCPC Paris, 1978.
(12) - B. Brulé, J. Liq. Chromatog., 1979, 2 (2), 165.
(13) - H. Benoit, Z. Grubisic et coll., J. Chim. Phys., 1966, 63, 1507.
(14) - A.C. Ouano, J. Polym. Sci., 1972, A1, 10, 2169.
(15) - J. Lesec, C. Quivoron, Analusis, 1976, V 4, 10, 456.
(16) - K.H. Altgelt, Bitumen Teere Asphalt Peche, 1970, 11, 475.

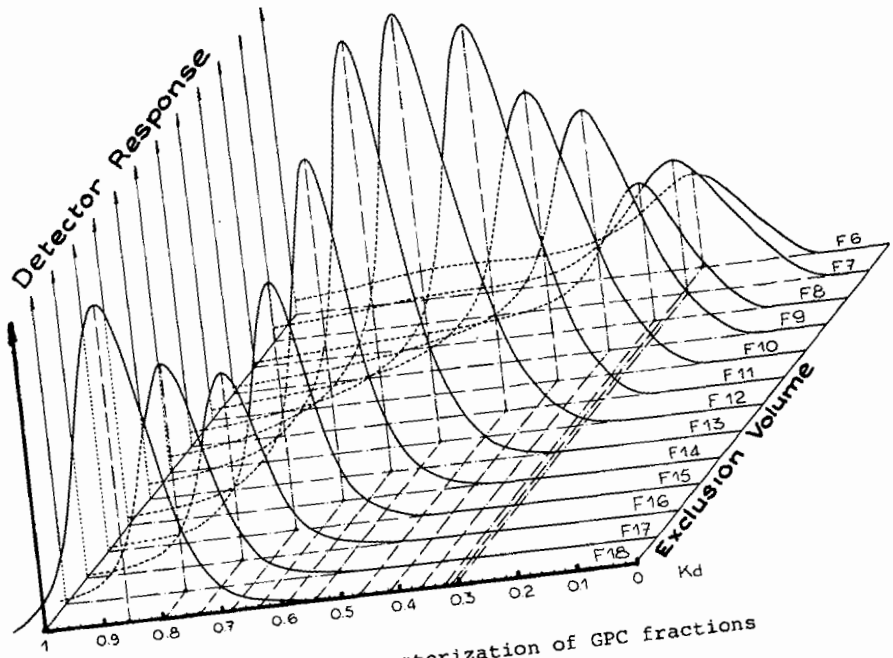

Figure 1. Characterization of GPC fractions

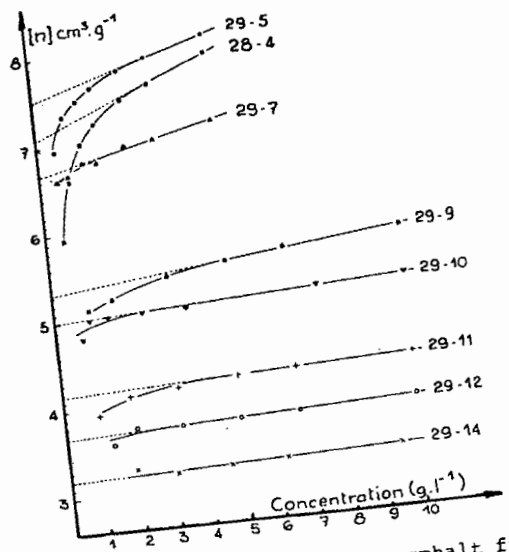

Figure 3. Viscosimetric curves for asphalt fractions

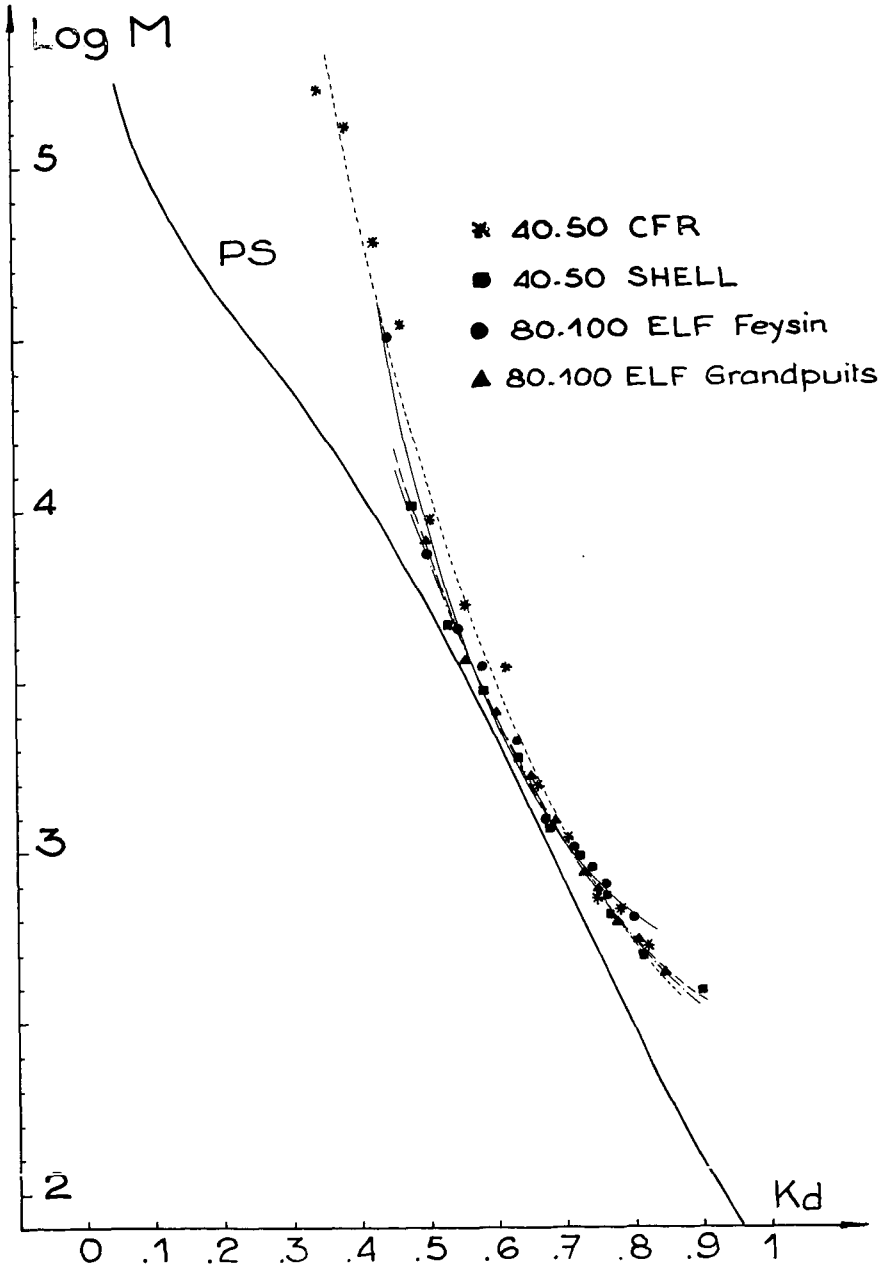

Figure 2. Calibration curve for asphalts by VPO and membrane osmometry

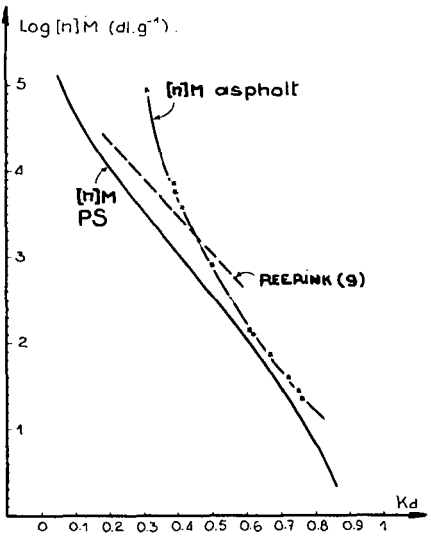

Figure 4. $[\eta]M$ calibration curve for asphalt fractions

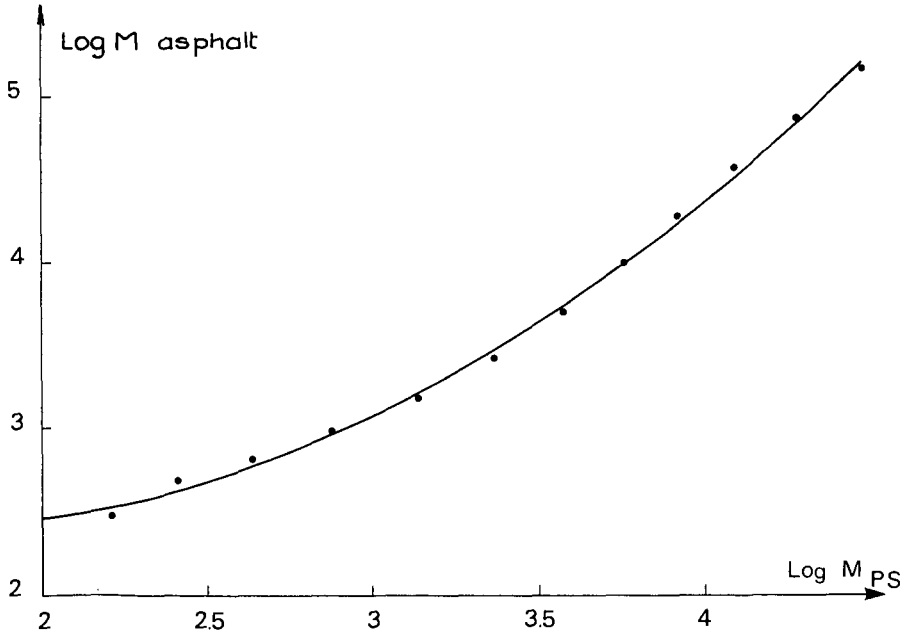

Figure 6. Relation between calibration curve for asphalt and calibration curve for PS

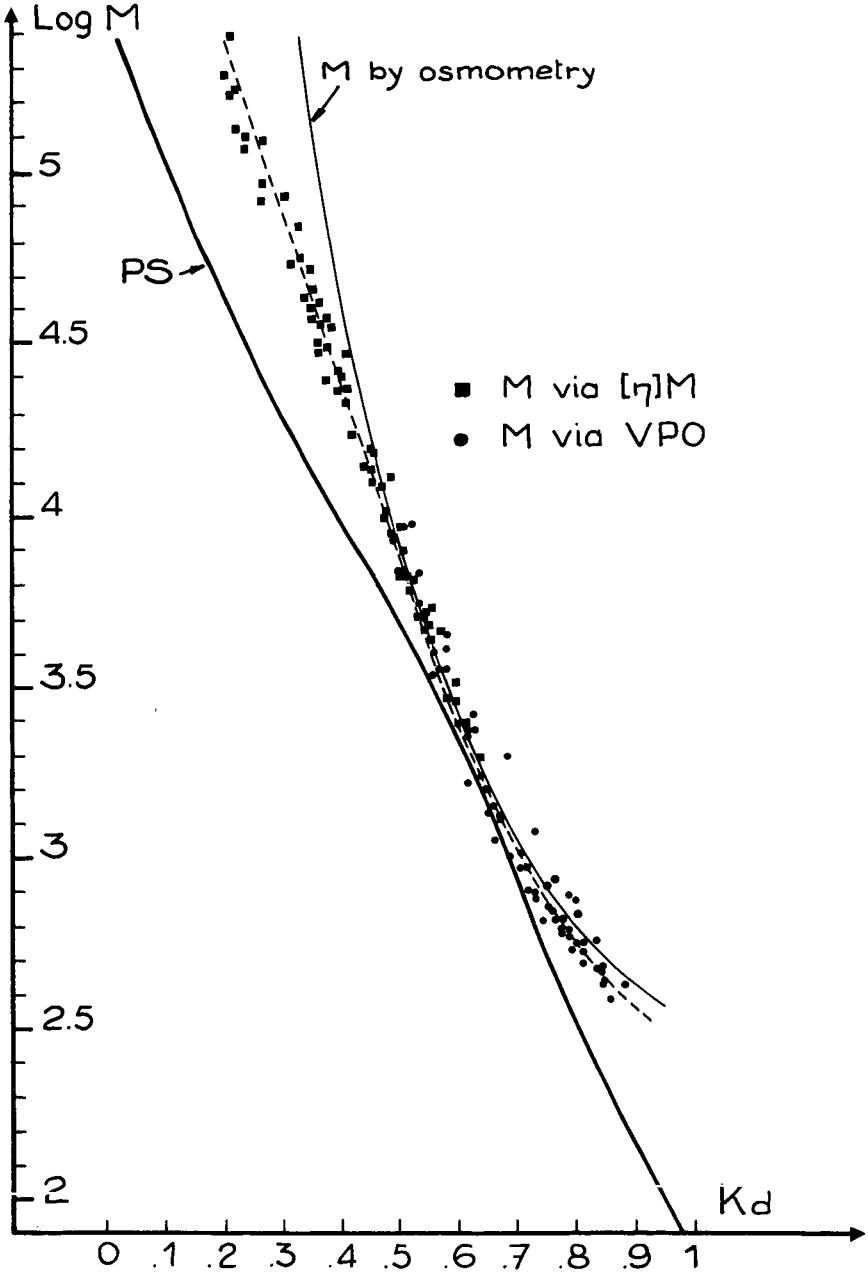

Figure 5. Calibration curve for asphalts from |η|M

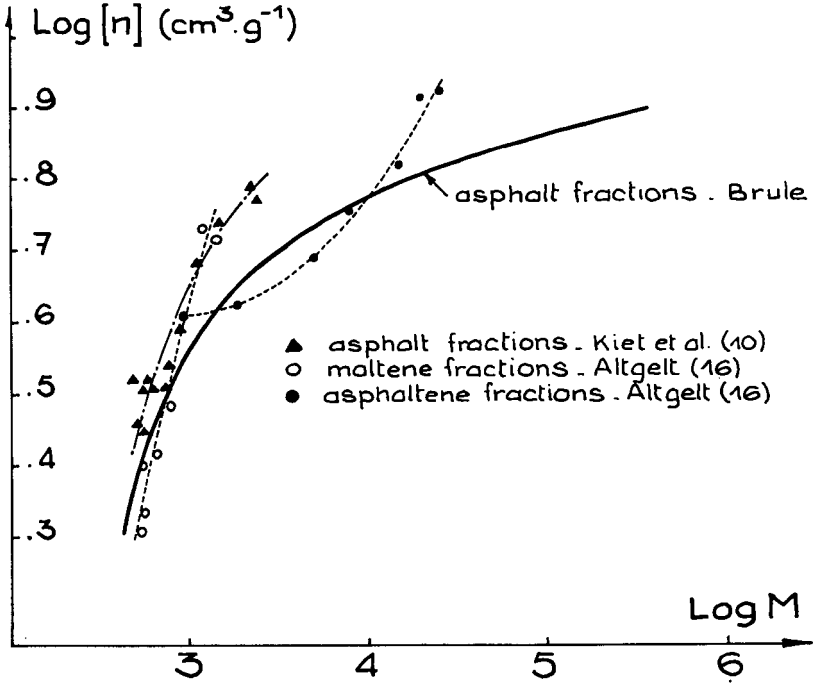

Figure 7. Relation between viscosity and molecular weight for asphalt fractions

SEPARATION AND CHARACTERIZATION OF LIGNITE DERIVED PREASPHALTENES BY GEL PERMEATION CHROMATOGRAPHY AND NUCLEAR MAGNETIC RESONANCE SPECTROMETRY

Richard J. Baltisberger, Kundanbhai M. Patel, David G. Wettlaufer
John W. Rovang, Neil F. Woolsey and Virgil I Stenberg

Chemistry Department
University of North Dakota
Grand Forks, ND 58202

INTRODUCTION

Methods for the separation and chemical characterization of the preasphaltene components in lignite liquefaction products has been understudied by our group for several years. Preasphaltenes for purposes of this study are defined as that portion of a lignite derived product which is soluble in tetrahydrofuran but insoluble in toluene. The preasphaltenes studied would fall into the seventh and eighth fractions of the sequential elution by solvent chromatography (SESC) procedure developed by Farcasiu (1). Further elution chromatography of the tetrahydrofuran preasphaltene fraction on silica or alumnia did not appear to be justified in view of the highly polar nature of the fractions. The preasphaltene fraction was chromatographed for size separation using Bio-Beads S-X3 columns and pyridine as the eluent (2). The distribution and functionality of nitrogen and oxygen were then monitored in the molecular size fractions formed at different operating conditions. The study shows the structure and distribution of oxygen is the most important parameter. Work of our group has centered on the development of procedures of the quantitation of oxygen functionality in this material. For this report we are only able to identify the amount of phenolic hydroxyl groups present. Work is continuing on the development of a number of quantitative ether cleavage reactions (3).

EXPERIMENTAL

Materials.

Solvent refined lignite (SRL) was produced at 404°, 460° and 480°C, 26.2 MPa (3850 psi) from Beulah 3 North Dakota Lignite. The reducing gas used was a 1:1 mol mixture of carbon monoxide and hydrogen. The SRL was produced in a 5-lb coal/hr continuous process unit at the Grand Forks Energy Technology Center (GFETC) using anthracene oil and 7% wt tetralin as the donor solvent in single pass tests in a continuous-stirred tank reactor (4). The preasphaltene fraction was recovered from the toluene insoluble portion of an SRL using tetrahydrofuran as the solvent in a Soxhlet extractor. Tetrahydrofuran was chosen to define the solubility of preasphaltenes in place of pyridine so that the results could be correlated with data obtained during the liquefaction runs at GFETC (4). Standard compounds used to calibrate the GPC and to acetylate the SRL were obtained from commercial sources.

Preparative Scale GPC.

Preparative scale GPC separations were carried out with a 22 mm i.d. X 1 m glass column packed with Bio-Rad, SX-3, Bio-Beads (200-400 mesh, 3% cross linked, styrene-divinyl benzene). The preasphaltene was acetylated by reaction with acetic anhydride in pyridine for 24 hr at 25°C. We found the total preasphaltene sample to be soluble in chloroform. Upon attempting to use this solvent with 1g of sample we found that some precipitation occured on the GPC column during separation. The elution solvent was changed to pyridine. About one gram of sample dissolved in 5 ml of solvent was charged to the column. A flow rate of 1.5 ml/min was maintained by a constant head devise. Fractions were collected every 5 ml which were then stripped of solvent in a rotary evaporator, added to 3-5 ml of benzene and free dried to remove the last traces of pyridine. The last traces of benzene were removed by drying in an abderhalden apparatus at 80°C under vacuum.

Analyses.

Elemental analyses were performed by Spang Microanalytical Laboratory, Eagle Harbor, MI. Molecular weights were determined at our laboratory with a Wescan Vapor Pressure Osmometer. Molecular weights were measured over a range of 0.1 to 4 g/kg using the solvent pyridine. Several fractions were run at three different concentrations for extrapolation to infinite dilution. No evidence for intermolecular association in pyridine was noted so single point analyses were measured because of the large number of fractions to be analyzed.

Proton NMR spectra were obtained on a Varian EM-390 Spectrometer. Samples were dissolved in d_5-pyridine containing a known amount of s-trioxane as an internal standard. Correction for residual pyridine protons was based on the standard versus residual pyridine integration. Generally, seven integrations were run and averaged. The data was analyzed using modified Brown-Ladner equations (5).

All samples of preasphaltenes were acetylated with 1-^{14}C acetic anhydride in pyridine under argon. The samples of acetylated SRL were weighed in combustocones (Packard Instrument CO, Downers Grove, ILL.) and then oxidized in a Packard Model 306 automatic sample oxidizer for subsequent liquid scintillation measurement. The counting was carried out in a Packard model 3375 liquid scintillation spectrometer. When SRL was allowed to react at room temperature for 24 hr only the hydroxyl and amine sites are derivatized. If the acetylation is carried out a reflux temperature (115°C) some aromatic carbon acetylation results (6).

RESULTS AND DISCUSSION

Molecular Weight Distribution

Seven to eight fractions each of five ml were collected for each GPC run. The fraction of total weight recovered from the original weight of material is reported in Table 1. Two solvent refined coal preasphaltene samples are added to the table from comparison with the lignite derived

material. The average molecular weight distribution goes to higher molecular weights with increased reaction temperature for the lignite preasphaltenes. The coal derived preasphaltenes have much higher molecular weights. The lignite preasphaltenes were 38, 25 and 21% wt, maf of the 400°, 460°, and 480°C lignite derived products. The molecular weight increase for the 480°C material is an indication the extent of recombination that occurs at the high temperature. The fact that the 400°C material has similar $\bar{M}n$ values as the 460°C may occur because higher molecular weight portions may lie in the tetrahydrofuran insoluble portion which is 35% wt of the original lignite at 400°C as compared to 15% wt at 460°C.

Nitrogen and Sulfur Distribution

Table 1 shows that the distribution of nitrogen and sulfur is spread evenly throughout the fractions. The distribution of nitrogen and sulfur is only slightly reduced with increased temperature for the lignite preasphaltene samples. Both of the above facts would be consistent with the nitrogen and sulfur being present in ring systems such as carbazoles, pyridines, and thiophenes. Nonaqueous titration data shows that approximately 50% of the nitrogen is present as basic nitrogen (7).

Oxygen Distribution

The hydroxyl contents were determined by carbon-14 counting of the labeled acetate added by the acetylation process. Earlier work has shown that there are few alcoholic hydroxyl or amine sites present in these type of samples (6). Carbazole acidic hydrogen does not react under the acetylation conditions used (6). Greater than 95% of the added acetate is due to phenolic hydroxyl sites and for purposes of this study was assumed 100%. The total oxygen content of each fraction was determined by difference with the carbon, hydrogen, nitrogen and sulfur analyses. In the past we have checked the validity of this assumption by comparison of neutron activation analysis data with this procedure and found the agreement was within ± 5% relative error (7).

Table 2 and 3 show the distribution of total oxygen, phenolic oxygen and other oxygen reported in millimoles per gram or per mole of sample. Insight is gained about the structure by comparison of the concentration of oxygen in several ways. The total oxygen content expressed in millimoles per gram is nearly constant with molecular weight for a given liquefaction temperature. There is a small increase in total oxygen millimoles per gram with decreasing molecular weight but this explained by the an increase in phenolic oxygen per gram as the molecular weight decreases. The millimoles of phenol per mole of lignite preasphaltene is near 1 phenolic site per average molecule. The constant concentration of other oxygen per gram at constant temperature could be due to a repeating structure of aromatic centers connected by ether or furan linkages as shown in the hypothetical models in figures 1-2. For the lignite preasphaltenes one finds there are 8-9, 20-23 and 16-23 aromatic carbon molecules per other oxygen mole, for 404, 460, and 480°C respectively, as shown in table 2. This is reflected in the structures drawn on figure 1 where benzene rings predominent for the 404°C material. As the reaction temperature is raised the aromatic centers begin to show more and more condensation as in figure 2.

Carbon Structure

Table 4 shows the values of f_a, the fraction of aromatic carbons, and D, the degree of condensation, calculated from modified Brown-Ladner equations:

$$f_a = \frac{C/H - (H\alpha^*/2 + Ho^*/2 + OH/2H)}{(C/H - 2OH/H)} \quad (1)$$

The term was OH/H is included in equation 1 to remove the carbonyl carbon present because of the acetylation.

$$D = \frac{H^*_{ar} + H^*_{\alpha}/2 + n[OH/H] + OH/H}{fa(C/H - 2OH/H)} \quad (2)$$

Equation 2 assumes that all the other oxygen is present in the polymeric molecules as connecting furan linkages (n=4) or ether linkages (n=2). This has not been proven in this study. The development of a furan or ether analysis technique is a major objective in our studies and we add the ether linkages only to show the importance of oxygen to the preasphaltene structure. Figures 1-2 show the furan and ether linkages with the corresponding values of f_a and D as counted from the hypothetical average molecule and from equations 1 and 2 using the NMR data. The calculated values are in good agreement with the model. The true value of D depends upon the correct assignment of n through a quantitative ether analysis.

Comparison to Asphaltene

Table 5 shows the oxygen distribution for a series of asphaltene samples. The main difference between the preasphaltenes and the asphaltenes is other oxygen concentration. The phenol concentrations, molecular weights, and f_a are approximately equal.

Conclusions

Gel permeation chromatography offers the opportunity to observe subtle changes in preasphaltene structure that would be rather difficult to observe by another procedure. The postulated aromatic core plus ether links polymer structure requires precise information about the concentration of phenolic sites as they change with molecular weight. The type of preasphaltene structure suggested by this study would explain why preasphaltenes are insoluble in benzene even through their acidities, bascities and fraction of aromatic carbons may be equal to those of asphaltenes. Their insolubilities results from ether and furan linkages locking the aromatic systems into very rigid condensed molecules.

ACKNOWLEDGMENT

This research was supported by the DOE through contract number EX-76-01-01-2211.

LITERATURE CITED

1. Farcasiu, M., Fuel, 56, 9 (1977).

2. Coleman, W.M., Wooton, D.L., Dorn, H.C., Taylor, L.T., J. of Chrom., 123, 419 (1976).

3. Baltisberger, R.J., Woolsey, N.F., Stenberg, V.I. and Klabunde, K.J., Quarterly Rpt, Conversion of Solvent Refined Lignite into Premium Fuels, FE-2211, April-June, 1980.

4. Wilson, W.G., Knudson, C.L., Baker, G.C., Owens, T.C. and Severson, D.E., Application of Liquefaction Process to Low-Rank Coals, 1979 Symposium on Technology and Use of Lignite, Grand Forks, ND, May, 1979.

5. Brown, J.K. and Ladner, W.R., Fuel, 39, 87 (1960).

6. Baltisberger, R.J., Klabunde, K.J., Woolsey, N.F. and Stenberg, V.I., Final Rpt, Chemistry of Lignite Liquefaction, FE-2211, August, 1980; Submitted to Fuel for publication.

7. Baltisberger, R.J., Klabunde, K.J., Stenberg, V.I., Woolsey, N.F., Saito, K. and Sukalski, W., ACS Symposium Series No. 71, Organic Chemistry of Coal, J.W. Larsen Ed. pp 294-300, 1978.

Table 1. Distribution of Nitrogen and Sulfur

Preasphaltene Samples

Sample	$\%_{wt}$,N	$\%_{wt}$,S	$M\bar{n}$	Wt, %[a]
Y-15-2	1.48	0.52	582	0.15
(400°C)	1.30	0.57	573	0.26
	0.89	0.48	373	0.17
	0.85	0.47	218	0.07
	0.86	0.45	219	0.07
	0.89	0.52	224	0.07
26-Y-7	1.90	0.51	568	0.09
(460°C)	1.63	0.75	626	0.23
	1.37	0.54	429	0.20
	1.24	0.67	302	0.14
	1.14	0.49	240	0.08
	1.05	0.59	240	0.07
26-Y-11	1.43	0.46	1165	0.22
(480°C)	1.26	0.47	831	0.31
	1.27	0.46	607	0.22
	1.22	0.64	463	0.09
Beulah 3 Lignite	.80	3.03	---	---
Tacoma[b]	2.63	---	2400	0.08
	2.32	---	1600	0.24
	2.07	---	1450	0.22
	1.95	---	800	0.17
	2.15	---	800	0.12
	1.96	---	655	0.08
Indiana[c]	2.22	---	2300	0.10
	1.97	---	1600	0.22
	2.11	---	1300	0.21
	1.85	---	830	0.17
	1.76	---	810	0.12
	1.88	---	560	0.07

[a] wt% of recovered starting material

[b] prepared at 450°C, 10MPa H_2, recycle solvent

[c] prepared at 441°C, 12MPa H_2, recycle solvent

Table 2. DISTRIBUTION OF ETHERAL AND ACID OXYGEN IN GFETC PREASPHALTENE SAMPLES

Sample	Mole wt gm/mole	Total O_2 mmol/gm	OH		Etheral O_2	
			mmol/gm	mol/mol	mmol/gm	mol/mol
15-Y-2	582	8.9	1.8	1.0	5.3	3.1
(400°C, 26MPa)	573	9.1	1.9	1.1	5.3	3.0
	373	9.7	2.4	0.9	4.9	1.8
	218	10.6	2.7	0.6	5.2	1.1
	219	10.8	2.9	0.6	5.0	1.1
	224	10.6	2.9	0.6	4.8	1.1
26-Y-7	568	6.5	1.4	0.8	3.7	2.1
(460°C, 26MPa)	626	5.8	1.5	0.8	2.8	1.8
	429	7.0	1.7	0.7	3.6	1.5
	302	7.6	2.3	0.7	3.0	0.9
	240	8.2	3.0	0.7	2.2	0.5
	240	8.8	3.3	0.8	2.2	0.5
26-Y-11	1165	5.6	1.0	1.2	3.6	4.2
(480°C, 26MPa)	831	5.7	1.4	1.2	2.9	2.4
	607	5.9	1.5	0.9	2.9	1.8
	463	6.5	1.9	0.9	2.7	1.3

Lignite, Beulah 3 - 19.57% O_2 (MAF); 10.6 meq/gm $\approx$ 15% O_2

Table 3. Distribution of Ethenal and Acid Oxygen in SRC Samples

Sample	$\bar{M}n$	Total O_2 mmol/gm	Phenolic OH mmol/gm	Phenolic OH mol/mol	Etheral O_2 mmol/gm	Etheral O_2 mol/mol
Tacoma	2400	5.4	1.3	3.1	2.8	6.7
	1600	5.6	1.4	2.2	2.8	4.5
	1450	5.8	1.5	2.2	2.8	4.1
	800	5.9	1.5	1.2	2.9	2.3
	800	5.3	1.6	1.3	2.1	1.7
	655	4.6	1.65	1.1	1.3	0.9
Indiana	2300	6.5	1.5	3.5	3.5	8.05
	1600	7.2	1.65	2.6	3.9	6.2
	1300	6.0	1.8	2.3	2.4	3.1
	830	6.5	1.9	1.6	2.7	2.2
	810	6.1	2.0	1.6	2.1	1.7
	560	6.4	2.0	1.1	2.4	1.3

Table 4. Structural Features of GFETC Preasphaltenes

Sample	$\bar{M}n$	f_a	D (n = 2)	D (n = 4)	C_1
15-Y-2	582	0.735	0.94	1.02	2.0
	573	0.76	0.91	0.99	2.1
	373	0.75	0.91	1.01	1.8
	218	0.73	1.02	1.14	1.6
	219	0.69	1.01	1.27	1.6
	224	0.68	1.07	1.32	1.6
26-Y-7	568	0.84	0.72	0.85	1.8
	626	0.83	0.65	0.75	1.8
	429	0.84	0.73	0.86	1.8
	302	0.795	0.80	0.92	1.4
	240	0.76	0.84	0.94	1.4
	240	0.74	0.94	1.05	1.4
26-Y-11	1165	0.86	0.68	0.80	1.6
	831	0.84	0.69	0.79	1.5
	607	0.84	0.71	0.81	1.4
	463	0.83	0.73	0.83	1.4

Table 5. Asphaltene

Sample	$\bar{Mn}$	O, mmol/gm	OH, mmol/gm	Ref	Etheral O_2 mmol/gm
Asphaltene 1	615	2.2	---	a	---
Asphaltene 2	860	2.6	---	a	---
Asphaltene 3	415	2.5	---	a	---
Synthoil	---	2.4	1.8	b	0.6
FMC-COED	---	4.4	3.6	b	0.8
SRC, Catalytic	---	2.9	2.25	b	0.65

[a] B.C. Bockrath, Anal Chem, 51, 1168 (1979).

[b] T.F. Yen, Anal Chem, 51, 569 (1979).

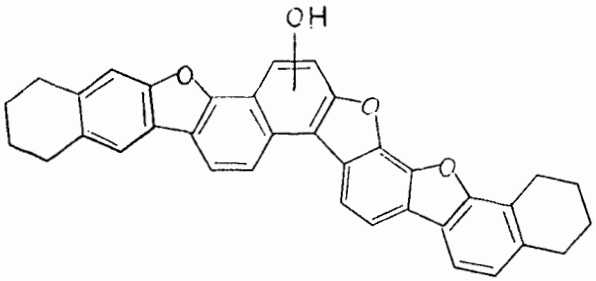

$C_{35.2}H_{25.8}(OH)_1O_{3.2}N_{0.6}S_{0.1}$

$f_a = 0.77$; 0.74(NMR)

D = 0.93 ; 1.02(NMR, n=4), 0.94(NMR, n=2)

$C_l = 2.0$; 2.0

Figure 1. Fraction one, 404°C

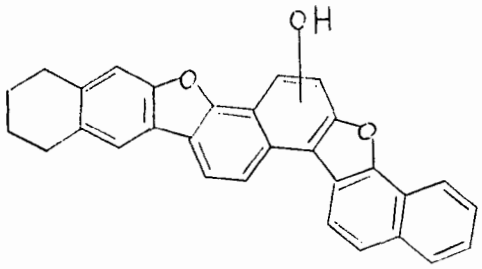

$C_{28}H_{17.8}(OH)_{0.7}O_{1.7}N_{0.4}S_{0.07}$

$f_a = 0.86$; 0.84(NMR)

D = 0.85 ; 0.86(NMR, n=4), 0.73(NMR, n=2)

$C_l = 2.0$; 1.8

Figure 2. Fraction three, 460°C

THE USE OF MACRORETICULAR RESIN FOR SEPARATION OF COAL CONVERSION PROCESS WASTEWATER

James I. S. Tang, F. K. Kawahara* and T. F. Yen

School of Engineering
University of Southern California
Los Angeles, CA 90007
and
Environmental Protection Agency
Environmental Support Laboratory
Cincinnati, Ohio 45268*

INTRODUCTION

A three-dimensional co-polymer resin possessing macroreticular or macroporous structure is considered to be the most effective means of preliminary separation of organics in aqueous sample. These porous polymeric resins will function as the sorbing agent for organics. The full line of macroreticular adsorbent resins includes a spectrum of surfaces from the least polar to the most polar for adsorbing compounds with different polarities.

Gasification and liquefaction of coal will generate at least hundreds of organic species which will contaminate the water associated with the conversion processes, and thereafter pose a possible threat to the environment. A majority of coal plant waste streams released to the environment are process wastewaters from coal conversion process steps (Oak Ridge National Laboratory, 1977). This includes wastewater originating as moisture in the coal, water of constitution or decomposition, water added for stoichiometric process requirements, and water introduced for by-product recovery gas scrubbing. This type of wastewater contains most of the soluble and suspended organics and is produced in both the coal gasification and liquefaction processes. This wastewater is formed under the following conditions:

1. When gases are scrubbed to remove soluble contaminants, quenched to control operating temperature, compressed, or dehydrated;
2. When steam is used in the unit process cools and condenses or is reformed during methanation or hydrotreating;
3. When the product oil is formed by hydrogenation or pyrolysis and is allowed to settle for product recovery; or
4. When slags and ash are water-quenched for slurry removal.

The chemical species in waste effluents are considered varied and numerous because they represent practically all the organic compounds found in coal. The structure of coal, can be visualized as consisting of islands of aromatic and heterocyclic clusters connected by weak linkages, such as hydrogen bonding, quaternization, or donor-acceptor complexation. The coal conversion processes involve a variety of reactions with pressure, heat, catalysts, and/or water. These reactions produce many classes of organic species, such as polynuclear aromatic hydrocarbons (PAH), phenolics, nitrogenous compounds, other oxygen-functional compounds, and organometallics. Most of these species fall under the classification of potentially hazardous materials.

We are developing methods to separate the organics in coal-derived wastewater into a few major classes. One of the approaches is the preseparation of hydrophobic and hydrophilic nature by macroreticular resin such as XAD-8 (1). The subsequent use of ion-exchange resin can again subclassify the hydrophobic or hydrophilic fractions into acidic, neutral or basic (Fig. 1).

EXPERIMENTAL

The following two wastewater samples, representative of coal gasification and liquefaction processes, were obtained:

1. Scrubber water from a coal hydrocarbonization process, derived from a gasification plant fluidized bed operation at 300 psi and 1035°F. Oak Ridge Division of Union Carbide Corporation.

2. Recycle process water No. 1511, from a coal liquefaction plant. PAMCO at DuPont, Washington.

The first classification step was the separation of the organic into hydrophobic (HO) and hydrophilic (HI) compounds on Amberlite XAD-8 macroreticular resin. Further classification was based upon acid-base characteristics (Fig. 2)

Hydrophobic acids and bases were desorbed by aqueous alkali (0.5 N NH_4OH) and acid (0.1 N HCl), respectively. Hydrophobic neutral were eluted with methanol. Hydrophilic acids and bases were adsorbed on cation and anion exchange resins. The bases were concentrated on H^+ -form AG MP-50 cation exchange resin and eluted in 0.5 N NH_4OH. Hydrophilic acids were concentrated on OH^--form AG MP-1 anion exchange resin and eluted with 0.5 N HCl. Hydrophilic neutrals passed through all columns and were collected.

The XAD-8 resin was supplied as an industrial grade product (20-40 mesh) which was purified by first rinsing with 0.1 N NaOH, 0.1 N HCl, and then by Soxhlet extracting for 24 hours successively in acetonitrile, ethyl ether, and methanol. The resin was then packed in a column and rinsed with distilled water for testing of organic compounds background.

The AG MP-50 and AG MP-1 resins were washed successively by 1 N HCl, 1 N NaOH, and then Soxhlet extracted for 24 hours in methanol, methylene

chloride, and n-pentane successively for column packing. Test samples of model compounds were made and tested for the extent of the separation.

One liter of water sample No. 1 was diluted to 3:1 volume with distilled water and passed through a 300 ml bed (3 bed volume) XAD-8 resin column. The flow rate of the sample was 10 ml/min. The column was then eluted with 500 ml 0.1 N HCl, 0.5 N NH_4OH, and CH_3OH to collect HO base, acid, and neutral compounds, respectively. The aqueous effluents were passed through a column of H^+ form cation exchange resin (BioRad AG MP-1) to separate HI components. HI bases were collected by eluting with 500 ml 0.5 NH_4OH. Acids were recovered by eluting with 2.0 HCl. HI neutrals remained in the aqueous effluent. The water sample No. 2 was also separated via the same procedures. However, it was diluted with distilled water by the ratio of 1:1. This is because the total organic carbon concentration of water sample No. 2 is about one half of No. 1. The purpose of dilution is to reduce solute-solute interactions at high solute concentrations.

RESULTS

There are six separated fractions for each sample from the column absorption separation process. The organic components in these fractions are classified as HI acid, base, neutral and HO acid, base, and neutral compounds.

Total organic carbon (TOC) concentration of these fractions was detected by using a Dohrmann Envirotech DC-50 Model TOC analyzer. Preliminary data of TOC distribution among these fractions are shown in Table 1.

The separate organic fractions from coal process wastewater were subjected to GC-MS analysis. All the fractions are in aqueous solution except the HO neutral fraction which was eluted with CH_3OH through the column. Benzene was used to recover the pure organic component in HO neutral fraction. Samples of HO neutral fraction then were diluted to 1 ml in benzene for GC-MS analysis. All the other fractions were extracted by dicholoromethane (CH_2Cl_2). After phase separation occured, a 2.0 µl aliquot of the CH_2Cl_2 was analyzed by GC-MS. Compounds identified on one of the fractions is illustrated in Table 2.

From the data obtained both qualitatively and quantitatively the following summary can be made (2).

a. hydrophobic acid fraction -- phenolic compounds, e.g. phenol, cresol, xylenol.
b. hydrophobic neutral fraction -- polynuclear aromatic hydrocarbons, e.g. naphthalene, anthracene, pyrne, benzo(a)anthracene, chrysene, fluoranthene, biphenyl.
c. hydrophobic base fraction -- aza-aromatics and nitrogen base compounds, e.g. diphenylhydrazine, indole, nitrobenzene, pyridine, quinoline, benzamine.
d. hydrophilic acid fraction -- phenolic compounds, aromatic acids, and volatile acids, e.g., phenol, cresol, xylenol, carboxylic acid,

benzoic acids, fatty acids.

e. hydrophilic neutral fraction -- cyclic polar compounds, e.g., ethylphthalate, benzylphthalate, cyclopentenone.

f. hydrophilic base fraction -- methoxybenzene (2).

DISCUSSION

The pre-separation of organics in coal wastewater via these resins is due to the following reasons:

1. It has a homogeneous surface, permitting the operation of only one adsorption mechanism at a time. Hence solutes can be quantitatively adsorbed or desorbed.
2. The large surface area produces high exchange capacity as well as good chemical and structural stability.
3. No high energy process (such as heat) is used which might alter the nature of the organic solutes or evaporate the volatile compounds which have relatively low boiling points.

The polymer resin used in this study is able to fractionate organic solute mixtures into more homogeneous fractions based on sorption mechanisms without serious alteration of the solutes or solute matrix. The general theory that hydrophobic (HO) or nonpolar molecules are attracted to hydrophobic surfaces, and hydrophilic (HI) or polar molecules to hydrophilic or polar surfaces, is adopted in this scheme. Thus adsorbents of intermediate polarity such as Amberlite XAD-7 and XAD-8 have an attraction for molecules of completely hydrophobic nature, or essentially hydrophobic compounds with some polar functionality. To adsorb hydrophilic compounds of polar of neutral functionalities, ion exchange resins were used.

The TOC data indicate the recovery efficiency is ca. 70-80%. The significant information is that the compounds found in the six fractions are largely different. This demonstrates that a sample method for characterizing the chemical nature of coal-derived wastewater effluents is available.

A drawback of the present method is that species do absorb strongly at the resin surface sites and cannot recover completely with most powerful eluents such as acids and bases. Another inconvenience is that the inorganics contained in the wastewater will alter the sorbing nature of the macroreticular resin.

REFERENCES

(1) Leeheer, J. A. and Huffman, E. W. D., Jr. Res. U.S. Geol. Survey 4, No. 6 737-751 (1976).

(2) Tang, J. I. S., Kawahara, F. K. and Yen, T. F., Second Chemical Congress of North American Continent., Div. Geochemistry, paper 19, 1980.

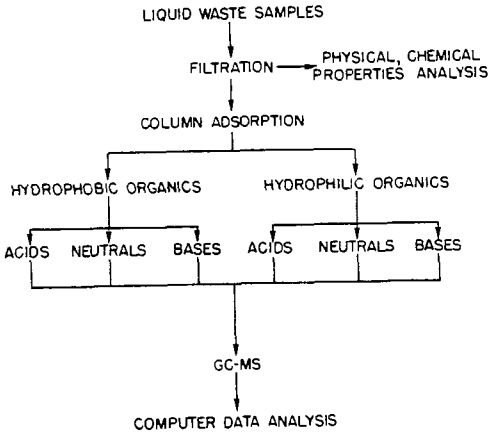

Figure 1. Schematic Diagram of Analytical Procedures for Coal Wastewater

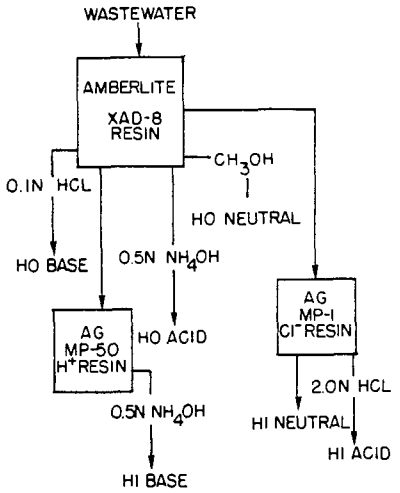

Figure 2. Flow Diagram of Column Adsorption to Separate Organics in Coal Wastewater

TABLE 1 PERCENTAGE OF TOTAL ORGANIC CARBON DISTRIBUTION IN SEPARATED FRACTIONS

Separated Fraction	% of origin in-put TOC* No.1	No.2
HI acid	2.7	3.4
HI base	2.4	6.8
HI neutral	10.7	15.2
HO acid	9.4	14.5
HO base	7.1	12.6
HO neutral	48**	40**

*The original in-put TOC for No.1 and No.2 are 2083 ppm, 1755 ppm, respectively.

**Values approximated from GC peaks of Solvent.

TABLE 2 COMPOUNDS IDENTIFIED FROM HYDROPHOBIC FRACTION IN NO. 1 WATER SAMPLE

GC SCAN NO.	BASE M/E	MOLECULAR WEIGHT	COMPOUND
77	91	92	Methylbenzene
131	43	88	Ethyl acetate
193	108	108	Methoxybenzene
244	94	94	Phenol
264	107	108	2-Methylphenol
286	107	108	3-Methylphenol
303	107	122	3,5-Dimethylphenol
315	107	122	2,5-Dimethylphenol
324	107	122	3,4-Dimethylphenol
331	121	136	4-(1-Methylethyl)-phenol
335	121	136	2-Ethyl-5-methylphenol
343	121	136	2-Ethyl-4-methylphenol
352	121	136	4-Ethyl-2-methylphenol
382	133	134	3,4-Dimethylbenzaldehyde
394	133	148	Pentamethylbenzene
451	144	144	3-Phenylfuran
506	170	170	(1-1-Biphenyl)-3-ol

Separation and Characterization of Polycyclic Aromatic Hydrocarbons and Alkylphenols in Coal Derived Solvents

R. J. Hurtubise, T. W. Allen, and A. Hussain

Chemistry Department

H. F. Silver

Chemical Engineering Department, University of Wyoming

Laramie, Wyoming 82071

Introduction

Polycyclic aromatic hydrocarbons (PAH) and alkylphenols in coal derived solvents are important in the conversion of coal to solvent refined coal (1). A knowledge of the composition of coal derived solvents used in coal liquefaction will allow the adjustment of processing conditions to improve the solvent effectiveness in liquefying coal and thus improve the overall yield of coal derived liquids. Selective and efficient methods are reported for the separation and characterization of PAH and alkylphenols in coal derived solvents.

Experimental

The coal derived solvents were obtained from Wilsonville, Alabama and Tacoma, Washington. The Wilsonville sample was a Wyodak coal derived recycle solvent from which a light distillate (533K-) and a heavy distillate (533K+) were obtained. The Tacoma sample was a Kentucky recycle solvent.

The liquid chromatograph used was a Waters model ALC/GPC 244 equipped with a model 6000-A pump, a U6K injector, a free standing ultraviolet detector set at 254 nm, and a 10-mV strip chart recorder. For normal-phase work, a μ-Bondapak NH_2 column and n-heptane:2-propanol mobile phases were used. For reversed-phase work a μ-Bondapak C_{18} column was used with methanol: water mobile phases.

All corrected fluorescence excitation spectra were obtained with a Farrand MK-2 spectrofluorometer, a Farrand excitation correction module, and a Farrand Autoprocessor I.

Results and Discussion

Polycyclic Aromatic Hydrocarbons

Dry-column chromatography with an aluminum oxide (activity II-III) stationary phase and a n-hexane-ether (19:1) mobile phase was used to separate PAH by ring size (3-, 4-, 5-, and 6-ring). Prior to the dry-column chromatography step, the coal derived solvents were added to an acid

treated silica gel column and eluted with chloroform. This step removed pyridine-type nitrogen heterocycles (2). Snyder (3) has shown that PAH can be separated according to ring size by using an aluminum oxide stationary phase and a relatively weak mobile phase. These concepts were applied in developing the dry-column chromatographic method for PAH in coal derived solvents. After separation of the individual ring fractions, the fractions were further separated by either thin layer chromatography (TLC) or high performance liquid chromatography (HPLC).

If TLC was used, then after separation fluorescence profiles of each PAH ring fraction distributed on 30%-acetylated cellulose chromatoplates were obtained with a spectrodensitometer. The fluorescence profiles were essentially a plot of fluorescence intensity for a given PAH ring fraction versus distance on the chromatoplate. The profiles were simple in that only one or two fluorescence peaks were obtained. Measurement of fluorescence peak heights gave an approximate measure of the amount of the 3-, 4-, 5-, and 6- ring PAH.

For HPLC separation, the 3- and 4- ring PAH fractions obtained from the dry-column chromatography step were separated with a μ-Bondapak C_{18} column. Figure 1 shows a typical HPLC chromatogram of a 3-ring PAH fraction from a Wyodak coal derived solvent using a μ-Bondapak C_{18} column and methanol:water (65:35) mobile phase. Identical separation steps were carried out with the Kentucky coal derived solvent and differences with the Wyodak coal derived solvent were compared. The HPLC separated PAH were characterized by chromatographic correlation factors and corrected fluorescence excitation spectra. The chromatographic correlation factors were described earlier (4). Corrected fluorescence excitation spectra were obtained because they are identical to absorption spectra and allow for ready comparison with literature spectra. In addition, the corrected fluorescence excitation spectra of substances can be obtained at very low concentrations. This is important when small amounts of material are obtained in the several fractions collected in a separation scheme. Figure 2 shows fluorescence excitation spectra for standard fluoranthene and fluoranthene isolated from a Wyodak coal derived solvent using the dry-column chromatography and HPLC steps. Several 3- and 4- ring PAH in coal derived solvents were separated and characterized by the approaches described above. Similar approaches will be used for the 5- and 6- ring PAH.

Alkylphenols

HPLC methods developed previously for ortho and nonortho alkylphenols in coal derived solvents were improved (5,6). A theoretical equation developed by Scott and Kucera (7) was applied for the prediction of retention volumes of alkylphenols and mobile phase compositions which improved the resolution of alkylphenols in normal phase HPLC systems.

Acknowledgement

The support of this research by the U. S. Department of Energy under Contract No. DE-AC01-79ET14874 is gratefully acknowledged.

References

1. D. D. Whitehurst, T. O. Mitchell, and M. Farcasiu, "Coal Liquefaction: The Chemistry and Technology of Thermal Processes," Academic Press, New York, 1980.

2. R. J. Hurtubise and J. D. Phillip, Anal. Chim. Acta, 110, 245 (1979).

3. L. R. Snyder, "Principles of Adsorption Chromatography, Marcel Dekker, Inc., New York, 1968.

4. J. F. Schabron, R. J. Hurtubise, and H. F. Silver, Anal. Chem., 49, 2253 (1977).

5. J. F. Schabron, R. J. Hurtubise, and H. F. Silver, Anal. Chem., 50, 1911 (1978).

6. J. F. Schabron, R. J. Hurtubise, and H. F. Silver, Anal. Chem., 51, 1426 (1979).

7. R. P. W. Scott and P. Kucera, J. Chromatogr., 112, 425 (1975).

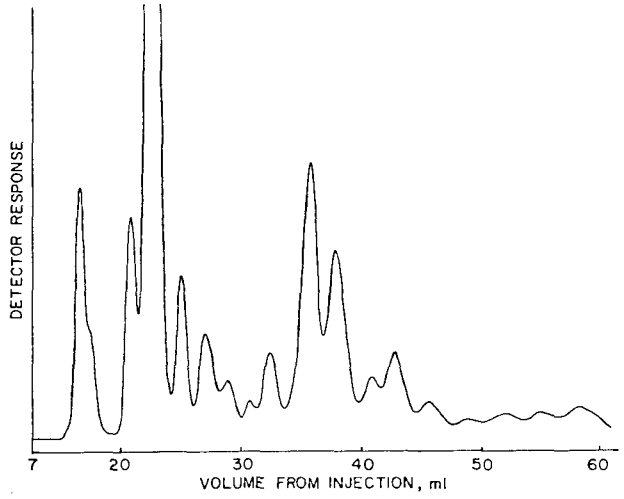

Figure 1. HPLC Chromatogram of 3-Ring PAH Fraction from 533K+ Wyodak Solvent from Willsonville

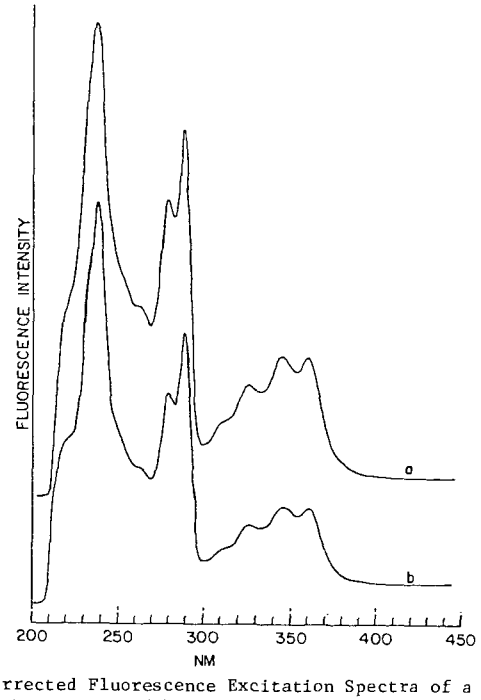

Figure 2. Corrected Fluorescence Excitation Spectra of a Standard Fluoranthene Sample (a) and Suspect Component (b) from HPLC Separation of 533K+ Wyodak Solvent

A Comparative Study of HPLC Column Packings for the Separation of Aromatic and Polar Compounds in Fossil Fuel Liquids

Atsushi Matsunaga and Sampo Kusayanagi

Lubricants and Petroleum Products Laboratory, Nippon Mining Co., Ltd.
3-17-35, Niizo-Minami, Toda, Saitama 335, Japan

INTRODUCTION

The upgrading of petroleum residuals, tar sand bitumens, shale oil and coal liquefaction products is a matter of current concern. Polynuclear aromatic hydrocarbons, nitrogen and oxygen compounds are present in relatively large amount in these fuel sources. These compounds can cause serious problems in processing and in the quality of the products. Then, the character and content of these compounds must be known to choose appropriate catalysts and conditions for refining.

Many works on compositional analyses of each liquid have been reported, most of which involve the combination of classical chromatographic separation and spectrometric characterization. Although this approach is undoubtedly most useful, it is very time-consuming to apply to routine analysis for the purpose of process control or product evaluation. Also, the poor separation due to the low efficiency or tailing problems of classical adsorbents causes cross-contamination of fractions in many cases.

Recently, high performance liquid chromatography (HPLC) has been applied to the rapid analysis of petroleum products and alternative fuel sources. Many of the works dealt with the type analysis as a substitute of FIA method (1,2) or so-called SARA method (3,4). Selucky et al. used HPLC on μ-Porasil as a fingerprinting technique of petroleum products (5). Wise et al. employed μ-Bondapak NH_2 column for the separation of polynuclear aromatic hydrocarbons (PAHs) in crude oil (6), while Mourey et al. used microparticulate pyrrolidone column for the analysis of PAHs in shale oil (7). μ-Bondapak NH_2 was also used by Dark et al. for the analysis of anthracene oil (8). It seems apparent that normal phase chromatography is adequate for the class separation of heavy fractions, since the long alkyl chains govern the retention characteristics rather than polar group in the reversed phase mode (6,9). This paper reports a study on normal phase HPLC separations of aromatic and polar compounds using several packing materials.

EXPERIMENTAL

The instrument used was a Varian Aerograph model 5020 Liquid Chromatograph equipped with a UV 254 nm absorbance detector and a ternary solvent programmer. Column packings used are listed in TABLE I. Hexane, methylene chloride and methanol of LC grade were obtained from Wako Chemicals, Tokyo, and used as received.

TABLE I. HPLC COLUMN PACKINGS STUDIED

Packing	Functionality	Particle Diameter (um)	Column Length (cm)	Column ID (mm)	Theoretical Plate Number	Supplier
Nucleosil NO_2	Nitro-	5	15	4.6	4000	Machery-Nagel Co. (Germany)
Nucleosil NH_2	Amino-				5000	
Nucleosil CN	Cyano-				4900	
Nucleosil SA	Sulfonic Acid-				4600	
Lichrosorb Si-5	Silica				7500	E. Merck (Germany)
Lichrosorb Al-5	Alumina		25		3000	
TSK 111	Styrene-Divinylbenzene Copolymer				3000	Toyo Soda (Japan)

(Functionality: group bonded on silica)

RESULTS AND DISCUSSION

MODEL COMPOUND STUDY. TABLE II summarizes the retention data of model aromatic compounds on each stationary phase. The largest capacity factor (k') was obtained using Nucleosil NO_2 column, with the exception of activated alumina. Selectivity (α) for the separation between naphthalene and chrysene is given by the ratio of the capacity factor for both compounds and is also shown in TABLE II. Again, Nucleosil NO_2 gave the largest selectivity. This could be attributed to the large charge-transfer capability of nitrophenyl group with polynuclear aromatic hydrocarbons. Nucleosil NH_2 seems to posess the similar, but weaker, ability, as it gave a better selectivity than silica regardless of the weaker retention for naphthalene. Nucleosil CN and Nucleosil SA columns showed smaller capacity factor than silica. It was difficult to obtain reproducible retention data with alumina/hexane system. Alumina is,however, an important adsorbent since it exhibits the most strong retention for aromatic compounds at activated state and it gives the most distinctive separation between mono- and diaromatics (10). TSK 111 (polystyrene gel) exerts a unique adsorption of aromatic compounds with hexane as eluant, probably due to π-π electron interaction. The difficulty with this system is that retention is very dependent on the size of alkyl substituent and steric exclusion can occur in some cases, that causes the impossibility of separation of substituted compounds by aromatic ring number.

The retention behavior of selected polar compounds are summarized in TABLE III. Pyridine and its benzologues are the known main "basic" nitrogen compounds in fossil liquids. Indole and its derivatives are the typical "nonbasic" nitrogen compounds. Phenols are typical polar components containing oxygen. Carboxylic acids were not studied here as they did not give a clear peak in these LC modes, probably because of association.

Good separation of polar compounds from aromatic hydrocarbons was obtained except for that on TSK 111 as shown in TABLE III. As TSK 111 has no polar group on it, interaction with polar group in sample molecule is weak. The rather strong retention of phenols and indoles will be due to their electrophilic nature. Polar compounds were preferentially retained on the stationary phases other than TSK 111. Gradient elution was carried out for rapid elution of strongly retained molecules. From the data shown in TABLE III, it is considered that polar-polar interactions including hydrogen bonding or acid-base interaction are the predominant separation mechanism, although the effect of alkyl substitution, especially at sterically hindered positions to polar group, is not negligible (e.g. 8-methylquinoline and 2,4-dioctylphenol).

Both Nucleosil NO_2 and Nucleosil CN have neutral functional group and the elution order of compounds on these packings are similar and in accordance with the order of so-called polarity: nonbasic nitrogen compounds$<$phenols$\leq$basic nitrogen compounds. The capacity factors are larger for all compounds with NO_2 column than CN because of its strong polarity. NO_2 showed stronger retention for phenols, with decreasing the selectivity for the resolution between phenols and basic nitrogen compounds (see TABLE III). Nucleosil NH_2 have weakly basic character, and showed strong retention of phenols. Basic and nonbasic nitrogen compounds were not separated each other. The nonbasic nitrogen compounds are weak acids and the interaction with amino group can occur. It is well known that alumina contains a number of strongly basic sites. Then, alumina showed preferential adsorption of nonbasic nitrogen compounds relative to basic compounds. To elute phenols from alumina column, eluant containing a more polar solvent (e.g. methanol) was required. In contrast, Nucleosil SA has strongly acidic functionality and showed strong retention of basic nitrogen compounds. In the case of silica, the elution order approximately depends on sample polarity, although tendency for a preferential adsorption of basic compounds is also observed.

The comparison of selectivities in TABLE III shows that Nucleosil NH_2 and silica give better resolution between phenols and nitrogen compounds and that better separation of nitrogen compounds by types is obtained using silica and Nucleosil SA. The effect of alkyl substitution on separabilities by compound types depend on its position, number and size. From TABLE III, substitution at sterically hindered positions appears to affect most largely. The tendency of this effect seems to be

common to all polar stationary phases studied.

APPLICATION STUDY. Examples of HPLC separations on coal tar and heavy petroleum fractions are described here. FIGURE 1 is the chromatograms on coal tar. With Nucleosil NH_2 column, separation of aromatic compounds by ring number (three-ring aromatics as predominant) and separation between nitrogen compounds and phenols were achieved. Nonbasic nitrogen, phenols and basic nitrogen compounds were separated each other using silica. In the case of alumina, gradient elution using three solvent including methanol was performed to elute phenols. Here again, separation of aromatics by ring number and separation of nitrogen compounds and phenols were obtained. A reversed trace of gradient profile was carried out to regenerate alumina column.

FIGURE 2 demonstrates the HPLC separations on heavy petroleum fractions. Silica, Nucleosil NO_2, NH_2 and CN columns all gave the similar patterns of chromatograms; with NO_2 and CN columns some overlap were observed between polynuclear aromatics and weakly polar components. Two main peaks in polar region seem to be attributed to basic and nonbasic nitrogen compounds. To examine the HPLC behavior of these components present in the fraction, basic and nonbasic (acidic) compounds were concentrated by chromatography on ion-exchangers (Amberlyst 15 and A29, Rohm and Haas), and collected fractions were injected into HPLC system. Although cross-contamination was observed, particularly in the A29 adsorbate, the attribution of two peaks was proved to be proper. Due to the long and several alkyl substitutions, nitrogen compounds were not retained so strongly as model compounds, while some separability by types still remains. The heavier is the fraction, the more difficult is the separation as shown in FIGURE 2B. FIGURE 2C shows the chromatogram of hydrogenated product of fraction in FIGURE 2A. Broader distribution of nitrogen compounds were observed in FIGURE 2C. These new peaks can be those of the hydrogenated intermediates or products of nitrogen compounds, which posess a variety of basic or nonbasic characters. Separation of aromatic compounds by types was not so clear in petroleum heavy fractions, because of the large alkyl or naphthenic substituents. Some characteristic profiles can be obtained, though, especially with Nucleosil NO_2. Mono-, di- and polynuclear aromatic fractions were collected by preparative scale chromatography on activated alumina (10) and the well-defined fractions were chromatographed on Nucleosil NO_2. As shown in FIGURE 3, separability by ring number can be recognized, although clear resolution was not obtained.

REFERENCES

(1) Suatoni, J.C., Garber, H.R. and Davis, B.E., J. Chromatogr. Sci. 13, 367 (1975).
(2) Suatoni, J.C. and Garber, H.R., J. Chromatogr. Sci. 14, 546 (1976).
(3) Suatoni, J.C. and Swab, R.E., J. Chromatogr. Sci. 13, 361 (1975).
(4) Suatoni, J.C. and Swab, R.E., J. Chromatogr. Sci. 14, 535 (1976).
(5) Selucky, M.L., Rue, T.C.S. and Strausz, O.P., Fuel 57, 585 (1978).
(6) Wise, S.A., Chesler, S.N., Hertz, H.S., Hilpert, L.R. and May, W.E., Anal. Chem. 49, 2306 (1977).
(7) Mourey, T.H., Siggia, S., Uden, P.C. and Crowley, R.J., Anal. Chem. 52, 885 (1980).
(8) Dark, W.A., McFadden, W.H. and Bradford, D.L., J. Chromatogr. Sci. 15, 454 (1977).
(9) Schabron, J.F., Hurtubise, R.J. and Silver, F., Anal. Chem. 49, 2253 (1977).
(10) Matsunaga, A. and Yagi, M., Anal. Chem. 50, 753 (1978).

TABLE II. CAPACITY FACTORS AND SELECTIVITY OF AROMATIC COMPOUNDS[a]

Compounds	Nucleosil NO_2	Nucleosil NH_2	Nucleosil CN	Nucleosil SA	Lichrosorb Si-5	TSK 111
Capacity factor						
Dodecylbenzene	0.09	0.00	0.06	0.05	0.14	-0.08
Toluene	0.09	0.05	0.06	0.14	0.25	-0.03
Tetraline	0.14	0.05	0.06	0.18	0.33	0.22
Naphthalene	0.68	0.23	0.22	0.23	0.44	0.67
Biphenyl	0.68	0.25	0.29	0.23	0.61	0.67
Fluorene	1.55	0.36				1.03
Anthracene	1.91	0.54	0.53	0.45	0.75	1.67
Fluoranthene	4.64	0.86	0.61			2.11
Pyrene	3.18	0.91		0.55	0.83	2.25
Chrysene	6.27	1.32	0.80	0.82	1.33	3.50
Benzo(e)pyrene	12.18	1.82	1.00		1.69	5.00
Dibenzofuran	1.23	0.36				0.94
Dibenzothiophene	1.72	0.50				1.61
Selectivity(α_1)[b]	9.22	5.74	3.64	3.57	3.02	5.22

a) Carrier: Hexane. 1 ml/min.
b) α_1 = k'(chrysene)/k'(naphthalene).

TABLE III. CAPACITY FACTORS AND SELECTIVITIES OF POLAR COMPOUNDS[a]

Compounds	Nucleosil NO_2	Nucleosil NH_2	Nucleosil CN	Nucleosil SA	Lichrosorb Si-5	Lichrosorb Al-5	TSK 111
Capacity factor							
Indole	9.82	10.73	6.45	8.36	6.89		5.17
2-Methylindole	9.82	10.09	5.82	7.41	6.72		4.53
3-Methylindole	9.27	9.73	5.12	6.68	6.44		3.94
Carbazole	10.73	11.18	7.00	8.27	7.67	6.45	9.08
Pyridine	14.00	11.18	10.29				
Quinoline	13.73	10.82	9.98				1.38
2-Methylquinoline	13.64	10.55					
4-Methylquinoline	14.45		10.29				
7-Methylquinoline	13.91	11.55	9.82				
8-Methylquinoline	8.73	7.64					
2,6-Dimethylquinoline	13.82	11.18	10.29				
Isoquinoline	14.55	12.00	10.37				
Acridine	13.64	10.82	9.04	22.64	16.00	5.55	2.47
Aniline	10.36						
1,2,3,4-Tetra-hydroquinoline	9.36	7.18	2.45				
Phenol	13.64	16.27	8.88	13.68	11.00	N.E.[e]	3.94
o-Cresol	11.82	13.55	7.71	10.45			2.81
p-Cresol	14.00		9.27	13.00			3.50
2,5-Xylenol	11.27		7.00				8.39
2,6-Xylenol	8.18		3.16				
3,4-Xylenol	14.00	15.27	8.88				
p-Nonylphenol	12.18	13.73	7.78	11.91	10.11	N.E.	1.69
2,4-Dioctylphenol	6.91		3.16	4.86	6.44		0.47
α-Naphthol	13.55	17.73	9.67				8.39
Selectivity α_1 [b]	1.27	1.46	1.27	1.65	1.43	large	2.30
α_2 [c]	1.00	1.50	1.02	1.65	1.45	large	1.60
α_3 [d]	1.27	1.03	1.29	2.74	2.09	1.16	3.68

a) Gradient elution for Nucleosil and Lichrosorb: Hexane(10 min) then to methylene chloride at 2.5%/min. With TSK, isocratic with hexane. 1-ml/min.
b) For phenol & carbazole. c) For phenol & acridine. d) For carbazole & acridine.
e) not eluted.

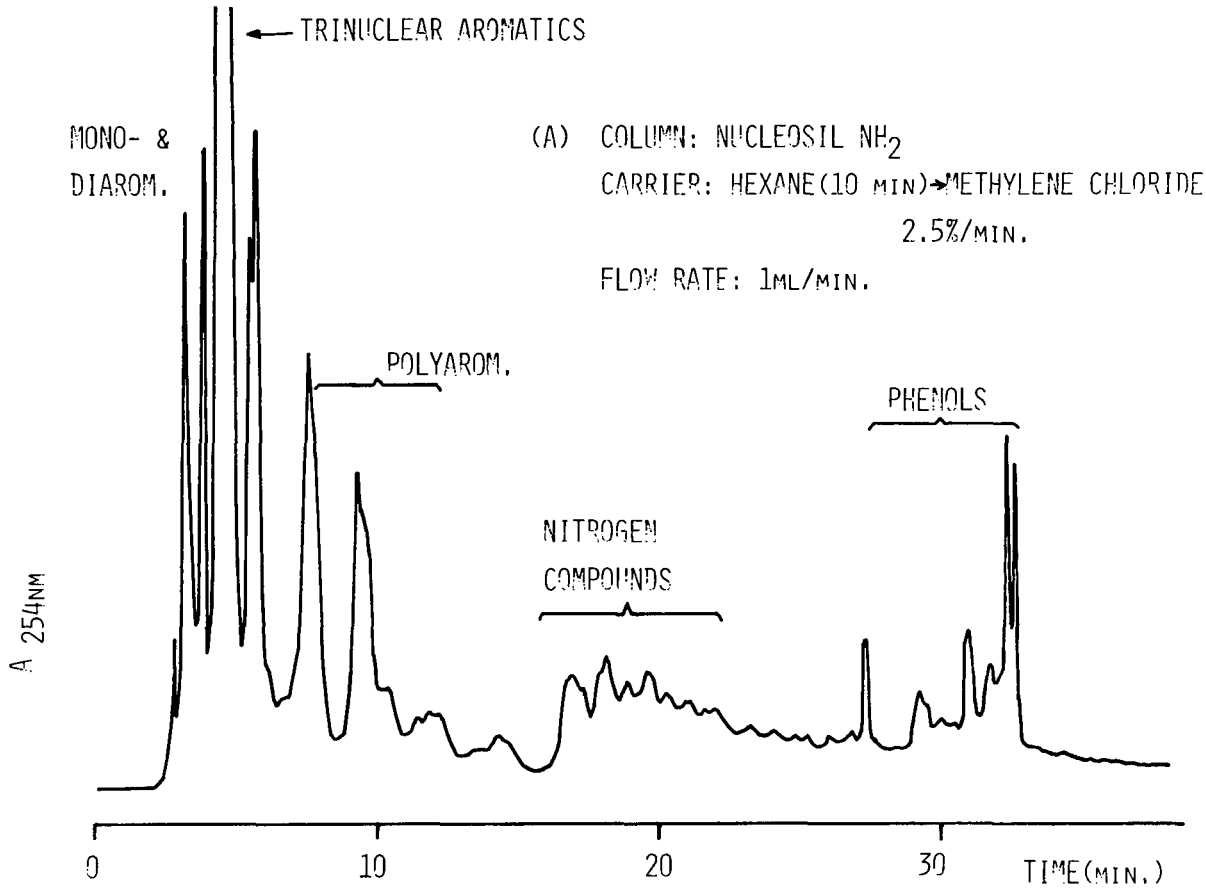
TRINUCLEAR AROMATICS
MONO- &
DIAROM.
(A) COLUMN: NUCLEOSIL NH2
CARRIER: HEXANE(10 MIN)→METHYLENE CHLORIDE
2.5%/MIN.
FLOW RATE: 1ML/MIN.
POLYAROM.
PHENOLS
NITROGEN
COMPOUNDS
A 254NM
0
10
20
30
TIME(MIN.)

FIG. 1A

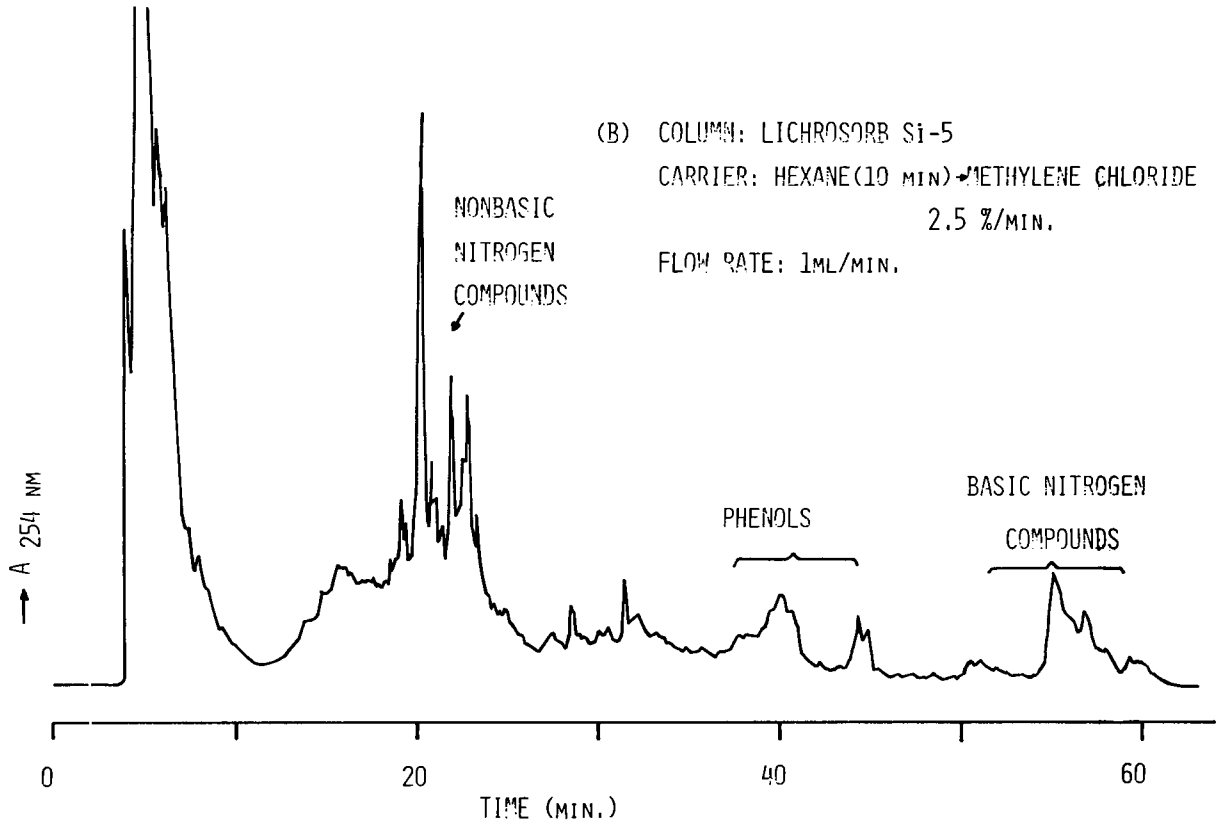
(B) COLUMN: LICHROSORB Si-5
CARRIER: HEXANE(10 MIN)→METHYLENE CHLORIDE
2.5 %/MIN.
FLOW RATE: 1ML/MIN.
NONBASIC
NITROGEN
COMPOUNDS
PHENOLS
BASIC NITROGEN
COMPOUNDS
A 254 NM
0
20
40
60
TIME (MIN.)

FIG. 1B

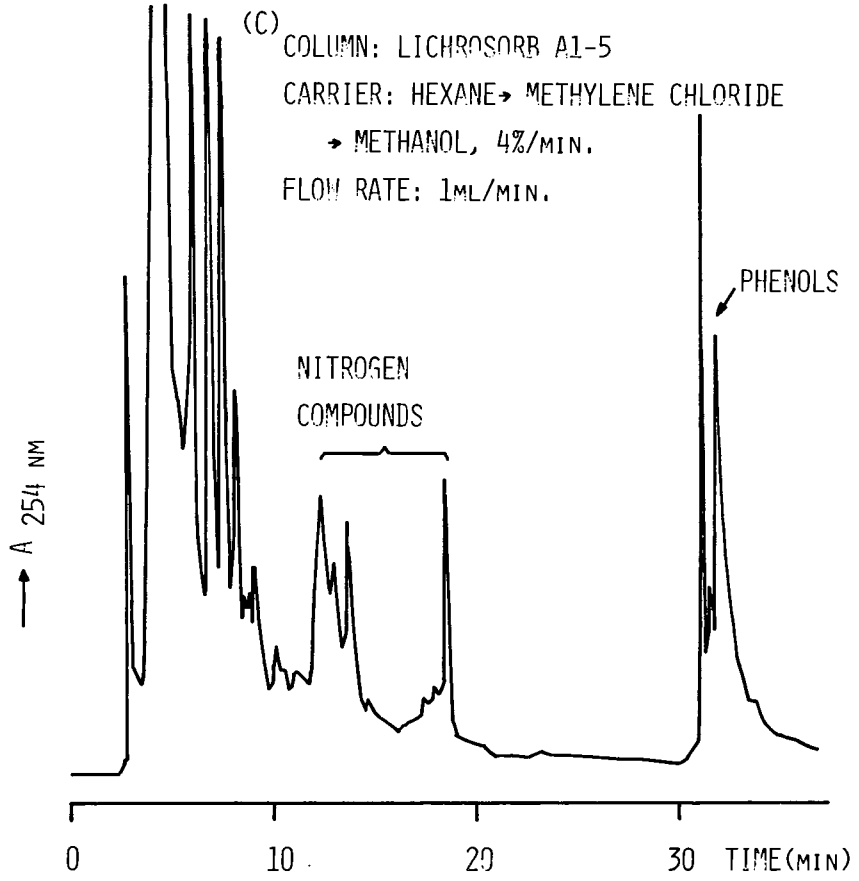

FIGURE 16 CHROMATOGRAMS OF COAL TAR

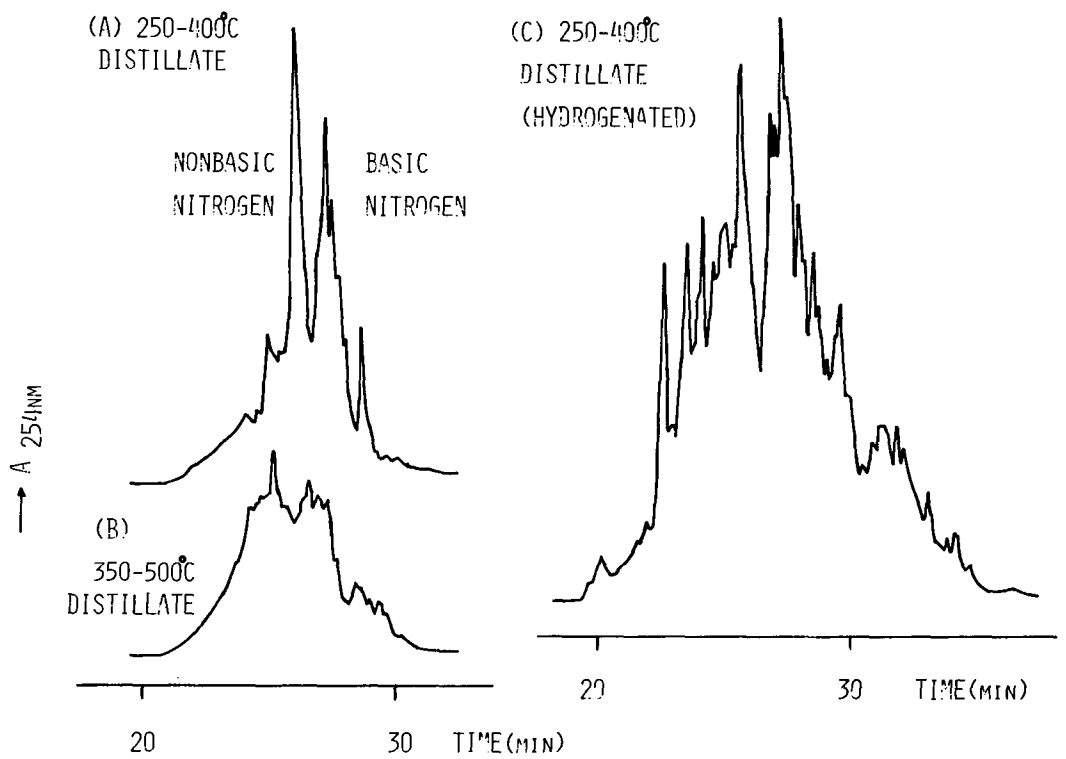

FIGURE 2. CHROMATOGRAMS OF HEAVY PETROLEUM FRACTIONS.(POLAR COMPOUNDS REGION)
CONDITIONS AS IN FIGURE 2(B)

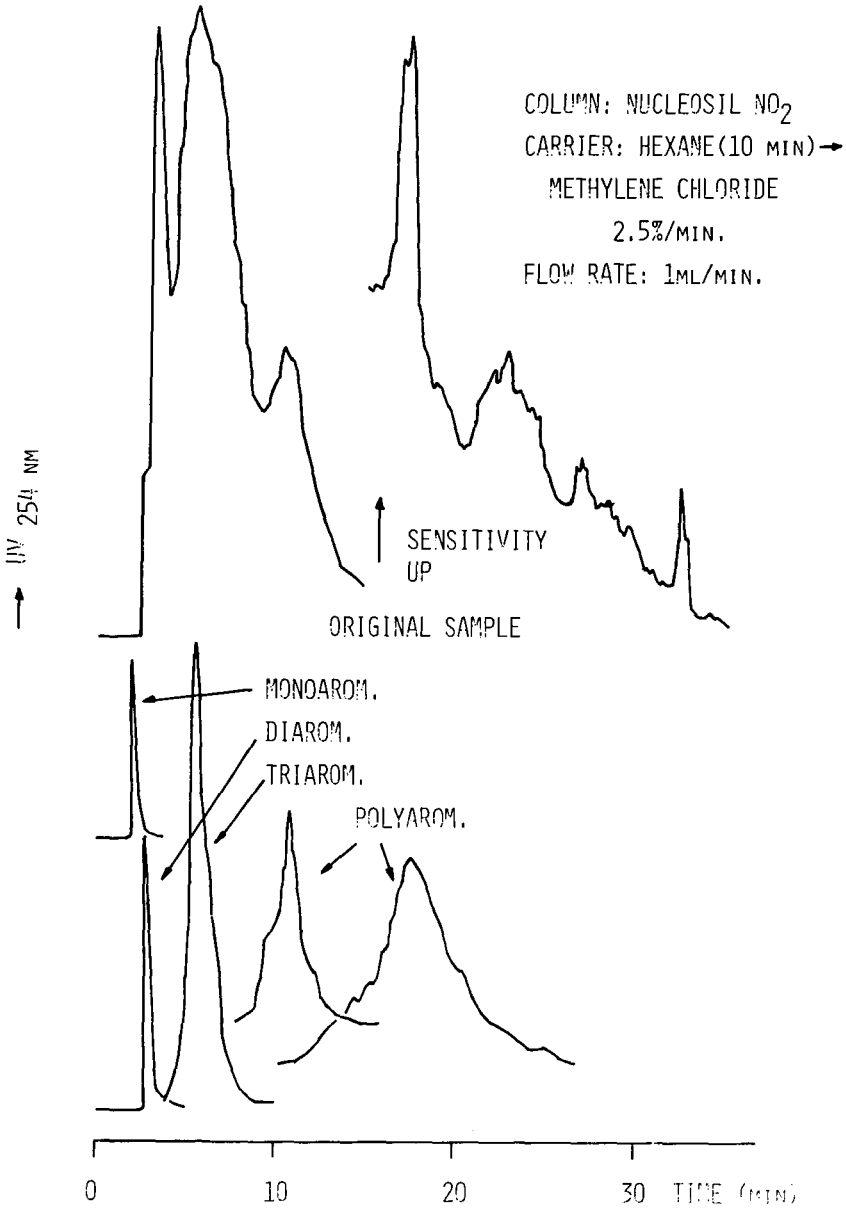

FIGURE 3. CHROMATOGRAMS OF 350-480°c DISTILLATE AND ITS SEPARATED FRACTIONS BY ALUMINA CHROMATOGRAPHY

REVERSE PHASE LIQUID CHROMATOGRAPHY OF COAL LIQUEFACTION SOLVENTS

F. P. Burke, R. A. Winschel and T. C. Pochapsky

Conoco Coal Development Company
Research Division
Library, Pennsylvania 15129

INTRODUCTION

In the various processes for the direct liquefaction of coal a liquefaction solvent is employed which consists, at least in part, of a distillate boiling in the 200 x 500°C range. The composition of this material can have a significant effect upon process performance([1,2]). In our work with SRC-I and H-Coal recycle oils([2,3]), we found it desirable to have a method for separating these distillates into component classes which can be quantified to provide a compositional analysis of the material, in a manner similar to the SESC technique([4]). Group separations of this kind have been reported([5,6]) using silica or alumina columns with some sequence of solvents of increasing polarity. We felt that the chromatography of these recycle solvents on an ODS reverse phase column might be advantageous in avoiding the problems of irreversible absorption, low selectivity, and alteration of the sample which can occur with the absorption column. The binary gradient used with the ODS column offered much greater flexibility in terms of solvent programming to tailor the separation to a specific type of sample, than was available with the absorption method.

Results are presented on the RPLC separation of Wilsonville SRC-I solvents. These data are quantified and the relative amounts of the eluted fractions provide an explanation of the relative values of these solvents as liquefaction media. Results are also presented on the RPLC separation of H-Coal recycle distillates. It was found that, for the RPLC elution program used, a strong linear correlation exists between the retention time of the component and a "structural vector" consisting of ten parameters which describe that component's molecular structure. This allows one to predict the retention time of a component of interest for qualitative identification, and can also be used to support the identification of a component observed to elute at a given retention time.

EXPERIMENTAL

Separation of Wilsonville Solvents

The Wilsonville solvents were separated using a 25 cm x 6.35 mm ODS column from Lyon Technology. The sample was eluted from the column using a step-wise methanol/water gradient indicated at the top of the chromatogram in Figure 1. Eluted fractions were quantified using a Pye-Unicam moving wire flame ionization detector, and component identifications were made by GC/MS analyses of each fraction. The elutant flow rate was 1.5 ml/min. The chromatogram was divided into twelve more-or-less arbitrary fractions, the fraction cutpoints corresponding to minima in the chromatogram.

Separation of H-Coal Samples

The H-Coal recycle distillates were separated on an Altex C-18 Ultrasphere ODS column (25 cm x 4.6 ml). As above, fractions were quantified usind the Pye-Unicam FID. The elutant flow rate was 1.0 ml/min, and the elution sequence is shown in Figure 2. A 2 min gradient was programmed for each step change in solvent strength. Twenty-eight fractions collected from the RPLC separation of the H-Coal samples,

as indicated in Figure 2, were analyzed by GC/MS to make component identifications. Note that for both separations, the final fraction was removed by a tetrahydrofuran (THF) flush.

RESULTS AND DISCUSSION

Wilsonville SRC-I Solvents

In the course of a program on short residence time liquefaction done under EPRI sponsorship([2]) we received relatively large and representative samples of Wilsonville SRC-I recycle distillates over a period of fourteen months. The first sample, Batch I, was hydrogenated in a fixed-bed unit to produce a solvent identified as Hydro II. These were found to be acceptable solvents for bench-scale short residence time liquefaction work. The later batches, Batch III and VI, were found to be unacceptable for use in the continuous short residence time bench-scale unit. The results of this work have been presented in considerable detail elsewhere([2]). For the present purposes it is sufficient to note that Batch I and Hydro II solvents were significantly superior to Batch III and VI solvents in terms of their ability to act as hydrogen donor liquefaction solvents.

The reverse phase liquid chromatogram of Hydro II solvent is shown in Figure 1. Table 1 lists representative compounds in each of the twelve fractions and the approximate weight percentage of each fraction as determined by the FID detector response. Because of the high resolution of the commercial ODS columns used in this study, there was essentially no overlap of components even between two adjacent fractions. Therefore, the functional components occur primarily in fractions 1 through 5, the nonfunctional aromatics in fractions 6 through 11 and the saturated hydrocarbons exclusively in fraction 12. Note also that the sequence of diaromatics (e.g., fluorenes, naphthalenes, dibenzofurans) begins around fraction 5 and each successive fraction contains the next alkylated homologue. Phenanthrene elutes in fraction 7 and pyrene in fraction 8 and again the alkylated homologues appear in order in successive fractions. Hydroaromatics appear earlier than alkyl substituted molecules with the same number of saturated carbons. Thus, dihydrophenanthrene elutes with the methylphenanthrene in fraction 8, and tetra and octahydrophenanthrene in the next two fractions. Fraction 11 contains very highly alkylated aromatics (e.g., C_7 through C_9 naphthalenes).

The RPLC data show a steady increase in the amount of hetero molecules (principally phenols and indanols) upon going from Batch I to Batch VI solvent. Taking fractions 1 through 4 as a group, polar molecules increased from 15.8% (Batch I) to 20.0% (Batch III) to 27.1% (Batch VI). Hydrogenation of Batch I decreased the polar fractions to 10.0% (Hydro II). At the other end of the chromatogram, the saturates approximately double on going from Batch I to Batch VI. Hydrogenation of Batch I increases the saturates by about 50%. The hydroaromatic hydrogen donor molecules are found principally in fractions 7 through 10. Batch III and Batch VI solvents are depleted in these fractions relative to Batch I and Hydro II.

The RPLC data on the Wilsonville recycle solvents can be readily related to the quality of these solvents as hydrogen donors. The Batch I and Hydro II solvents are richer in those fractions which contain the partially hydrogenated aromatics which can serve as hydrogen donors. In Batch III and Batch VI solvents these fractions are displaced by the monoaromatic phenols and indanols and also by saturated hydrocarbons. The more alkylated Batch III and Batch VI solvents are, therefore, expected to be both poorer hydrogen donors and poorer physical solvents than Batch I or Hydro II.

RPLC Separation of H-Coal Recycle Distillate

Figure 2 shows the RPLC chromatogram of a distillate recycle sample from Run 9 of the H-Coal PDU, operated by HRI in Trenton, New Jersey. This chromatogram was obtained as part of a program to analyze recycle oils in the H-Coal process and more

complete details are reported elsewhere([3,7,8]). The elution gradient used is shown at the top of Figure 2. Because a better column was used for the H-Coal distillate, the chromatogram shows higher resolution and was divided into 28 fractions as opposed to the 12 used for the Wilsonville solvent. The purpose of this was to obtain a better qualitative identification by GC/MS of the components in the H-Coal samples. We have found that these components elute in a predictable manner based on a set of standard parameters (i.e., "structural vectors") which define the molecule. By correlating retention times with vectors which describe the molecules we can support identifications and predict the fraction which a given component will elute. In all, we obtained mass spectra for over 500 components of the H-Coal distillate. Grouping isomers as individual components, this list is reduced to 153 entries. Components are represented as structural vectors for correlation with retention times. The ten categories used for structural components are shown in Table 2. We believe the listing in Table 2 is the minimum number of parameters necessary to specify each component to the extent that the GC retention times and mass spectra allow identification. That is, higher level parameters such as points of alkyl substitution cannot be derived for all components from the GC/MS data, and are therefore excluded.

Table 3 gives the tentative identifications of 153 components which were correlated on the basis of structural parameters, with retention times in the RPLC run. The percentage of each fraction in the RPLC chromatogram of the mixture was determined from the integrated response of the Pye-Unicam moving wire FID. The relative amounts of each component in a given fraction were determined from the total ion chromatograms of the GC/MS runs used for component identifications. In most cases the sum of the percentages of the components in a given fraction does not equal 100. This is because: (1) some fractions contained unidentified components which were not used in the correlation, and (2) some of the gas chromatograms were of poor quality because of the small sample size available and accurate quantitation was not possible. The percentages of components in a given fraction do allow a distinction between major and minor components, and, for those components which were found in more than one fraction, show in which fraction the majority of that component elutes. The RPLC eluate was collected in 28 fractions and the mean retention time of each fraction used in the linear multiple regression correlation. The correlation coefficient is 0.988 and the slope of the observed versus calculated retention times is 0.976. No usable GC/MS data were obtained for fractions 1, 2 and 27. Fraction 28, which is eluted with THF, contains naphthenes and normal and branched alkanes from C_{14} through about C_{35}. The average error in the correlation is 2.5 min. Since the average fraction width is over 4 min, and the mean retention times were used for each component in a given fraction, we have an inherent error of $\pm \sim 2$ minutes in the observed retention times.

The calculated retention time coefficients are given in Table 2. Factors which increase molecular size (number of aromatic rings, aliphatic and hydroaromatic carbons) increase the retention time. Parameters which reduce molecular size (aromatic condensation, hydroaromatic rings) decrease retention time.

Hydroxyls and basic and non-basic nitrogens have strong negative correlations. Surprisingly, etheric oxygen has a positive correlation coefficient. However, since only two ethers, dibenzofurans, were detected this parameter is uncertain.

That such a strong linear correlation exists between retention times and the structural parameters is surprising. It is clearly dependent on the solvent program used in the RPLC run. However, we have developed similar correlations for different solvent programs and samples other than H-Coal liquids. Therefore, we conclude that this solvent program is not unique. This suggests that a different program may produce a predictable separation which may have specific advantages for the problem at hand. One use of this method is as a pre-separation when the intent is to detect a specific component. The approximate retention time can be calculated for a given

component, and a fraction of the RPLC eluate can be taken which covers this retention time. This fraction can then be analyzed, probably by GC/MS, to determine if the component is present. This will eliminate the interferences in the GC from structurally dissimilar components with similar GC retention times. This method also allows concentration of the sample to improve sensitivity.

CONCLUSIONS

Reverse phase liquid chromatography is a promising method for analytical or preparative separation of coal derived distillates. The high resolution and selectivity of commercially available ODS columns allows specific component classes (e.g., polars, aromatics, saturates) to be separated without cross contamination. A wide variety of elution programs is readily available. The inertness of the column substrate should minimize problems of irreversible adsorption and chemical alteration of sample components on the column. The rather unexpected result that retention time can be accurately predicted on the basis of a simple structural representation of a component opens up interesting possibilities for refinement and application of the method.

REFERENCES

1. L. E. Furlong, E. Effron, L. W. Vernon and E. L. Wilson, Chem. Eng. Prog., 72, 69 (1976).

2. J. A. Kleinpeter, F. P. Burke, P. J. Dudt and D. C. Jones, "Process Development for Improved SRC Options: Short Residence Time Sutdies," EPRI Project 1134-1, Final Report, EPRI AP-1425, June 1980.

3. F. P. Burke, R. A. Winschel and T. C. Pochapsky, "Development of a Correlation Between Slurry Oil Composition and Process Performance," DOE Contract DE-AC05-79ET-14503, Topical Report 1, FE-14503-1, April 1980.

4. Farcasiu, M., Fuel, 56, 9 (1977).

5. D. D. Whitehurst, M. Farcasiu, T. O. Mitchell and J. J. Dickert, Jr., "The Nature and Origin of Asphaltenes in Processed Coals," EPRI Report AF-430, Annual Report, July 1977.

6. J. S. Shiller and D. R. Mathiason, Anal. Chem., 49, 1225 (1977).

7. F. P. Burke, R. A. Winschel and T. C. Pochapseky, "Development of a Correlation Between Slurry Oil Composition and Process Performance," DOE Contract DE-AC05-79ET-14503, Topical Report 2, FE-14503-2, August 1980.

8. F. P. Burke, R. A. Winschel and T. C. Pochapsky, "Development of a Correlation Between Slurry Oil Composition and Process Performance," DOE Contract DE-AC05-79ET-14503, Final Report, FE-14503-3, November 1980.

Table 1

Reverse Phase Liquid Chromatographic
Separation of Wilsonville Solvents

Fraction	Representative Compounds	Wilsonville Batch,* approximate, wt % I	II	VI	Hydro II
1	phenol, cresols	0.9	1.0	0.7	0.1
2	quinoline, indole, indanol, xylenols	2.2	2.1	4.7	1.1
3	methyl indanols, C_3-phenols, methyl quinoline	4.4	6.7	9.0	2.3
4	carbazole, C_4 + C_5-phenols, C_6-indanols	8.3	10.2	12.7	6.5
5	methyl carbazoles, diphenylether, C_2-quinolines, naphthalene	8.3	8.2	8.6	7.9
6	dibenzothiophene, dibenzofuran, C_2-carbazole, fluorene, acenaphthene, methylnaphthalene, biphenyl, tetralin	2.5	5.5	2.0	1.3
7	methyl fluorene, C_2-naphthalene, C_1-tetralin, phenanthrene	14.2	12.2	6.7	13.8
8	C_1-phenanthrene, C_3-naphthalene, pyrene, dihydrophenanthrene	11.7	4.6	6.5	9.4
9	tetrahydrophenanthrene, phenyl naphthalene, C_3-naphthalene, C_2-phenanthrene, C_2-biphenyl	7.0	6.2	5.6	4.2
10	octahydrophenanthrene, C_4 + C_5-naphthalenes, C_1 + C_2-tetrahydroacenpahthenes, C_1-phenyl naphthalene, C_3-biphenyl, C_3 + C_4-tetralins	30.3	28.9	21.7	37.2
11	highly alkylated aromatics	3.2	2.5	7.2	5.1
12	saturated hydrocarbons	7.1	11.8	14.6	10.9

* FID detector response

Table 2

Structural Parameters and Coefficients for Reverse Phase
Liquid Chromatogram of H-Coal Hydroclone Overflow Distillate

Structural Factor (X_i)	Coefficient, min, (C_i)
Constant	-10.45
Number of Aromatic Rings	24.28
Degree of Condensation	-5.35
Number of 6-Membered Saturated Rings	-3.80
Number of 5-Membered Saturated Rings	-4.86
Number of Alkyl Carbons	8.78
Number of Naphthenic Carbons	8.79
Number of Hydroxyl Groups	-25.26
Number of Ether Oxygens	11.53
Number of Non-Basic Nitrogens	-11.23
Number of Basic Nitrogens	-28.53

$$\text{Retention Time} = \sum_i C_i X_i$$

Tabl. 3. Component Identifications - RPLC Separation of H-Coal Hydroclone Overflow Distillate - PDU Run 9 - Period 20

Fraction	% of Total	Component	% of Component in Fraction	Calc. Retention Time, min	Fraction Mean Retention Time, min	Δ, min
3	1.1	C_2-Phenol	48	6.1	10.2	4.1
		Indole	2	9.9		0.4
		Indanol	47	10.0		0.2
4	1.5	C_3-Phenol	34	14.9	16.3	1.4
		C_1-Indanol	58	18.8		-2.5
		C_2-Quinoline	2	21.8		-5.5
		Phenylphenol	2	12.9		3.4
5	1.0	C_4-Phenol	20	23.7	21.8	-1.9
		C_1-Phenylphenol	5	21.6		-0.1
		C_2-Indanol	21	27.6		-5.8
		C_1-Indole	2	18.7		3.1
		Carbazole	18	22.0		-0.3
6	1.6	C_4-Phenol	10	23.7	25.4	1.7
		C_2-Indanol	40	27.6		-2.2
		C_1-Phenylphenol	5	21.6		3.7
7	1.9	C_5-Phenol	21	32.4	30.0	-2.4
		C_3-Indanol	13	36.4		-6.4
		C_2-Phenylphenol	5	30.4		-0.4
		C_1-Carbazole	20	30.8		-0.8
8	2.2	C_5-Phenol	1	32.4	36.7	4.3
		C_1-Phenol	6	41.3		-4.5
		C_3-Indanol	11	36.4		0.4
		C_4-Quinoline	2	39.3		-2.6
		C_1-Acridine	3	31.9		4.8
		C_2-Carbazole	1	39.6		-2.8
		C_2-Acridine	10	40.7		-4.0
9	2.7	C_6-Phenol	1	41.2	44.1	2.9
		C_4-Indanol	5	45.1		-1.0
		C_2-Carbazole	21	39.6		4.6
		C_2-Acridine	2	40.7		3.4
		C_1-Azapyrene	12	40.2		3.9
		C_3-Phenylphenol	12	39.2		4.9
10	4.1	C_2-Naphthalene	16	50.3	49.4	-1.0
		Acenaphthene	5	45.5		3.9
		Fluorene	25	42.0		7.3
		Dihydroanthracene	1	51.9		-2.5
		Phenanthrene	35	51.7		-2.3
		C_3-Carbazole	1	48.3		1.0
11	2.7	C_2-Naphthalene	1	50.3	52.2	1.8
		C_1-Acenaphthene	2	54.2		-2.1
		C_1-Fluorene	10	50.8		1.4
		Dihydrophenenathrene	6	51.9		-0.3
		Phenanthrene	2	51.7		0.5
		C_1-Dibenzofuran	1	53.6		-1.4
		Benzindan	70	54.2		-2.1
12	2.8	C_1-Tetralin	1	53.9	55.0	1.0
		Tetrahydroacenaphthene	1	57.8		-2.9
		C_3-Naphthalene	15	59.1		-4.1
		C_1-Fluorene	20	50.8		4.2
		C_1-Phenanthrene	7	60.5		-5.5
		Cyclopenta (d,e,f) Phenanthrene	2	55.6		0.7
		Fluoranthene	7	52.2		2.8
		Pyrene	1	59.9		-5.0
		C_1-Dibenzofuran	1	53.6		1.4
		C_4-Carbazole	2	57.1		-2.2
		C_2-Biphenyl	1	55.7		-0.7
		C_1-Acenaphthene	30	54.2		0.7

Table 3. (continued)

Fraction	% of Total	Component	% of Component in Fraction	Calc. Retention Time, min	Fraction Mean Retention Time, min	Δ, min
13	5.5	C_3-Naphthalene	2	59.1	58.4	-0.7
		Pyrene	28	59.9		-1.6
		C_1-Phenanthrene	38	60.5		-2.1
		Phenylnaphthalene	6	57.0		1.3
		C_1-Fluorene	3	50.8		7.6
		C_2-Fluorene	8	59.6		-1.2
		C_2-Biphenyl	5	55.7		2.7
14	1.2	Dihydropyrene	33	65.5	60.6	-4.8
		C_1-Phenanthrene	9	60.5		0.2
		C_1-Dihydrophenanthrene	5	60.6		0.0
		C_2-Acenaphthene	7	63.0		-2.4
		C_1-Benzindan	3	63.0		-2.4
		C_3-Biphenyl	1	64.4		-3.8
15	4.6	Tetrahydrophenanthrene	21	64.1	62.9	-1.2
		Acephenanthrene	9	64.4		-1.5
		C_4-Naphthalene	3	67.9		-4.9
		C_2-Tetralin	1	62.7		0.2
		C_1-Dihydrophenanthrene	8	60.6		2.3
		C_2-Fluorene	6	59.6		3.3
		C_1-Tetrahydroacenaphthene	1	66.6		-3.7
		C_1-Fluoranthene	1	61.0		2.0
		C_5-Carbazole	1	65.9		-3.0
		C_1-Phenanthrene	1	60.5		2.4
		Tetrahydropyrene	1	65.6		-2.7
		C_3-Biphenyl	4	64.4		-1.5
		C_2-Acenaphthene	22	63.0		-0.1
		Tetrahydrofluoranthene	1	64.6		-1.6
		C_1-Benzindan	13	63.0		-0.1
16	5.0	C_4-Naphthalene	1	67.9	66.5	-1.4
		C_2-Phenanthrene	31	69.3		-2.8
		C_1-Pyrene	24	68.7		-2.2
		Chrysene	3	70.6		-4.2
		Acephenanthrene	3	64.4		2.1
		Tetrahydrocyclopenta (d,e,f) Phenanthrene	1	68.0		-1.5
		C_2-Fluorene	11	59.6		6.9
		C_1-Benzindan	5	63.0		3.5
		C_2-Dihydrophenanthrene	4	69.4		-2.9
17	2.5	C_2-Phenanthrene	23	69.3	69.1	-0.1
		C_1-Dihydropyrene	12	74.2		-5.1
		C_1-Pyrene	30	68.7		0.4
		Chrysene	1	70.6		-1.5
		C_1-Tetrahydrophenanthrene	1	72.9		-3.7
		C_2-Benzindan	3	71.8		-2.7
		Tetrahydrocyclopenta (d,e,f) Phenanthrene	7	68.0		1.1
		C_4-Biphenyl	6	73.2		-4.1
		C_3-Fluorene	4	68.4		0.8
		C_2-Dihydrophenanthrene	1	69.4		-0.3
18	2.1	C_1-Pyrene	40	68.7	70.6	1.9
		C_2-Phenanthrene	20	69.3		1.3
		C_1-Tetrahydropyrene	4	74.4		-3.8
		C_1-Chrysene	1	79.4		-8.8
		C_2-Fluoranthene	4	69.4		0.9

Table 3. (continued)

Fraction	% of Total	Component	% of Component in Fraction	Calc. Retention Time, min	Fraction Mean Retention Time, min	Δ, min
19	5.5	C_3-Tetralin	1	71.5	73.8	2.4
		C_5-Naphthalene	4	76.6		-2.8
		C_3-Phenanthrene	8	78.0		-4.2
		C_2-Pyrene	1	77.5		-3.7
		C_1-Dihydropyrene	8	74.2		-0.4
		C_2-Phenylnaphthalene	1	74.6		-0.8
		C_2-Tetrahydroacenaphthene	1	75.4		-1.5
		C_1-Tetrahydrobenzindan		72.9		1.0
		C_2-Tetrahydrophenanthrene		75.4		-1.6
		C_3-Acenaphthene		71.8		2.1
20	7.6	Octahydrophenanthrene	1	76.5	79.0	2.6
		C_5-Naphthalene	4	76.6		2.4
		C_3-Phenanthrene	15	78.0		1.0
		C_2-Pyrene	14	77.5		1.5
		C_1-Chrysene	2	79.4		-0.4
		Benzpyrene	1	78.9		-0.1
		C_2-Dihydropyrene		83.0		-4.0
		C_1-Dihydropyrene	7	74.2		4.8
		C_4-Acenaphthene		80.6		-1.5
		C_2-Tetrahydrophenanthrene		81.6		-2.6
21	3.0	Tetrahydrochrysene	5	83.0	83.7	0.7
		C_4-Chrysene	8	79.4		4.3
		Benzpyrene	1	78.9		4.8
		C_6-Naphthalene	1	85.4		-1.7
		C_3-Phenanthrene	14	78.0		5.7
		C_4-Tetralin	1	80.2		3.5
		Dihydrobenzpyrene	1	84.4		-0.7
22	2.1	C_4-Phenanthrene	21	86.8	87.1	0.3
		C_3-Pyrene	11	86.3		0.8
		C_2-Chrysene	2	88.2		-1.1
23	2.7	Benzchrysene	1	89.6	90.4	0.8
		C_3-Pyrene	19	86.3		4.1
		C_4-Phenanthrene	8	86.8		3.6
24	3.0	C_5-Tetralin	8	89.0	94.4	5.4
		C_1-Octahydrophenanthrene	7	85.2		9.2
		C_5-Phenanthrene	5	95.6		-1.2
		C_6-Tetralin	2	97.8		-3.4
25	5.5	C_6-Tetralin	5	97.8	99.0	1.2
		C_3-Octahydrophenanthrene	9	94.0		5.0
		C_5-Phenanthrene	11	95.6		3.5
		C_4-Pyrene	7	95.0		4.0
26	6.5	C_6-Phenanthrene	2	104.4	106.6	2.3
		C_5-Pyrene	11	103.8		2.8
27	10.2	No Components Identified				
28	11.0	Alkanes and Naphthenes				

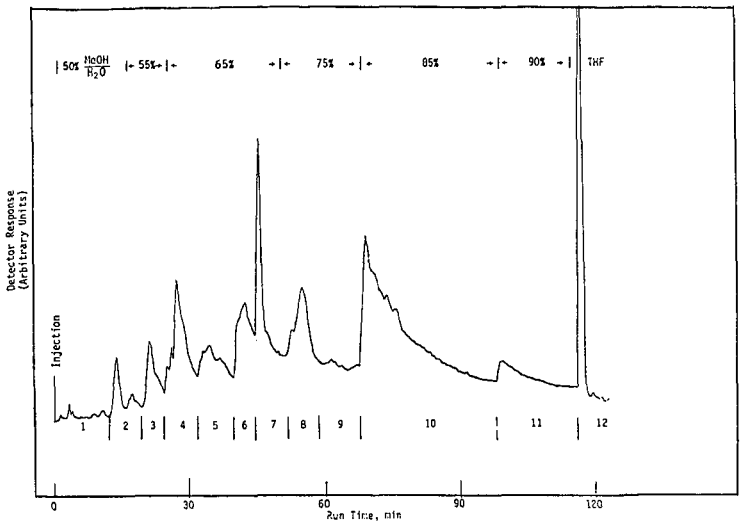

Figure 1. RPLC of Wilsonville Hydro II SRC-I Solvent

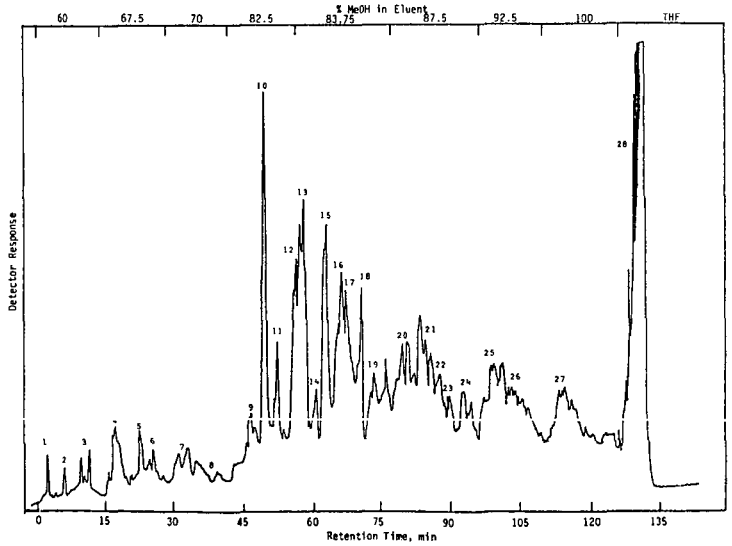

Figure 2. RPLC of H-Coal Hydroclone Overflow Distillate (Period 20 - PDU Run 9)

A COMPUTERIZED DATA REDUCTION SYSTEM FOR TABULATING DATA FROM GC RUNS AND CORRELATING CHANGES IN PRODUCT COMPOSITION WITH PROCESS CONDITIONS OR MUTAGENICITY

by

Leo A. Raphaelian
Argonne National Laboratory
9700 South Cass Avenue
Argonne, Illinois 60439

Even with the sophisticated analytical instrumentation presently available, a complete and exhaustive analysis of the organics in energy or environmental samples is not only time-consuming but also difficult due to the complexity of such samples. Generally, when organic analytical analysis is done on a number of samples, a GC/MS is run on each and every sample and, for quantification, the peak area of each peak in the GC/MS total ion chromatogram or in a corresponding GC chromatogram is determined and compared to peak areas derived from standards. Since the analysis of GC/MS data is cumbersome and time consuming, typically only a few of the more important analyses are performed. If the analysis of one or more representative samples could be done by GC/MS and data of a "standard representative" sample developed, then many samples could be done "rapidly" with a GC (rather than with a GC/MS) and a data system provided the samples were similar to the "standard representative" sample.

In this study, software was developed to carry out, with the assistance of a computerized data system, the rapid analysis of a series of samples containing complex mixtures of organic compounds. One of the samples to be analyzed was chosen as a standard or reference sample. With capillary column GC/MS, it was analyzed exhaustively and identification versus retention time data were stored in the data system. To this reference sample data, identification versus retention time data from capillary column GC/MS runs on other reference samples or standard mixtures was added to make up a "super" reference sample of identification versus retention time data. Now, all samples to be analyzed were compared to this reference sample. However, in place of GC/MS, capillary column GC was used and retention time and peak area data were automatically transferred from the GC to the data system. The data system then carried out those tasks typically done by the analyst, that is, the complex sorting and matching of GC peaks, the tabulation and recording of the identification of the compounds present, the calculation and recording of the concentration, and the presentation of charts and tables for comparing the data from several samples.

The software includes programs for matching the data for several GC runs, adjusting for dilution factors and response factors, compensating for drift in retention time, multiplying in factors for presenting tables of concentration in ppb, %, µg/L, etc., and doing regression analysis on the variation in product composition as a function of such variables as process conditions or on the variation in mutagenicity as a function of product composition.

Representative output of the data system is shown in Tables 1 and 2. In Table 1, the identification, amount (in grams of compound per 100 cubic feet of LTR gas), and total for the three samples are tabulated. In Table 2, the totals for five samples (from fifteen samples) are shown. The matching of peaks, identification, determination of concentration, totaling of more than one sample, and tabulation are easily and rapidly done by the data system.

TABLE 1: SCRUB SAMPLE ANALYSIS-GRAMS OF COMPOUND PER 100 ft^3 OF LTR GAS

Compound No.	Compound Name	SAMPLE 7 Top	SAMPLE 7 Bottom	SAMPLE 8 Top	SAMPLE 8 Bottom	SAMPLE 9	Total
		.000	.000	.000	.018	.000	.018
		.000	.089	.001	.058	.010	.158
999	SOLVENT	.249	1.792	3.855	65.084	11.560	82.540
		.000	.000	.001	.000	.000	.001
		.000	.009	.002	.036	.007	.054
		.000	.000	.001	.012	.000	.013
		.000	.022	.001	.016	.005	.044
		.000	.000	.000	.007	.000	.007
1	BENZENE	2.942	.595	.380	6.445	2.530	12.891
46	THIOPHENE	.021	.003	.002	.032	.016	.073
		.007	.000	.000	.000	.000	.007
2	TOLUENE	52.181	8.030	2.261	38.748	14.523	115.743
54	METHYL THIOPHENE	.037	.000	.001	.022	.006	.066
		.000	.012	.000	.005	.000	.017
7	ETHYL BENZENE	.590	.056	.010	.173	.052	.880
6	P AND M-XYLENE	1.489	.156	.025	.441	.131	2.242
58	DIMETHYL THIOPHENE	.031	.000	.000	.000	.000	.031
59	DIMETHYL THIOPHENE	.023	.000	.000	.000	.000	.023
340	STYRENE	.042	.000	.000	.000	.000	.042
5	O-XYLENE	.390	.034	.005	.095	.027	.551
60	DIMETHYL THIOPHENE	.012	.000	.000	.000	.000	.012
25	C3-BENZENE	.359	.028	.003	.053	.012	.456
26	C3-BENZENE	.140	.010	.001	.022	.005	.179
27	C3-BENZENE	.203	.013	.001	.028	.005	.252
28	C3-BENZENE	.369	.041	.001	.026	.018	.456
29	C3-BENZENE	.122	.000	.001	.013	.000	.136
364	BENZOFURAN	.098	.000	.000	.000	.000	.098
30	C3-BENZENE	.422	.035	.003	.058	.007	.525
385	ANILINE	.150	.032	.000	.006	.000	.239
31	C3-BENZENE	.091	.000	.000	.009	.000	.101
82	INDAN	.230	.010	.001	.024	.004	.269
125	INDENE	.354	.019	.001	.029	.006	.410

Table 2: SCRUB SAMPLE ANALYSIS-TOTAL GRAMS OF COMPOUND PER 100 ft^3 OF LTR GAS (TOTALS OF THE SCRUB SETS)

Compound No.	Compound Name	SAMPLES 1-3	SAMPLES 4-6	SAMPLES 7-9	SAMPLES 10-12	SAMPLES 101-103
		.0659	.0440	.0179	.0000	.0000
		.1596	.4950	.1578	.1112	.0825
999	SOLVENT	481.5288	320.0175	82.5404	207.3195	1549.8337
		.0174	.0478	.0011	.0196	.0557
		.2053	.1447	.0543	.0930	.0364
		.0000	.0386	.0125	.0079	.0000
		.0396	.0780	.0439	.0590	.0000
		.0000	.0171	.0067	.0000	.0082
1	BENZENE	15.1490	14.3839	12.8909	17.8191	58.8526
45	THIOPHENE	.0821	.0726	.0735	.1107	.7915
		.0000	.0162	.0071	.0012	.0000
		.0000	.0310	.0000	.0454	.1285
2	TOLUENE	102.1856	138.7792	115.7428	127.2517	100.7699
54	METHYL THIOPHENE	.0369	.0646	.0659	.0900	.0000
		.0237	.0623	.0169	.0346	.0578
7	ETHYL BENZENE	.4462	.8009	.3803	.6178	.3401
6	P AND M-XYLENE	1.1335	1.9830	2.2421	1.5764	1.0254
58	DIMETHYL THIOPHENE	.0151	.0346	.0308	.0108	.0000
59	DIMETHYL THIOPHENE	.0060	.0258	.0229	.0069	.0000
340	STYRENE	.0193	.0407	.0423	.0129	.0000
5	O-XYLENE	.2553	.4709	.5512	.3523	.1730
25	C3-BENZENE	.1652	.3355	.4557	.2500	.0000
26	C3-BENZENE	.0653	.1378	.1787	.1202	.0000
27	C3-BENZENE	.0819	.1777	.2516	.0760	.0000
28	C3-BENZENE	.0965	.2803	.4560	.1119	.0000
29	C3-BENZENE	.0399	.0928	.1361	.0379	.0000
364	BENZOFURAN	.0257	.0503	.0979	.0297	.0000
30	C3-BENZENE	.1690	.3283	.5253	.2045	.0000
385	ANILINE	.0311	.1468	.2387	.0125	.1127
31	C3-BENZENE	.0295	.0665	.1007	.0233	.0000
82	INDAN	.0758	.1561	.2692	.0737	.0000
125	INDENE	.0829	.1556	.4100	.0889	.1234

Fuel

A Computerized Data Reduction System for Tabulating Data From GC Runs and Correlating Changes in Product Composition with Process Conditions or Mutagenicity

20

X

Leo Raphaelian Argonne National Laboratory X
EES/12 X
9700 S. Cass Avenue
Argonne, IL 60439

ACS Membership number MUST be indicated for at least one author 0249990E120 IG1 AR5812 SM 1
(Please use number as it appears on C&EN mailing label)

Argonne National Laboratory

X Analytical Chemistry

No

A COMPUTERIZED DATA REDUCTION SYSTEM FOR TABULATING DATA FROM GC RUNS AND CORRELATING CHANGES IN PRODUCT COMPOSITION WITH PROCESS CONDITIONS OR MUTAGENICITY, Leo A. Raphaelian, Argonne National Laboratory, 9700 S. Cass Ave., Argonne, IL 60439.

Even with the sophisticated analytical instrumentation presently available, a complete and exhaustive analysis of the organics in energy or environmental samples is not only time-consuming but also difficult due to the complexity of such samples. More often, one is interested in such specific tasks as identifying and quantifying the major components or determining the PNAs present or determining which component or components in a fraction are causing mutagenicity.

In this study, software was developed to carry out, with a computerized data system, the rapid analysis of the major components of a complex mixture of organic compounds. With the software, one can also present data from several runs in a table in a variety of forms (%, ppb, µg/L, area counts, etc.), that is useful for making comparisons. Moreover, statistical analysis of the data can be performed such as regression analysis on the variation in product composition as a function of such variables as process conditions or on the variation in mutagenicity as a function of product composition. Such manipulations and presentations of data are rapidly handled by the data system.

A outline is presented of the software required for performing the matching of data from several GC runs, doing the adjustments for dilution factors, response factors, retention time drift, etc., multiplying in factors for presenting data in ppb, %, µg/L, etc., and doing regression analysis on the data from several runs. Data will be presented to demonstrate the performance of the data reduction system.

LIQUID CHROMATOGRAPHIC CLASS SEPARATION AND HIGH RESOLUTION GAS CHROMATOGRAPHY OF SHALE OIL POLAR COMPOUNDS

Peter C. Uden, Raymond J. Crowley, William F. Joyce and Sidney Siggia

Department of Chemistry, GRC TWRA, University of Massachusetts, Amherst, MA 01003

The largest reserves of fossil fuels in the United States lie in coal and oil shale. Yen (1) has estimated the United States petroleum reserves from shale in the Green River Formation (located in Colorado, Utah and Wyoming) to be some 600 billion barrels. This figure is based on an oil yield of 25-100 gallons of oil per ton of raw shale. Oil shale has been broadly defined as any shallow rock yielding oil in commercial amounts upon pyrolysis. The major organic component of shale is known as 'Kerogen' which is a high molecular weight macromolecular material that is insoluble in most organic solvents. Shale oil is generated when raw shale is heated to temperatures ca. 500°C in a process known as 'retorting.' The high temperatures cause breakdown of the macromolecular kerogen into smaller organic molecules, producing oil.

The organic content of oil shales, and the subsequent amount of oil produced, is dependent upon the source of the original organic precursor species (2). If it is from a terrestrial source the kerogen formed will be closely related to coal and will yield very little oil upon pyrolysis. An example of this type of deposit is in the Chattanooga shales of the Tennessee-Georgia area which yield only about 10 gallons per ton upon pyrolysis. If, however, the kerogen was formed from organic matter in a marine or lacustrine environment, the shale will yield substantial amounts of oil. Shale of this origin is typical of the Green River shales which may yield 25-100 gallons of oil per ton. A second source of organic substances in shale are the bitumens. These are defined as the extractable organic material originally present in the rock. One-three percent of the organic content of Green River shale is present as bitumens. Important differences in chemical composition exist between crude shale oils and typical petroleum crudes; for example in the high olefin content of middle distillates for the former (30 - 50%) with nitrogen content in the 1.8 - 2.1% range, in contrast to the 0.3 - 0.4% range of natural crudes.

To date, no large scale retort has been built in the United States; the only production has been from small pilot plants. However, with the world's dwindling petroleum reserves the prospects for development of this resource now seem favorable. Development must take place in the areas of mining of the raw shale, production of the oil, disposal of the spent shale, and refining of the crude shale oil. The development of new analytical techniques to characterize and evaluate each step in the production of the oil is also needed. In terms of refining operations a careful monitoring of the nitrogen and oxygen containing compounds is needed. In general, shale oil must be modified by hydrotreating or some other process to make it suitable for refining. Without detailed characterization of the hydrocarbons and heterocompounds at each step of the process it is not possible to determine the probable origin of hydrocarbons in the final product. Also, from an environmental standpoint monitoring of organic and inorganic components in both the raw crude and the spent shale is vital. Shale oil also has potential as a petrochemical source due to the diversity of compound types and functionalities present. As a result there is a need to develop new analytical techniques which quantitate shale oil by chemical compound class and in terms of each compound individually.

Crude oils generally comprise four chemical compound classes: (i) asphaltenes (hexane insolubles); (ii) alkanes/alkenes; (iii) aromatics; and (iv) polars (N- and O-containing compounds. Extensive separation schemes for petroleum have been

reported in the literature (3,4). These separations generally deal with distillate fractions which are important to product characterization. The scheme that is most widely employed for the class separation of crudes is the ASTM Clay-Gel Adsorption Chromatographic Method (5). However, the majority of the methods reported for the analysis of petroleum are unsatisfactory for samples containing olefinic unsaturation or non-hydrocarbon material (N- and O-containing compounds), and since shale oil has a high concentration of both these classes either modifications or existing techniques or the development of new techniques is required.

Numerous separation schemes have been reported in the literature for the alkane/alkene, aromatic, and polar fractions of shale oil which rely on conventional gravity columns packed with silica or alumina or on solvent/solvent extractions but these methods are both time consuming and inefficient. An ideal separation scheme should have the following properties: (i) it should be rapid and highly efficient; (ii) it should require minimal sample preparation; (iii) it should consist of a minimal number of steps; and (iv) it should be reproducible. Preparative high pressure liquid chromatography on microparticulate bonded stationary phases meets the criteria noted above. Suantoni et al. (6) performed hydrocarbon group type analysis on petroleum distillate fractions by HPLC on μ-Porasil. Saturate and aromatic fractions were eluted with hexane while the polar fraction was eluted with methylene chloride. Dark et al. (7) employed preparative HPLC to evaluate a hydrotreated coal liquefaction aromatic fraction by ring number. In our study, shale oil from different retorting processes has been resolved into individual chemical compound classes by HPLC using preparative columns packed with i) cyano-bonded and ii) amino-bonded stationary phases. Following the separations, each fraction was further characterized by high resolution gas chromatography and by analytical HPLC. GC detection was by nitrogen specificity, UV absorption and mass spectrometry.

Experimental

Analytical and preparative HPLC was carried out with a gradient system (Laboratory Data Control - Constametric I and II G pumps and 1601 gradient former), with preparative (20 μm) and analytical (10 μm) bonded cyano (LC-8) and bonded amino (LC-9) (Johns Manville Corp.). UV detection was employed. Gas chromatography was carried out on Varian Model 3700 and 2760 instruments using fused silica or glass wall-coated capillary columns. GC-MS was performed on a Hewlett-Packard 5985A mass spectrometer system. Shale oil samples were obtained from The Oil Shale Corporation (TOSCO II above ground retort), the Paraho project and a modified In Situ process (DOE, Laramie, Wyoming). Samples were pre-treated before liquid chromatography by dissolution in hexane, filtration of asphaltenes and removal of hexane prior to injection.

Results and Discussion

The chromatographic conditions for the shale oil class separation utilizing the cyano-bonded LC-8 column have been reported (8). In general isocratic hexane elution was followed by an exponential gradient to 100% n-butanol. The overall class elution sequence was i) alkanes/alkenes, ii) aromatics, and iii) polar compounds. A 20 μm preparative column could be readily re-equilibrated with hexane after elution of oil samples.

Gas chromatography of alkane/alkene fractions, carried out on a 25 meter SP-2100 200 μm bore fused silica column (Hewlett Packard), clearly exhibited characteristic homologous hydrocarbon series from C_{10} - C_{29} (8). Prominent doublets seen at each carbon number sequenced 1-alkenes and n-alkanes, alkene content for TOSCO II oil being much greater than in Paraho or In Situ oils.

Aromatic fractions were chromatographed on the same fused silica column and also on a glass Carbowax 20 M wall coated capillary column (8). Figure 1 shows

a comparison of the aromatic fraction of TOSCO II oil from the cyano-bonded column with a number of aromatic standards, obtained on the SP 2100 fused silica column from which systems of up to 5 rings may be eluted. No alkane/alkene pattern is discernible on this fraction and a minimum of 95% resolution of the aromatic fraction is apparent.

Carbowax 20M was the preferred phase for the general characterization of the polar HPLC fraction. A nitrogen specific non-flame thermionic detector (TSD) proves helpful in determining the nitrogen content of this fraction and a typical dual detector chromatogram is shown in Figure 2 for Paraho shale oil. The nitrogen species are primarily heterocyclic compounds with a maximal concentration in the 3-4 ring area, at a somewhat higher molecular weight range than TOSCO II or In Situ. The nitrogen content of the three oils decreases in the order Paraho > TOSCO II > In Situ, as shown both by microanalysis and TSD peak envelope areas. The In Situ oil has the lowest nitrogen content of the oils, attributable to the high degree of coking losses present in this retort process. The larger shale blocks heat slowly, causing low effective retorting temperatures and as a result extensive liquid phase polymerization occurs. Since the N-compounds selectively condense and polymerize they are in effect removed from the oil.

Identification of compounds by GC alone relies on the resolution of the columns and the ability to match retention times against standards. For full identification and characterization GC-mass spectrometer interfacing has great advantages particularly in a field as complex as petroleum analysis where it has been heavily used (9,10). To illustrate the utility of capillary gas chromatography/mass spectrometry with selective ion monitoring in characterization of shale oil classes resolved by the preparative HPLC procedures, two typical analyses are presented. Capillary GC was performed on an OV-101 WCOT fused silica column (19 meter x 200 micron i.d., Quadrex), the capillary being connected directly to the ion source of the mass spectrometer via a Pt/Ir transfer line. Sample introduction was by splitless injection with 1 mL/minute helium carrier gas flow. Mass spectral scans were at 70 eV electron impact ionization voltage, being recorded between 50-350 AMU at a scan rate of 128.6 AMU/sec.

Shale oil aromatic fractions in general show predominantly alkyl substituted benzenes, naphthalenes, indans and tetralins. Alkylbenzenes are characterized by a series of ions corresponding to masses with an empirical formula $C_6H_5C_nH_{2n+1}$ (77, 91, 105, 119, 133, 147, 161, etc.). The most characteristic ions in these spectra correspond to the rupture of the benzylic bond of the largest alkyl group. This cleavage produces the characteristic $C_7H_7^+$ tropylium ion in the case of phenylalkyls or ions of higher mass/charge ratios in the case of polyalkylbenzenes. Total ion current and specific ion detection chromatograms are shown in Figure 3 where C_4, C_5 and C_6 substituted alkyl benzenes are characterized at m/e 133, 147, and 161 respectively. An important class of compounds which co-elute with the aromatic fraction are thiophenes, which are characterized by a series of ions corresponding to masses of empirical formula $C_4H_3SC_nH_{2n}$ (83, 97, 111, 125, etc.). The total ion and selective ion chromatogram for this class is shown in Figure 4.

The total polar HPLC fraction is too complex for direct analysis by GC-MS. The polars are normally further separated by ion exchange chromatography or acid/base extraction which, however partially degrades the sample by, for example, polymerization of the pyrroles. Resolution of the polars into acidic, neutral and basic fractions by HPLC has not been reported. Using a modified amino bonded stationary phase shale oil has been separated into four chemical classes. An analytical and preparative amino-bonded LC-9 column were washed once with two column volumes of 1% phosphoric acid in water and then reequilibrated to hexane. The chromatographic conditions were isocratic elution with hexane, a step gradient to 5% acetic acid in

hexane followed by an exponential gradient to 100% isopropanol. The overall class elution sequence was i) alkanes/alkenes/1-ring aromatics, ii) polynuclear aromatics, iii) acidics/neutral nitrogen compounds, iv) basic nitrogen compounds.

Figure 5 shows a chromatogram of In Situ shale oil on an analytical amino-bonded column. Figure 6 depicts a comparison of In-Situ shale oil bases chromatographed on a 10 meter SE-30 wide bore (300 micron i.d.) fused silica column (A - obtained by acid extraction, B - obtained by preparative HPLC. Below 140°C the chromatograms show the same pattern except for some initially lower relative peak heights in A due to evaporation losses. Above 140°C curve A shows much lower relative amounts of compounds due presumably to inefficiency of acid extraction of the higher molecular weight basic nitrogen compounds.

References

1. T. F. Yen, "Science and Technology of Oil Shale," Ann Arbor Science, Ann Arbor, Mich., 1976, p.1.
2. I. D. Breger, "Analytical Chemistry Pertaining to Oil Shale and Shale Oil," S. Siggia and P. C. Uden, eds, Report of NSF Conference Workshop, Washington, D.C. 1974, p. 11.
3. L. R. Snyder, Anal. Chem., 41, 315 (1969) and citations therein.
4. J. R. McKay, J. H. Weber and D. R. Latham, Anal. Chem., 48, 981 (1976).
5. ASTM Standards, D 2007, Characteristic Groups in Rubber Extender and Processing Oils by the Clay-Gel Adsorption Chromatographic Method, part 24, p. 163 (1974).
6. J. C. Suantoni and H. R. Garber, J. Chrom. Sci., 14, 546 (1976) and citations therein.
7. W. A. Dark, W. H. McFadden and D. L. Bradford, J. Chrom. Sci., 15, 454 (1977).
8. R. J. Crowley, S. Siggia and P. C. Uden, Anal. Chem., 52, 1224 (1980).
9. E. J. Gallegos, "Analytical Chemistry of Liquid Fuel Sources," P. C. Uden, S. Siggia and H. B. Jensen, eds., Amer. Chem. Soc., Advances in Chemistry Series, V. 170, p. 13 (1978) and citations therein.
10. H. Solli, S. R. Larter and A. G. Douglas, J. Anal. and Applied Pyrolysis. 1, 231 (1980).

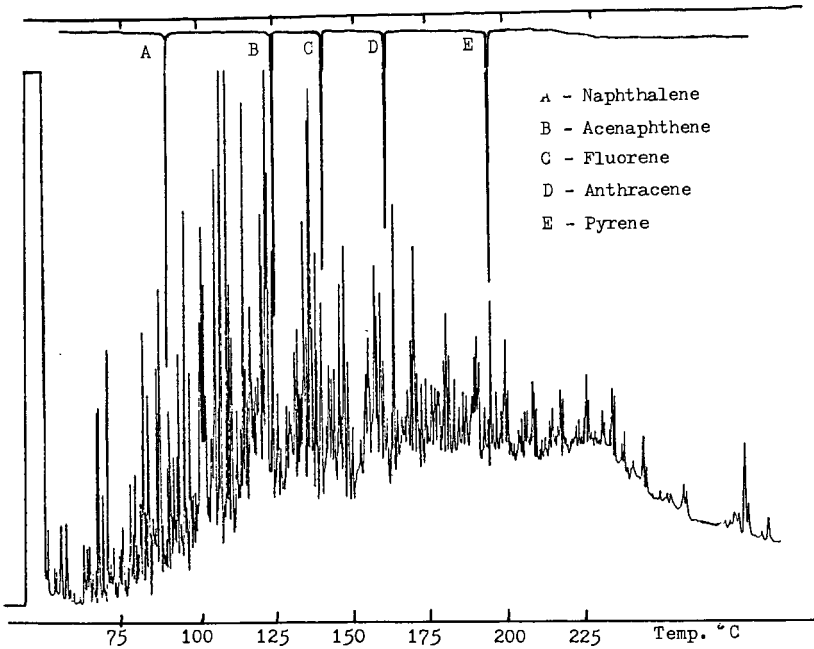

Figure 1. SP 2100 fused silica capillary chromatograms; TOSCO aromatic fraction.

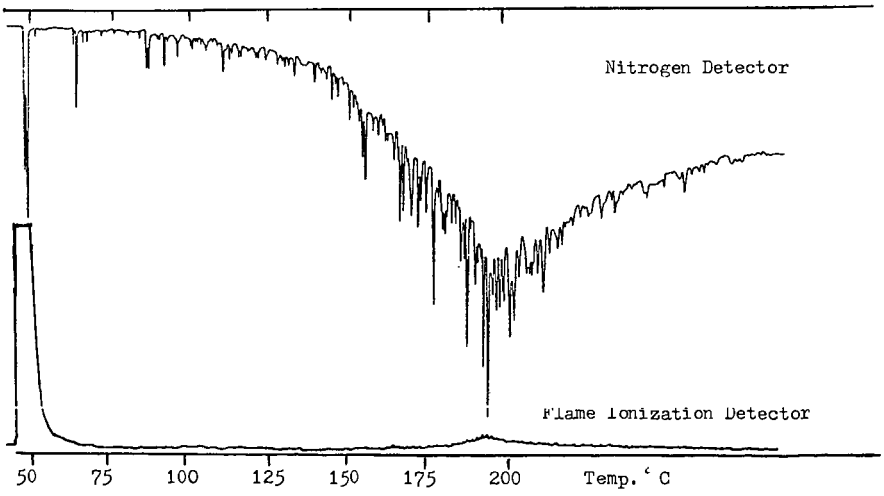

Figure 2. Simultaneous flame ionization and nitrogen specific detection of Paraho Polar fraction on Carbowax 20M glass WCOT column.

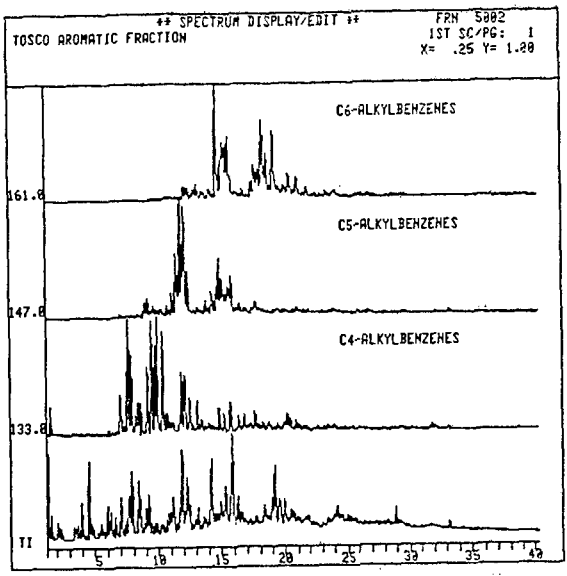

Figure 3. Tosco aromatic fraction; total ion current and selective ion chromatograms. C_4, C_5 and C_6 alkyl benzenes at m/e 133, 147 and 161.

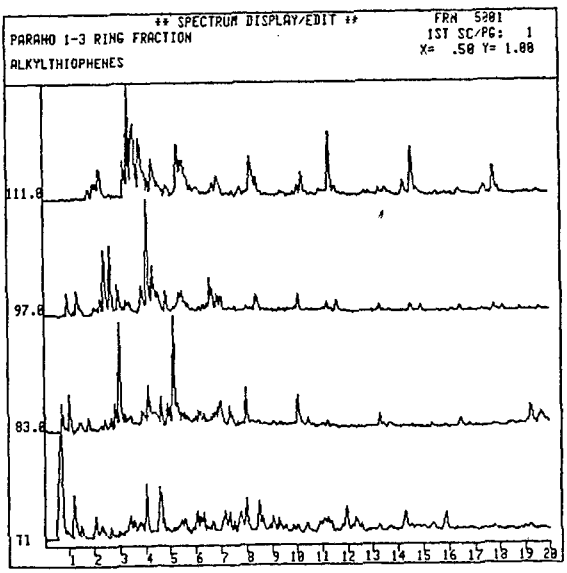

Figure 4. Paraho 1-3 ring fraction; total ion and selective ion chromatograms Alkylthiophenes $C_4H_3SC_nH_{2n}$.

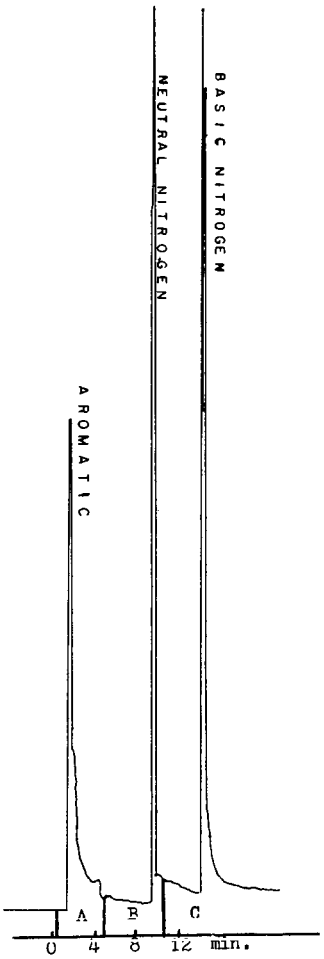

Figure 5. Chromatogram of 4 µl of In Situ shale oil (50% in n-hexane) on 10 micron LC-9 amino-bonded HPLC column. Solvents: A - n-hexane; B - 5% acetic acid/n-hexane C - isopropanol.

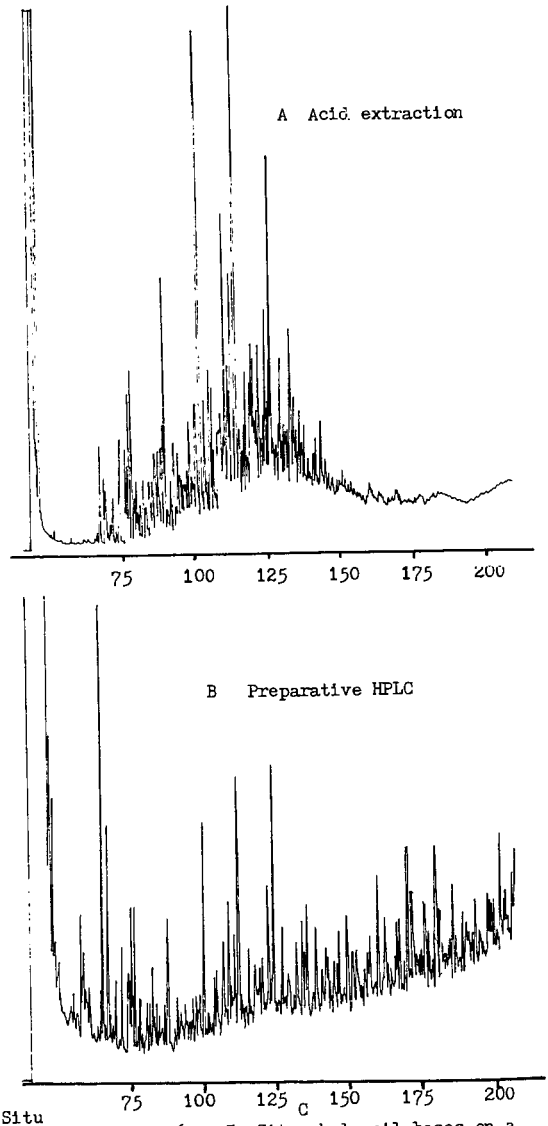

Figure 6. In Situ shale oil bases on a 10 meter SE 30 fused silica column (300 micron i,d.) A - acid extraction; B - preparative HPLC.

CHROMATOGRAPHIC SEPARATION OF FUNCTIONAL GROUP CLASSES FROM PROCESS DERIVED RECYCLE SOLVENTS

by
G. A. Odoerfer, L. R. Rudnick and D. D. Whitehurst

Mobil Research and Development Corporation, Central Research Division
P.O. Box 1025, Princeton, New Jersey 08540

INTRODUCTION

To gain a more thorough understanding of the chemistry of coal-solvent interaction in coal liquefaction and to effectively utilize a solvent for this process, detailed information on the chemical composition of the recycle solvent is needed.

The solvent, to be termed a good solvent, must have four critical qualities: it must (1) be able to donate hydrogen to the coal and/or act as a hydrogen transfer agent; (2) function as a physical solvent; (3) prevent char formation; and (4) be chemically stable and be reversibly regenerable to its hydrogen donor form. To identify and quantitatively assess the chemical structures responsible for these actions a chemical characterization method for solvents has been developed.

The development and utilization of this method for separation of a coal derived solvent in terms of different chemical functionalities was our primary objective in this study. The solvent used, Hydrogenated SRC-1 Recycle, is an example of a solvent currently utilized in coal liquefaction studies.

BACKGROUND

Several liquid chromatographic techniques can be found in the literature which potentially could be used for characterization of solvent range coal liquids.

Initially, one such method, the SESC chromatographic procedure (1,2) was employed. This method, based on chromatographic fractionation by sequential elution with specific solvents on silica gel columns, although yielding a good overview of the chemical functionalities present in the samples does not give fine separation of hydrocarbons. This led to the development of the liquid chromatographic technique (RSMC) (3), utilized by us, for the past two years, in the fractionation of coal derived solvents principally of SRC origin.

In the initial portion of this technique, similar to the SARA procedure developed for petroleum liquids (4), fractionation is performed by sequential elution liquid chromatography over basic alumina. The sequence of solvents and chemical species present in each fraction are as follows:

Fraction	Solvent	Chemical Species
1	Petroleum ether*	Saturated hydrocarbons
2	95% Petroleum ether* 5% Benzene	Monoaromatic hydrocarbons with aliphatic substituents (including tetralin and tetralin homologs)
3	85% Petroleum ether* 15% Benzene	Diaromatic hydrocarbons (naphthalene and alkyl derivatives)
4	Tetrahydrofuran; 1% Ethanol	Polyaromatic hydrocarbons Dibenzofuran and other furan derivatives Nonbasic nitrogen compounds
5	Tetrahydrofuran; 10% Water	Phenols and basic nitrogen compounds
6	(Non-eluted)	Polyfunctional Compounds

* These fractions are now being developed using heptane instead of petroleum ether.

Although this sequence allows good separation of hydrocarbons, and though an improvement over other methods, the technique is not without fault. One difficulty is that phenols, basic components and acidic nitrogen species are sometimes mixed in the same fraction (Fraction 5). Also, polyfunctional molecules, comprising as much as 20% in some process derived solvents (1,3), are generally non-elutable.

To circumvent the problem of non-eluted material a silica column in front of the alumina column could be used to absorb polyfunctional compounds which could then be eluted separately. For the isolation of acidic and basic components, an alternative method is the use of ion-exchange resins as in the SARA procedure.

Two resins, Amberlyst-26 and Amberlyst-15, manufactured by Rohm and Haas, are potentially useful for coal derived solvent separations of this type. The desirability of the Amberlyst type resins is that they are intrinsically porous and can be used for non-aqueous applications as they do not require solvent swelling to become effective. The resin, Amberlyst-26, was used in prior work (5) to isolate the heavy phenol fraction (450°F+), so designated in that it contains no simple single-ring compounds, from a recycle solvent obtained from the Wilsonville, Alabama, Process Demonstration Unit operated by Catalytic, Incorporated for Southern Services, Incorporated. The isolation was quantitative and provided a mixture of phenols and acidic nitrogen compounds (e.g. carbazole). In conjunction with this, reviewing the development of RSMC it was noted that although basic nitrogen and phenols elute in the same fraction (RSMC-5) it appeared that the retention factors were different enough that by introducing an elution solvent of 5% EtOH in THF, separation could be possible.

Considering all past work, a procedure has been developed, using sequential columns of silica, and/or alumina in combination with a strong base ion exchange resin column for separation of a coal derived solvent.

EXPERIMENTAL

Sample

The sample used was an Hydrogenated SRC-1 recycle solvent prepared by Conoco Research and Development Corp., and contained 9.67% H. It was initially distilled and the distillation fraction (400-600°F) was used for these studies.

Material

A. Reagents

n-heptane obtained from Aldrich Chemical Company.

Benzene obtained from Fisher Scientific, Fair Lawn, NJ.

Chloroform, Ether(anhydrous) and Methanol were obtained from J. T. Baker Chemical Co., Phillipsburg, NJ.

Tetrahydrofuran (uninhibited) obtained from Burdick & Jackson.

B. Ion-Exchange Resin (Amberlyst A-26)

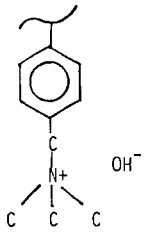

Skeletal Structure	Styrene - DVB
Ionic Function	Quaternary
Porosity (%)	27
Surface Area m^2/g	28
Exchange Capacity:	
meq/g	4.4
meq/ml	1.0
Stability	in OH^- form not above 60°C

This resin was rigorously cleaned prior to use by exhaustive washing with MeOH and THF in both Cl^- and OH^- forms.

C. Chromatographic Supports

Silica

Preparative - Prep Pack - 500 cartridges (5.7 x 30 cm) obtained from Waters Associates.

Analytical - LPS-2 37-53 μm silica gel obtained from Whatman Inc., Clifton NJ.

Alumina

Basic Alumina Woelm Activity - 1 obtained from ICN.

PROCEDURE

The overall procedure is shown schematically in Figure 1. The initial separation utilized a modified version of our SESC (1,2) procedure and was performed on a 10 g scale.

The sample, Hydrogenated SRC-1, was dispersed on glass beads (Regular 170/230 mesh) and loaded in a pre-column. Chromatographic separation was then accomplished, using a system similar to the Waters LC/Prep 500 System containing two silica cartridges, at a flow rate of approximately 50 cc/min. The fractions obtained are presented in Table 1.

Each fraction isolated in the initial step was analyzed by analytical SESC, utilizing a stainless steel column (3 x 1000 mm) and 1 cc/min flow rate, to determine the quality of the separation. Vapor-phase chromatograms of each fraction were also obtained on a Hewlett Packard 5750 Research Chromatograph utilizing a Dexsil 300 column (10% on Chromasorb; 1/8" x 10 ft) and programmed at 6°C per minute from 50°C to 350°C.

The hydrocarbons and monofunctional compounds were further fractionated by preparative chromatography over alumina. An Altex analytical glass

column (15 x 1000 mm) equipped with an adjustable plunger and a flow rate of 5 cc/min was used for development of fractions as shown in Figure 1. These fractions were analyzed by vapor phase chromatography.

Both analytical and preparative fractionations were monitored using a Pye 2 Unicam moving wire detector and an Autolab Minigrator. The data from both chromatographic separations are summarized in Table 2.

The chemical and structural nature of the components of each of these fractions are presently being examined by FIMS as well as by other spectral methods and will be the subject of a future publication.

RESULTS AND DISCUSSION

The preparative scale chromatography data indicates total recovery of sample from the silica was achieved. Analytical SESC indicates that greater than 90% of the hydrocarbon fraction is saturates and mono, di and polyaromatics. Similar analysis of heterocyclic and functional compound fractions indicate that there is some overlap but that in general the separation obtained appears to be quite good.

Preparative scale separation of both the hydrocarbon and functional compound fractions into sub-groups by RSMC method indicates good separation between chemical groups as outlined in Figure 1. The results, within experimental error, are well in agreement with analytical SESC data and thus give good indication that non basic N, O, S - heterocyclics are contained in fraction B. This fraction may then be further fractionated by ion exchange.

CONCLUSIONS

The described fractionation scheme, using sequential columns of silica, alumina and a strong base ion exchange resin, provides separation of process derived coal liquefaction recycle solvents into chemically different fractions containing various hydrocarbons, mono, di and polyaromatics

including sulfur containing heterocycles; furans; non basic N; basic nitrogen species; mono-phenols and polyfunctional compounds.

The combination of fractionation with additional study by elemental analyses, FIMS as well as by other spectral methods leads to a good chemical characterization of each fraction, and the total solvent.

The developed method allows for the circumvention of any problems normally encountered in separating the desired functionalities. The utilization of such method coupled with characterization of the chemical groups obtained allows for the gain of a more thorough understanding of the chemistry of coal-solvent interaction and can lead to a more detailed identification of the chemical composition of recycle solvents.

The latter premise is presently being investigated, for a variety of full range process derived recycle solvents (400-800°F).

REFERENCES

1. D. D. Whitehurst, M. Farcasiu and T. O. Mitchell, "The Nature and Origin of Asphaltenes in Processed Coals," EPRI Report AF-252, First Annual Report Under Project RP-410, February 1976.
2. M. Farcasiu, Fuel, 56, 9 (1976).
3. D. D. Whitehurst, M. Farcasiu, T. O. Mitchell and J. J. Dickert, Jr., "The Nature and Origin of Asphaltenes in Processed Coals," EPRI Report AF-480, Second Annual Report Under Project RP-410, July 1977.
4. E. Lecte, JACS 83, 3645 (1961).
5. D. D. Whitehurst, T. O. Mitchell, M. Farcasiu and J. J. Dickert, Jr., "The Nature and Origin of Asphaltenes in Processed Coals," EPRI Report AF-1298, Final Report Under Project RP-410, Vol. 2, December 1979.

ACKNOWLEDGEMENT

This work was conducted under Electric Power Research Institute (EPRI) Contract No. RP-1655 which is jointly funded by EPRI and Mobil Research and Development Corporation. Mrs. L. F. Atherton is the EPRI Project Manager.

The authors wish to acknowledge Dr. J. Kleinpeter, D. C. Jones, and P. J. Dudt from Conoco Coal Development Corporation for providing the sample used in this study.

Figure 1. Schematic Diagram of the Separation Scheme

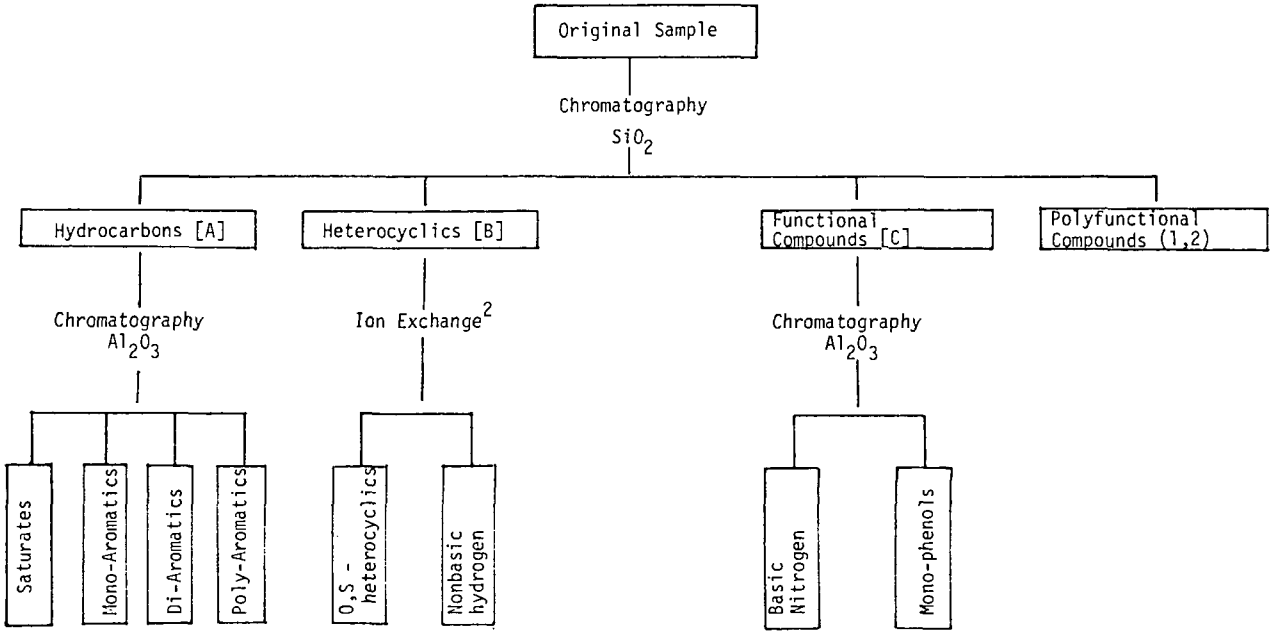

1. Fraction was combined with functional compounds for development of the procedure.

2. Actual separation not performed during procedure development. This will be an individual fraction for full range solvent separations.

Table 1

DATA FROM INITIAL PREPARATIVE CHROMATOGRAPHY

Fraction	Components	Elution Solvent	%
A	Saturates, Mono, Di & Polyaromatics	→ Heptane/ 15% Benzene	∿ 80
B	S, O, Heterocyclics and nonbasic N	Chloroform	∿ 10
C	Basic Nitrogen & phenols	$ChCl_3/Et_2O$ → $CHCl_3/EtOH$	∿ 10

Table 2

SEPARATIONS OF INITIAL FRACTIONS

Analytical SESC: (Normal Mode)

	Composition		
	Weight %	Response Factor	Normalized %
Fraction A			
Frac. 1-2	76.4	(1.81)*	90.61
" 3	1.2	(1.30)	1.00
" 4	8.4	(0.52)	2.89
" 5	8.4	(0.42)	2.83
" 6	5.5	(0.87)	3.16
Fraction B			
Frac. 3	59.4	(1.30)	78.2
" 4	28.1	(0.52)	14.8
" 5	8.7	(0.42)	3.7
" 6	3.8	(0.87)	3.3
Fraction C			
Frac. 3	2.1	(1.30)	4.4
" 4	63.6	(0.52)	53.4
" 5	8.3	(0.42)	5.6
" 6-7	21.1	(0.87)	29.6
" 8	2.1	(0.78)	2.6
" 9	2.7	(0.97)	4.2

* Response factors as determined for solvent 6663. (1,3)

RSMC OF SESC Fractions

Fraction	Fraction A %	Fraction C %
1	27.7	-
1A	8.6	-
2	10.2	-
3	11.4	-
4	15.0	7.0
4A	10.0	42.0
5	10.1	45.0
6	-	∿ 5.0*

* Non-eluted by difference

SPECIFIC METAL DETECTION IN THE SIZE EXCLUSION SEPARATION OF SEPARATION OF SOLVENT REFINED COAL

L. T. Taylor and D. W. Hausler(1)

Department of Chemistry
Virginia Polytechnic Institute and State University
Blacksburg, VA 24061

INTRODUCTION

The high sensitivity of Inductively Coupled Plasma Atomic Emission Spectroscopy (ICP-AES) for metal analysis(2) makes this system a potentially powerful metal-specific detector for liquid chromatographic separations. Several reports have recently appeared regarding a chromatography-ICP interface(3). Practically all of these investigations have involved an aqueous mode where the characteristics of the plasma are much better understood(2).

Exceptions to this are the simultaneous determination of 15 different wear metals in lubricating oils dissolved in 4-methyl-2-pentanone(4) and the separation with toluene eluent of a test mixture of ferrocene compounds via adsorption chromatography with ICP-AES as a single element detector(5). The extension of LC-ICP to a variety of organic solvents wherein organometallic compounds are more compatible has not been made. To accomplish this task one requires an efficient interface which can handle a variety of solvents with their accompanying differences in nebulization efficiencies since the plasma is extremely sensitive to changes in solvent delivery, solvent composition and solvent volatility. A change of solvent can lead to changes in background emissions, coupling of the radio frequency to the plasma and differences in optimal viewing height of the plasma. A jacketed spray chamber whereby coolant can flow or be pumped around the exterior proved to be the choice interface(6). Metal detection limits in such solvents as pyridine, chloroform, toluene and heptane have been shown to be comparable to those found in aqueous static ICP-AES operation.

Pyridine has a number of features as a solvent that makes it interesting for development both as a LC solvent and a solvent for ICP-AES. Pyridine is particularly desirable for most all synfuel materials in that it dissolves, for example, approximately 98% of solvent refined coal solid product. In addition, we have shown it to be an acceptable solvent for size exclusion chromatography (SEC) of coal derived products(7). The results of the SEC separation in pyridine of a variety of coal derived fractions utilizing ICP as a specific metal detector are described herein.

EXPERIMENTAL

An ARL (Sunland, CA) ICP-AES Model 137000 was used as obtained for metal detection. The software utilized was significantly modified from that which is commercially available and can be obtained from the authors. The argon gas flows for the nebulizer and coolant were as delivered when setting the regulators at 15 and 40 psi, respectively. The system, including torch position, was optimized for pyridine. Pyridine was purchased as a chromatographic grade solvent with no special precautions as to metal content. The pumping system for the chromatographic separations was a Waters 6000A dual piston pump (Milford, MA). The separations were achieved using a 100Å μ-Styragel column (Waters, Milford, MA) at a flow rate of either 1 or 0.5 ml/min.

All tubing between the sample injection valve (Valco, 50 μl loop) and the nebulizer was fabricated from either 316 stainless steel or Teflon. The nebulizer,

composed of Pyrex glass, was obtained from ARL. A thermostated Pyrex glass spray chamber, developed in this laboratory, to facilitate the interface and also be compatible with volatile organic solvents was utilized. The plasma was maintained at 1400 watts incident power and zero watts reflected power.

Separation of solvent refined coal by selective elution solvent chromatography (SESC)(8) was carried out by slurrying approximately 200 grams of silica gel (70-230 mesh) (MC/B Manufacturing Chemists Inc.) in one liter of dry methanol and filtering through a Whatman #1 cellulose filter. The silica gel was further washed with three 200 ml of volumes of methanol and dried at 120°C in a gravity convection oven. The chromatographic column was a 1 3/4 inch o.d. x 10 inch long stainless steel tube with fritted reducers that lead to 1/16 inch o.d. tubing outlets. To gravity pack the column, approximately 130 grams of the prepared silica gel was slurried in 500 ml of HPLC grade hexane and poured into the chromatographic column. Once drained of hexane, a sample mixture of SRC and silica gel (1:1) was dry packed onto the column head. The solvents used for the chromatography were those previously reported (8). Having isolated the nine SESC fractions, each was individually reduced in volume through rotary evaporation at 40°C (60°C for pyridine) under vacuum. Each fraction was further dried at 60°C and 5 torr for 24 hours.

For size exclusion chromatography, these SESC fractions were redissolved in pyridine at approximately 0.5 grams of fraction to 10 milliliters of solvent. The solutions were filtered through 0.45 micrometer Millipore syringe filters. Fifty microliters of each of the resulting solutions was then injected on a 100Å μ-Styragel column and eluted with pyridine.

RESULTS AND DISCUSSION

We have developed a LC-ICP interface which can simultaneously detect (ICP) and speciate (LC) up to 34 elements at concentrations between 10 ppm and 0.5 ppb depending on the element and the matrix. A variety of organic matrices have been successfully used. Preliminary experiments using this interface have monitored 15 elements simultaneously (Al, Ca, Cd, Co, Cr, Cu, Fe, Hg, Mg, Mn, Mo, Ni, Ti, V and Zn). The mode of separation of process derived coal liquefaction solvents and Amax solvent refined coal has been size exclusion chromatography.

The metals present in a process solvent obtained from the SRC Wilsonville, AL facility and metal distribution according to effective molecular size are presented in Figure 1. Very low levels of Mg, Mn, Ti, Cd and Hg are observed. A rather broad molecular size distribution is found for Mg; whereas, Ti appears to be more monodispersed with an average molecular size via retention volume approximately equivalent to a 500 molecular weight n-alkane. A definite bimodal distribution is observable for Mn. Of the elements which were monitored, Cr surprisingly exhibits the largest concentration unlike the other coal-derived materials which have been examined via LC-ICP. The source of Cr in this case may well be from corrosion of the reactor equipment. Both Cr and Fe show a similar molecular size distribution with most of the material eluting near the totally excluded volume. Cu and Zn, on the other hand, show a much smaller size distribution with Cu having at least two groups of "sized" species; while, Zn appears to be incorporated in a relatively small number of single "sized" species. The remainder of the elements monitored did not shown detectable peaks above ambient noise level.

A moderately hydrotreated process solvent that had been previously separated into four distillation ranges: IBP (initial boiling point) -800°F, 400-800°F, 400-600°F and 600-800°F was subjected to SEC-ICP. Figure 2 shows three such distillation cuts

separated on a 100Å μ -Styragel SEC column using pyridine as the eluting medium. Since the 400-600°F and the 600-800°F fractions were taken from the ICP-800°F distillate, one would hope that these should be additive. Indeed, if one looks at the Fe "metallogram" of the 400-600°F cut, one sees a distribution that is bimodal with the predominant fraction being of smaller molecular size, while the 600-800°F Fe metallogram is likewise bimodal but the predominant fraction being of larger molecular size. The original IBP-800°F distillate also appears to be bimodal but with equal distribution of smaller and larger molecular sized compounds. It is also satisfying that the higher temperature range distillate exhibits an increased concentration of larger (less volatile) compounds.

Zn appears to be concentrated in the lower temperature distillate. The higher temperature distillate has smaller sized Zn compounds although the reason is not clear. This may imply that these Zn containing species are more polar and hence more highly associated. No detectable levels of Mn were observed in the SEC of both the 400-600°F and 600-800°F cut. The IBP-800°F cut, however, showed a low Mn lost in the distillation or severely diluted as a result of the distillation. On the other hand, Cu is retained upon distillation and is equally divided between the two more narrow boiling cuts. Of the 15 elements monitored, only the metals shown in Figure 2 were above the minimum detectable limit.

ICP alone will not yield speciation information; coupled, however, with specific types of chromatography some knowledge of the nature of metal species can be obtained. A preparative separation of SRC solid product via polarity on silica gel has been performed employing selected elution solvent chromatography (SESC) into nine fractions, designated saturates (#1), aromatics (#2), polar aromatics (#3), simple phenols (#4), nitrogen heterocycles (#5), highly functional molecules (#6), polyphenols (#7), and molecules that possess increasing oxygen and nitrogen content (#8 and #9). We found significant quantities of a variety of metals in each SESC fraction (9). After removing the eluting solvent, we separated each SESC fraction further according to effective molecular size by elution with pyridine with the ICP "on-line" to obtain fifteen "metallograms", one for each metal and SESC fraction monitored.

Copper, iron and zinc metallograms show the richest variety of metallic species detected (Figure 3). All nine SESC fractions contain varying amounts of these metals. SESC #1 and #8 have the highest concentration of copper; SESC #1 and #6 have the highest concentration of iron; and SESC #8 has, by far, the highest concentration of zinc. The multiple chromatographic peaks registered in most metallograms testify to the wide variety of organically bound copper, iron and zinc species in the SRC studied. The sharpness of many of the peaks, especially in the case of zinc, suggests exclusive elution of closely related components or even of just a single species. Elution of iron species commences at the totally excluded volume for each SESC fraction. This is not the case with copper and zinc; for these metals, molecules of size less than an $n\text{-}C_{35}$ alkane are predicted to elute. Iron-containing materials eluting in highly polar SESC fractions are large "sized" entities, while a much broader "sized" distribution is observed in less polar fractions (SESC #1-6). Major copper and zinc peaks eluting from SESC #1 correspond to approximately 1.3 ppm (Cu) and 0.4 ppm (Zn). Other relatively sharp peaks where concentration can be estimated are provided in the copper metallogram derived from SESC #7. Progressing to smaller "sized" species (increasing elution volume) the copper concentrations are approximately 0.8, 2.3 and 1.1 ppm, respectively. Since SESC #7 is reputed to be polyphenols, it seems reasonable to suggest that these copper signals are due to elution of copper phenolates. The zinc metallogram derived from SESC #6 exhibits the largest number of discrete peaks. Four zinc containing species in this highly functional fraction are revealed upon separation by effective molecular size. The

apparent largest "sized" zinc compound elutes at the totally excluded volume and represents approximately 6 ppm zinc. Elution of the species at 10.5 ml is representative of a molecule corresponding to n-decane in size. SESC #8 has a zinc concentration of about 45 ppm, all of which apparently elutes in a relatively narrow band corresponding in size to an n-C_{24} alkane. Finally, an interesting bimodal separation of totally excluded and selectively permeated (~0.25 ppm) zinc-containing material is observed in the size exclusion separation of SESC #9.

A capability to perform metal analyses in pyridine and other organic solvents and the interfacing of LC and ICP provide researchers a tool for metal speciation in synfuels. Further work must be undertaken to ascertain specific chemical environments of each metal. However, solubility of these materials in a wide variety of organic solvents, repeated filtration through 5μm filters, and selective separation via two chromatographic procedures (SESC and SEC) indicates that metals in organic combination are present(10).

Acknowledgement - The generous financial assistance provided by Department of Energy Grant DE-AC22-80PC30041 and the Commonwealth of Virginia is appreciated.

REFERENCES

1. Present address: Phillips Petroleum Co., Bartlesville, OK.

2. V. A. Fassell and R. N. Kniseley, Anal. Chem., 46, 110A (1974).

3. D. M. Fraley, D. Yates and S. E. Manahan, Anal. Chem., 51, 2225 (1979).

4. V. A. Fassell, C. A. Peterson, F. N. Abercrombie and R. N. Kniseley, Anal. Chem., 48, 516 (1976).

5. C. H. Gast, J. C. Fraak, H. Poppe and F.J.M.J. Maessen, J. Chromatogr., 185, 549 (1979).

6. D. W. Hausler and L. T. Taylor, submitted for publication.

7. D. W. Hausler, J. W. Hellgeth, H. M. McNair and L. T. Taylor, J. Chromatogr. Sci., 17, 617 (1979).

8. M. Farcasiu, Fuel, 56, 9 (1977).

9. W. M. Coleman, P. Szabo, D. L. Wooton, H. C. Dorn and L. T. Taylor, Fuel, 56, 195 (1977); W. M. Coleman, P. Perfetti, H. C. Dorn and L. T. Taylor, Fuel, 57, 612 (1978); D. W. Hausler and L. T. Taylor, Fuel, 59, 0000 (1980).

10. H. J. Gluskoter, Adv. Chem. Scr., 141, 1 (1975); P. Zubovic, Adv. Chem. Ser., 55, 221 (1966); R. R. Ruch, H. J. Gluskoter and N. F. Shimp, "Environmental Geology Notes", Illinois State Geological Survey, No. 72, 1974.

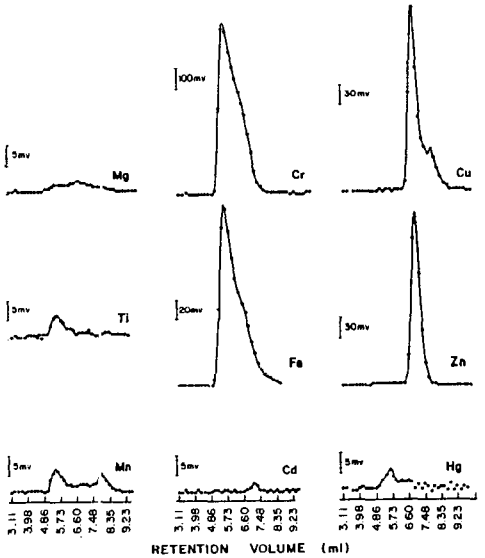

Size Exclusion Chromatographic Metallogram of Wilsonville Process Solvent employing specific metal detection and pyridine elution

FIGURE 1

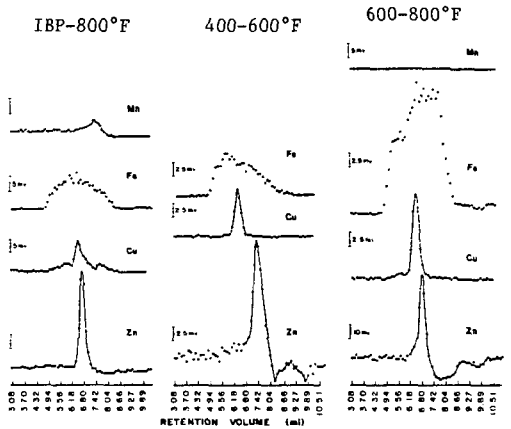

Size Exclusion Chromatographic metallogram of hydrotreated process solvent employing specific metal detection and pyridine elution

FIGURE 2

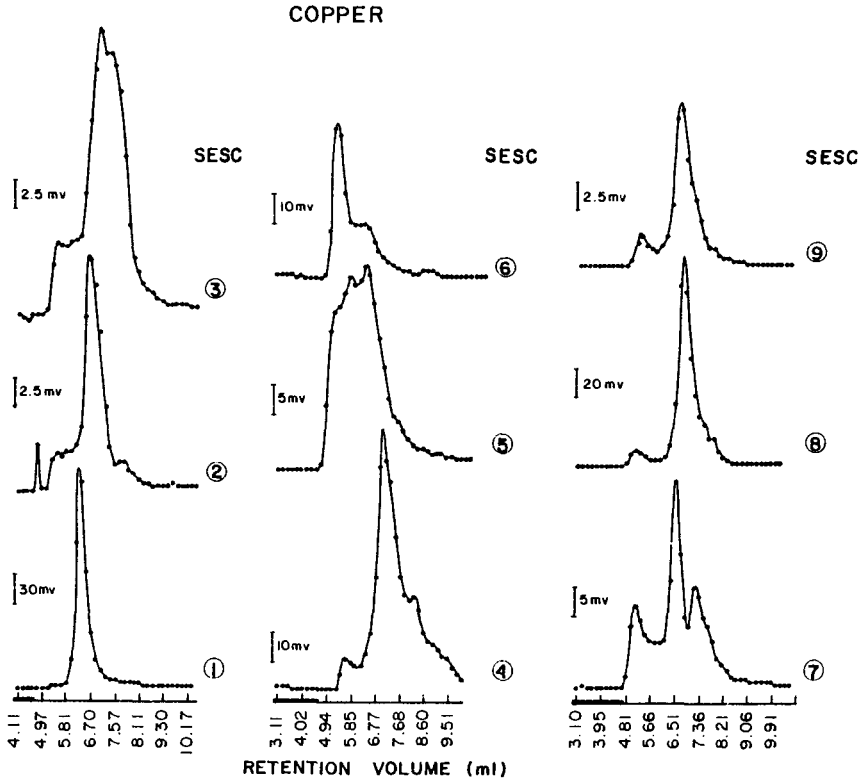

Size Exclusion Chromatographic metallogram of nine SESC fractions employing pyridine elution and Cu detection

FIGURE 3A

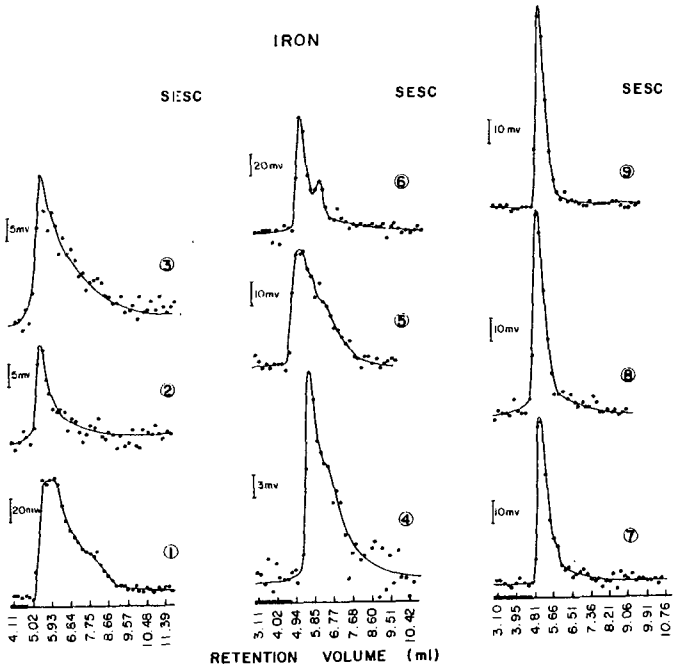

Size Exclusion Chromatographic metallogram of nine SESC fractions employing pyridine elution and Fe detection

FIGURE 3B

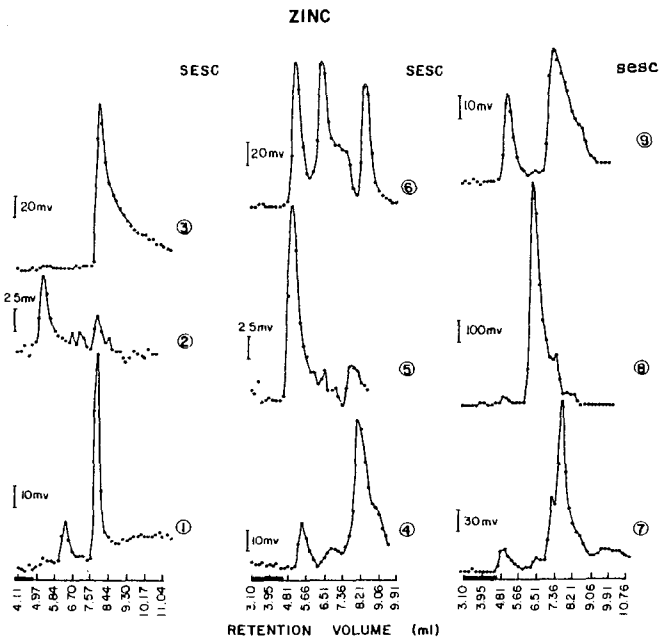

Size Exclusion Chromatographic metallogram of nine SESC fractions employing pyridine elution and Zn detection

FIGURE 3C

Pyrolysis/$(GC)^2$/MS as a Coal Characterization Technique

B. Mason Hughes and J. Troost

Gulf South Research Institute
P. O. Box 26518, New Orleans, Louisiana 70186

R. Liotta

Exxon Research and Engineering Company
Corporate Research Science Laboratory
P. O. Box 45, Linden, New Jersey 07036

INTRODUCTION

With the commercial availability of mini-pyrolyzers coupled with gc/ms intrumentation, many studies[1-7] have been conducted on fossil fuels. However, the studies conducted to date have been limited in two important areas. The first is the lack of a suitable quantification method to describe the patterns of pyrolysates formed and the second is the absence of absolute quantitative yields for the major degradation products. These two features have been included in this present work to demonstrate a generally applicable method for quantifying a wide range of coal pyrolysis products. By employing rapid pyrolysis, that is, a 20°C per millisec heat-up rate with a helium gas sweep, many secondary reactions are avoided. Many of the volatilized coal pyrolysates are swept out of the Pyroprobe hot zone quickly enough so that they still retain much of their structural identity. Analysis of the major chromatographable compounds, therefore, provides some information of the original coal structure.

EXPERIMENTAL

Py/$(GC)^2$/MS System

A Chemical Data Systems Pyroprobe 100 solids pyrolyzer was interfaced to the conventional capillary chromatographic injection port of a Hewlett-Packard 5993 $(GC)^2$/MS/DS system, using glass-lined metal tubing. Alltech 50-meter SCOT SE-30 and OV-17 glass capillary columns with 0.5 mm internal diameters were installed in-line with the pyrolysis interface. Less volatile degradation products were cold trapped on the head of the SE-30 capillary column by maintaining the column oven at either 0° or 10°C. In studies where volatile degradation products were analyzed, volatile degradation product peak widths were minimized by continually sweeping the 5993 injection port with approximately 16 mls/min backflush helium flow, while approximately 4 mls/min helium flow through the OV-17 capillary column was maintained. In addition, the 1.5 mm x 6 cm glass-lined interface line between the pyrolyzer and the capillary column contained several hundred milligrams of Porapak Q Chromatographic support to improve chromatographic separation of the most volatile degradation products.

The pyrolyzer interface and gas chromatographic injection port were maintained at 240°C and 260°C, respectively. A coil type pyrolyzer was used. Solid coal samples were placed in 3 mm i.d. quartz tubes and these tubes inserted in the pyrolysis coil. For the quantitative analysis of volatile degradation products, coal samples were placed on a small amount of quartz wool within the quartz tube and weighed before and after pyrolysis. The coil was heated to 1000°C with a heating ramp of 20°C/msec and maintained at 1000°C for 10 sec.

Previous studies[8,9] reported that a coil temperature of 1000°C results in a sample temperature of approximately 750°C, when similar conditions are used. Degradation products from the inert gas pyrolysis of coal were chromatographed using either a 6°C/min or 8°C/min chromatographic oven heating rate from the starting, subambient temperature, to 250°C.

Quantitative yields of volatile degradation products were determined by using a 0.5 ml gas sampling loop in-line with the pyrolyzer. Characteristic mass responses were determined daily by injecting known volumes of CO_2, CO, CH_4, C_2H_6, C_3H_8, and C_4H_{10} quantitative gas standards, which were supplied by Matheson.

Mass spectral data were stored for later analysis and interpretation using the standard Hewlett-Packard data acquisition system. The mass spectrometer data system was scanned from 35-450 amu for the analysis of less volatile degradation products. Information on volatile degradation products was obtained by scanning the instrument from 10-450 amu. Typical mass spectrometric operating conditions resulted in complete 70 eV mass spectra being obtained every 2 seconds.

Nitrogen compounds were not analyzed in this study. The Illinois No. 6 and Rawhide coals were ground to -80 U.S. mesh and dried at 100°C under vacuum. No further preparation was performed. The compositional analysis of these two coals have been reported[10].

RESULTS AND DISCUSSION

Table I gives a summary of all pyrolysis products identified. A large number of isomers was observed for many methyl-substituted degradation products. Since mass spectra of various isomers are generally very similar, no attempt was made to identify specific isomers using the retention times of known isomers, except for the methyl and dimethyl phenols. In addition, compounds which are identified to contain several methyl groups could also be ethyl or propyl substituted. Therefore, all alkyl-substituted degradation products are listed as isomers under the corresponding methylated compounds.

As can be seen from Figure 1, the total ion chromatogram of the coal pyrolysis products consists of several regions where several degradation products are not completely resolved chromatographically, even though capillary chromatographic separation of the degradation products is used. However, this problem can be minimized if rather than the total ion chromatogram, selected ion chromatograms are used for quantitation. An example of the use of this approach in the quantification of phenols can be seen in Figures 2 and 3. Figure 2 shows the total ion chromatogram, along with molecular ion chromatograms for phenol and methyl phenol isomers produced in the degradation of Illinois No. 6 coal. As can be seen from the comparisons of these molecular ion chromatograms with the total ion chromatogram, only phenol and methyl phenols give peaks at the respective retention times in the ion chromatograms, while the total ion chromatogram yields a large number of overlapping peaks because of the overlapping elution of various degradation products. Figure 3 shows an isometric display of mass spectral data for masses 90-110 at the same retention region shown in Figure 2. Response of masses 94 and 95 are seen to be characteristic of phenol, masses 105 and 106 of trimethylbenzenes and masses 107-109 of methylphenols.

Table I is a summary of the pyrolysates from each coal. The identification of the characteristic mass ions used for quantification of each compound, the characteristic ion percent of total ionization, and the characteristic ion areas, normalized to naphthalene in the Py/$(GC)^2$/MS analysis, are listed for Illinois No. 6 and Rawhide coal degradation products. The values that are given for normalized characteristic ion areas are an average of two Py/$(GC)^2$/MS analyses for each coal sample type and the range of values for each compound in each pyrolysis can be obtained from the variance of each compound listed in the table.

Qualitative differences emphasized by arrows in Figure 1 are also seen in the quantitative comparison of coal degradation products. Good reproducibility, as measured from the variance of each degradation product is obtained for the quantities of all degradation products measured using this technique. For pyrolysates in this volatility range, the quantitative differences observed between the Illinois No. 6 and Rawhide coals are due solely to sulfur-containing heterocyclic compounds. The nonsulfur-containing degradation products are quantitatively similar for the two coals. The one class of compounds which shows the largest variablility in the quantitative determinations of duplicate analyses are the phenols. This is likely due to the fact that these acidic compounds are difficult to chromatograph. While most other degradation product characteristic ion areas vary by 10-15 percent, the phenols typically vary by as much as 30 percent.

High-Volatility Degradation Products

Since a detailed quantitative and qualitative comparison of the relatively nonvolatile degradation products, described above, gives useful information for the characterization of these coals, the same approach was taken to evaluate the differences in the more volatile pyrolysates produced in the inert gas degradation of them. Figure 4 shows the comparison of total ion chromatograms for masses 10-450, produced from the Py/$(GC)^2$/MS analysis of these coals. As in Figures 1 and 2, the numbers listed above each peak refer to peak numbers in Table I and II. Isometric displays of masses 10-46 for Illinois No. 6 and Rawhide coal degradation products are given in Figures 5 and 6. These displays show that methane, carbon monoxide, and carbon dioxide are the degradation products responsible for the major ionization in this mass range. Also, these figures show that the yields of carbon monoxide and carbon dioxide relative to methane are larger in Rawhide coal than in Illinois No. 6. The relatively larger mass 12 shown in Figure 6 is due to C^+ from carbon dioxide and is, therefore, also relatively larger in the mass spectra produced from Rawhide coal degradation products due to the increased yield of this degradation product.

The shoulders on the mass 28 peaks in Figures 5 and 6 show that the normalized area listed for mass 28 as the characteristic ion for carbon monoxide is from more than one compound. The ion chromatograms of masses 25-30 shown in these figures demonstrate that in addition to carbon monoxide, ethane and ethylene are also important degradation products which can produce mass 28. Therefore, unlike other characteristic ion areas listed in Table II, that listed for carbon monoxide is probably due in part to carbon monoxide with some contribution from ethane and ethylene.

To emphasize other degradation products, methane, carbon monoxide, and carbon dioxide degradation products have been excluded from Figure 7 by starting the mass summation range at mass 46. In addition to these three major degradation products, the broad elution of water, which is identified by an asterisk in Figure 3, is also eliminated in Figure 7. The peaks labeled with arrows in Figure 7 are sulfur-containing degradation products and are major pyrolysates which differentiate these two coals (Table II).

Quantitative Yields of Degradation Products

In addition to the normalized yields of products based upon characteristic ion areas, also reported in Tables I and II are the percent of total ionization which these characteristic masses represent in the total mass spectrum of each compound quantified. Since 70 eV electron ionization cross sections of most compounds with masses greater than 70 amu is constant, the absolute naphthalene yield given in Table IV and the compound class yield, relative to naphthalene, given in Table III, can be used to estimate the quantitative yields of all minor degradation products summarized in Table III. If the total relative characteristic ion yields in Table III are normalized to the absolute naphthalene yield of approximately 1 ug/mg of coal, then the sum of all compound classes, in µg/mg of coal would be 27.5 and 25.8 for Illinois No. 6 and Rawhide, respectively. If these yields are added to the major degradation products listed in Table IV, a total of 66.5 and 91.3 ug/mg coal are measured using this analysis technique. Both Illinois No. 6 and Rawhide coals loose approximately 50 percent of their total weight in the 750°C pyrolysis. Therefore, of the weight lost by these two coal samples, approximately 13 and 18 percent is accounted for in the chromatographable degradation products. The data in Table III shows that major differences in the pyrolysates of the two coals appear to result in the formation of large amounts of thiophenes and benzothiophenes.

All other degradation products, with the exception of the carbon oxides are similar for these different ranked coals. The striking similarities of the isomer distributions for the methylthiophenes, dimethylbenzenes, dimethyl thiophenes, methyl phenols, dimethyl phenols, methyl naphthalenes, trimethyl benzenes, dimethyl naphthalenes and methyl dibenzofurans, produced from both coals indicate that the organic structures producing these degradation products in the two coals are very similar.

One additional important conclusion which may be drawn concerning the organic structure of coal is reflected in the complete absence of substituted furans. No oxygen heterocyclic degradation products were observed from either the eastern or western coals which were alkylated furans. However, about one-half of the sulfur-containing organic degradation products are the sulfur-containing analogue of furan, i.e., alkylated thiophenes. While it is possible that the alkylated phenol degradation products could be a result of furan degradation, the complete absence of alkyl furans may imply that only benzofuran structures are the important heterocyclic oxygen-containing structures present in the primary coal structure.

To measure absolute yields for the major volatile degradation products listed in Table II, a calibrated gas standard was used to calibrate the $(GC)^2/MS$ analysis system. Weighed quantities of coals in the low milligram range were pyrolyzed and the characteristic ion areas produced from the analysis of the pyrolysates were compared to this quantitative gas standard. Approximately 50 percent of the coal sample weight was lost when heated under the conditions listed above. Table IV gives the absolute yields of methane, carbon monoxide, carbon dioxide, ethane, carbonyl sulfide, and naphthalene determined in this manner.

As can be seen from Table IV, a major difference observed in the major degradation products of these two coals is in the carbon dioxide yields. From studies reported by Schafer[11,12] on the pyrolytic yields of carbon dioxide produced from brown coals at various degradation temperatures, complete decarboxylation of the coals yielding carbon dioxide was observed at temperatures greater than 700°C. In addition, he deduced that carbon monoxide, which is also produced with different yields from these two coals, is due to phenolic groups present in the coal. If this is the case then from the absolute quantities of the major degradation products shown in Table IV, it can be seen that not only does Rawhide contain approximately 3 times more carboxylic acid groups than Illinois No. 6, but also in Rawhide coal, these groups comprise approximately 3.7 percent by weight, of the total coal sample.

REFERENCES

1. C. J. Wolf, M. A. Grayson, and D. F. Fanter, "Pyrolysis Gas Chromatography of Polymers," Anal. Chem 52:348A (1980).

2. J. L. Wupper, "Pyrolysis Gas Chromatographic/Mass Spectrometric Identification of Intractable Materials," Anal. Chem. 51:997 (1979).

3. R. O. Gardner, and R. F. Browner, "Determination of Polymer Pyrolysis Products by Gas Chromatography and Gas Chromatography/Mass Spectrometry," Anal. Chem. 52:1360 (1980).

4. E. J. Gallegos, "Analysis of Five U. S. Coals," Analytical Chemistry of Liquid Fuel Sources, ed. E. C. Uden, S. Siggia, and H. B. Jensen, Advances in Chemistry Series 170, p. 13, 1978.

5. R. L. Ganson, N. E. Vanderborgh, and D. G. Brookins, "Characterization of Coal by Laser Pyrolysis Gas Chromatography," Anal. Chem. 49:390 (1977).

6. C. S. Glam, T. E. Goodwin, P. Y. Glam, K. F. Rion, and S. G. Smith, "Characterization of Lignites by Pyrolysis-Gas Chromatography," Anal. Chem. 49:1540 (1977).

7. D. A. Hickman, and I. Jane, "Reproducibility of Pyrolysis-Mass Spectrometry Using Three Different Pyrolysis Systems," Analyst 104:334 (1979).

8. F. D. Hileman, "New Techniques for the Analysis of Thermolysis Products," Dissertation, The University of Utah, 1978.

9. G. O. Tremblay, "Qualitative and Quantitative Studies of Volatiles from Coal Pyrolysis Using Mass Spectrometry and Gas Chromatography," Dissertation, The Pennsylvania State University, 1977.

10. R. Liotta, "Selective Alkylation of Acidic Hydroxyl Groups in Coal," Fuel 58, 724 (1979).

11. H. N. S. Schafer, "Pyrolysis of Brown Coals. 1. Decomposition of Acid Groups in Coals Containing Carboxyl Groups in the Acid and Cation Forms," Fuel 79, 667 (1979).

12. H. N. S. Schafer, "Pyrolysis of Brown Coals. 2. Decomposition of Acid Groups on Heating in the Range 100°C-900°C," Fuel 79, 673 (1979).

Table 1. *Characteristic Ion Areas Measured for the Major Inert Gas Degradation Products with Volatilities Less Than or Equal to Toluene Obtained from the Py/(GC)^2/MS Analysis of Illinois No. 6 and Rawhide Untreated Coals.*

Peak Number	Retention Time (Min)	Degradation Product	Characteristic Masses Used for Quantitation	Percent of Total Ionization	Illinois No. 6	Rawhide
1	7.8	Toluene	91 - 93	60.5	2.91 ± 0.48	3.16 ± 0.53
		Methyl Thiophenes	97 - 99			
2	7.9	Isomer #1			0.341 ± 0.039	0.062 ± 0.015
3	8.2	Isomer #2		66.1	0.209 ± 0.016	0.035 ± 0.008
		Dimethyl Benzenes	91-92, 105-106			
4	11.7	Isomer #1			0.193 ± 0.020	0.259 ± 0.029
5	11.9	Isomer #2		55.3	1.063 ± 0.16	1.175 ± 0.228
6	12.5	Isomer #3		55.7	0.396 ± 0.062	0.486 ± 0.096
7	12.4	Styrene	77-79, 102-105	61.5	0.667 ± 0.023	0.718 ± 0.100
8	15.0	Phenol	65-66, 94-95	54.7	1.139 ± 0.295	1.87 ± 0.65
		Dimethyl Thiophenes	111 - 113			
9	11.8	Isomer #1			0.108 ± 0.016	0.012 ± 0.007
10	12.1	Isomer #2		39.0	0.130 ± 0.008	0.017 ± 0.007
11	12.3	Isomer #3			0.085 ± 0.001	0.011 ± 0.005
12	15.1	Benzofuran and methyl styrene	89-90, 117-119	50.5	0.562 ± 0.066	0.707 ± 0.117
13	16.1	Indane	115-119		0.061 ± 0.012	0.052 ± 0.009
14	16.3	Indene	115-117	65.5	0.767 ± 0.115	0.606 ± 0.106
		Methyl Phenols	77-81, 107-109			
15	16.5	Isomer #1		58.6	0.673 ± 0.26	0.642 ± 0.333
16	16.9	Isomer #2		67.5	2.336 ± 0.76	1.923 ± 0.959
17	17.4	Methyl benzofuran	102-105, 131-133	45.6	0.374 ± 0.021	0.301 ± 0.047
18	18.3	Methyl Indene	115, 127-131	57.9	0.345 ± 0.121	0.299 ± 0.121
19	18.4	Dihydronaphthalene	115, 127-131	56.1	0.455 ± 0.140	0.425 ± 0.144
20	19.1	Naphthalene	126-129	62.0	1.000	1.000
21	19.2	Benzothiophene	134-136	53.9	0.229 ± 0.010	0.057 ± 0.032
		Dimethyl phenols	107-108, 121-123			
22	18.3	Isomer #1		51.5	0.717 ± 0.304	0.390 ± 0.236
23	18.8	Isomer #2		50.0	0.641 ± 0.246	0.434 ± 0.242
24	19.6	Dimethyl benzofuran	145-147		0.120 ± 0.027	0.148 ± 0.054
		Methyl Naphthalene	115, 139-143			
25	21.1	Isomer #1		71.1	0.768 ± 0.030	0.651 ± 0.013
26	21.4	Isomer #2		67.3	0.522 ± 0.039	0.512 ± 0.036
27	22.4	Acenaphthene or biphenyl	151-155	62.6	0.140 ± 0.006	0.117 ± 0.007
28	23.5	Acenaphthalene or biphenylene	150-153	68.6	0.413 ± 0.010	0.296 ± 0.031
29	24.5	Dibenzofuran	139, 168-170	69.8	0.157 ± 0.002	0.191 ± 0.012
		Trimethyl benzenes	105-106, 120			
30	14.6	Isomer #1			0.171 ± 0.011	0.236 ± 0.023
31	14.7	Isomer #2		61.9	0.082 ± 0.006	0.077 ± 0.019
32	14.9	Isomer #3			0.044 ± 0.002	0.064 ± 0.006
33	15.2	Isomer #4			0.255 ± 0.031	0.251 ± 0.053
34	15.8	Isomer #5			0.088 ± 0.012	0.188 ± 0.028
		Dimethyl naphthalenes	141, 155-157			
35	22.8	Isomer #1			0.167 ± 0.021	0.116 ± 0.003
36	23.2	Isomer #2 and 3			0.372 ± 0.068	0.345 ± 0.024
37	23.5	Isomer #4			0.177 ± 0.010	0.119 ± 0.007
38	23.7	Isomer #5			0.062 ± 0.012	0.066 ± 0.006

Continued

Table 1. Continued

Peak Number	Retention Time (Min)	Degradation Product	Characteristic Masses Used for Quantitation	Percent of Total Ionization	Illinois No. 6	Rawhide
		Methyl dibenzofurans	181-184			
39	26.0	Isomer #1		53.9	0.092 ± 0.005	0.083 ± 0.001
40	26.3	Isomer #2		63.5	0.203 ± 0.006	0.131 ± 0.003
41	28.2	Phenanthrene	176-179	65.6	0.397 ± 0.043	0.258 ± 0.051
42	28.3	Anthracene	176-179	68.6	0.141 ± 0.014	0.087 ± 0.017
43	25.5	Fluorene	163-167	78.9	0.344 ± 0.006	0.286 ± 0.017
44	9.7	C_8-alkene	41-43, 55-57		0.105	0.229 ± 0.064
45	10.0	C_8-alkane	41-43, 55-57		0.099	0.128 ± 0.007
46	12.8	C_9-alkene	41-43, 55-57	73.1	0.091 ± 0.006	0.214 ± 0.065
47	13.2	C_9-alkane	41-43, 55-57	55.7	0.088 ± 0.011	0.127 ± 0.009
48	15.4	C_{10}-alkene	41-43, 55-57		0.088 ± 0.0010	0.235 ± 0.070
49	15.7	C_{10}-alkane	41-43, 55-57		0.073 ± 0.015	0.119 ± 0.004
50	17.5	C_{11}-alkene	41-43, 55-57		0.075 ± 0.002	0.187 ± 0.042
51	17.7	C_{11}-alkane	41-43, 55-57		0.068 ± 0.004	0.116 ± 0.000
52	19.5	C_{12}-alkene	41-43, 55-57		0.056 ± 0.002	0.152 ± 0.033
53	19.7	C_{12}-alkane	41-43, 55-57		0.094 ± 0.033	0.106 ± 0.005
		Methyl benzothiophenes	147-148			
54	20.8	Isomer #1		48.8	0.060 ± 0.001	0.010 ± 0.004
55	21.0	Isomer #2			0.125 ± 0.007	0.018 ± 0.007
56	21.1	Isomer #3		41.7	0.094 ± 0.020	0.018 ± 0.005
57	21.2	Isomer #4		55.5	0.100 ± 0.004	0.016 ± 0.005
58	21.4	Isomer #5			0.017 ± 0.006	0.003
		Dimethyl benzothiophenes	161-163			
59	22.6	Isomer #1		58.0	0.061 ± 0.009	0.0038
60	22.7	Isomer #2			0.024 ± 0.005	0.0164
61	22.8	Isomer #3			0.100 ± 0.007	0.0066
62	22.9	Isomer #4			0.050 ± 0.001	0.0027
63	23.1	Isomer #5			0.039 ± 0.005	0.0044
64	23.2	Isomer #6			0.022 ± 0.003	0.0091
65	27.8	Dibenzothiophene	184-186	60.3	0.091 ± 0.003	--
		Trimethyl thiophenes	111, 125-126			
66	14.9	Isomer #1			0.094 ± 0.037	--
67	15.6	Isomer #2			0.034 ± 0.012	--

Table 2. Characteristic Ion Areas Measured for the Major Inert Gas Degradation Products with Volatilities Greater than Toluene Obtained from the Py/$(CC)^2$/MS Analysis of Illinois No. 6, and Rawhide Utreated Coals.

Peak Number	Retention Time ** (Min)	Degradation Product	Characteristic Masses Used for Quantitation	Percent of Total Ionization	Illinois No. 6	Rawhide
68	4.9	Methane	15-16	81.1	38.8 ± 1.6	48.5 ± 14.8
69	4.9	Carbon Monoxide	28	>90.0	25.2 ± 2.4	63.2 ± 12.0
70	5.1	Carbon Dioxide	44	60.2	7.75 ± 1.06	32.7 ± 9.1
71	-	Ethylene	No Unique Masses	-	-	-
72	5.0	Ethane	30	*13.5	0.78 ± 0.05	0.60 ± 0.13
73	5.2	Propene	42	*19.7	0.99 ± 0.00	1.03 ± 0.07
74	-	Propane	No Unique Masses	-	-	-
75	5.7	Butene	55-56	*20.0	0.60 ± 0.02	0.58 ± 0.04
76	6.0	Butadiene	53-54	*39.1	0.55 ± 0.08	0.56 ± 0.08
77	5.2	COS	60	44.5	0.46 ± 0.06	0.09 ± 0.01
78	5.2	H_2S	34	*51.8	0.56 ± 0.20	-
		Methyl butadienes	67-68	*34.7		
79	8.9	Isomer #1			0.11	0.051
80	9.1	Isomer #2			0.19 ± 0.03	0.10 ± 0.02
81	9.3	Cyclopentadiene	65-66	*57.4	0.66 ± 0.04	0.64 ± 0.04
82	12.5	Cyclohexadiene (2 isomers)	77-80	*73.9	0.45 ± 0.05	0.34 ± 0.01
83	13.6	Benzene	77-79	*63.6	2.34 ± 0.01	2.62 ± 0.08
84	9.3	CS_2	76,32	*78.7	0.38 ± 0.08	--
85	14.5	Thiophene	45,58,84	60.5	0.32 ± 0.02	--

* Percent of Total Ionization obtained from Reference 21.

** Coal pyrolysis occurs at 2.0 minutes.

Table 3. Comparison of classes of pyrolysates listed in Tables 1 and 2 in the inert gas degradation of untreated coals.

Compound class	Characteristic Ion Yields (Relative to Naphthalene) Illinois No. 6	Rawhide
alkyl benzenes*	8.21	9.23
polynuclear aromatic hydrocarbons	6.13	5.24
benzofurans*	0.95	0.85
phenols	5.51	5.26
thiophenes	1.32	0.14
benzothiophenes	1.01	0.17
alkenes (C_8-C_{12})	0.42	0.60
alkanes (C_8-C_{12})	0.42	1.02
alkenes (C_3-C_6)	3.55	3.30

*Exclusive of benzofuran and methyl styrene

Table 4. Quantatative yield of major volatile degradation products formed in the inert gas degradation of untreated coals.

Degradation Product	Yield (microgram/milligram) Illinois No. 6	Rawhide
Methane	11.9 ± 0.3	10.4 ± 1.0
Carbon Monoxide	8.0 ± 0.7	14.6 ± 3.1
Carbon Dioxide	12.4 ± 1.5	36.6 ± 4.6
Ethane	4.2 ± 0.2	2.4 ± 0.5
Carbonyl Sulfide	2.5 ± 0.2	0.3 ± 0.0
Naphthalene	1.2 ± 0.0	0.9 ± 0.4

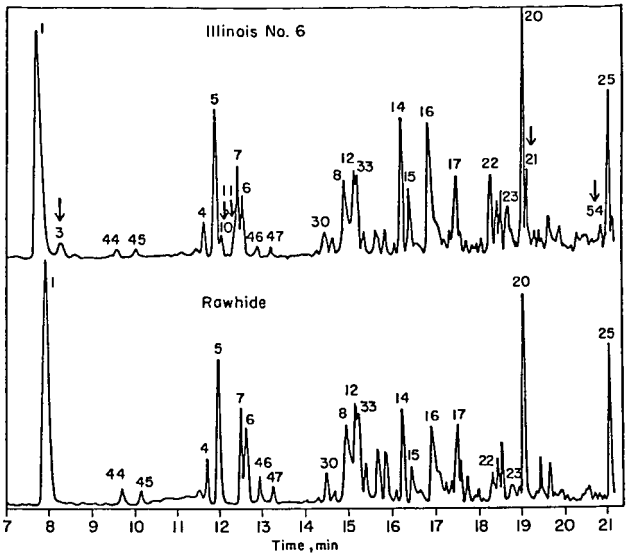

Figure 1. Comparison of pyrolysates from untreated coals. Arrows indicate significant visual differences between the two samples.

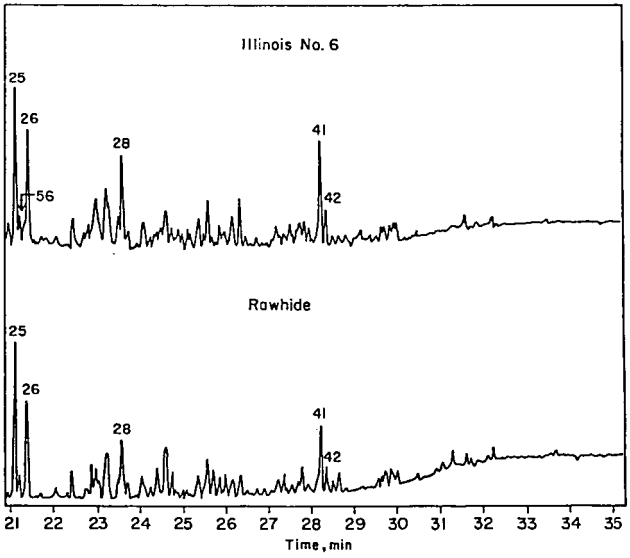

Figure 1. (continued)

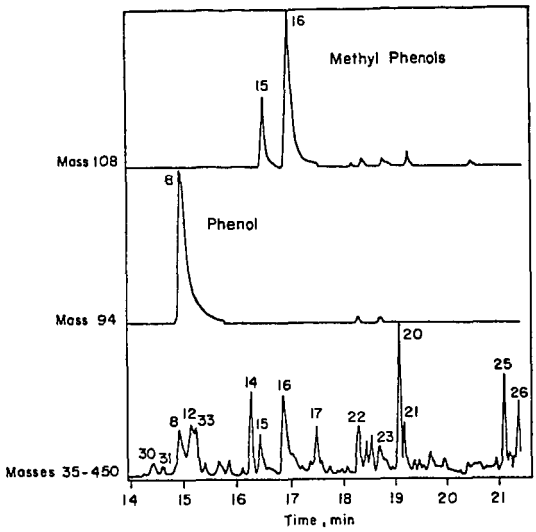

Figure 2. Comparison of Masses 35-450 total ion chromatogram and characteristic ion chromatograms used for the quantitation of phenol and methyl phenol present as pyrolysates of Illinois No. 6 coal.

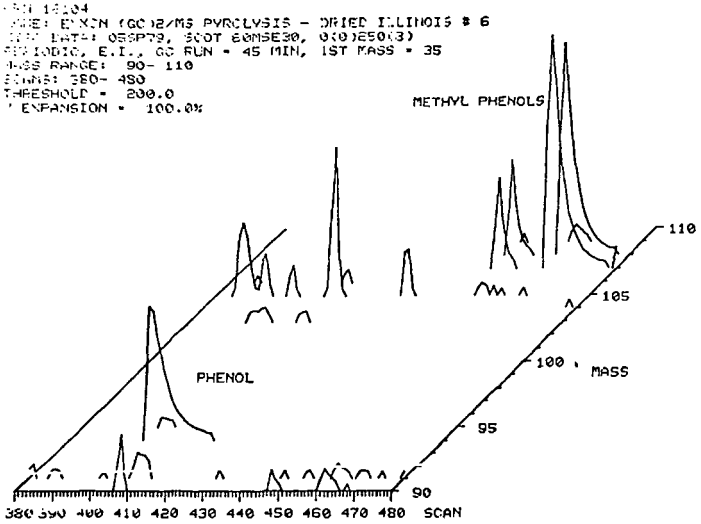

Figure 3. Isometric display of Masses 90-110 in the retention time region of phenol and methyl phenol, produced in the inert gas degradation of Illinois No. 6 coal.

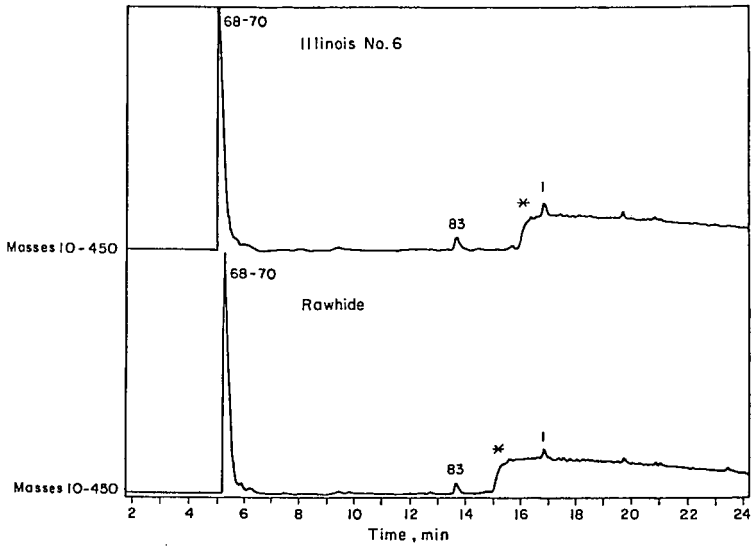

Figure 4. Comparison of Masses 10-450 total ion chromatograms of volatile pyrolysates from untreated coals.

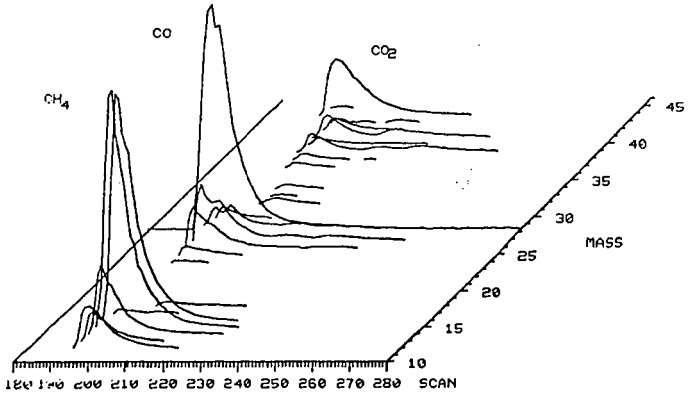

Figure 5. Isometric display of Masses 10-46 in the retention time region of volatile pyrolysates produced in the inert gas degradation of Illinois No. 6 coal.

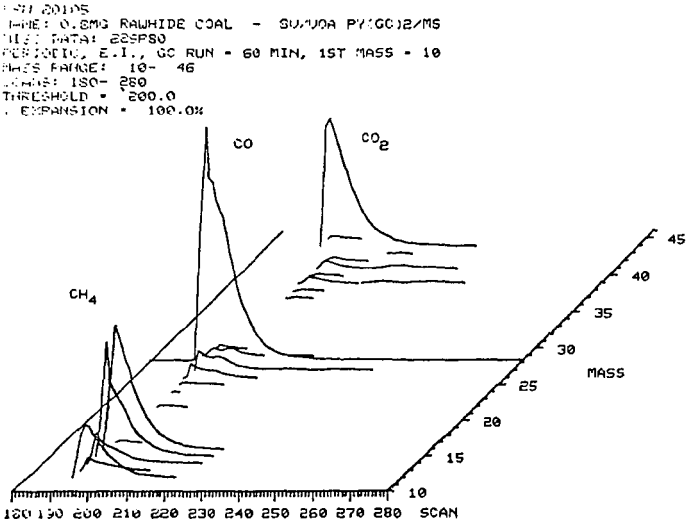

Figure 6. Isometric display of Masses 10-46 in the retention time region of volatile pyrolysates produced in the inert gas degradation of Rawhide coal.

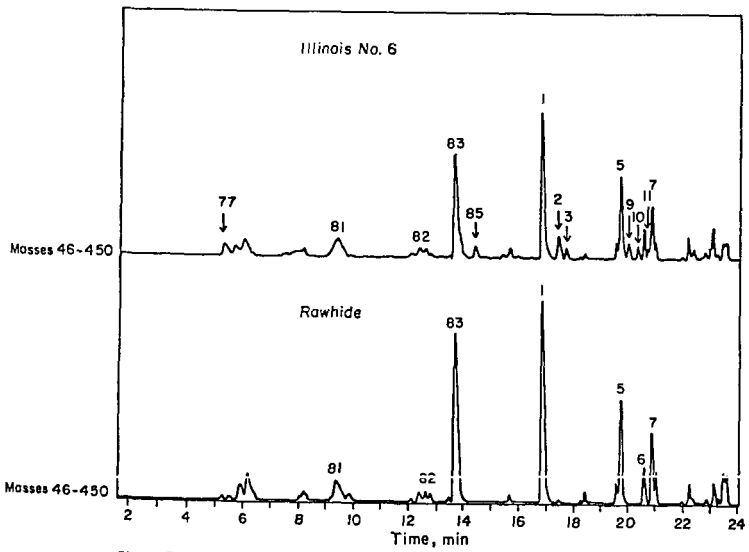

Figure 7. Comparison of Masses 46-450 total ion chromatograms of untreated coals. *Arrows indicate significant visual differences between the two samples.*

EFFECTS OF CALCIUM MINERALS ON THE RAPID PYROLYSIS OF A BITUMINOUS COAL

Howard D. Franklin, William A. Peters, Jack B. Howard

Department of Chemical Engineering and Energy Laboratory,
Massachusetts Institute of Technology, Cambridge, Mass. 02139

INTRODUCTION

Previous research at M.I.T. on rapid coal pyrolysis has dealt with the kinetics of evolution of individual products as a function of temperature, pressure, particle size, reactive gas, and coal type (1-5). Since recent studies elsewhere have shown that certain minerals occurring in coal affect significantly other types of coal conversion reactions, the present study was undertaken to determine what effects these minerals may have on rapid coal pyrolysis. This paper presents results on the pretreatment of coal with calcite ($CaCO_3$) and lime (CaO). These minerals have already been shown to influence fluidized-bed pyrolysis (6), steam gasification (7,8,9), and CO_2 gasification (10,11) of coal. Results obtained with other mineral additives will be reported later.

EXPERIMENTAL

The coal used was a Pittsburgh No. 8 Seam bituminous coal (Table 1) ground to -270+325 mesh (45-53 μm dia.). The native mineral matter was removed from the sample by extraction with HF and HCl followed by float-sink separation, resulting in a coal containing 4.3 percent by weight mineral matter, most of it pyrite. The demineralization procedure was shown to have no effect on the subsequent pyrolysis behavior of the coal (12). A fraction of the demineralized sample was co-slurried in water with 0.1 μm diameter calcite grains for 24 hours and dried at room temperature. The resulting mineral-treated coal contained 20.2 percent by weight $CaCO_3$. A second fraction of demineralized coal was similarly treated with CaO, resulting in a sample containing 5.9 percent by weight of a mixture consisting of 74 percent $Ca(OH)_2$ and 26 percent $CaCO_3$. Details of the pretreatment procedures are described elsewhere (12).

The pyrolysis apparatus (Fig. 1) and procedures have been described previously (2,12,13). Briefly, a thin horizontal layer of coal (≈15 mg) is sandwiched between the folds of a 325 US mesh stainless steel screen held between two electrodes in either a length of glass pipe or a stainless steel pressure vessel. The coal is heated by electrically heating the screen. The vessel and its gaseous contents remain at close to room temperature throughout the run, and thus the volatiles are quenched almost instantaneously on escape from the coal particles. The entire time-temperature history of the sample is recorded by use of a chromel-alumel thermocouple (75 μm bead diameter) positioned within the folds of the screen alongside the coal particles. Heat transfer calculations show that at pressures of 1 atm and heating rates of 1000 K/s or less, coal particles and thermocouple beads 80 μm or less in diameter closely follow the temperature of the screen and are spatially isothermal.

All reaction products were collected. Gases and low boiling liquids were trapped on lipophilic sorbents and subsequently analyzed by gas chromatography. Char was determined gravimetrically, and was further characterized by elemental analysis. Tar (room temperature condensibles) was collected on a filter at the reactor outlet and by a methylene chloride wash of the reactor internals, and its yield was determined gravimetrically. Total material balances usually exceeded 95 percent.

All runs were performed at heating rates of 1000 K/s with holding times of 0 or 5 s at the maximum temperature attained and cooling rates of about 200 K/s. These elements of the time-temperature history pertain only to the parent sample since the volatiles, once formed, rapidly escape the sample and are quenched as mentioned above. Demineralized and calcite-pretreated samples were heated in 1 atm He to temperatures between 800 and 1400 K. Other demineralized as well as lime-pretreated samples were heated in He at 1 atm or 69 atm to temperatures in the range 1050-1300 K.

RESULTS

Total yields of volatile products from demineralized and calcite-pretreated coals pyrolyzed in 1 atm He for 5 s holding time runs are shown in Fig. 2. The calcite-pretreated sample had lower weight losses, and hence higher char yields, than did the demineralized sample. Tar yields were greatly reduced in the presence of $CaCO_3$, as shown in Fig. 3. The $CaCO_3$-pretreated coal had a high temperature tar yield of 22 percent by weight dmmf coal, as compared with a yield of 30 percent by weight dmmf coal from the demineralized sample. Yields of lighter hydrocarbons were also reduced in the calcite-pretreated sample, although to a lesser extent than were yields of tar. The results for CH_4, shown in Fig. 4, are typical for those of the light hydrocarbon gases. The effect of $CaCO_3$ on these products manifested itself only at temperatures above 1200 K for 5 s holding time runs.

While addition of $CaCO_3$ to coal reduced the yields of all hydrocarbon products, yields of carbon oxides were strongly enhanced. Carbon monoxide yields, shown in Fig. 5, were larger for the $CaCO_3$-pretreated coal than for demineralized coal for all 1000 K and higher runs. At the limit of 1300 K, the yields were three times those from the demineralized sample. Yields of CO_2 for both 5 s and 0 s holding time runs are shown in Figs. 6 and 7, respectively. These plots show yields of CO_2 from demineralized and $CaCO_3$-pretreated coals, uncorrected for mineral carbonate decomposition. Yields of CO_2 from pyrolysis of samples of pure $CaCO_3$ under the same conditions and converted to a basis of percent by weight dmmf coal are shown on the same graphs for comparison. The high temperature, 5 s holding time yields of CO_2 from calcite-pretreated coal are approximately equal to those obtained from pure calcite mineral under the same conditions. For 0 s holding times or low temperatures, however, yields from the $CaCO_3$ pretreated sample were much higher than the combined yields of CO_2 from separate pyrolysis of demineralized coal and calcite at equivalent conditions. The CO_2 yields in 5 s runs from calcite-pretreated coal have in fact already reached an asymptote in the 1050-1200 K range, where the rate of CO_2 evolution from calcite itself is at its maximum. These results all seem to indicate that calcite in the

presence of coal decomposes yielding CO_2 at lower temperatures than it would when pyrolyzed alone.

Elemental compositions of chars resulting from 5 s holding time runs are shown in Fig. 8. Data are plotted as the percent of the element (C, H, or O) in the original coal sample that is retained in the char. Chars from calcite-pretreated coal have greater retentions of carbon and hydrogen, and much lesser retentions of oxygen, than do chars from demineralized coal.

In Table 2, yields from pyrolysis of CaO-pretreated coal at 1 atm and 69 atm He are compared with those from demineralized coal under similar conditions. Since product yields are temperature independent for 5 s holding time runs at high temperatures, results for several runs have been grouped together and reported by means of an average value and a standard deviation. The effects of CaO pretreating and $CaCO_3$ pretreating on hydrocarbon yields are similar. The $CaCO_3$-pretreated sample, however, gave a much higher CO yield than did the CaO-pretreated sample.

Fewer runs were done at 69 atm than at 1 atm, and the standard deviations are thus much larger for the high pressure data. These uncertainties tend to reduce the sigificance of the effects observed for CaO addition to coals pyrolyzed at 69 atm. These effects are, however, very similar to those seen for pyrolysis at 1 atm. The effect on tar of CaO addition tends to be obscured at the higher pressure since, as can be seen in the table, increased pressure itself leads to decreased tar yields and hence to less opportunity for an enhancement of tar cracking by CaO.

DISCUSSION

The yields from coal samples pretreated with calcite and those pretreated with lime are quite similar. This is consistent with the indication in Figs. 6 and 7 that for most runs conducted with calcite pretreated coal, the $CaCO_3$ decomposed to CaO. Thus, lime is the likely active species for the effects observed in either coal.

Addition of $CaCO_3$ to coal reduces the yields of all volatile hydrocarbon products. Yields of heavy hydrocarbons such as tar are reduced considerably at temperatures above 900 K for 5 s holding time runs, while yields of lighter products are reduced to a lesser extent, and only at temperatures above 1200 K. These results point to a catalysis by CaO of secondary hydrocarbon cracking/repolymerization reactions, a conclusion consistent with results of other work. Yeboah *et al.* (6) showed that addition of calcined dolomite or limestone to a fluidized-bed coal pyrolyzer reduces tar yields. No reduction in light hydrocarbon yields was seen, but temperatures in that study did not exceed 1050 K. Solano *et al.* (14) showed that calcite promotes CH_4 cracking to char at 1200 K, while Mead (15) observed that lime is particularly active for the cracking of single-ring aromatic compounds. The latter result may account for the much larger reduction of aromatic-rich liquids obtained by adding calcite, as compared with the reduction of light aliphatic gas products. Some of the tar is converted to CO as well, and thus the amount by which tar hydrocarbon cracking exceeds light hydrocarbon gas reduction is unclear. Since all volatile

hydrocarbon product yields are reduced by CaO, the resulting cracking products must in all cases include char and H_2. Char yields are indeed higher for the calcite-pretreated coal (Fig. 2), and carbon and hydrogen retention in this char is higher than it is in demineralized coal (Fig. 8). High temperature H_2 yields are also higher for calcite-pretreated coals (12). Hydrocarbon yield reductions were almost identical for both calcite- and lime-pretreated samples, despite the fact that the former sample had almost four times as much calcium as the latter. This would seem to point to the presence of a saturation effect for CaO catalysis of hydrocarbon cracking.

The CO_2 evolution data, shown in Figs. 6 and 7, seem to indicate that the presence of coal in some way catalyzes the decomposition of $CaCO_3$ to CaO and CO_2. Similar results have been observed in two other recent studies dealing with different carbon-carbonate systems. McKee (11) pyrolyzed mixtures of graphite and alkaline earth carbonates under He and CO_2 atmospheres in a thermogravimetric analyzer. Weight loss of these mixtures in helium occurred at temperatures much lower than the decomposition temperature of the carbonates alone. He postulated, based on the degree of weight loss observed, that the carbonates react with graphitic carbon yielding the corresponding oxide and CO. No analysis of the exit gas was conducted to verify the presence of CO. Other workers (16) heated mixtures of Illinois coal and ^{14}C labeled K_2CO_3 at 775 K. The carbonate decomposed completely to CO_2 under these conditions, and no carbonate carbon was detected as either CO or hydrocarbon products. The decomposition temperature of pure K_2CO_3 is well above 775 K. The authors proposed that a reaction of K_2CO_3 with the coal forms a surface complex and CO_2, a mechanism said to generate well-dispersed active sites for catalysis of subsequent reactions of the coal or char. This hypothesis is consistent with the data of the present work, although the mechanism for the apparent solid-solid reaction is not yet well-established. One possibility might be the reaction of carbonates with the phenolic groups in coal (21). This would agree with the finding of Sears et al. (10) that CO_2 gasification rates of chars correlate with the cross correlation of char oxygen and calcium contents, an indication of a calcium/coal-oxygen gasification site.

$CaCO_3$-pretreated samples gave considerably higher yields of CO than did demineralized samples. CO_2 yields from calcite-pretreated coals are always greater than or equal to CO_2 yields from calcite mineral at corresponding conditions, and hence the excess CO cannot be explained by postulating reactions of carbonate CO_2 with the coal or its volatile products. H_2O yields (not plotted) were also increased by calcite addition, thus ruling out steam gasification as a source of the excess CO. The oxygen in this excess CO is therefore organic in origin, and is derived from oxygen groups that end up in the tar and char fractions in demineralized coal pyrolysis. Most organic oxygen in bituminous coals is phenolic (17), and this phenomenon must therefore be examined in terms of decomposition mechanisms for the phenolic groups in coal.

Evidence that phenol decomposes along two parallel pathways was obtained by Cyprès and co-workers (18,19,20) in a study of the rapid pyrolysis of phenol, cresols, and xylenols using ^{3}H- and ^{14}C- labeled compounds. One pathway is a condensation of two phenol molecules to form dibenzofuran plus water and H_2.

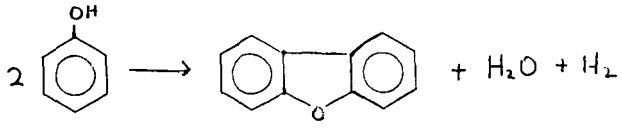

Dibenzofuran is itself stable at temperatures up to 1150 K. This reaction is important at low temperatures (920–1020 K) at which phenol just starts to decompose, but accounts for only a small fraction of the phenol pyrolysis that occurs at higher temperatures. At temperatures above 1020 K, the major pathway is unimolecular decomposition by way of a keto-enol shift to either H_2O and benzene, or to CO and a C_5 moiety which would then further condense to tetralin, naphthalene, and ultimately char.

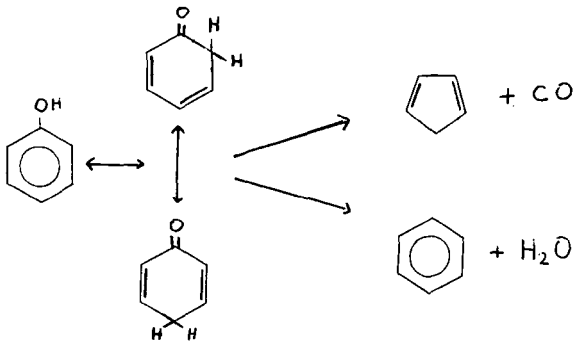

The CO pathway is preferred, the molar ratio of CO/H_2O generated at 1120 K being 1.7/1.

Assuming this mechanism for decomposition of phenolic groups in coal, the effect of $CaCO_3$ addition is predictable. The initial step of the decomposition to CO, the keto-enol shift, is a strongly base catalyzed reaction and the CaO generated by calcite decomposition is a strong solid base. Calcium carbonate or oxide addition will thus promote the decomposition of phenolics to CO at the expense of their evaporation as components of tar, or their condensation to species such as polycyclic furans, which remain in the char. Any of the latter compounds formed may also be cracked by CaO, which has been shown to strongly catalyze the cracking of furan itself (15). These proposed mechanisms are all supported by the results in Fig. 8, which show a much lower retention of oxygen in chars from calcite-pretreated coal than in chars from demineralized coal. Tar oxygen contents could not be obtained owing to the small absolute tar yields.

These results seem to conflict with a previous study on fluidized-bed pyrolysis of coal (6) which showed that CO yields from bituminous coal were lower when lime was used as the fluidizing medium than when sand was used. This apparent discrepancy can be explained by the differing conditions present in the two reactors. The temperatures in the fluidized bed were below 1050 K, where $CaCO_3$ rather than CaO is the stable species. Consequently, the lime removed CO_2 from the gas phase in a secondary reaction independent of the pyrolysis. As a result CO yields were reduced through the water-gas shift which was important in the fluidized bed where the volatiles were not immediately quenched. These gas-phase secondary reaction effects would mask any effects of the lime on the pyrolysis itself.

The calcite-pretreated sample gave much larger CO yields than did the lime pretreated sample. This behavior can probably be explained by the fact that there was 3.8 times as much Ca in the former sample as in the latter. The excess CO yield, that is CO yield from the mineral-pretreated sample less the yield from demineralized coal, is 4.4 times as great for the calcite-pretreated sample as for the lime-pretreated sample. This almost linear relationship between excess CO and Ca content might be due to an association of CaO molecules with the phenolic groups, either during pretreatment (for the lime-pretreated coal) or by reaction of $CaCO_3$ with the phenolic groups (for the calcite-pretreated coal).

CONCLUSIONS

Addition of $CaCO_3$ or CaO to coal reduces the high temperature yield of hydrocarbon products and increases the yield of CO in rapid coal pyrolysis. The former effect is probably attributable to lime-catalyzed secondary cracking reactions, while the latter results from base catalysis of a step in the decomposition of the phenolic groups. Calcite in the presence of coal decomposes to lime and CO_2 at lower temperatures than it will when pyrolyzed alone.

ACKNOWLEDGEMENTS

Frank Cariello obtained the data on CaO and $CaCO_3$ pretreated coal samples. This work was supported by a grant from the United States Department of Energy, under Contract EX-76-A-01-2295, Task Order No. 26.

REFERENCES

1. Anthony D.B., Howard J.B., AIChE J. 22, 625 (1976).

2. Suuberg E.M., Peters W.A., Howard J.B., Ind. and Eng. Chem. Proc. Des. and Dev. 17, 37 (1978).

3. Suuberg E.M., Peters W.A., Howard J.B., Proc. 17th Symp. (International) on Combustion, p. 117, The Combustion Institute, Pittsburgh Pa, (1979).

4. Suuberg E.M., Peters W.A., Howard J.B., ACS Adv. in Chem. Ser. 183, 239 (1979).

5. Suuberg E.M., Peters W.A., Howard J.B., Fuel 59, 405 (1980).

6. Yeboah Y.D., Longwell J.P., Howard J.B., Peters W.A., Ind. and Eng. Chem. Proc. Des. and Dev. 19, 646 (1980).

7. Haynes W.P., Gasior S.J., Forney A.J., ACS Div. of Fuel Chem. Prepr. 18(2), 1 (1973).

8. Forney A.J., Haynes W.P., Gasior S.J., Kenney R.F., ACS Div. of Fuel Chem. Prepr. 19 (1), 111 (1974).

9. Feldmann H.F., Chauhan S.P., Longanbach J.R., Hissong D.W., Conkle H.N., Curran L.M., Jenkins D.M., Battelle Columbus Laboratories Report BMI-1986 (1977).

10. Sears J.T., Muralidhara H.S., Wen C.Y., Ind. and Eng. Chem. Proc. Des. and Dev. 19, 358 (1980).

11. McKee D.W., Fuel 59, 308 (1980).

12. Franklin H.D., PhD Thesis Dept. of Chem. Eng. Mass. Inst. of Tech. (1980).

13. Anthony D.B., Howard J.B., Meissner H.P., Hottel H.C., Rev. Sci. Instrum. 45, 992 (1974).

14. Solano A.L., Mahajan O.P., Walker P.L., Fuel 56, 452 (1977).

15. Mead D.W., M.S. Thesis Dept. of Chem. Eng. Mass. Inst. of Tech. (1979).

16. Mims C.A., Pabst J.K., ACS Div. of Fuel Chem. Prepr. 25 (3), 258 (1980).

17. Yarzab R.J., Abdel-Baset Z., Given P.H., Geochim. et Cosmochim. Acta 43, 281 (1979).

18. Cyprès R., Bettens B., Tetrahedron 30, 1253 (1974).

19. Cyprès R., Bettens B., Tetrahedron 31, 353 (1975).

20. Cyprès R., Bettens B., Tetrahedron 31, 359 (1975).

21. Mims C.A., personal communication (1980).

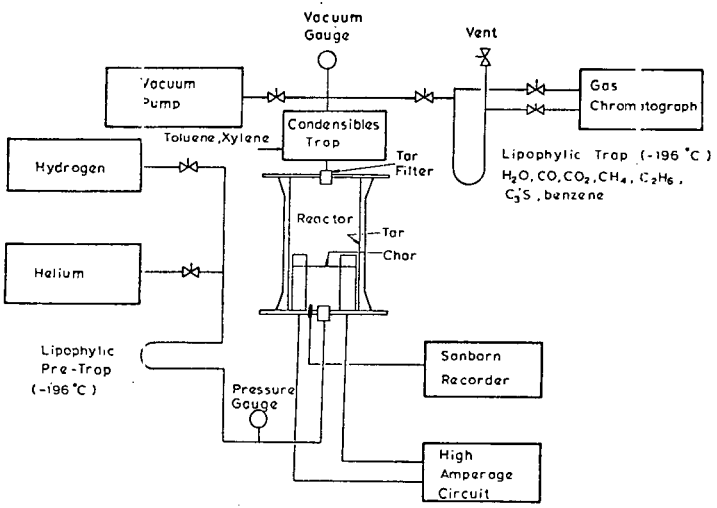

Fig. 1 Schematic of Captive Sample Apparatus

TABLE 1

CHARACTERISTICS OF COAL EXAMINED

Proximate Analysis	Wt.% (as received)
Moisture	2.0
Volatile Matter	36.2
Fixed Carbon*	51.0
Ash	10.8
	100.0

Ultimate Analysis	Wt.% (dry)	Wt.% (dmmf)
Carbon	71.74	82.91
Hydrogen	4.84	5.65
Oxygen*	6.22	7.19
Nitrogen	1.14	1.32
Organic Sulfur**	2.54	2.94
Mineral Matter	13.47	
	100.00	100.00

Petrographic Analysis	Wt.% mineral matter free
Vitrinite	81.5
Semi-Fusinite	6.0
Fusinite	2.5
Micrinite	3.0
Macrinite	1.2
Exinite	5.2
Resinite	0.6
	100.0

Mineral Matter Analysis	Wt.%
Kaolinite	13
Calcite	10
Quartz	7
Montmorillonite	14
Illite	9
Pyrite*	45
	100

* by difference

**calculated from total sulfur (5.77% by weight dry coal) and measured pyrite content

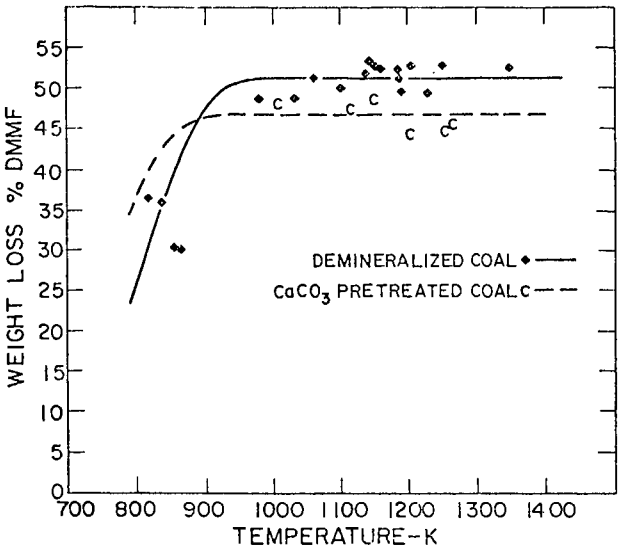

Fig. 2 Total Yield of Volatiles from Pyrolysis in 1 atm He of Demineralized and $CaCO_3$ Treated Coals, 5 s Holding Times.

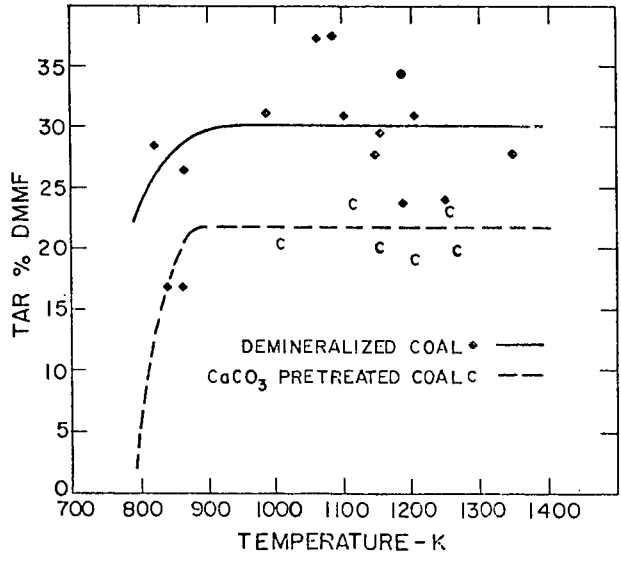

Fig.3 Yield of Tar from Pyrolysis in 1 atm He of Demineralized and $CaCO_3$ Treated Coals, 5 s Holding Times.

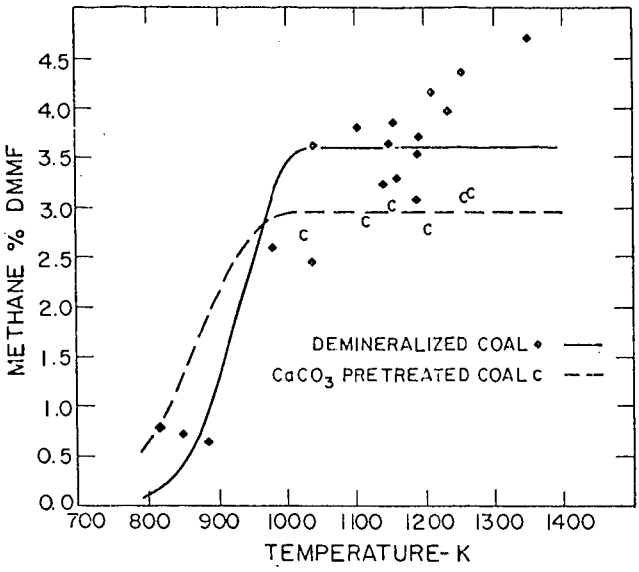

Fig. 4 Yield of Methane from Pyrolysis in 1 atm He of Demineralized and $CaCO_3$ Treated Coals, 5 of Holding Times.

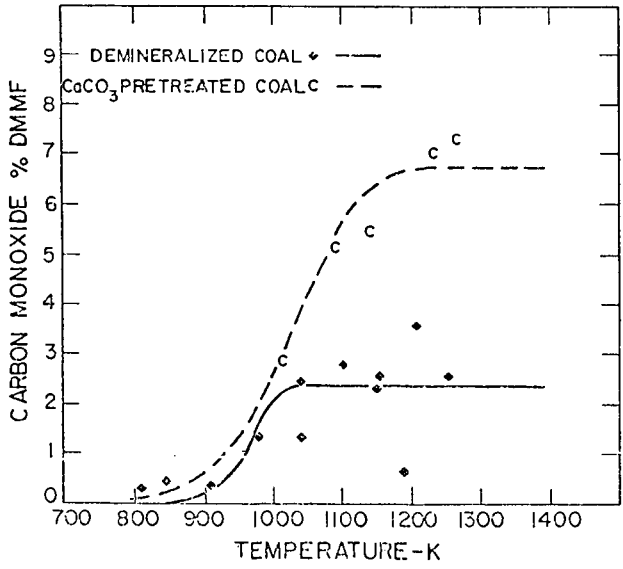

Fig. 5 Yield of Carbon Monoxide from Pyrolysis in 1 atm He of Demineralized and $CaCO_3$ Treated Coals, 5 s Holding Times.

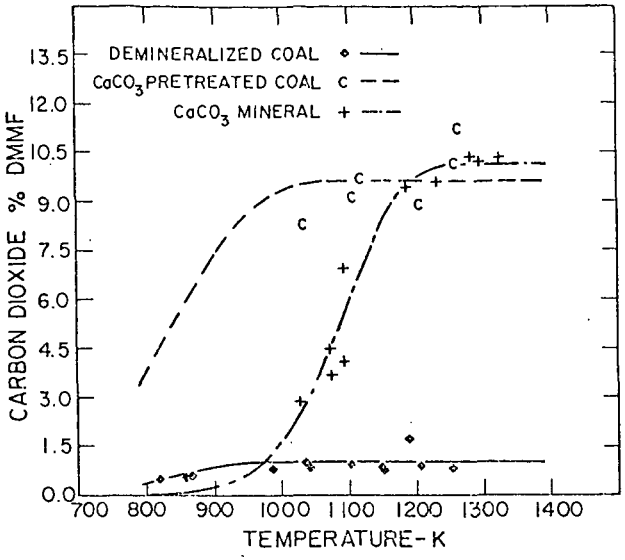

Fig. 6 Yield of Carbon Dioxide from Pyrolysis in 1 atm He of Demineralized and $CaCO_3$ Treated Coals, $CaCO_3$ Mineral, 5 s Holding Times.

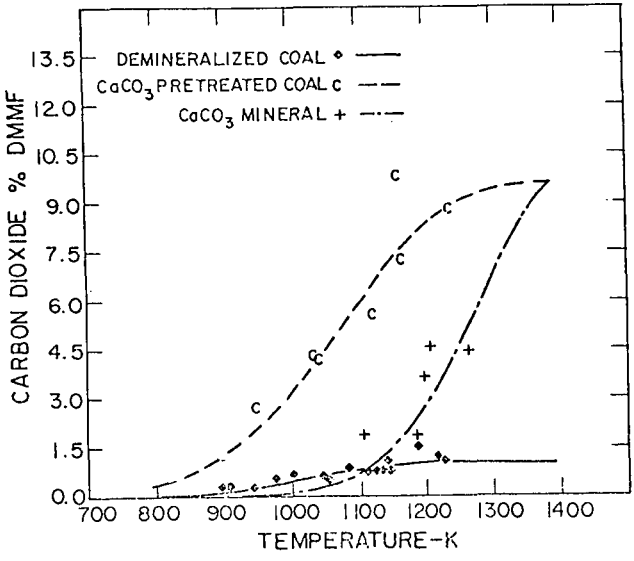

Fig. 7 Yield of Carbon Dioxide from Pyrolysis in 1 atm He of Demineralized and $CaCO_3$ Treated Coals, $CaCO_3$ Mineral, 0 s Runs.

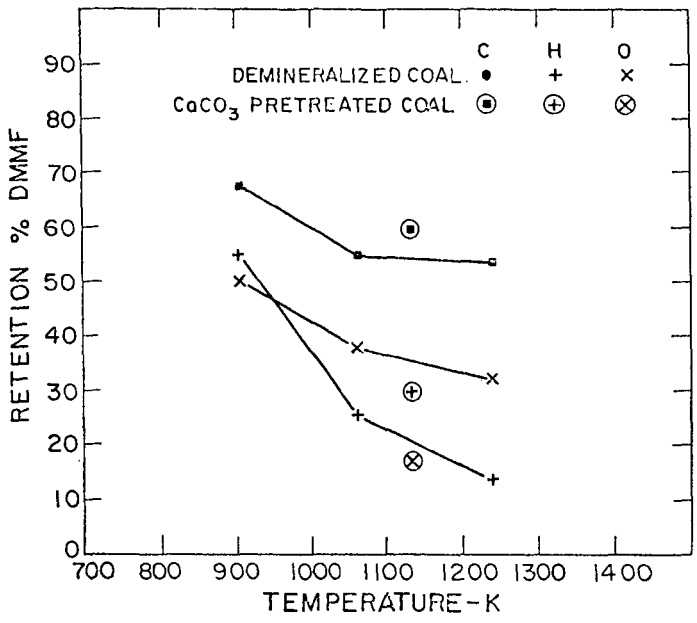

Fig. 3 Fraction of Elements in Demineralized and $CaCO_3$ Treated Coals that Remain in Chars from Pyrolysis in 1 atm He, 5 s Holding Times.

TABLE 2

YIELDS FOR 5 S RUNS IN He 1050 K - 1300 K

	1 ATM		69 ATM	
	DEMIN	CaO	DEMIN	CaO
ΔW/W	51.38±1.13	47.95	35.12±1.47	35.93
TAR	30.24±1.35	23.67	16.76±2.27	14.03
CH_4	3.62±0.11	2.93	5.79±1.11	5.36
C_2H_4	0.96±0.04	0.87	1.12±0.11	1.03
C_2H_6	0.74±0.03	0.73	0.83±0.21	0.73
C_3	0.89±0.03	0.75	0.67±0.15	0.58
C_4^+	1.26±0.04	0.79	0.69±0.19	0.48
LIQ HC	3.37±0.10	2.23	2.50±0.46	1.82
CO	2.40±0.15	3.42	3.73±0.92	4.36
CO_2	1.03±0.07	2.50	1.15±0.17	2.71
H_2O	3.01±0.30	--	2.91±1.76	3.76

An Investigation of Yields and Characteristics of Tars Released During the Thermal Decomposition of Coal

J. D. Freihaut and D. J. Seery

United Technologies Research Center
East Hartford, CT 06108

Introduction

Reported results indicate that tar yields obtained from a wide variety of coals and reactor conditions can represent a significant fraction of the mass of the parent coal.[1-6] Tar yields and characteristics appear to reflect not only the nature of the parent coal but also the experimental conditions of the decomposition process.[1,2, 6-9] The variation in tar yields and characteristics with intrinsic characteristics of the coal and process parameters underscores the possibility of relating such observations to fundamental aspects of the decomposition process.

This report contains some results of an initial investigation of tar yields and properties obtained from eight coals. Results are shown for variations with 1) coal rank characteristics; 2) apparent thermal history; and 3) ambient pressure. Apparent heating rates of 10^2 C/sec to 10^3 C/sec and final temperatures of 500 C to 1780 C were utilized. Ambient pressures were varied from near vacuum to 760 torr. The results indicate that tar yields and characteristics are sensitive functions of intrinsic characteristics of the coal and the process parameters associated with the decomposition process. Prediction of tar yields may involve coal rank characteristics as a basis but the nature of the transforms introduced by the process conditions (ambient pressure, heating rate, final temperature, particle size) are equally important.

Experimental Design

Figure 1 represents schematically the apparatus employed to perform the thermal decomposition experiments. The procedure involves placing small samples (20-50 mg) of finely ground coal (-100+325 mesh) between the folds of a fine (325 mesh) metal screen (stainless steel, molybdenum, tungsten). The grid is then driven to a predetermined temperature via the preset control circuitry. The apparent heating rate is monitored by a thermocouple bead placed between the folds of the grid. For vacuum runs the light gases evolved are immediately vented through a glass wool filter into the infrared cell of a Fourier Transform Infrared Spectrometer (FTIR). The total time for each run is 10 seconds.

For runs conducted with ambient nitrogen present, the reaction chamber is isolated from the infrared cell. The pressure is monitored by a pressure transducer attached to the reaction chamber. In addition, a fine mesh screen cylinder is placed around the grid with a baffle below the grid to prevent recirculation of the aerosol mist to the grid. In both configurations the tar mass is defined as the material which condenses on the room temperature walls, linings and filters.

In the cases where infrared spectra of the overall tar mass was desired a dry KBr pellet was placed in the reaction chamber and exposed to the evolving tar species. The pellets were then removed and scanned using the FTIR. Glass filters placed in the chamber were also removed and examined with a Scanning Electron Microscope (SEMC) to ascertain the nature of the tar release at various ambient pressures.

Infrared Characteristics and Elemental Analysis of Coals

The coals selected for these initial studies represent a wide cross section by rank and geologic province. Elemental analyses of these coals were provided by the institutions supplying the coals but each sample was also subjected to elemental analysis on a Perkin Elmer 240 Elemental Analysis System (EAS). In cases where substantial differences were observed between the reported values and the measured values, samples were sent to an independent laboratory for additional analysis. Table I contains the elemental analysis of the coal samples as well as the calculated H/C and O/C ratios. Figure 2 represents the location of the samples on the coalification band as revealed by the H/C and O/C values. The position of the Western bituminous coals relative to the Eastern bituminous coals reflects the differences in geologic sources.

The variation in chemical structural characteristics with position on the coalification band is reflected in the infrared spectra (Fig. 3) of the coals. The spectra are obtained from KBr pellets of finely ground coal samples and spectra are normalized with respect to 1 mg of coal. Identified mineral matter contributions to the spectra have been substracted. The spectra indicate, although at times indirectly, the manner in which the organic hydrogen and oxygen are distributed throughout the coal matrix. For example, the regions associated with aliphatic hydrogen (2800-3000 cm^{-1}, 1450-1475 cm^{-1}) show absorption increase with hydrogen content. The resolution of the aromatic hydrogen peaks (3020-3050 cm^{-1}, 700-900 cm^{-1}) increases with reductions in the H/C and O/C ratios. The regions associated with oxygen-containing functional groups (1500-1800 cm^{-1}) are more clearly defined for the higher oxygen-containing coals. The variation in infrared structural characteristics with position on the coalification band is clearly reflected in

the differences in the spectra of the bituminous coals from the different geological regions.

While the Eastern bituminous and Western bituminous coals are different structurally, the infrared spectra of the Utah and Colorado bituminous coals are similar. The two subbituminous coals also display infrared spectra similar to each other. On the basis of the infrared spectra and the elemental analysis, the Alabama bituminous coal appears more aromatic than the Pittsburgh bituminous coal. If thermal decomposition behavior is related to infrared structural characteristics, the behavior of the Western bituminous coals should be similar to each other, but measurably different than that of the Eastern bituminous coals. The Alabama bituminous coal should in turn exhibit thermal decomposition behavior different than the Pittsburgh bituminous coal. The Western subbituminous coals would be expected to be similar to each other in their thermal decomposition behavior.

Variations in Tar Yields/Characteristics with Coal

The maximum tar yields obtained from the vacuum devolatilization experiments are listed in Table I and displayed in Fig. 2. The results indicate that the fractional conversion of the parent coal to tar is not a simple linear function of the H/C ratio, O/C ratio, hydrogen or oxygen percentages. For example, the Pittsburgh bituminous coal has a maximum tar yield 40-60% greater than the other bituminous coals. The hydrogen content of the Pittsburgh coal is ~ 3% lower than the Western coals and ~ 15% greater than the Alabama coal. The Alabama coal has a hydrogen content approximately 15% lower than the Western bituminous coals but has a maximum tar yield only 4% lower than the Colorado bituminous coal and about 9% less than the Utah coal. Differences in H/C ratios show a similar pattern.

Inspection of the infrared spectra of the parent coals also reveals no simple relationship between infrared spectral characteristics of a coal and its maximum tar yield. For example, the Pittsburgh bituminous coal has weaker absorption in the aliphatic hydrogen regions than either of the Western bituminous coals. The Alabama coal on the other hand gives a tar yield nearly the same as the Western coals, though it also displays weaker aliphatic absorption than these coals. The tar yields from the Western subbituminous coals are very nearly equal as are the tar yields from the two Western bituminous coals. As noted above, these pairs of coals have similar infrared spectra in the regions of interest - aliphatic type H, aromatic H, and oxygen - containing functional groups. The coals of similar infrared spectra do produce similar tar yields, but a coal with a dissimilar spectra can also produce comparable tar amounts.

The variations of maximum tar yield with elemental composition and infrared spectral characteristics both indicate the multi-parameter nature of the yield dependence. As a path from the low rank side of the coalification band is followed the tar-producing potential of a coal reaches a maximum in the H/C-O/C region near that of the Pittsburgh bituminous coal. It is interesting to note that this is not a point of maximum H/C nor does the infrared spectra of the coal show more aliphatic-type H than the other, lower rank coals. Beyond the Pittsburgh coal the tar yield drops with further decreases in H/C and O/C ratios. In this region the H/C ratio is changing more rapidly than the O/C ratio. The infrared spectra of these coals show well-defined aromatic hydrogen regions, reduced aliphatic hydrogen absorption and a reduction in oxygen-containing functional group absorption. Tar yields are increased as the O/C ratio is decreased from the low rank side of the coalification band. They are also increased as H/C ratios are increased from the high rank side of the band. Inspection of the infrared spectra indicates that tar yields do not vary directly with change in absorption characteristics associated with a particular structural characteristic. Such a relationship may be valid for samples from a limited region on Fig. 2. It appears that tar yields are related to a mix of structural characteristics present in the parent coal and as revealed by infrared and elemental analysis.

Tar Yields and Apparent Thermal History

Figures 4-6 show plots of tar yields obtained for various final temperatures. Figure 4 contains the results for the two Western subbituminous coals. Figure 5 displays the Western bituminous coal, and Fig. 6 the Eastern bituminous coals as well as the anthracite and lignite.

The tar yields obtained from the two Western subbituminous coals show a close resemblance both with respect to magnitude and final temperature dependence (Fig. 4). The Western bituminous coals also show a close resemblance to each other with respect to magnitude and final temperature dependence of the tar yields (Fig. 5). As noted above, these coals have similar infrared spectra. Both the subbituminous and Western bituminous coals show a maximum in tar yield at low final temperatures. This maximum occurs at approximately 775 C for the subbituminous coals but at a slightly lower temperature for the bituminous coals. The reduction in tar yield at final temperatures greater than the maximum is not as sharp as the rise to the maximum yield.

The Eastern bituminous coals also show a low temperature maximum in tar yield (Fig. 6). The Pittsburgh seam bituminous coal gives a maximum tar yield around 600 C whereas the Alabama bituminous coal shows a maximum around 700 C. The reduction in tar yields with final temperatures greater than these is not as sharp as

that of the Western subbituminous and bituminous coals. However, these coals do display the same steep gradient for the change in tar yield with final temperature on the low temperature side of the tar maximum.

Figure 7 shows typical char yields obtained during the runs. The char yield decreases sharply with final temperature in the 500-800 C range, the temperature range of greatest increase in tar yields. At final temperatures from 800 C to 1000 C, production is not as sensitive to changes in final temperature. The tar yields are decreasing significantly in this final temperature regime. For final temperatures greater than 1000 C total volatile yields do not increase appreciably. Tar yields continue to decrease to final temperatures of 1400 C at which point a high temperature asymptote is nearly achieved.

Examination of the thermocouple data for a decomposition run associated with a particular final temperature indicates that the apparent heating run did vary with final temperature setting. The initial slopes of the temperature-time data are taken as the apparent heating rate. The variation in apparent heating rate with final temperature is shown in Fig. 8. A final temperature setting of 500 C corresponds to an initial apparent rate of ~ 100 C/sec whereas a setting of 1000 C corresponds to an apparent rate of ~ 600 C/sec. Thus, the coal particles experience slightly different thermal conditions with variations in final temperature setting. The tar yields for the two Western bituminous coals and the Alabama coal are maximimzed under conditions of an apparent heating rate of approximately 200 C/sec and a final temperature temperature of ~ 700 C. The Western subbituminous coals on the other hand show tar maximums at a heating rate of ~ 250 C/sec to a final temperature of 775 C. The Pittsburgh bituminous coal has a tar maximum at 150 C/sec and ~ 625 C. The lignite and anthracite show no clearly defined maximum.

In light of these results and those of other investigations[8,9] it is obvious that further investigation of tar yields from bituminous coals under a wider range of thermal drive conditions is needed.

Tar Characteristics and Apparent Thermal History

Figure 9 illustrates the changes in the infrared spectral characteristics of tars collected for different final temperatures. As has been reported elsewhere[10,11,12], low temperature vacuum tars give infrared spectra similar to that of the parent coal but with enhanced absorption in regions associated with aliphatic hydrogen. As indicated, however, the high temperature tars show considerable reduction in absorption in regions associated with functional groups attached to aromatic rings. The low temperature tars apparently thermally decompose when subjected to

the longer times at higher temperatures that accompany the increase in thermal drive with final temperature. The condensed high temperature tars are noticeably darker than the low temperature tars, indicating a more aromatic nature.

Figure 10 shows typical paths followed by evolved chars in a H/C vs. O/C plot for different final temperatures. As reported elsewhere[13] the char shows a rapid decline in H/C and O/C values as volatiles are evolved. The low-temperature tars have H/C and O/C ratios greater than those of parent coal whereas the high temperature tars have values below those of the parent coal.

The nitrogen content of the evolved tars is of particular interest. Figure 11 shows fractions of parent coal mass evolved as tar vs. the fraction of parent coal nitrogen evolved as tar nitrogen. The fraction of fuel nitrogen evolved as tar is directly proportional to the fraction of coal mass evolved as tar.

Infrared spectra of the light gases evolved reveal that HCN is the principal nitrogen-containing gas species that is observed. Figure 12 is a plot of the fuel nitrogen distribution in the gaseous, tar and char species as observed for the Utah bituminous coal. The distribution pattern for the other subbituminous and bituminous coals were similar although the magnitudes of the distribution varied with rank characteristics of the coal. The main chracteristics of these nitrogen distribution plots are:

1. A low temperature evolution of fuel N as HCN-usually about 10% of the coal nitrogen to the point of maximum tar evolution.

2. The fuel nitrogen evolved as a tar component is directly proportional to the coal mass evolved as tar.

3. HCN is observed to be the major nitrogen-containing light gas.

4. As the tar fraction is reduced with higher final temperatures, HCN is a principal nitrogen-containing by-product.

5. Around 1100 C nitrogen is evolved from the char product as HCN. Little increase in total volatiles is observed at those temperatures but a substantial increase in nitrogen evolution as HCN is observed.

6. The nitrogen retained in the high temperature chars is a function of coal rank. Higher coal ranks retain a greater fraction of the coal nitrogen in the char product.

The nitrogen distribution in the thermal decomposition products reflects both the coal type and the conditions of thermal decomposition in a manner similar to the tar yields and properties.

Tar Yields and Ambient Pressure

Figure 13 displays the tar and char yields obtained from the bituminous coals as a function of ambient nitrogen pressure. The two Eastern bituminous coals and one Western bituminous coal produced tar yields as low as 50% of the vacuum value. The other Western bituminous coal gave an approximately 25% reduction in tar yield upon increasing the ambient pressure from near vacuum to one atmosphere of nitrogen. This coal showed a gradual reduction in tar yield with increases in pressure throughout this range. The other coals however showed much greater changes in tar yield per unit of pressure change in the range from near vacuum to 190 torr of nitrogen than from 190 torr to 760 torr.

The decrease in tar yield with increase in ambient pressure did not result in a proportionate reduction in total volatiles yield for any of the coals investigated (Fig. 13). The Pittsburgh bituminous coal produced about a 20% reduction in total volatiles yield while the tar yield dropped by 50%. Two other bituminous coals displayed only 10% reductions in total yield. The coal giving the gradual reduction in tar yield over the entire pressure range showed no significant decrease in total yield as the tar yield decreased.

There has been no direct measurement of the gas species produced at various ambient pressures while the tar yield is being reduced. However, the decrease in tar yield per unit mass of coal is accompanied by a proportionate increase in internal pressure within the reactor above the initial pressure. Thus, there appears to be a significant increase in light gas yield as the tar yield is decreased due to ambient pressure effects.

Apparently the ambient pressure serves to decrease the rate of escape of the large tar species from the devolatilizing coal mass. Such effects have been reported elsewhere.[3,6] The increased contact time of the large hydrocarbon species with the hot coal mass promotes further cracking of these species to lighter gases. As a result more light gas species are produced per unit of total yield. The thermal degradation of the tar mass in contact with the coal/char results in some secondary deposition of carbon on the devolatilizing particles. The amount of secondary deposition seems to be dependent upon the specific coal and its properties during the decomposition process.

Tar Characteristics and Ambient Pressure

In order to determine if any overall changes in the chemical nature of the tars released occurred due to changes in ambient pressure, dried KBr pellets were placed above the grid within the reaction chamber. After a run the pellets were removed and scanned with the FTIR. The infrared spectra of the tars formed in vacuo closely resemble the spectra of the parent coal from which it was derived. However, the infrared spectra of the tars formed under pressure showed reduced absorption in the regions associated with functional groups of vacuum tars. The greatest reductions occur in the near vacuum to 190 torr region, corresponding to the greatest reducing in tar yield per unit change of ambient pressure. As pressures are increased beyond 190 torr further reductions in absorption due to functional groups are slight. The Utah bituminous coal showing the least change in tar yield per unit pressure increase also displays the least change in functional group absorption per unit pressure increase.

The tar pellets from the pressure runs scattered the infrared beam considerably, where as the pellets from the vacuum runs did not. It is believed that the scatter is due to the physical form of the tars condensed on the pellets. In the case of the devolatilization runs performed with an ambient pressure, the tars released immediately form an aerosol mist. It is these mists which condense on the KBr pellets. The particle-like nature of the condensed tar mass on the pellets scatters the infrared signal. No mist is observed in the case of the vacuum runs. The vacuum tars apparently coat the KBr pellets in more of a molecular-layering like condensation. Scanning Electron Microscope photographs of the tars condensed on glass fiber filters placed in the reaction vessel reveal crystallite-like structure formed on the filters from the vacuum runs. The filters from the pressure runs displayed particle-like droplets coating the filters. Tar droplet formation similar to this has been observed elsewhere but under different devolatilization conditions.[9,14]

In order to demonstrate the propensity of the tar mass to form aerosol mists when released in ambient pressure conditions high speed films were made of the devolatilizing Pittsburgh bituminous coal. A cross flow of nitrogen across the heating grid immediately swept any released volatiles from the grid so that a clear view of the decomposing coal mass could be maintained. The plasticizing Pittsburgh coal was selected for the initial film study since the release of volatile matter during the plastic stage of decomposition can be observed to occur via bubble rupture. By means of a framing projector one can obtain a rough estimate of the time interval between the rupture of a specific bubble and the formation of a visible aerosol mist in the flow stream around the grid. Examination of such films

reveals that the aerosol mist formation in a one atmosphere cold flow is rapid, taking place during the first few milliseconds of the bubble rupture.

Summary and Conclusions

Based on these initial investigations the following general observations can be formulated:

1. In vacuo tar yields can be related to structural characteristics of the parent coal:

   a. For coals with O/C values less than ~ 0.09 the tar yield appears to be proportional to the H/C parameter. In this region as previously reported,[15] the maximum tar yield appears to be proportional to the aliphatic-type functional groups of the parent coal as revealed by infrared analysis of the coal.

   b. For coals with O/C values greater than 0.1 the tar yield is inversely proportional to the O/C values of the coal. In this region the tar yield appears to be proportional to a mix of aliphatic and oxygen-containing functional groups as revealed by infrared analysis.

   b. Consequently, predictive equations for in vacuo tar yields which are to be valid for a range of coals along the coalification band must consider the multi-parameter nature of the dependence of tar yield on intrinsic coal structural paramters.

2. In vacuo tar yields are dependent on the thermal drive experienced by the coal particles. Subbituminous and bituminous coals produce a maximum tar yield when heated to a final temperature in the 600 C to 800 C range with an apparent heating rate of ~ 100-200 C/sec. Coals with higher O/C ratios display a sharper reduction in tar yields with an increase in thermal drive characteristics beyond these values.

3. Tar yields for bituminous coals are sensitive functions of ambient pressure in the near vacuum to one atmosphere region. Reduction in tar yields up to 50% of the in vacuo value are observed. Total volatile yields are not proportionately reduced.

4. Physiochemical characteristics of tar species are dependent on parent coal structural characteristics as well as the conditions of devolatilization. Vacuum formed low temperature tars closely resemble the parent coal in structural characteristics. Changes in apparent thermal drive and ambient conditions produce changes in tar characteristics. In general, functional group characteristics are reduced with increases in thermal drive and ambient pressure. HCN appears to be a principal nitrogen-containing light gas species released as tar yields are reduced with an increase in thermal drive.

Since tar yields and characteristics are sensitive functions of coal characteristics and devolatilization conditions, predictive relationships are of necessity multi-parameter in nature. Both intrinsic and process parameters must be considered as the tar yields and characteristics are shown to be sensitive functions of both. The sensitivity of yields and characteristics to parameter changes for a wide variety of coals is indicative of the coupled chemical kinetic-transport nature of coal devolatilization.

ACKNOWLEDGMENTS

The authors would like to express gratitude to David Santos and Gerald Wagner for their technical assistance and to Marty Zabielski for assistance in the grid temperature measurements and interpretations. We are grateful for the financial support of the Department of Energy under Contract ET-78-C-01-3167, Energy and Environmental Research Corporation under Contract EER-8318-8, and United Technologies Corporation financial support under its Chemistry of Coal Gasification project.

REFERENCES

1. Peters, W. and Bertling, H. Kinetics of the rapid degasification of coals, Fuel, 44, 317 (1965).

2. Loison, R. and Chauvin, F. Pyrolyse rapide due charbon. Chem. Ind. (Paris), 91, 269 (1964). Reported by Field, et. al. Combustion of pulverized fuel. BCURA, 31, No. 4, 193 (1967).

3. Anthony, D. B. and Howard, J. B. Coal devolatilization and hydrogasification. AIChe, 22, No. 4. 625 (1976).

4. Suuberg, E. M., Peters, W. A. and Howard, J. B. Product composition and kinetics of lignite pyrolysis. Amer. Chem. Soc. Div. of Fuel Chem. Preprints 22, No. 1, 112 (1977).

5. Solomon, P. R. and Colket, M. B. Coal devolatilization. In "Seventeenth Symp. (Intern) on Combustion," The Combustion Institute, Pittsburgh, PA (1978).

6. Suuberg, E. M., Peters, W. A. and Howard, J. B. Product composition in rapid hydropyrolysis of coal. Fuel, 59, 405 (1980).

7. Lowry, H. H. (ed.), Chemistry of Coal Utilization-Supplementary Vol., Wiley & Sons, Inc., New York, Chapters 13, 14 (1963).

8. Mentser, M., O'Donnel, J. and Ergun, S. Rapid thermal decomposition of bituminous coals. Amer. Chem. Soc. Div. of Fuel Chem. Preprints, 14, No. 5, 94 (1970).

9. Freihaut, J. D. and Vastola, F. J. A numerical and experimental investigation of rapid coal pyrolysis. Technical Report 19 to DOE (FE-2030-TR19). Dept. of Mat. Sci, Pennsylvania State U.

10. Orning, A. A. and Greifer, B. Infrared spectrum of solid distillate from high vacuum pyrolysis of a bituminous coal. Fuel, 35, 381 (1956).

11. Solomon, P. R. Relation between coal structure and thermal decomposition products. Amer. Chem. Soc. Div. of Fuel Chem. Preprints, 24, No. 2, 185 (1979).

12. Brown, J. K. et. al. Some experiments on the fundamentals of coking properties. Jr. Inst. Fuel, 31, 259 (1958).

13. Van Krevelen, D. W., Van Herden, C. and Huntjens, F. J. Physiochemical aspects of the pyrolysis of coal and related organic compounds. Fuel, 30, No. 11, 253 (1951).

14. Lowry, H. H. (e.d.) Chemistry of Coal Utilization-Supplementary Volume, Wiley-Since, Inc., New York, 617 (1973).

15. Solomon, P. R. The characterization of coals during thermal decomposition. Fifth EPA Fundamental Combustion Research Workshop. Newport Beach, CA, January, 1980.

TABLE I

ELEMENTAL ANALYSIS (DMMF) AND TAR YIELDS

	Mon Lig(L)	WY Sub(S1)	WY Sub(S2)	Utah Bit(UB)	Col Bit(CB)	Pitt Bit(PB)	Ala Bit(AB)	Anth. (AN)
C	0.6827	0.7540	0.7550	0.7818	0.8100	0.8197	0.8497	0.9369
H	0.0457	0.0490	0.0517	0.0552	0.0553	0.0536	0.0463	0.0259
O	0.2547	0.1807	0.1699	0.1386	0.1119	0.0936	0.0818	0.0189
N	0.0102	0.0128	0.0171	0.0169	0.0163	0.0142	0.0173	0.0108
S_o	0.0067	0.0035	0.0063	0.0076	0.0064	0.1089	0.0052	0.0072
H/C	0.803	0.780	0.822	0.847	0.819	0.785	0.654	0.332
O/C	0.280	0.180	0.169	0.133	0.104	0.086	0.072	0.015
Max Tar%	18	20	21	27	26	39	25	2
T_{max} tar (^oC)	-----	750-800	750-800	675-725	675-725	600-650	700-750	-----

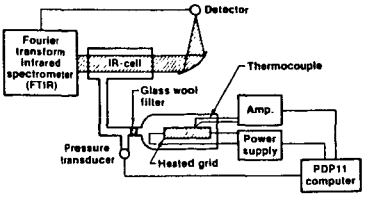

Figure 1: Heated Grid Pyrolysis Apparatus

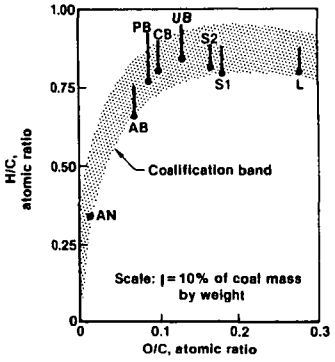

Figure 2: Tar Yields and Coalification Band Position (See Table I for Abbreviation Key) Tar Yields Are Maximum Tar Yields Obtained in Vacuo

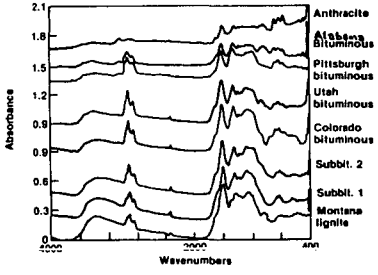

Figure 3: IR Spectra of Coals

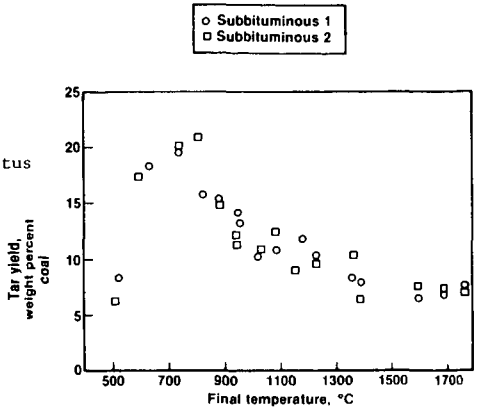

Figure 4: Tar Yields as a Function of Final Temperature for Western Subbituminous Coals

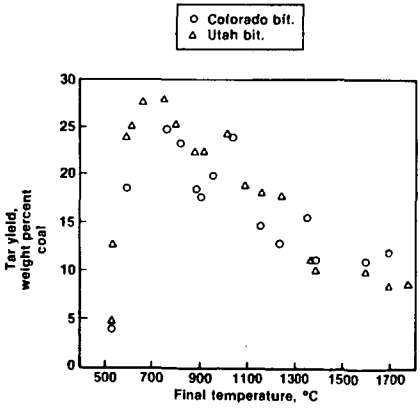

Figure 5: Tar Yields as a Function of Final Temperature for Western Bituminous Coals

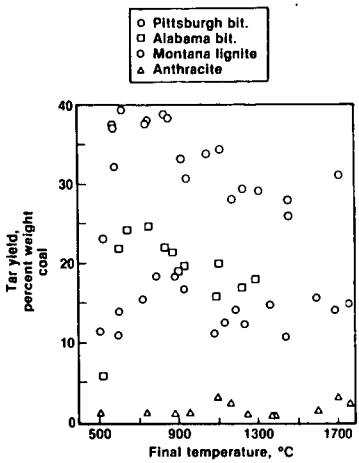

Figure 6: Tar Yields as a Function of Final Temperature for Eastern Coals and Montana Lignite

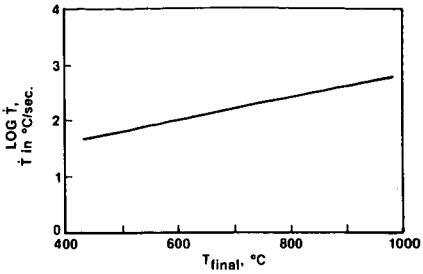

Figure 8: Temperature - Heating Rate Correlation: 75 μm Thermocouple Bead Placed Between Folds of Grid

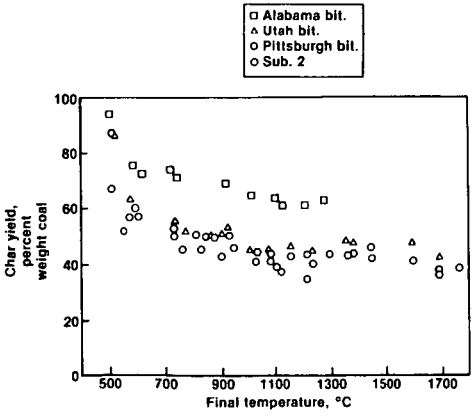

Figure 7: Char Yields as a Function of Final Temperature

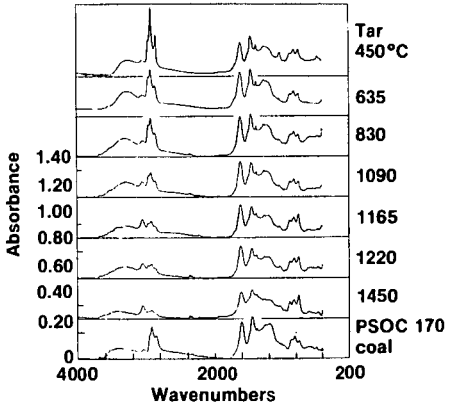

Figure 9: IR Spectra of Tars from Pittsburgh Bituminous Coal Tars from 10 Sec Vacuum Pyrolysis at the Indicated Final Temperature

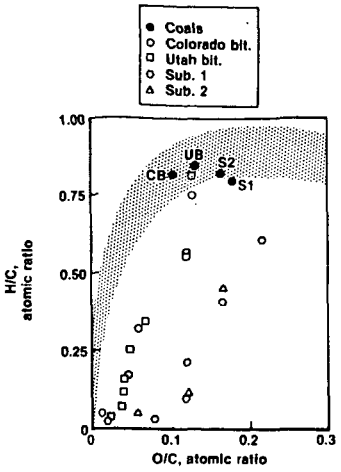

Figure 10: H/C - O/C Paths During Thermal Decomposition Process

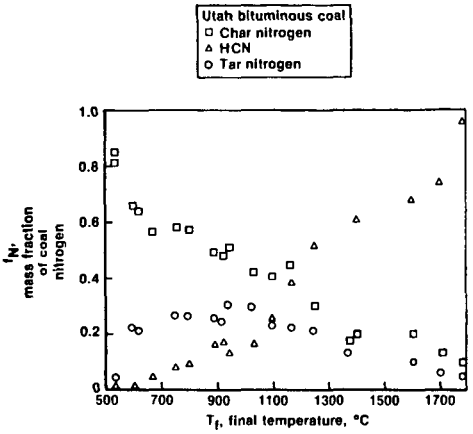

Figure 12: Nitrogen Distribution in Thermal Decomposition Products of The Utah Bituminous Coal

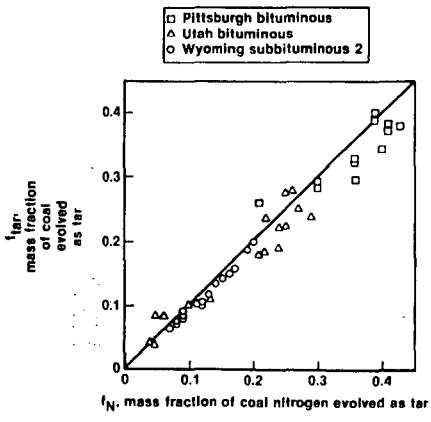

Figure 11: Mass Fraction of Coal Mass Vs. Mass Fraction of Coal Nitrogen

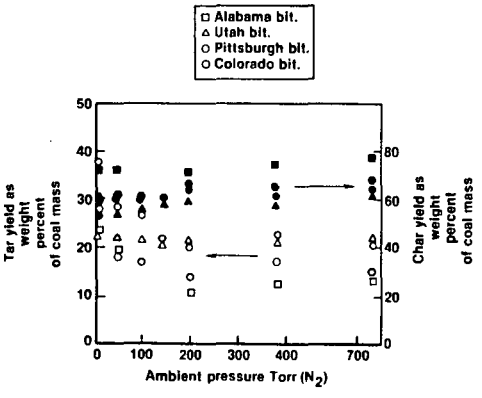

Figure 13: Tar and Char Yield Variation with Ambient Pressure Open Symbols → Tar; Closed Symbols → Char; Final Temperature ~ 635°C, Thermocouple Heating Rate ≈ 150°C/sec

CONVERSION OF BITUMINOUS COAL IN CO/H_2O SYSTEMS
II-pH DEPENDENCE*

David S. Ross,* James E. Blessing
and Quyen C. Nguyen

SRI International
333 Ravenswood Avenue
Menlo Park, California 94025

Introduction

We have reported that strongly basic conditions promote the conversion of Illinois No. 6 coal in CO/H_2O systems at 400°C to a product that is fully pyridine-soluble and has 50% benzene solubility and 18% hexane solubility. (1) This work used 4 M aqueous KOH, and CO_2 and H_2 were the product gases. No organic H-donor solvents were used in the conversions; water was the only medium used.

We have since shown in control experiments that (a) with N_2 in place of CO, the strongly basic medium alone only decreases the already small benzene solubility of the coal and (b) CO used with only water provides a product with a benzene solubility of only about 10%. (2) Thus both the base and CO must play an important role in the conversion, and in accord with the suggestion by Appell et al., (3) we have considered that formate was the active reducing agent in the system. (1)

Conversion Chemistry

We report here on the study of the conversion at considerably lower basicities and on the question of the intermediacy of formate in the conversion. The data for runs carried out at 400°C for 20 minutes in a stirred autoclave are shown in Figure 1, in which the benzene solubilities of the products are plotted against the pH of the starting aqueous phase determined at 25°C. It is seen that the conversion in a system 4 M in OH^- is little different from that in a system with a starting pH of 12.6 (OH^- = 0.04 M). The conversion is thus effective down to that basicity level, but then falls suddenly under less basic conditions. This striking loss of conversion effectiveness provides the S-shaped curve shown in the figure.

Also shown in Figure 1 are the product gas analyses. In the effective runs above pH = 12.6, the CO was largely consumed and the product gases were almost equimolar quantities of H_2 and CO_2. The runs below pH 12.6, however, neither yielded substantially converted coal nor consumed CO. There would seem to be a parallel in this system between the conversion of coal and operation of the water gas shift reaction, which provides equal quantities of H_2 and CO_2.

$$CO + H_2O \rightarrow CO_2 + H_2$$

The product analyses for two runs at pH 12.6 are shown in Table 1 along with the composition of the starting coal. Since no organic H-donor solvent is used, the products are uncontaminated and are fully coal-derived. This conditions is in contrast to the common finding from conversions in tetralin or other organic media in which there is incorporation of portions of the organic medium into the products. The contaminant commonly cannot be fully removed, even under high temperature and full vacuum. (4) It is thus possible to calculate a detailed mass balance with our data, using both the elemental analyses of the product fractions and the gas analyses. Such a procedure is presented in Table 2, which compares the quantities of C and H (in mmoles) in both the starting and final systems.

---

*Paper I in this series is cited as reference 1.

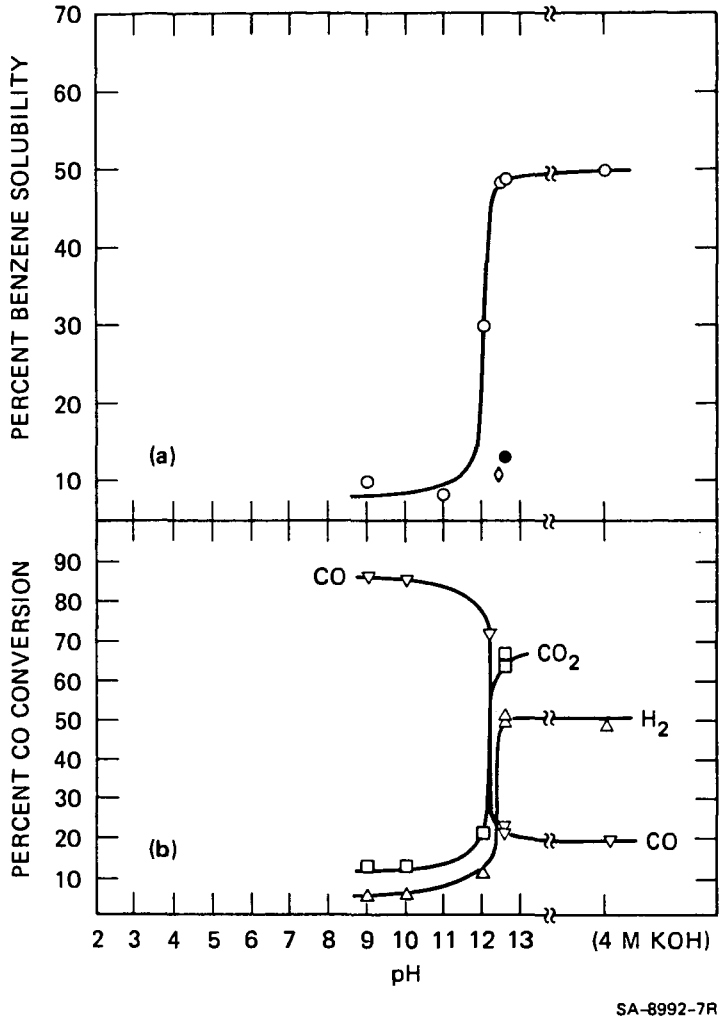

FIGURE 1 (a) CONVERSION OF COAL TO BENZENE-SOLUBLE FRACTIONS VERSUS pH OF INITIAL MEDIUM (○ = CO; ◇ = H_2; ● = formate/N_2); (b) CO CONVERSION (▽ = CO; △ = H_2; □ = CO_2)

Table 1

COAL CONVERSION AT 400°C FOR 20 MIN IN CO/H_2O SYSTEMS AT pH 12.6

	Benzene-Soluble Product					Benzene-Insoluble Product				
Run No.	% Soluble	%H	%C	%N	%S	% Insoluble	%H	%C	%N	%S
Starting Coal	--	--	--	--	--	1	4.66	75.05	1.1	2.1 (org)
26	48	7.26	85.12	1.4	--[a]	41	5.01	79.53	2.0	--[a]
28	48	8.25	83.55	0.6	--[a]	39	4.92	80.75	1.8	--[a]

NOTE: The coal used in this work is from Pennsylvania State University, number PSOC 26. It has been beneficiated by PSU through its flotation procedure. The runs are conducted on 10 g coal, using 36 g H_2O.

[a]Pending.

The recovery in coal-carbon in this case is 95%, which is a typical value for our studies in these systems. The product gases contain only traces of methane, and we have found only trace quantities of phenolic materials in the final aqueous phase.

Table 2

DETAILED MASS BALANCE FOR RUN 26
(Quantities in mmoles)

Starting Coal (10.0 g)			Product Coal* (8.7 g)		Remarks
C	625	→	C	594	95% C recovery
H	460	→	H	585	125 H gain
Starting Gas			**Product Gas**		
CO	478	→	CO	103	84% C recovery
			CO_2	297	
			H_2	237	120 H lost

*Composite values for both benzene-soluble and benzene-insoluble product fractions.

The CO_2 and H_2 quantities in the product gases are not the same, although on the basis of the water gas shift reaction we would expect equal quantities of these two gases. The deficit in hydrogen (120 mmole H) is that taken up by the coal. The match in this case may be better than we might expect, but for most runs the agreement is good.

The C-recovery in the gas product CO_x here is typical, and it is likely that the missing C is in the aqueous phase in the form of formate and bicarbonate. We have made no attempt to quantify the inorganic, water-soluble carbon.

This type of mass balancing is readily performed with the products of these conversions. Because the system is "clean," the close balances obtainable provide us with the opportunity to work with coal almost as a "pure" organic compound.*

Figure 1 shows further that at pH = 12.6 the replacement of CO with H_2 was ineffective; the use of potassium formate with N_2 was equally unproductive. A closer look at these results is presented in Table 3, which includes the product gas composition.

Clearly, hydrogen present at the beginning of a run in place of CO does not provide effective conversion of the coal. The considerable contrast to the results obtained in systems containing CO shows that the hydrogen produced in the latter systems is formed concurrently with the coal conversion and does not play a role in the conversion itself.

For the formate case, the quantity of added formate salt was equivalent on a molar basis to twice the hydrogen added to the coal in the high conversion pH 12.6 runs with CO. Thus there was enough hydrogen present for the conversion; however, the system was

*Further study with these "clean" systems is planned. In some preliminary work along these lines with the focus on oxygen balance, it has been observed that the ratio of the hydrogen gained in the coal produce (ΔHg) to oxygen lost (ΔO_g) was close to 2.0 for several runs. This finding is similar to that discussed by Whitehurst for work with conventional conversion systems. (5)

Table 3

TEST OF THE ROLE OF HYDROGEN AND FORMATE AT pH = 12.6 IN CO-H_2O CONVERSION SYSTEMS AT 400°C/20 MIN

Run No.	Conditions	Benzene-Soluble %	Gas Composition (%)		
			CO	H_2	CO_2
26	CO-H_2O	48	14	35	47
27	H_2/H_2O	11	8	86	2
66	N_2-H_2O-HCOOK[a]	13	1[b]	90[b]	9[b]

[a] 167 mmoles potassium formate.
[b] Relative quantities, ignoring the N_2.

Table 4

COMPARISON OF CO/H_2O AND TETRALIN CONVERSION SYSTEMS

Conversion Medium	Benzene Solubility (%)	H/C[a]		H_{ali}/H_{arom}[d] (BS)
		BS[b]	BI[c]	
Tetralin	37	1.01	0.72	∿ 2.7
CO/H_2O	48	1.01	0.65	∿ 3.0

[a] Molar.
[b] Benzene-soluble fraction.
[c] Benzene-insoluble fraction.
[d] By ^1H nmr.

completely nonconverting. In addition, except for the starting N_2, the product gas composition was primarily H_2, with virtually no CO_2 formed. In this case the formate was probably converted to oxalate, a well-known reaction. (6)

Products

A conventional conversion run was performed with tetralin at 400°C/20 min to provide product material for comparison with the products for the CO/H_2O systems. Both products were fully pyridine-soluble. A detailed comparison is provided in Table 4.

The products are thus very similar in terms of their H/C ratios and H_{ali}/H_{arom} ratios. Other comparisons were made using hplc, ^1H nmr, and field ionization mass spectrometry (FIMS) as shown in Figures 2, 3, and 4. The hplc profiles for the benzene-soluble fractions are very similar, with virtually identical retention volumes.

The ^1H nmr spectra in Figure 3 are of the benzene-soluble fraction for both the tetralin and CO/H_2O systems and include a spectrum of the benzene-soluble fractions of an SRC sample of Illinois No. 6 coal from the Wilsonville, Alabama plant. The tetralin-derived material clearly contains incorporated tetralin; however, except for that factor the spectra are qualitatively very similar. The H_{ali}/H_{arom} for the SRC is $\sim$ 1.1, considerably smaller than that value for the other two samples. This difference is most likely due to the higher temperature at which the SRC is produced.

Field ionization mass spectrometry is a mass spectral procedure using low energy ionization, and most molecules are observed with the technique as molecular ions. (7) The procedure is particularly useful applied to coal liquefaction studies, since it can provide a true molecular weight profile for any given fraction.

In Figure 4, which represents the FIMS spectra of the same three benzene-soluble fractions, some differences emerge between the three conversion products. The SRC fraction has the most narrow distribution, followed by the tetralin and CO/H_2O fractions, respectively. The last in particular displays a rather broad distribution, and the detailed differences are expected to be the subject of future study.

Discussion

Our observations can be summarized as follows:

- CO/H_2O systems at initial pH values above 12.6 successfully convert Illinois No. 6 coal to a product that is fully pyridine-soluble and has benzene and hexane solubilities of 50% and 18%, respectively.
- The product gases are H_2 and CO_2. However, the expected H_2/CO_2 ratio of 1.0 based on the water gas shift reaction is not observed, with the deficit in hydrogen being found in the increased hydrogen content of the coal product.
- These clean systems provide good elemental balances, with typically 95% coal carbon recovery and a good hydrogen balance. The $\Delta H_g/\Delta O_\ell$ ratio is close to 2 in preliminary work.
- The system with H_2 in place of CO is not effective, and potassium formate under an N_2 atmosphere is equally ineffective.
- The products are very similar to those obtained in conventional tetralin conversions.

These results can be considered from two points of view. First, it is of interest to consider the advantages this chemistry might provide in a large-scale coal conversion process. The conversion is catalytic in base, with the turnover number for OH^- (the molar ratio of H added to the coal to the quantity of base present) calculated from the values in Tables 1 and 2 to be 80-90.* It is thus an efficient process, and while catalyzed, its homogeneous nature would avoid the common problem of catalyst fouling due to carbon deposition. The system thus has good recycle potential and small catalyst/coal loading requirements. Hydrogen is a product gas and useful for subsequent upgrading of the coal product.

*For run 26, 125 mmole H is gained by the coal in a system 0.04 M in OH^- of volume 36 ml. Thus the turnover number = 125/(36 x 0.04).

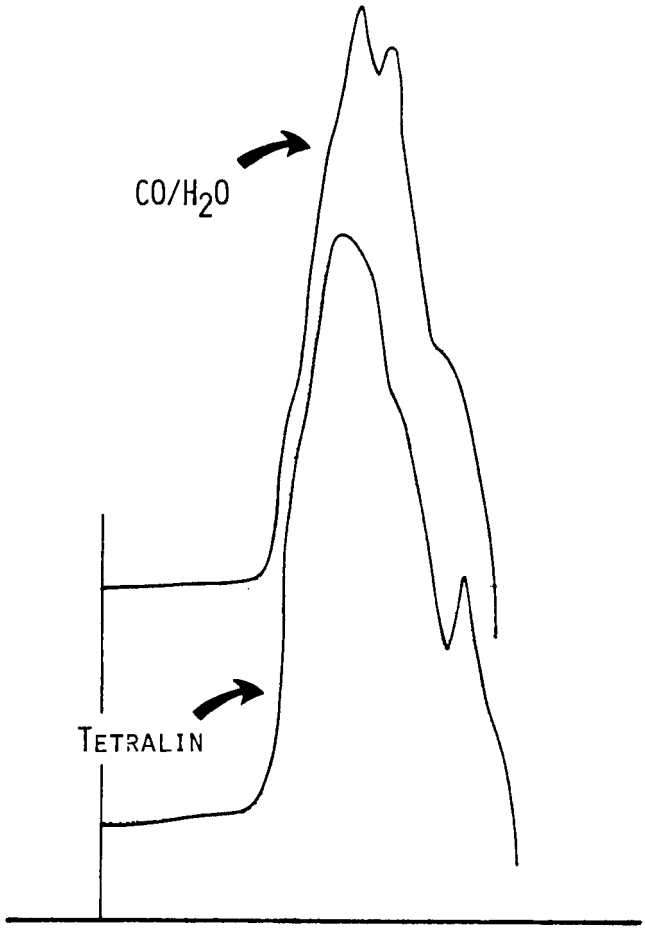

Figure 2. High pressure liquid chromatographs of the benzene-soluble fractions from conversions with Tetralin and CO/H_2O.

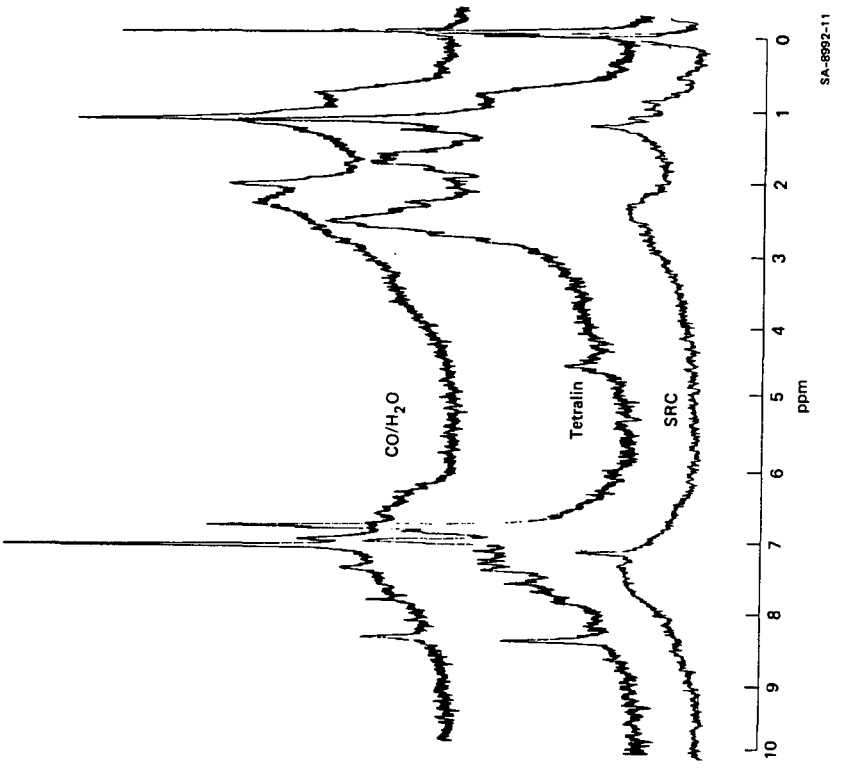

Figure 3. ^{1}H-nmr spectra of the benzene-soluble fractions of SRC, tetralin, and CO/H_2O conversions.

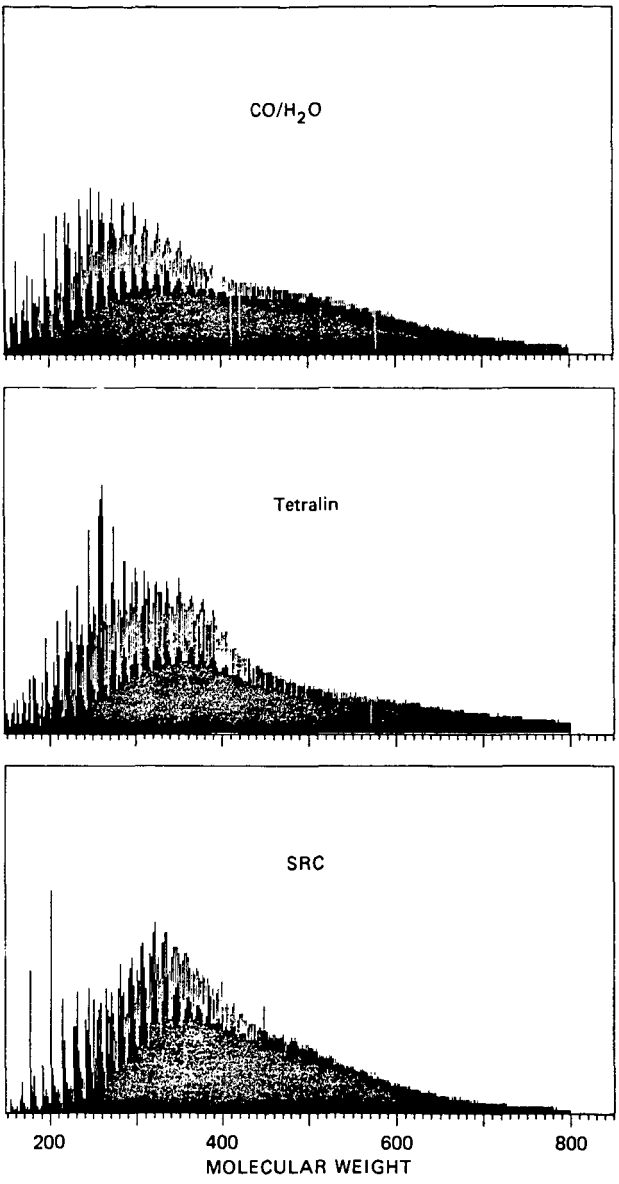

Figure 4. FIMS spectra of the benzene-soluble fractions of SRC, Tetralin, and CO/H_2O conversion.

The second view to be taken of these results concerns the clean nature of the conversions. We suggest that the system would be useful for studies in coal structure and conversion mechanisms since the recoveries are very high, and there is no organic medium to deal with. Both nmr and mass spectrometry studies could be applied to the products from these conversions, and we expect this work to continue along those lines.

Acknowledgment

We acknowledge the support of the U.S. Department of Energy for this research.

References

1. D. S. Ross and J. E. Blessing, Fuel, 57, 379 (1978).
2. D. S. Ross, J. E. Blessing, and Q. Nguyen, Paper presented at the 88th National AIChE Meeting, June 10, 1980, Philadelphia, PA.
3. H. R. Appell, R. D. Miller, and I. Wender, "On the Mechanism of Lignite Liquefaction with Carbon Monoxide and Water," presented before the Division of Fuel Chemistry of the American Chemical Society, 163rd National Meeting of the American Chemical Society, April 1972.
4. C. Collins, B. Benjamin, V. Raaen, P. Maupin, and W. Rouk, preprints of the Division of Fuel Chemistry, American Chemical Society, 22, (5) 98 (1977).
5. D. Whitehurst in Organic Chemistry of Coal, ACS Symposium Series 71, J. Larsen, Ed. (1978).
6. P. A. Florio and G. R. Patel, in Kirk-Othmer Encyclopedia of Chemical Technology, 2nd ed., Vol. 14, (John Wiley and Sons, Inc., New York, 1967) p. 356.
7. G. A. St. John, S. E. Buttrill, and M. Anbar, American Chemical Society Division of Fuel Chemistry Preprints, 22 (5), 141 (1977).

Effect of Preoxidation on Reactivity of Chars in Steam

K. Gomi

New Energy Development Authority of Japan, Department of Coal Technology Development, 3-1-1, Higashi-Ikebukuro, Toshima-ku, Tokyo, Japan

Y. Hishinuma

Hitachi Research Laboratory, Hitachi Ltd., 4026 Kuji-machi, Hitachi-shi, Ibaraki-ken, 319-12, Japan

The investigation of the rate of reaction of char-steam is very important in the development of a coal gasification process and also in the production of activated cokes from coal. The objective of this work is to measure the rate of reaction of preoxidized coal char in steam and to investigate the effect of changes in the preoxidation conditions, especially in the preoxidation temperature and the degree of burn-off, on the reactivity of the char in steam.

Apparatus and Procedure

The coal used here was Taiheiyo coal, a non-caking bituminous coal from Hokkaido, Japan. The raw coal was ground and 0.35-0.42mm fractions were used. They were carbonized in N_2 at 1000°C for 2h.

The Cahn R.G. balance was used for reactivity measurements. About 100 mg of char was placed on a quartz pan (20mm i.d.), which was suspended from the balance at the center ot the furnace. The sample was then heated to the desired preoxidation temperature (400-550°C) in N_2 and the N_2 was replaced by a N_2-O_2 mixture with an O_2 concentration of 20%. The progress of the preoxidation process was followed until the desired weight decrease occurred. After that, the N_2-O_2 mixture was replaced by N_2 and the sample was heated to the desired reaction temperatures (800-900°C). Then a N_2-H_2O mixture containing water vapor at a partial pressure of 13.2 KPa was admitted to the apparatus. This water-vapor pressure was generated by bubbling N_2 through deairated distilled water of a temperature of 60°C. The weight of the sample was recorded continuously as a function of time.

The amount of CO and CO_2 given off by the preoxidized chars was measured with the induction heating pyrolyzer. The product gases were analyzed with a gas chromatograph which was coupled to the pyrolyzer.

Results and Discussion

Effect of preoxidation on char reactivity in steam

The gasification rates were determined for each of the preoxidized chars using the following rate expression:

$$\frac{dXc}{dt} = k\ (1 - Xc) \qquad 1)$$

where Xc represents the fractional conversion of carbon (daf) and k is the rate constant.

In Figure 1, the (dXc/dt) for typical samples are plotted against (1-Xc). As can be seen in Figure 1, the curve for the

char that was not preoxidized rises slowly to a plateau and then falls away gradually. On the other hand, the curves for the preoxidized char show a continuous gradual falling away, with no initial slow rise and no plateau.

Effect of carbon burn-off during preoxidation on char reactivity in steam

$(dXc/dt)i$ at 850°C for chars preoxidized to different burn-off levels at various temperatures are also calculated with the above procedure and plotted against the burn-off during preoxidation as a function of the preoxidation temperature, as shown in Figure 2. $(dXc/dt)i$ is the rate of reaction observed at zero conversion.

As seen in Figure 2, the $(dXc/dt)i$ for the preoxidized chars increase with burn-off during preoxidation. The extent of this is rather large for the chars preoxidized at relatively lower temperatures (400-430°C). On the other hand, as the oxidation temperature rises, the degree of increase in the rates is smaller.

Effect of carbon burn-off during preoxidation on amount of CO and CO_2 given off

In Figure 3, the total amounts of CO and CO_2 given off, when heated at 920°C, by samples that were preoxidized to varying degrees of burn-off at temperatures between 400 and 550°C are plotted against the burn-off that occurred during the preoxidation. As shown in the Figure 3, the total amounts of CO and CO_2 given off by the chars preoxidized at lower temperatures increased markedly with increases in burn-off, but the total amounts given off by the chars preoxidized at higher temperatures increased very little with increases in burn-off.

It is interesting to note that the relationship between the initial rate of reaction of char-steam and the burn-off that occurs during preoxidation, shown in Figure 2, is similar to the relationship between the total amounts of CO and CO_2 given off by samples at 920°C and the burn-off that occurs during preoxidation shown in Figure 3. In both cases, an increase along one axis yields an increase along the other.

From earlier works (1) (2), it is well known that during the reaction of pure carbon with oxygen a surface oxide is formed and that the thermal decomposition of the oxide yields a mixture of CO and CO_2. Phillips et al. (3) found that the amount of a surface oxide formed on a sample of particular burn-off decreased with increasing reaction temperature. From the experimental results shown in Figure 3, we conclude that the amount of a surface oxide increases with burn-off during preoxidation and the amount on a sample of particular burn-off decreases with increasing preoxidation temperature. Phillips et al. (3) suggested that decomposition of the surface oxide leaves highly reactive sites. Considering these works, our results suggest that the increase in the initial rate of reaction of the preoxidized char in steam is due to an increase in the number of highly reactive sites left by the decomposition of the surface oxide.

Conclusions

The reactivity of preoxidized char in steam has been investigated. It has been found that preoxidation of char markedly enhances the initial rate of reaction of steam-char and that the degree of the increase parallels the increase in burn-off during

preoxidation. However, the preoxidation temperature strongly affects the degree to which the reaction rate can be increased. It has also been found that there is a very intimate relationship between the degree to which the reaction rate can be increased and the amount of CO and CO_2 given off by preoxidized char.

References

1. Phillips, R., Vastola, F.J. and Walker, P.L., Jr., Carbon, 8, 197 (1970)

2. Laine, N.R., Vastola, F.J. and Walker, P.L., Jr., Carbon, 67, 2030 (1963)

3. Phillips, R., Vastola, F.J. and Walker, P.L., Jr., Carbon, 7, 479 (1969)

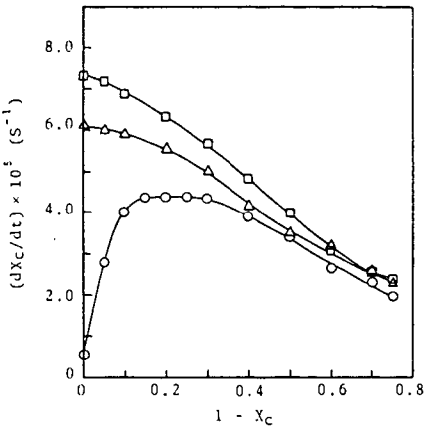

Fig.1 Variation of reaction rates in steam at 13.2 kPa and 850°C with conversion of chars. Burn-off during preoxidation at 430°C (%, daf): ○ none; △ 7.5; □ 11.1.

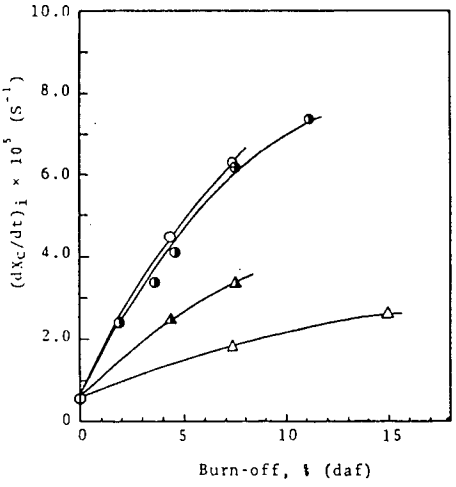

Fig.2 Effect of carbon burn off during preoxidation on char reactivity in steam at 850°C. Preoxidation temperature: ○ , 400°C; ◑ , 430°C; ▲ , 480°C; △ , 550°C.

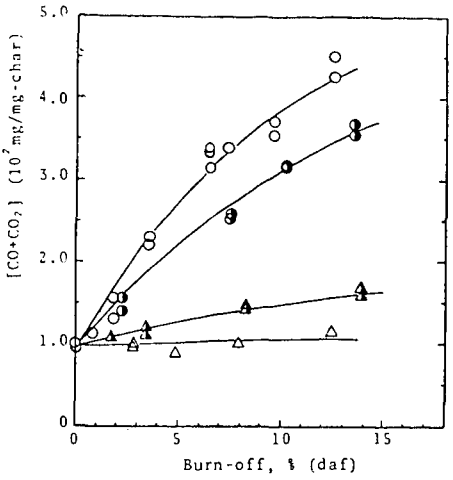

Fig.3 Effect of carbon burn-off during preoxidation on amount of CO and CO_2 given off at 920°C. Preoxidation temperature: ○, 400°C; ◑, 430°C; ▲, 480°C; △, 550°C.

A Study of Deactivation and Regeneration of Catalysts Used in the LC-Fining of Solvent Refined Coal

C. W. Curtis, J. A. Guin, R. Nalitham, A. Mohsin, and A. R. Tarrer

Department of Chemical Engineering, Auburn University, Auburn University, AL 36849

J. D. Potts and K. E. Hastings

Cities Service Research and Development Company, P.O. Box 3908, Tulsa, OK 74102

Introduction

Lummus Cities-Fining (LC-Fining) was developed by Cities Service over the past twenty years and is licensed by the CE Lummus Company. The technology has been successfully applied to the upgrading of low quality petroleum crudes and refinery residues. LC-Fining is currently being applied to the upgrading of coal extracts.

The cost of commercial cobalt molybdenum and nickel molybdenum catalysts has escalated by a factor of four over the last five years. This has produced a strong economic incentive to regenerate used LC-Fining catalysts. The Auburn University research program was undertaken to obtain detailed information on the effect of various solvent and SRC types on the deactivation of a commercial Shell 324 nickel-molybdenum catalyst, to understand the mechanism of catalyst deactivation in catalytic upgrading of coal extracts and to develop effective regeneration methods.

Experimental

Materials. The solvents used in this study were Koppers heavy residue creosote oil, hydrogenated to 7.0%, 7.5% and 8.0% hydrogen and labeled for this study as "solvent D," "solvent C," and "solvent AB," respectively. The solvent refined coals (SRC) used in this study were from (1) Pyro Kentucky #9 coal processed at the Wilsonville SRC Pilot Plant using Kerr McGee critical solvent deashing as the solids separation method and labeled as SRC I-A (Wilsonville Run 161 and 163); (2) Kentucky #9 coal processed at the Fort Lewis, Washington SRC Pilot Plant and labeled as SRC I-B; and (3) Fies coal processed at the Wilsonville SRC Pilot Plant also using Kerr McGee deashing and designated as Fies SRC (Wilsonville Run 209). The catalyst used was Shell 324 nickel-molybdenum, 1/32 inch extrudate. The catalyst was presulfided according to the manufacturer's suggested procedure before use. Spent catalysts were obtained from the CE Lummus LC-Fining PDU (Process Development Unit) operation in New Brunswick, New Jersey. Spent catalyst A was obtained after processing a 70/30 volume blend of SRC I-A/solvent AB for 28 days, and spent catalyst B was obtained after processing a 50/50 volume blend of SRC I-B/solvent AB for 24 days. Elemental analyses of the solvents and SRC's are given in Table I. Naphthalene (Fisher, scintanalyzed) and hexadecane (Pfaltz and Bauer) were used in the model compound hydrogenation reactions.

Equipment and Analysis. Batch catalyst deactivation experiments and naphthalene hydrogenation reactions were performed in tubing bomb reactors of volumes of 46 cc and 17.5 cc, respectively. The tubing bomb was immersed in a fluidized sand bath maintained at 430° ± 2°C and was agitated at 860 CPM. Hydrogen was charged to the tubing bomb through a Nupro fine metering valve.

Products from the naphthalene hydrogenation reactions were analyzed by gas chromatography using a Varian Model 3700 equipped with a SP2250 column (2.4 m x 0.3 m O.D.), FID detection and temperature programming from 60° to 165°C at 5°C/min. Surface area measurements of the catalysts were obtained by nitrogen adsorption. Catalyst

pellets were regenerated by low, medium and high temperature ashing. A four chamber L.F.E. Model 504 low temperature asher (LTA) operated at 0.5 mm Hg oxygen and 250 watts was used for the LTA experiments.

Reaction Procedures. The batch catalyst deactivation study was performed in a 46cc tubing bomb at 430°C and 1250 psig initial hydrogen pressure charged at 25°C. A 70/30 SRC/solvent charge (weight basis) was used with an initial fresh catalyst weight of 1.25 g. Four deactivation cycles were performed; each cycle was followed by a separate hydrogenation reaction on a catalyst aliquot using a 10 wt.% naphthalene in hexadecane solution reacted in a 17.5 cc tubing bomb at the reaction conditions of 410°C and 1250 psig.

Results and Discussion

Catalyst Deactivation. Deactivation of Shell 324 Ni/Mo catalyst used in the upgrading of SRC was examined in four cycle batch deactivation experiments using various SRC/solvent feed blends. The loss of catalyst hydrogenation activity after the SRC reaction was measured by the degree of naphthalene hydrogenation after each cycle. As shown in Table 2, the catalyst showed deactivation in each SRC/solvent system as measured by a decrease in naphthalene conversion. A comparison of the activity level of the fresh presulfided Ni/Mo catalyst is also given. Of the various combinations of SRC and solvent employed, the SRC I-A/solvent C and SRC I-B/solvent C systems appear to have the least catalyst deactivation after four reaction cycles.

When solvent and catalyst with no SRC present are reacted in a similar set of experiments, essentially no catalyst deactivation was observed as measured by changes in naphthalene conversion. However, comparisons of the entire product distributions between the fresh presulfided catalyst and the solvent treated catalysts showed a definite difference as illustrated in Table 3. Less decalin formation and more tetralin formation of the solvent treated catalyst represents a decrease in the hydrogenation activity of the catalyst after contact with the solvent.

Tailoring of the solvent and SRC/solvent combination for maximal SRC upgrading and minimal catalyst deactivation may be an important factor in catalytic upgrading according to preliminary evidence. This certainly warrants further investigation. A comparison of the five different SRC/solvent combinations using catalyst prepared in the same batch indicates that solvent AB in concert with the SRC's used may have a more pronounced deactivating effect than that of solvent C. The deactivation behavior plotted in terms of the naphthalene conversion after each cycle is given in Figure 1.

Since coking occurs at high carbon loadings, elevated reaction temperatures and conditions of hydrogen starvation, experiments were performed to investigate the effect of each of these parameters on catalyst deactivation at the SRC/solvent reaction temperature. Deactivation data has been obtained with a range of SRC loadings in two cycle hydroprocessing reactions. The effect of increased SRC loading on catalyst activity is evident after one cycle and becomes more pronounced after two. Catalyst activity definitely decreases with increased SRC loadings (Figure 2). Experiments were also performed at constant SRC loading at elevated temperatures and at conditions involving both excess and limited hydrogen. Experiments using SRC I-A and SRC I-B with solvent AB and fresh presulfided catalysts show high levels of activity at 430°C after one cycle which rapidly dropped off to essentially no activity at 500°C (Table 4). Hydroprocessing reactions were performed using 1250 psig hydrogen and no hydrogen at 500°C. The catalysts used were both the spent catalysts from the LC-Fining PDU operation and fresh presulfided catalyst. A 45% increase was observed in the hydrogenation activity level of the fresh sulfided catalyst with hydrogen present as opposed to no hydrogen being present. No difference in catalyst activity was observed for the spent catalyst regardless of hydrogen

presence. A more substantial effect of the hydrogen presence would most likely be observable at lower processing temperatures.

Deactivation Mechanism. Regeneration of spent catalysts from the LC-Fining PDU operation was attempted using controlled oxidation at three temperature levels: low, ~150°C in an excited oxygen atmosphere; medium, 370°C with an air atmosphere; and high, 950°C also with air atmosphere. A histogram of the regeneration levels achieved after oxidation or grinding are shown in Figure 3. The hydrogenation activity of both spent catalyst A and B is low before oxidative treatment, with catalyst A showing greater deactivation (PDU run at 70/30 SRC/solvent ratio). Spent catalyst B can be essentially regenerated to its original activity level as based on naphthalene conversion by a combination of medium temperature ashing followed by presulfiding. Presulfiding alone provides significant regeneration for spent catalyst B and a definite increase in activity of spent catalyst A. Presulfiding of the spent catalyst pellets apparently increased the catalyst activity by activating or sulfiding sites which had lost their activity during the coal extract upgrading reaction and removal of hydrocarbon deposits. Grinding the spent catalyst pellets to -200 mesh provides increased activity for both spent catalysts possibly by exposing fresh active sites. Both high temperature and low temperature ashing show slight increases in the activity of spent catalyst B, but none for spent catalyst A.

The rate of carbonaceous material removal from the spent catalysts during medium temperature oxidation is shown in Figure 4. After forty hours of oxidation, spent catalyst B pellets and pellets of both spent catalyst A and B ground to -200 mesh reached constant weight. However, ninety hours are required for spent catalyst A to reach constant weight. These results indicate that spent catalyst A obtained from a higher SRC loading in PDU feed may have more carbonaceous material blocking the pores. The carbonaceous material may also be more refractory.

Surface area analyses were performed using both spent catalysts A and B and catalysts A and B regenerated by medium temperature oxidation followed by sulfiding. The surface areas before and after treatment and the naphthalene conversions obtained are given in Table 5. A direct correlation between surface area and hydrogenation activity of the catalyst is observed and is shown in Figure 5.

Spent catalysts obtained after four batch reaction cycles of SRC I-B/solvent AB and Fies SRC/Solvent D were regenerated in the same manner as the spent catalysts obtained from the PDU operation. By medium temperature ashing followed by presulfiding, the batch deactivated catalysts are regenerated to essentially their original activity level. Medium temperature oxidation alone of the batch deactivated catalysts gives partial but not complete catalyst regeneration.

To determine the effect of metals deposition on catalyst deactivation, ash obtained from Kentucky #9 coal was added to solvent C and batch deactivation experiments were performed. The degree of catalyst deactivation at varying ash concentrations is shown in Figure 6.

Summary. Batch experiments as well as results from LC-Fining catalytic upgrading of coal extracts indicate deactivation of the Shell 324 Ni/Mo catalyst in the presence of SRC. At increased levels of SRC loading, deactivation increases. The chief cause of catalyst deactivation appears to be coking. The Shell 324 catalyst can be substantially regenerated after the upgrading reaction by medium temperature ashing followed by presulfiding.

Acknowledgement

Auburn University gratefully acknowledges the support of Cities Service Research and Development Company for this work.

Table 1

Analysis of Solvents and SRC

	Solvent A/B	Solvent C	Solvent D	SRC I-A	SRC I-B	Fies SRC
Elemental content, wt%						
Carbon	91.48	91.6	91.28	90.3±0.1	87±0.2	87.6±0.2
Hydrogen	8.01	7.5	7.03	6.4±0.2	6.2±0.1	6.2±0.1
Oxygen	<0.5	<0.5	0.88	-	-	-
Nitrogen	0.29	0.36	0.69	2.1±0.2	2.1±0.3	2.0±0.2
Sulfur	0.03	0.19	0.27	-	-	-
Ash, wt%				0.2	0.6	-
Distillation, °F						
276.8	0.0	0.0	0.0			
336.2	0.4	0.9	1.1			
395.6	1.4	3.9	1.8			
435.2	2.3	6.8	2.5			
464.0	3.3	9.6	3.0			
500.0	6.3	15.8	4.4			
582.8	21.6	34.6	12.6			
647.6	25.9	47.5	17.9			
674.6	35.8	57.5	24.5			
746.6	64.0	81.9	52.6			
820.4	100.0	99.9	99.9			

Table 2

Batch Catalyst Deactivation Tests With SRC and Solvent

Feed Blend	Presulfided Catalyst Batch Number	Naphthalene Conversion	Naphthalene Conversion in Activity Test Reaction With Deactivated Catalyst From 1st Cycle	2nd Cycle	3rd Cycle	4th Cycle
Fresh Pre-	1	94				
sulfided	2	90				
Catalyst	3	99.5				
SRC I-A/	1&2		83±5	44±3	33	32
Solvent AB	3		84	60		
SRC I-B/	1&2		86±4	66±5	40	34
Solvent AB	3		83±7	71±7	59	48
SRC I-A/						
Solvent C	3		86	74	67	-
SRC I-B/	3		86	73	68	64
Solvent C	3		85	70	-	-
Fies SRC/	3		92	80	43	22
Solvent D	3		84	75	64	35
Fies SRC/						
Solvent D	3		73	68	59	39

Table 3

Comparison of Product Distribution Before and After Solvent Aging

	Base Activity With Fresh Presulfided Catalyst	Solvent AB		Solvent C	
		1st Cycle	2nd Cycle	1st Cycle	2nd Cycle
Naphthalene conversion	99.5	98.9	98.9	98.9	98.9
Conversion to:					
Trans-decalin	74	34	28	40	29
Cis-decalin	19	11	10	13	11
Tetralin	6	46	58	39	54

Table 4

Effect of Elevated Temperature and Hydrogen Starvation on Catalyst Activity

Hydroprocessing Reaction Temperature, °C (initial H_2 pressure = 1250 psi)	Feed Blend	% Naphthalene Conversion in Activity Test
430	SRC I-A/Solvent AB	84
460	SRC I-A/Solvent AB	51
500	SRC I-A/Solvent AB	17
430	SRC I-B/Solvent AB	84
460	SRC I-B/Solvent AB	40
500	SRC I-B/Solvent AB	10

Catalyst	Feed Blend	Hydrogen Pressure psig (reaction temperature = 500°C)	Naphthalene Conversion in Activity Test
Spent Catalyst A	SRC I-A/Solvent AB	1250	6
Spent Catalyst A	SRC I-A/Solvent AB	0	5
Spent Catalyst B	SRC I-B/Solvent AB	1250	6
Spent Catalyst B	SRC I-B/Solvent AB	0	5
Fresh Presulfided Catalyst	SRC I-A/Solvent AB	1250	17
Fresh Presulfided Catalyst	SRC I-B/Solvent AB	0	12

Table 5

Surface Area and the Hydrogenation Activity of Different Catalysts

Catalyst	Surface Area m^2/g	% Naphthalene Conversion In Activity Test
Spent Catalyst A	2	34
Spent Catalyst B	87	73
Spent Catalyst A-oxidized at 370°C and presulfided	141	92
Fresh presulfided catalyst	188	99
Spent Catalyst B-oxidized at 370°C and presulfided	225	100

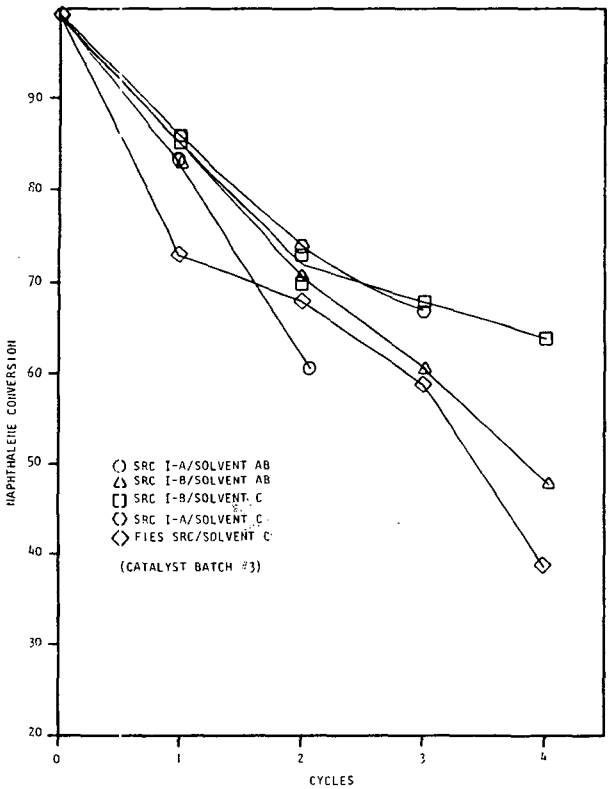

FIGURE 1. PERFORMANCE COMPARISON OF SRC I-A, SRC I-B, AND FIES SRC IN SOLVENT AB AND SOLVENT C

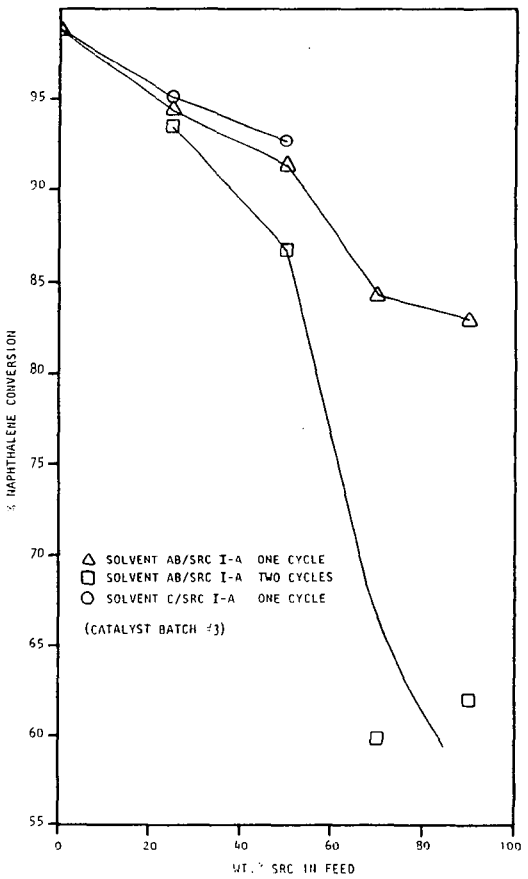

FIGURE 2. FEED BLEND SRC CONTENT EFFECT ON CATALYST DEACTIVATION

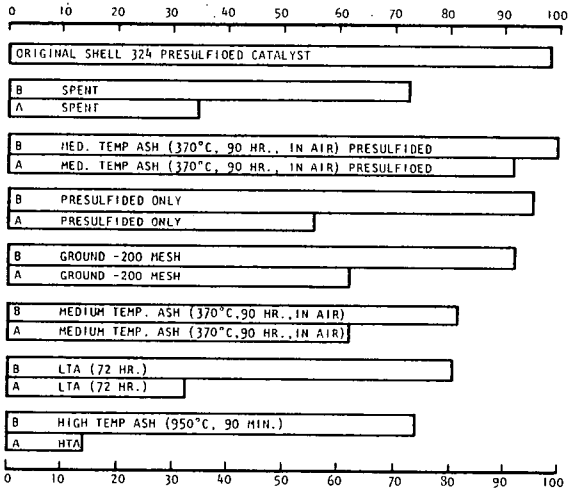

LTA = LOW TEMP ASH HTA = HIGH TEMP ASH

FIGURE 3. SPENT CATALYSTS A AND B REGENERATION

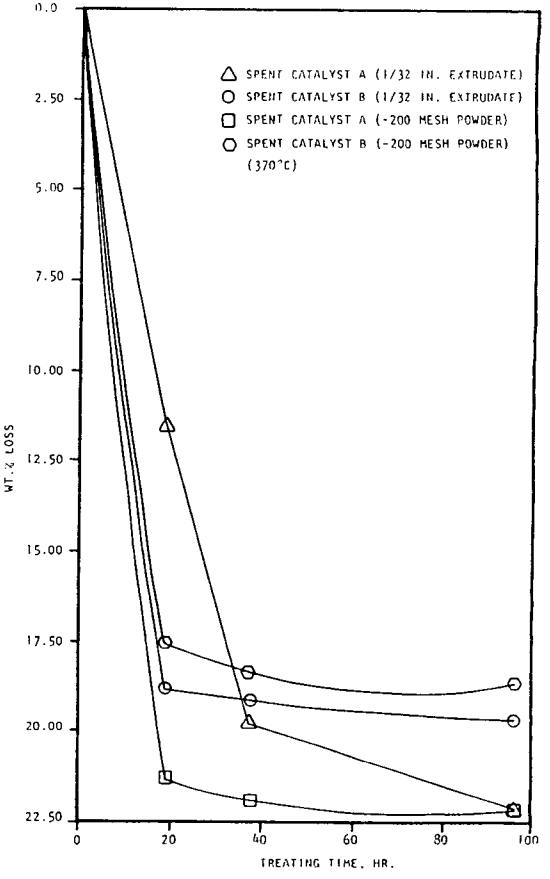

FIGURE 4. SPENT CATALYSTS OXIDATION WEIGHT LOSS CURVES

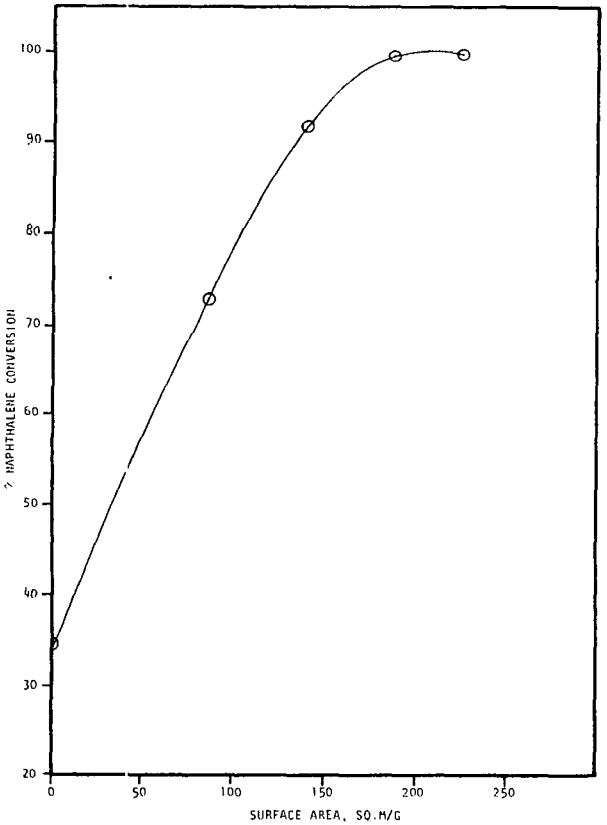

FIGURE 5. SURFACE AREA AND CATALYST ACTIVITY RELATIONSHIP

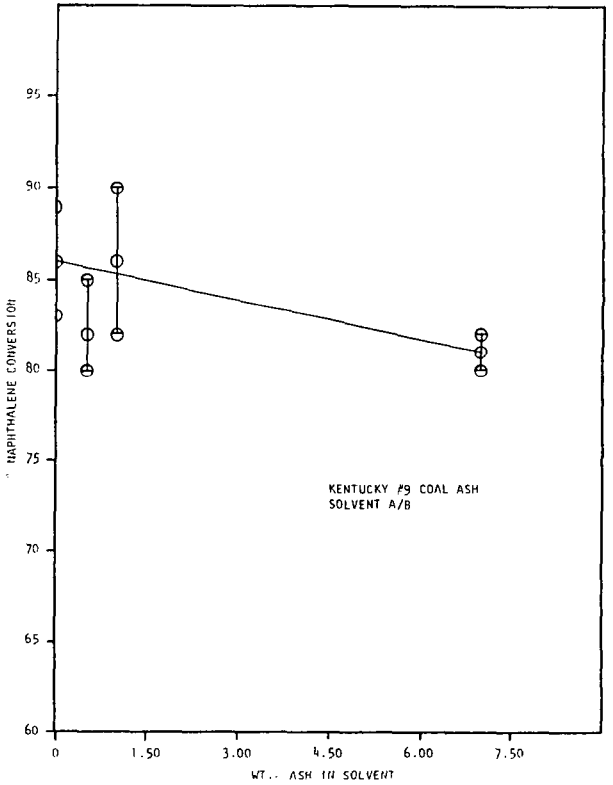

FIGURE 6. CATALYST DEACTIVATION WITH VARYING ASH CONCENTRATION

THE EFFECTS OF CATALYSTS ON SHORT CONTACT TIME COAL LIQUEFACTION*

M. G. Thomas, T. C. Bickel, B. Granoff

Process Research Division 4731, Sandia National Laboratories
Albuquerque, New Mexico 87185

Introduction

An understanding of the effects of inherent (1-3) (i.e., naturally occurring mineral matter) and externally added catalysts (4) is of prime importance for the production of synthetic liquid fuels by the direct liquefaction of coal. Future liquefaction process concepts will require an extensive research data base, including the rates and mechanisms of the various chemical steps that occur when solid coals are converted into useful liquid products. (5) In a generic direct coal liquefaction process (Figure 1), the coal/solvent slurry and hydrogen are first preheated to liquefaction temperatures (400-475°C), and are then fed to a catalytic reactor or dissolver. The average residence time in the reactor is generally an order of magnitude greater than that in the preheater. (6) The reactions that occur in the preheat stage involve the dissolution of coal; i.e., the conversion of coal to species (such as preasphaltenes) that are soluble in tetrahydrofuran (THF). (7) All current direct liquefaction processes utilize preheaters where coal dissolution takes place, and they also take advantage of the catalytic effects of the inherent mineral matter in coal.

Short-contact-time (SCT) liquefaction (8), as we define it, refers to the minimum time at a given temperature required for the complete dissolution of the coal. This time is sufficiently long to convert the coal to preasphaltenes, but is short enough so that secondary reactions (i.e., the conversion of preasphaltenes to toluene and pentane solubles) take place to only a limited extent. Traditionally, the initial dissolution step has not been considered in catalyst studies, generally due to the belief that this step cannot be catalytically enhanced. We will show that catalysts do have an effect on SCT liquefaction. First, however, we will describe a mechanistic pathway for coal liquefaction reactions. Following this, we will discuss the role of catalysts and the potential impacts of catalysis on current and future liquefaction processes.

Discussion

The following series reaction path for coal liquefaction is in agreement with the bulk of literature data: (9-10)

1. coal + solvent $\rightleftharpoons$ preasphaltene
2. preasphaltene $\rightleftharpoons$ asphaltene
3. asphaltene $\rightarrow$ oil

The first step of this reaction is usually considered to be noncatalytic; i.e., solid coal plus solid catalyst plus a source of hydrogen is a very unlikely type of reaction. In addition, molecular hydrogen does not appear to have a significant involvement in the dissolution process.

* This work supported by the U.S. Department of Energy.

The secondary reactions, 2 and 3, are considered to be solution phase reactions and do involve hydrogen transfer. Direct interaction between hydrogen gas and model compounds has been observed, but the more usual mechanism is the transfer of hydrogen through the solvent. (11-12) This reaction in particular appears to be catalytically enhanced.

At this point, one needs to reassess the possibility of catalyst affecting the dissolution step. There are marked solvent quality effects both in upgrading and in coal dissolution.(13-14) Because the interconversions of the preasphaltenes, asphaltenes and oil are affected by catalysts, and because these moieties are parts of the solvent which affects dissolution, it follows that catalysts are affecting coal dissolution. The existence of the solvent quality effect also unequivocably establishes that solvent is an integral reactant (not just a medium) in the first step of dissolution.

In Figure 2, two examples of catalytic effects of mineral matter on liquefaction are shown. (15) These examples are specific to FeS_2, since FeS_2 has been shown to be the most active catalytic species in mineral matter. In Figure 2a, we have shown enhanced conversion with the incremental addition of FeS_2. This indicates apparent rate enhancement although insufficient data were collected to compare rate constants. At constant conversion, Figure 2b, a selectivity to oil (as opposed to gas make) is obtained by the addition of 5 wt % pyrite and lowering the reaction temperature by 25°C.

An example specific to SCT liquefaction is shown in Figure 3. (16) Here we have shown the marked effect of the addition of FeS_2 on the dissolution and conversion of coal at temperatures where secondary reactions are not observed. An $\sim$ 15 wt % increase in THF solubles and a complete regime change from solvent imbalance (negative toluene solubles) to a small positive conversion to toluene solubles is observed.

These examples have demonstrated marked effects, both in apparent rate enhancement and in product selectivity. However, to optimize the possible catalyst effects, we need to properly utilize: (1) the Fe-S system; and (2) the reactivity of the coal-derived products.

The Fe-S system has been studied in detail both in the presence and absence of H_2. In 1947, Schwab and Phillinis (17) measured the decomposition of FeS_2 in a TGA apparatus and determined rates and activation energies. Although the rates were affected by the presence of hydrogen, the activation energy was measured to be $\sim$ 30 kcal/mole in each case. The measurements point out that hydrogen is not part of the activated complex of the rate determining step; i.e., hydrogen adsorption and dissociation may occur but does not affect the rate of decomposition of pyrite. A mechanism consistent with the data is:

$$FeS_2 \rightleftharpoons FeS + S$$
$$S + H_2 \rightleftharpoons HS + H$$
$$H + HS \rightleftharpoons H_2S$$

Paramount in this description is the concept that this in an equilibrium system and that no individual species involved can be described separately to explain the observed catalytic effects. In an operational sense, it is most likely the H_2S fugacity which controls the equilibrium and establishes our steady state activity.

The rate of decomposition is affected by coal and solvent, but the activation energy is not a function of the system (i.e., external atmosphere). Rate constants for the decomposition, at 350°C, in the presence of coal and solvent, solvent and hydrogen, and with hydrogen alone have been calculated, $k_{coal+solvent} = 4x10^{-2}$ mole/min, $k_{solvent} = 4.5x10^{-2}$ mole/min, $k_{H_2} = 1.9x10^{-1}$ mole/min. (18)

Our second approach to catalyst activity regards the response of the substrate molecules (e.g., preasphaltenes) to "catalytic" treatment. A method developed for obtaining and observing effects is shown in Figure 4. (6) Three preasphaltenes, differing in reactivity, were prepared in three separate autoclave runs at 350°C/30 minutes, 405°C/5 minutes, and 430°C/30 minutes, all at ∿ 1800 psig H_2. Preasphaltenes were isolated by solvent extraction techniques, and their subsequent reactivities were measured in microreactor experiments at 400°C, 10 minutes, and 450 psig H_2. The thermal reactivity (no added catalyst) is shown in Figure 4a as a cross-hatched plane, where the conversion of the preasphaltenes was plotted against the time and temperature at which they were prepared. The speckled plane was obtained by analogous experiments with the addition of a ground supported CoMo catalyst--American Cyanamid 1442A CoMo.

The slope of the plane for the catalyzed runs is greater than that observed for the thermal runs, which indicates a rate enhancement by CoMo. More importantly, the two-plane surfaces intersect. This intersection is a line by definition, Figure 4b. (Increasing the number of points would probably produce non-plane surfaces intersecting in a curve.) This line of intersection describes the demarcation of substrate reactivity between observable catalytic effects, and non-observable catalytic effects. This analysis is catalyst-specific, and our description is reaction-specific for the decomposition of preasphaltenes. Thus we have a way to: (1) test for catalytic activity; and (2) determine when and where catalyst should be employed.

Summary

The effects of catalyst on the early stages of coal liquefaction have been described in terms of changes in dissolution and product distribution. The major points established for SCT liquefaction include:

1. Catalysts of some form are present during the initial stages of all direct liquefaction processes;
2. Catalysts affect both dissolution (indirectly) and secondary reactions; and
3. Coal-derived materials that have been formed at short times are more thermally reactive and more sensitive to subsequent catalytic treatment than coal-derived materials that have been formed at longer residence times.

References

1. P. A. Montano, B. Granoff, Fuel, 59, 214 (1980).

2. J. A. Guin, J. M. Lee, C. W. Fan, C. W. Curtis, J. L. Lloyd, A. R. Tarrer, Ind. Eng. Chem. Process Des. Dev., 19, 440-446 (1980).

3. B. Granoff, P. M. Baca, M. G. Thomas, G. T. Noles, "Chemical Studies on the Synthoil Process: Mineral Matter Effects, Final Report," Sandia National Laboratories Report SAND-78-1113 (1978).

4. A. G. Comolli, R. R. Bernard, E. S. Johanson,, Proc. 14th Intersociety Energy Conv. Eng. Conf., 1, 815-820 (1979).

5. E. C. Moroni, "DOE Overview - Advanced Direct Coal Liquefaction," Fifth Annual Contractor's Conference, EPRI, Palo Alto, CA, May 7-8 (1980).

6. T. C. Bickel, R. M. Curlee, B. Granoff, T. D. Padrick, F. V. Stohl, M. G. Thomas, "Coal Liquefaction Process Research," Sandia National Laboratories Report SAND-80-1426 (1980).

7. R. C. Neaval, Fuel, 55, 237 (1976).

8. DOE Conference on Advanced Two-Stage Liquefaction, Albuquerque, NM February 26-27 (1980).

9. M. G. Thomas, R. K. Traeger, Prep. American Chemical Society, Division of Fuel Chemistry, 24 (3) 224 (1979).

10. Y. T. Shah, D. C. Cronauer, A. G. Mclluried, J. A. Pasaskos, Ind. Eng. Chem. Process Des. Dev., 17 (3) 288 (1978).

11. D. D. Whitehurst, T. O. Mitchell, Prep. American Chemical Society, Division of Fuel Chemistry, 21, 5, 127 (1976).

12. M. G. Thomas, T. C. Bickel, Prep. American Chemical Society, Division of Fuel Chemistry, 27, 38 (1980).

13. D. G. Cronauer, D. M. Jewell, Y. T. Shah, R. J. Modi, Ind. Eng. Chem. Fundam., 18 (2) 152 (1979).

14. J. A. Kleinpeter, F. P. Burke, P. J. Dudt, D. C. Jones, "Process Development for Improved SRC Options: Interim Short Residence Time Studies," EPRI Report AF-1158, Conoco Coal Development Company (1979).

15. B. Granoff, P. A. Montano, "Mineral Matter Effects in Coal Liquefaction," Conf. on the Chem. and Phys. of Coal Util., W. Va. Univ., June 2-4 (1980); also Ref. 3.

16. Unpublished results, Sandia National Laboratories.

17. George-Marin Schwab, J. Philinis, JACS, 69, 2588 (1947).

18. M. G. Thomas, T. D. Padrick, F. V. Stohl, "The Decomposition of Pyrite Under Coal Liquefaction Conditions: A Kinetic Study," submitted for pub. in Fuel, October (1980).

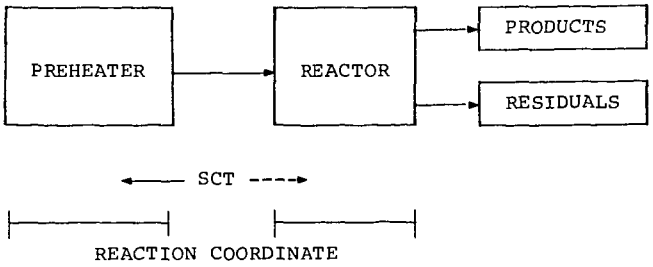

Figure 1. A Generic Description for Coal Liquefaction

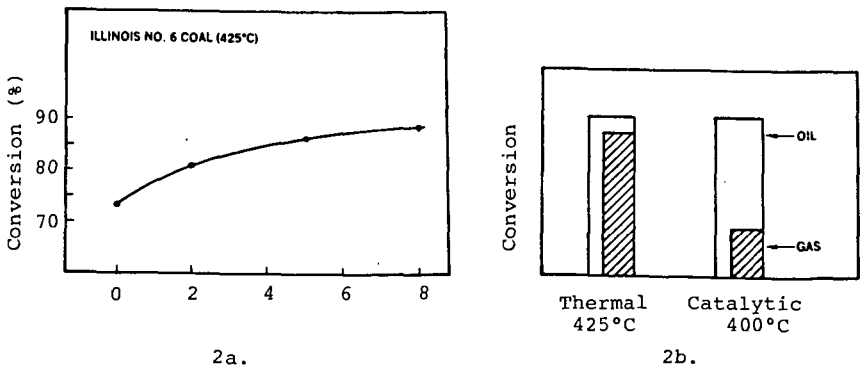

Figure 2. Effect of Mineral Matter on Liquefaction

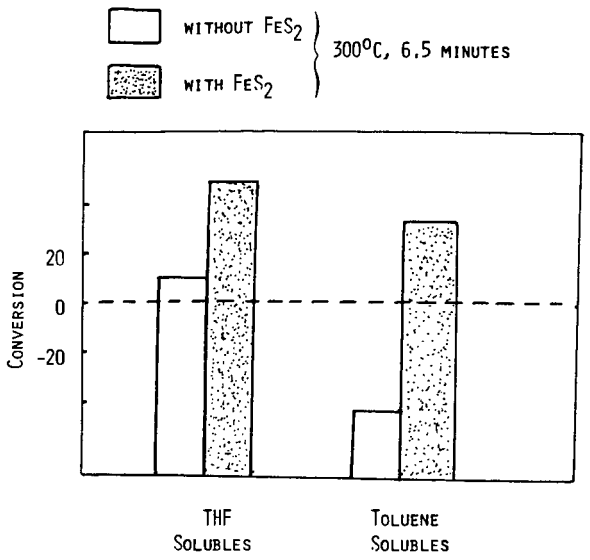

Figure 3. Catalysis of Dissolution by FeS_2

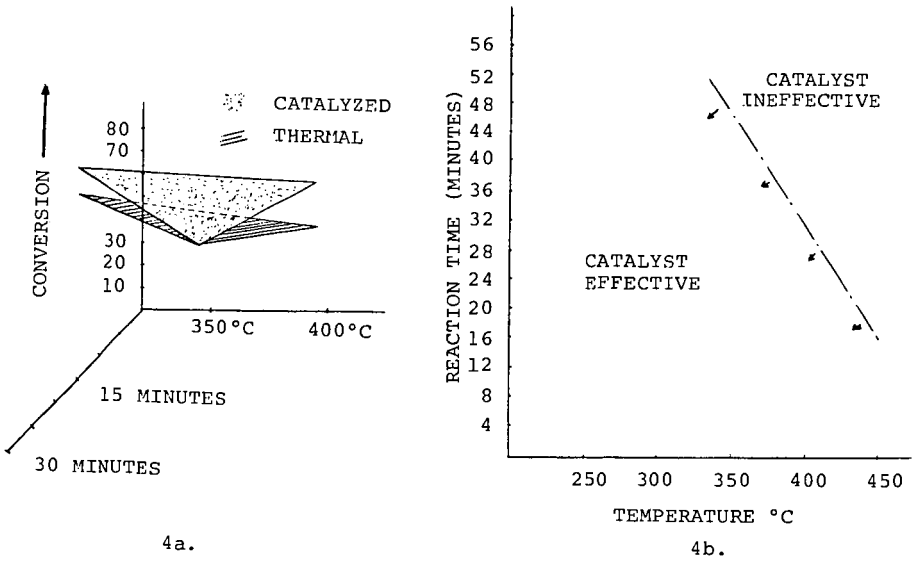

Figure 4. The Effect of Preasphaltene Reactivity on Obtaining and Observing Catalytic Responses

RECENT DEVELOPMENTS IN HIGH GRADIENT MAGNETIC SEPARATION (HGMS) FOR COAL DESULFURIZATION. Y. A. Liu. Department of Chemical Engineering, Auburn University, Auburn University, Alabama 36849.

The objectives of this paper are to describe the basic principles of HGMS, to discuss the general design features of laboratory and industrial HGMS units and to review the recent developments of HGMS processes applied to coal desulfurization. In particular, this paper summarizes the currently available, technical and economical information on various HGMS processes for desulfurization of coal/water slurry, dry pulverized coal, reacted coal slurries (liquefied coal), coal/oil mixture and coal/methanol slurry. In addition, the use of several physical and chemical methods as pretreatment steps for magnetic desulfurization is described. Of particular interest in this paper is a status report of novel continuous HGMS processes being developed for desulfurization of dry pulverized coal for utility applications.

INVESTIGATION OF THE HIGH-TEMPERATURE BEHAVIOR OF COAL ASH IN REDUCING AND OXIDIZING ATMOSPHERES. G. P. Huffman, F. E. Huggins and G. R. Dunmyre. U. S. Steel Corp., Research Laboratory, Monroeville, Pennsylvania 15146.

Ash samples from a large suite of coals were quenched from high temperatures under either a reducing (60% CO/40% CO_2) or an oxidizing (air) atmosphere, and investigated by Mossbauer spectroscopy, scanning electron microscopy/automatic-image-analysis, and X-ray diffraction. Significant partial melting of the ashes occurred at temperatures as low as 200 to 400°C below the initial deformation temperature (IDT) defined by the ASTM ash fusion test. Under reducing conditions, melting is normally controlled by the iron-rich corner of the FeO-Al_2O_3-SiO_2 phase diagram, as evidenced by the observation of such phases as wustite (FeO), fayalite (Fe_2SiO_4), hercynite ($FeAl_2O_4$), and ferrous glass in samples quenched from 900 to 1200°C. The percentage of glass increases rapidly between 900 and 1100°C, approaching 70 to 100% above approximately 1200°C. Ashes rich in CaS are an exception to this rule, exhibiting copious formation of iron sulfide and melting behavior associated with the FeO-FeS phase diagram. Under oxidizing conditions, the percentage of glass in samples quenched from below 1100 to 1200°C is proportional to the amount of the potassium-bearing mineral illite in the coal. Above 1200°C, calcium and to a lesser extent, iron, become effective fluxes; melting accelerates between 1200 and 1400°C and nears completion between 1400 and 1500°C for most ashes.

COAL STRUCTURE CLEAVAGE MECHANISMS: SCISSION OF DIPHENYLMETHANE AND DIPHENYL ETHER LINKAGES TO HYDROXYLATED RINGS

Donald F. McMillen, Walter C. Ogier, and David S. Ross

Department of Chemical Kinetics
SRI International, Menlo Park, CA 94025

INTRODUCTION

Recently a number of workers[1] have subjected model compounds to various coal conversion conditions to (1) confirm that certain coal structures are reactive during coal conversion and (2) infer the conversion mechanisms of real coals from the mechanisms determined for model compounds. Thus, Collins and coworkers recently reported the results of pyrolysis of many model compounds in tetralin at 400°C.[1a] Many, but not all, of the results can be interpreted as reactions involving straightforward unimolecular bond-scission/radical-capping mechanisms or as radical chain reactions involving β-scissions of appropriate bonds.

In one striking and unexplained exception, Collins observed that, although diphenylmethane is for practical purposes totally unreactive in tetralin at 400°C, hydroxydiphenylmethanes (HODPM) are converted to toluene and phenol relatively rapidly, almost as fast as the weakly bonded bibenzyl reacts to form two equivalents of toluene.[1a] This lability cannot indicate reaction by the same mode that has been shown to be operative for bibenzyl, i.e., rate-limiting bond scissions in the original model structures. Table 1 lists the estimated strengths of the weakest bonds of these HODPM compounds, estimated half-lives for unimolecular scission of these bonds, our measured half-lives, and observed products. The observed rates of conversion to phenol and toluene are faster than the estimated rates by a factor of at least 10^6. (The good agreement between estimated and observed rates for bibenzyl indicates both the level of success expected for moderate temperature liquid-phase predictions based on high temperature gas-phase measurements, and the good agreement between the present work and the results of Miller and Stein[1d] for a "well-behaved" system.) Oddly, the half-lives measured in our laboratory for HODPMs are 10 to 20 times longer than those of Collins, but are still very short relative to diphenylmethane. This high reactivity of the hydroxylated diphenylmethane linkage is consistent with earlier observations by Depp, Stevens, and Neuworth[4] of the pyrolysis of 4-pyrenylmethyl-2,6-xylenol, which also results in cleavage (with somewhat less specificity) of the bond between the methylene group and the aromatic ring bearing the hydroxyl group.

It is particularly significant that hydroxydiphenylmethane and hydroxydiphenyl ether structures should be susceptible to degradation by mechanisms other than those traditionally invoked in donor-solvent coal liquefactions because (1) the traditional view[5] of coal structure is that single methylene groups and diphenyl ether structures are common coal linkages. (Recent degradation studies[6] have provided contradictory evidence as to the importance of Ar–CH_2–Ar units in coals.); (2) bituminous coals typically possess one oxygen atom for every 20 carbon atoms, with 40% to 60% of this oxygen present as phenolic-OH;[7] and (3) elimination of part of this oxygen is a critical and time-consuming step in donor-solvent liquefaction processes.[1c,f]

Thus, elucidation of the mechanism(s) of conversion of these structures to lower molecular weight products in tetralin could be of significant importance to the technology of coal conversion

EXPERIMENTAL

Reactions were conducted as 5 wt% solutions in 300 μl of tetralin, in ampoules made from 4-mm fused silica tubing that had been washed in water and acetone and dried by heating under vacuum. When silanized silica surfaces were desired, they were prepared by treatment with hexamethyldisilazane vapor at 200°C for one hour. Samples were introduced and degassed by evacuation to $\leq$ 0.1 torr, frozen in liquid N_2, sealed, and placed with several cubic centimeters of tetralin in steel tubes with Swagelok caps. A thermostatted molten $NaNO_3$-KNO_3 bath provided steady reaction temperatures (± 0.2°C). All reactions were conducted for 21 ± 3 hours at 400 ± 1°C. Heat-up time was < 5 minutes.

Samples for gas chromatographic analysis were prepared by dilution with tetrahydrofuran and, in some cases, addition of an internal standard to determine mass balance. Analyses were carried out on a Hewlett Packard 5711 gas chromatograph with a 1.5 m x 2 mm glass column packed with 5% OV-17 on Chromosorb W. A flame ionization detector was used. Nonlinear calibration curves were constructed for the phenolic compounds. Identification and quantification of peaks was confirmed by GC/MS and capillary GC. Mass balances ranged from 77% to 108%, usually 90% to 100%.

Most compounds were purchased from major suppliers and purified in a sublimation apparatus to ≥ 99.5%. Tetralin was purified by distillation using spinning band columns. The m-HODPM was prepared by the method of Lamartine-Balme et al.[8] The o-MeODPM was prepared from basic o-HODPM and MeI.

RESULTS AND DISCUSSION

The most likely homogeneous mechanism for conversion of hydroxydiphenylmethanes to phenol and toluene in a hydrocarbon solvent involves a keto-enol tautomerism to produce a weakly bonded keto intermediate as shown in Scheme 1.

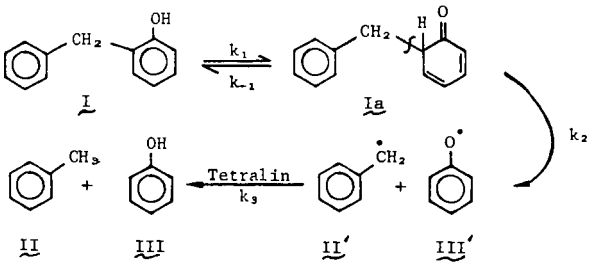

Scheme 1

Although the equilibrium constant for reaction (1) (k_1/k_{-1}) is $\sim 10^{-6}$ (based on estimated[2] enthalpy difference between the phenol and keto forms), unimolecular scission (reaction 2) of the keto-form Ia should proceed rapidly since the estimated strength[2] of the indicated bond is only $\sim$ 45 kcal/mole, at least 40 kcal/mole less than any bond in the original structure (Table 1). If k_{-1} is substantially greater than k_2, then equilibrium between the enol and keto forms will be established before homolysis, and the overall rate will be given by

$$-\frac{d[I]}{dt} = k_{obs}[I] = \frac{k_1[I]k_2}{k_{-1} + k_2} \simeq \frac{k_1}{k_{-1}}[I]k_2 \qquad 1)$$

Using, as a first-order estimate of the A-factor A_2, a value equal to that observed for bibenzyl,[1d,2] Equation 1 results in an estimated rate constant for overall reaction of 1.5×10^{-6}, very close to our observed value of 3.3×10^{-6} sec^{-1} at 400°C. This agreement is consistent with reaction by the mechanism shown in Equation 1 where $k_{-1} \gg k_2$. Observed reaction rates of ortho- and para-HODPM in tetralin are listed in Table 2 as percent reaction and as defined first-order rate constants.

Table 2 also shows the rates of ortho-hydroxydiphenylmethane decomposition in the presence of several potential heterogeneous catalysts. These data indicate that (1) C-C bond cleavage in hydroxydiphenylmethanes is subject to heterogeneous catalysis by a number of surfaces, notably iron oxides, and (2) nevertheless, the observed rates of C-C bond cleavage in hydroxydiphenylmethanes, which are the principal subject of this paper, contain no significant heterogeneous component. The latter conclusion is based on findings (Table 2) that (1) rates in fused-silica and pyrex ampoules are identical, and (2) silanization of the crushed fused-silica, which was shown to be catalytically active, markedly reduces catalysis by that surface. Unless otherwise noted, reaction rates discussed in the remainder of this paper will be limited to those observed in the "normal" fused-silica ampoules in which rate-limiting steps are purely homogeneous.

Reaction via a pre-equilibrium followed by rate-limiting homolysis is additionally supported by the following observations (Table 2). First, rearrangement is observed at $\sim$ 10% and 15% of the cleavage rates of ortho- and para-HODPM, respectively. This is consistent with solvent-caged radical recombination of structures II' and III' in Scheme 1, in which rearrangement of para-HODPM to the ortho isomer is statistically favored. The other possible recombination product, benzylphenylether, is not observed, having a half-life of less than 2 minutes at 400°C.[1c] Second, meta-HODPM, for which no weakly bonded keto form can be drawn, is stable in tetralin at 400°C. Third, variation of ortho-HODPM concentration from 0.5 to 33.3 wt% in tetralin and variation of the extent of conversion from 3% to 22%, produced no significant changes (> 10%) in the defined first-order rate constant. Thus the rate-limiting step is indeed first order in substrate. Fourth, addition of acids, bases, and a radical initiator as potential catalysts for the enol-keto equilibrium failed to cause a significant (> 15%) increase in rate, in accord with the fact that acceleration of the rate at which a keto-enol pre-equilibrium is established will not affect the overall reaction rate. These catalysts were added to 4.1% ortho-HODPM in tetralin in the following amounts: phenol (2:1 mole ratio to substrate), H_2O (10:1 to 20:1), KOH (0.5:1), para-toluenesulfonic acid (0.25:1, unstable at 400°C), diphenylether (0.2:1), and bibenzyl (0.2:1 to 1:1).

Table 1 ESTIMATED AND OBSERVED HALF-LIVES FOR BOND SCISSION OF MODEL COMPOUNDS

Model Compound	Estimated Bond Strength	Estimated $t_{1/2}$ [a] at 400°C	Measured $t_{1/2}$ at 400°C	Defined First-Order Rate Constant [f]	Principal Products in Tetralin
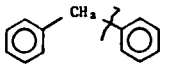	89 ± 3 kcal/mole [b]	10^9 hr	> 9000 hr	$< 2 \times 10^{-8}$	None
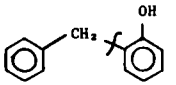	≥ 86 ± 3 kcal/mole [b]	≥ 10^8 hr	58 hr	3.3×10^{-6}	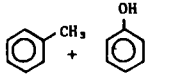
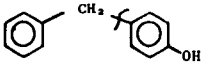	≥ 86 ± 3 kcal/mole [b]	≥ 10^8 hr	64 hr	3.0×10^{-6}	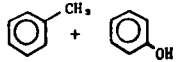
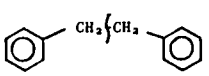	61.6 ± 2 kcal/mole [c]	10 hr	23 hr [d,e]	8.4×10^{-6}	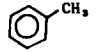

[a] Based on estimated bond strength and an assumed A factor of $10^{15.3}$ sec^{-1}.

[b] Based on values listed in References 2 and 3.

[c] Based on gas-phase rate measurements and an assumed A factor of $10^{15.3}$ sec^{-1} (Ref. 1d).

[d] From liquid-phase measurements (present work), which give log k = 16.4 - [(66.3±0.3/2.303 RT]. (Liquid-phase measurements from Reference 1d give log k = 16.0 - 64.8/2.303 RT and $t_{1/2}$ = 21 hr.)

[e] Data in Reference 1a indicate $t_{1/2}$ > 13 hr.

[f] When reaction is carried out in Tetralin at 400°C; units of sec^{-1}.

Table 2 CONVERSION OF COAL-MODEL COMPOUNDS IN TETRALIN AT 400°C IN THE PRESENCE OF HETEROGENEOUS CATALYSTS WITHOUT H_2 PRESSURE[a]

Coal-Model Substrate	Wt% in Tetralin	Catalyst or Surface/Amount	% Reaction at 20 hr	k_1 s^{-1}
o-Hydroxydiphenylmethane	4.1 (12.3 mg)	Fused-silica ampoule (normal reactor)	21	3.3×10^{-6}
		Pyrex ampoule	21	3.3×10^{-6}
		Silanized fused-silica ampoule	22	3.4×10^{-6}
		Stainless steel ampoule	28	4.5×10^{-6}
		Crushed fused-silica 0.5 g 100-200 mesh	94	3.8×10^{-5}
		Silanized crushed fused-silica 0.5 g, 100-200 mesh	55	1.1×10^{-5}
		α-Al_2O_3, 60 mg 1 μm diameter	46	8.5×10^{-6}
		Alundum (see text) 10.4 mg 325-400 mesh[b]	36	6.3×10^{-6}
		Crushed fused-silica 6.4 mg 325-400 mesh[b]	38	6.6×10^{-6}
		O_2, 150 torr (0.12:1 mole ratio to substrate)	26	3.8×10^{-6}
		$Na_2Cr_2O_7$, 1.5 mg	19	3.0×10^{-6}
		Fe_2O_3, 14.8 mg 325-400 mesh[b]	61	1.3×10^{-5}
		Fe_2O_3, 15 mg 0.2 μm diameter	78	2.1×10^{-5}
		Fe_3O_4, 15 mg 0.2 μm diameter	≥ 99.7	≥ 8×10^{-5}
		Fe_3O_4, 1.5 mg 0.2 μm diameter	58	1.2×10^{-5}
p-Hydroxydiphenylmethane	5.0 (15 mg)	--	19	3.0×10^{-6}
		Fe_3O_4, 15 mg 0.2 μm diameter	89	3.1×10^{-5}
m-Hydroxydiphenylmethane	5.0	--	≈ 0	≤ 2×10^{-6}
	5.2 (15.6 mg)	Fe_3O_4, 15 mg/0.2 μm diameter	48	9.0×10^{-6}
o-Methoxydiphenylmethane	4.1	--	90	3.2×10^{-5}
	4.1	Fe_3O_4, 1.5 mg/0.2 μm diameter	94	4.0×10^{-5}

[a] For the sake of comparison all rates are listed as defined first-order rate constants based on disappearance of starting material. In the case of ortho-hydroxydiphenylmethane and bibenzyl, the first-order rate constants varied by no more than 10% for 10-fold variations in concentration and 10-fold variations in extent of conversion. Mass balances (starting material plus identified products) were 97%-98% for noncatalyzed reactions, and 77%-88% for catalyzed reactions. Toluene and phenol account for ≥ 65% of the products of catalyzed reactions. The deficit in phenol and toluene was typically accounted for by 10% to 20% alkylation products and 15% to 25% high molecular weight products. The toluene/phenol ratios were typically 1.0 ± 0.2.

[b] Calculated to have equal surface areas, using a spherical particle assumption and density values from Chemical Rubber Co. Handbook of Chemistry and Physics.

Additional and more direct evidence that the rate-determining step is unimolecular scission of a keto intermediate is provided by the reaction of the methyl ether of ortho-hydroxydiphenylmethane (ortho-MeODPM). Five percent ortho-MeODPM in tetralin at 400°C gave a pseudo-first-order rate constant for disappearance of substrate which is ten times greater than that observed for ortho-HODPM. The major product was ortho-HODPM, formed via the reactions proposed in Scheme 2, at a rate that is consistent with the measurements of Colussi, Zabel, and Benson[9] and of Collins et al.[10] for the rate of homolytic ΦO-Et bond cleavage.

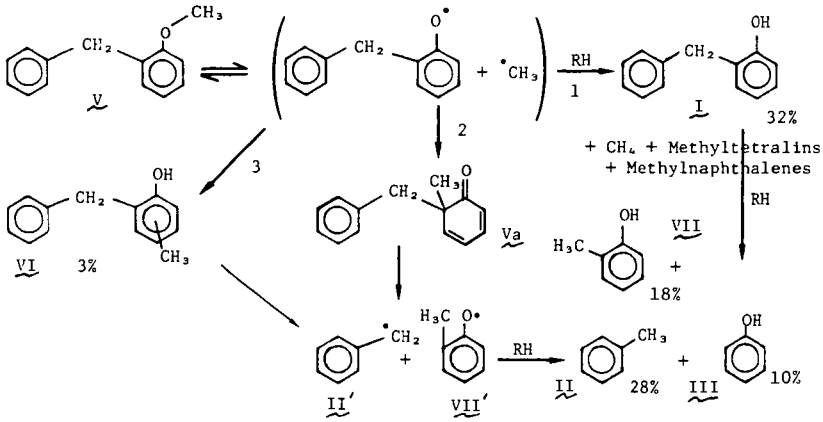

Scheme 2

The pertinent observations are (1) the total rate of formation of phenols is several times too large to be accounted for by reaction of HODPM as an intermediate, and (2) only one-third of the phenolic product is phenol; the other two-thirds is ortho-cresol. Evidently, the weakness of the Ph-Me bond provides an alternative pathway to the keto form: methyl shifts to the ortho position, either by solvent-caged radical recombination or by a symmetry hindered concerted [1,3] sigmatropic rearrangement. This shift produces an intermediate (Va) analogous to the keto tautomer in ortho-HODPM, except that in the present case establishment of a pre-equilibrium by reversal of this process is unlikely for the following reasons. There is no acidic proton to be lost in a very rapid acid-base reaction, and homolytic loss of a benzylic radical will be favored by ~ 15 kcal/mole (i.e., $> 10^4$ at 400°C) over either homolytic loss of the methyl radical,[2] or reversal of a [1,3] shift. Thus formation of Va leads inevitably to ortho-cresol and toluene at a rate that corresponds roughly to the rate of PhO-Me homolysis in the starting material.

Migration of the methyl group to the ring position ipso to the benzyl group seems to be fairly selective, suggested by the small amounts of VI formed. The selectivity of formation of other rearranged noncleaved products is an important factor in answering the question of whether methyl group migration is a scission-recombination process or a concerted reaction. Further details of these reactions and a discussion of this question will be presented in a subsequent publication.

The evidence presented above that the second and rate-limiting step is a unimolecular (i.e., homolytic) scission reaction provides no information about the mechanism by which tautomeric equilibrium is established. The equilibrium could be free radical in nature, as in Scheme 3, ionic, or surface catalyzed.

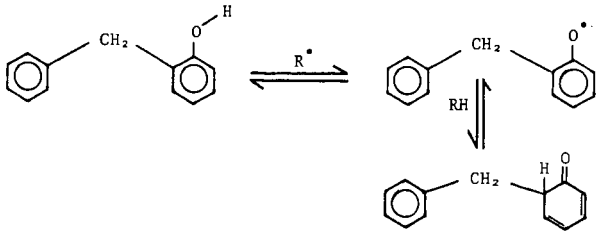

Scheme 3

Tautomerization by the radical chain mechanism shown in Equation 4 is plausible because tetralin is commonly observed to undergo significant rearrangement and degradation at 400°C by what have been argued to be radical chain reactions involving the 1- and 2-tetralyl radicals,[11] and because exchange of benzylic hydrogens is observed with coal models even when C-C bond scission is not observed.[12] On the other hand, tautomerization by an ionic mechanism is no less likely, since deuterium exchange at the ortho- and para- positions of phenols and naphthols is reported to occur at modest rates in tetralin even at temperatures ~ 200°C lower than the temperatures used in the study.[12] In fact, subsequent measurements of the rates carbon-oxygen bond cleavage in the anlogous hydroxydiphenyl ethers reveal that the fastest tautomerization process operative under the conditions of this study involve ionic reactions.

HYDROXYDIPHENYL ETHER DECOMPOSITION

The behavior of p-hydroxydiphenyl ether is analogous to that of o- and p-HODPM in that cleavage of the ether linkage is greatly accelerated by the presence of the hydroxy group, but differs in that the observed rate is more than two orders of magnitude too slow to result from rate-determining homolysis of the keto form. These results are illustrated in Table 3. This lack of agreement could be an indication that the general mechanism shown in Equation 1 does not apply to diphenyl ethers, or possibly even that the agreement of estimated with observed rates for the hydroxydiphenylmethanes was fortuitous. However, the results described below show that the disagreement actually results from the fact that in the case of hydroxydiphenyl ethers, tautomerization is significantly slower than it is with the HODPM. In contrast to ortho-hydroxydiphenylmethane decomposition, where addition of a number of different additives which would be expected to accelerate the tautomerization process failed to bring about any significant increase in the overall decomposition process (consistent with a tautomeric pre-equilibrium), the addition of KOH, p-cresol, or additional p-hydroxydiphenyl ether, all resulted in significant increases in the rate of decomposition of p-hydroxydiphenyl ether.

Table 3 ESTIMATED AND OBSERVED RATES OF C-O BOND SCISSION IN DIPHENYL ETHER STRUCTURES AT 400°C

Model Structure	Bond Strength[a], kcal/mole	Est. Bond Scission Rate[b]	wt % in Tetralin	Additive wt %	Est. Rate[c] via Tautomeric Equilibrium	Obs. Rate Constant[d], sec^{-1}	Principal Products
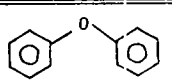	78 ± 2	5.5×10^{-11}	5.0	None	- - - - -	$\sim 0.2 \times 10^{-6}$	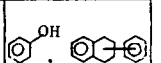
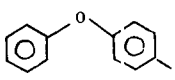	78 ± 4	5×10^{-11}	4.7	None	4.9×10^{-3}	1.7×10^{-6}	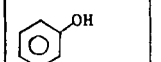
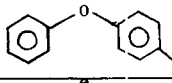	78 ± 4	5×10^{-11}	4.7	p-cresol / 34%	4.9×10^{-3}	5.5×10^{-6}	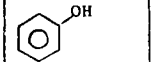
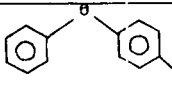	78 ± 4	5×10^{-11}	33	(additional substrate)	4.9×10^{-3}	11×10^{-6}	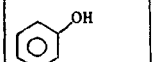
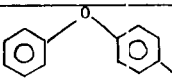	78 ± 4	5×10^{-11}	4.7	KOH[e] / 1%	4.9×10^{-3}	$\geq 100 \times 10^{-6}$	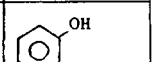

[a] Based on values listed in References 1d, 2, and 8.

[b] Expressed as first-order rate constant, sec^{-1}; based on an assumed A-factor of $10^{15.5}$ sec^{-1}.

[c] Expressed as first-order rate constant, sec^{-1}; calculated on the basis of Equation 2.

[d] Defined first-order rate constants, $k_1 = \ln (C_0/C)/t$.

[e] Heterogeneous reaction mixture.

These results are shown in Table 3 where it can be seen that in the case of added p-hydroxydiphenyl ether, a 7-fold increase in substrate concentration resulted in a 5.5-fold increase in the defined first-order rate constant for decomposition. This approaches the second-order behavior expected for ionic tautomerization of phenols in tetralin.

An ionic tautomerization process that is somewhat slower in the case of hydroxydiphenyl ethers is consistent with the fact that -OR substitution is known to be deactivating for the required electrophilic attack in the ipso position.[14] On the other hand, if tautomerization took place via a radical chain process, such as that shown in Equation 4, it would be difficult to rationalize such a process being significantly slower for diphenyl ether than for diphenylmethane structures.

SUMMARY AND CONCLUSIONS

The scission of strong carbon-carbon and carbon-oxygen bonds in hydroxydiphenylmethanes and diphenyl ethers during reaction in tetralin at 400°C has been shown to occur via ionic tautomerization to the respective keto forms which can undergo homolytic scission at rapid rates. In the case of the hydroxydiphenylmethanes, the tautomerization is rapid and constitutes a pre-equilibrium, but in the case of hydroxydiphenyl ethers, the tautomerization is slower and constitutes the principal rate-controlling step. Consistent with this picture, additives known to increase the rates of ring-hydrogen exchange in phenols have no effect on the decomposition rate of hydroxydiphenylmethanes, but markedly accelerate the rate of C-O bond scission in hydroxydiphenyl ethers. This latter observation suggests that the sometimes beneficial effects of added phenols in coal-conversion processes may be due, in part, to increased rates of tautomerization in diphenyl ether structures analogous to those studied in this work. Finally, an understanding of these and other details of the homogeneous decomposition mechanisms of hydroxydiphenylmethanes and hydroxydiphenyl ethers now provides a sound basis for elucidating the mechanism(s) of the facile heterogeneous cleavage that takes place in the presence of iron oxide surfaces.

Acknowledgement

The research reported here is supported by U.S. Department of Energy under contract number DE-AC22-79-ET14855.

REFERENCES

1. a) B. M. Benjamin, V. F. Raaen, P. H. Maupin, L. L. Brown, and C. J. Collins, Fuel, 57, 269 (1978).
   b) D. C. Cronauer, D. M. Jewell, K. A. Kueser, and Y. T. Shah, "Investigation of Mechanisms of Hydrogen Transfer in Coal Hydrogenation," Annual Report, July 1977, for U.S. Energy Research and Development Administration, Contract No. E(49-18)-2305.
   c) D. D. Whitehurst, M. Farcasiu, T. O. Mitchell, and J. J. Dickert, Jr., Annual Report, February 1977, for Electric Power Research Institute, EPRI AF-480.
   d) R. E. Miller and S. E. Stein, ACS Fuel Div. Preprints, 25, 271 (1979).
   e) K. R. Brower, Fuel, 56, 243 (1978).
   f) J. A. Franz, Fuel, 58, 405 (1979).
   g) M. L. Poutsma, Fuel, 59, 335 (1980).
2. a) S. W. Benson, Thermochemical Kinetics, 2nd Ed., John Wiley and Sons, New York, 1976, p. 309.
   b) J. D. Cox and G. Pilcher, Thermochemistry of Organic and Organometallic Compounds, Academic Press, New York, 1970.
3. J. S. Kerr and A. F. Trotman-Dickenson, in Handbook of Chemistry and Physics, 57th Ed., Chemical Rubber Co., Cleveland, Ohio, 1976, p. F-231.
4. E. A. Depp, C. M. Stevens, and M. B. Neuworth, Fuel, 35, 437 (1956).
5. L. A. Heredy and P. Fugassi, Adv. Chem. Series, 55, 448 (1968).
6. a) N. C. Deno, B. A. Greigger, and S. G. Stroud, Fuel, 57, 455 (1978).
   b) N. C. Deno, K. W. Curry, J. E. Cuynan, A. O. Jones, R. O. Minard, T. Potter, W. G. Rakitsky, and K. Wagner, ACS Fuel Div. Preprints 25, 103 (1980).
   c) N. C. Deno, K. W. Curry, B. A. Griegger, A. D. Jones, W. G. Rakitsky, K. A. Smith, K. Wagner, and R. D. Minard, Fuel 59, 694 (1980).
7. Abdel-Baset, P. H. Given, and R. F. Yarzab, Fuel, 57, 95 (1978).
8. Lamartine-Balme et al., C. R. Acad. Sci. Paris, Ser. C., 1969, 268 (11), 1064-6.
9. A. J. Colussi, F. Zabel, and S. W. Benson, Int. J. Chem. Kinetics, 9, 161 (1977).
10. C. J. Collins, V. F. Raaen, B. M. Benjamin, P. H. Maupin, and W. H. Roark, J. Amer. Chem. Soc., 101, 5009 (1979).
11. J. A. Franz and D. M. Camaioni, "Fragmentation of Free Radical Intermediates During Hydroliquefaction of Coals in Hydrogen Donor Media," Fuel, in press.
12. L. Stock, private communication.
13. a) I. F. Tupitsyn and V. I. Komarov, Reakts. Sposobnost Org. Soedin., 1969, 6 (3) 616-26.
   b) I. I. Kukhtenko, Dokladv Akad. Nauk. SSSR, 93, 487 (1953).
14. a) G. A. Olah, "Reactivity and Selectivity" in Friedel-Crafts and Related Reactions, G. A. Olah, Ed., Intersciences Publishers, New York, 1963, p. 853.
   b) H. H. Jaffe, Chem. Rev., 53, 191 (1953).